



**HAL**  
open science

# Changes in Calcium Cycling and Its Mechanisms in Sinoatrial-node underlying the TAC-induced Heart Failure in Mouse

Jianbin Xue

► **To cite this version:**

Jianbin Xue. Changes in Calcium Cycling and Its Mechanisms in Sinoatrial-node underlying the TAC-induced Heart Failure in Mouse. Cardiology and cardiovascular system. Université Paris-Saclay, 2020. English. NNT : 2020UPASQ009 . tel-03148869

**HAL Id: tel-03148869**

**<https://theses.hal.science/tel-03148869>**

Submitted on 22 Feb 2021

**HAL** is a multi-disciplinary open access archive for the deposit and dissemination of scientific research documents, whether they are published or not. The documents may come from teaching and research institutions in France or abroad, or from public or private research centers.

L'archive ouverte pluridisciplinaire **HAL**, est destinée au dépôt et à la diffusion de documents scientifiques de niveau recherche, publiés ou non, émanant des établissements d'enseignement et de recherche français ou étrangers, des laboratoires publics ou privés.

# Changes in Calcium Cycling and Its Mechanisms in Sinoatrial-node underlying the TAC-induced Heart Failure in Mouse

## Thèse de doctorat de l'université Paris-Saclay

École doctorale n° 569, Innovation Thérapeutique : du Fondamental à  
l'Appliqué (ITFA)

Spécialité de doctorat : physiologie, physiopathologie

Unité de recherche : Université Paris-Saclay, Inserm, UMR-S 1180,  
92296, Châtenay-Malabry, France

Référent : Faculté de pharmacie

Thèse présentée et soutenue à Châtenay-Malabry,  
Le 15 Octobre 2020, par

**Jianbin XUE**

### Composition du Jury

**Christian POÛS**

Professeur, Université Paris-Saclay,  
Châtenay-Malabry

Président

**Matteo Elia Mangoni**

Directeur de Recherche CNRS,  
Montpellier

Rapporteur & Examineur

**Héctor Valdivia**

Professeur, University of  
Wisconsin-Madison, USA

Rapporteur & Examineur

**Marcel Egger**

Professeur, University of Bern,  
Switzerland

Examineur

**Isabelle Marty**

Directeur de Recherche, Inserm,  
Grenoble

Examinatrice

**Ana Maria Gomez**

Directeur de Recherche, Inserm,  
Châtenay-Malabry

Directrice de thèse

## Résumé en Français

# Changements dans le cycle du calcium et ses mécanismes dans le nœud sino-auriculaire sous-jacent à l'insuffisance cardiaque induite par le TAC chez la souris

**Mots clés :** Insuffisance cardiaque ; nœud sino-auriculaire ; récepteurs de la ryanodine ;  $\text{Ca}^{2+}$

## Introduction

La circulation sanguine est contrôlée par les battements spontanés du cœur. Avec une fréquence de 50 à 90 battements par minute au repos, le cœur humain bat  $10^5$  fois par jour, soit 2 milliards de battements de cœur au cours d'une vie. Ces battements cardiaques sont initiés par la génération spontanée cyclique d'une activité électrique dépolarisante, qui quand elle atteint un seuil déclenche un potentiel d'action (PA) au niveau des cardiomyocytes du nœud sino-auriculaire (SAN). De manière générale, les mécanismes responsables de cette dépolarisation diastolique sont groupés en deux horloges : une « horloge membranaire », et une « horloge calcique », qui agissent en synergie de manière couplée ou redondante pour déclencher le PA des cellules du SAN. Cette impulsion électrique dépolarisante est ensuite transmise au reste de cœur générant des PAs qui entraînent la contraction cardiaque par le mécanisme de couplage excitation-contraction.

L'horloge membranaire est composée de canaux ioniques voltage-dépendants au niveau du sarcolemme, principalement le courant pacemaker (le courant  $I_f$  « funny »), mais aussi, les courants  $\text{Ca}^{2+}$  de type T ( $I_{\text{CaT}}$ ), et de type L ( $I_{\text{CaL}}$ ) par le canal Cav1.3, le Cav1.2 étant impliqué dans le PA lui-même.

L'horloge calciques est initiée par des canaux non-voltage-dépendants situés au niveau de la membrane intracellulaire du réticulum sarcoplasmique (SR) : les canaux de libération calcique, appelé récepteur à la ryanodine (RyR). Le  $\text{Ca}^{2+}$  libéré par ce canal pendant la dernière phase de dépolarisation diastolique, est expulsé de la cellule par l'échangeur  $\text{Na}^+/\text{Ca}^{2+}$  sarcolemmal, qui extrude 1 ion  $\text{Ca}^{2+}$  contre l'entrée de 3 ions  $\text{Na}^+$  générant ainsi un courant dépolarisant. Ce courant,  $I_{\text{NaCa}}$ , accélère la dépolarisation de la membrane, jusqu'au seuil de déclenchement du PA.

L'insuffisance cardiaque (IC) est un syndrome manifestant l'incapacité du cœur d'assurer sa fonction de pompe afin de maintenir le flux sanguin pour répondre aux besoins du corps, d'abord à l'effort, puis aussi au repos. En 2015, l'IC a touché environ 40 millions de personnes dans le monde. On considère qu'environ 2 % des adultes souffrent d'IC et chez les personnes de plus de 65 ans, cela passe à 6-10 %, voire au-delà pour les plus de 75 ans.

Les patients présentant IC présentent un remodelage significatif de la fonction du SAN caractérisée par une diminution de la fréquence cardiaque intrinsèque. Il a été montré, dans des modèles expérimentaux de lapin et chien, que cela est dû à l'altération des éléments de l'horloge membranaire, notamment une diminution du courant  $I_f$ .

À ce jour, peu de choses et souvent controversées ont été rapportées sur l'homéostasie  $Ca^{2+}$  des cellules du SAN dans le cadre de la IC. Cela peut être dû aux différents modèles utilisés (souris, lapin ou canine) et à la manière différente d'induire l'IC (rythme rapide imposé ou constriction de l'aorte transversale (TAC)).

## **Objectifs**

Le SAN est le pacemaker primaire du cœur. De nombreuses conditions pathologiques telles que l'IC, peuvent influencer la fonction SAN. L'homéostasie  $Ca^{2+}$  joue un rôle clé dans la régulation de la fonction de SAN. Le but de cette étude était d'analyser comment la fonction intrinsèque des cellules du pacemaker cardiaque est modifiée dans l'IC et si l'homéostasie de  $Ca^{2+}$  est impliquée dans cette dysfonction. En outre, notre travail c'est également penché sur le mécanisme possible sous-jacent au changement de l'homéostasie  $Ca^{2+}$ . Le but était de fournir une compréhension plus complète du dysfonctionnement pacemaker cardiaque au cours de l'IC afin de fournir des perspectives cliniques prometteuses.

# Résultats

## Partie 1

Nous avons analysé l'horloge calcique dans un modèle expérimental d'IC par constriction aortique transversale (TAC) chez la souris. Les animaux témoins (Sham) ont été soumis à une chirurgie factice. L'IC a été déterminée par une fraction d'éjection diminuée, estimée par échocardiographie en mode M. L'IC congestive a été déterminé par une augmentation du rapport poids de poumons/longueur du tibia. Les électrocardiogrammes enregistrés par télémétrie n'ont pas montré de modification du rythme cardiaque (HR) de base. Cependant, la variabilité du HR était plus faible chez les souris IC, ainsi que le HR intrinsèque du SAN, après blocage du système nerveux autonome (SNA) par injection intrapéritonéale d'atropine et de propranolol (2 mg / kg chacun). Ces résultats montrent un dysfonctionnement intrinsèque du SAN chez les souris IC.

Afin d'analyser le mécanisme sous-jacent, le SAN a été disséqué, chargé avec un indicateur fluorescent de  $Ca^{2+}$ , le fluo-4 AM, et observé par microscopie confocale. La fréquence des transitoires  $[Ca^{2+}]_i$  était plus lente dans le SAN d'IC et leur durée significativement plus longue, suggérant une altération de la fonction de la  $Ca^{2+}$ -ATPase du RS (SERCA) et/ou de l'échangeur  $Na^+/Ca^{2+}$  (NCX). De fait, dans le groupe IC, l'expression protéique de NCX était déprimée, avec une expression accrue de phospholamban (PLB, un inhibiteur naturel de SERCA lorsqu'il n'est pas phosphorylé) ainsi qu'une moindre phosphorylation au site T17, site phosphorylation par la  $Ca^{2+}$ /Camoduline Kinase II (CaMKII). Ainsi, le temps de décroissance plus long des transitoires  $[Ca^{2+}]_i$  pourrait être le résultat d'une moindre d'expression de NCX et/ou d'une plus grande inhibition de SERCA. La diminution de la fonction de la SERCA diminuait la charge calcique du SR, comme cela a été constaté par une perfusion rapide de caféine dans les cellules isolées du SAN du groupe IC.

Afin d'évaluer l'activité des récepteurs à la ryanodine (RyR2), nous avons analysé les transitoires calciques localisés ( $Ca^{2+}$  sparks), événements élémentaires produits par l'activation d'un cluster de RyR2s. La fréquence des sparks  $Ca^{2+}$  est plus petite dans le groupe IC, avec une amplitude et une durée aussi réduite. Ainsi, la quantité de  $Ca^{2+}$  libéré pendant la diastole par les  $Ca^{2+}$  sparks était plus petite dans le groupe IC, indiquant une diminution de la fonction de l'horloge  $Ca^{2+}$ .

Nous avons ensuite étudié plus en détail les altérations des RyR2s au niveau moléculaire, par immunoblot. Avec l'IC, le niveau d'expression des RyR2s était significativement diminué, ainsi que leur

phosphorylation relative au site S2814. Combiné avec la réduction de la phosphorylation relative du phospholambane (PLB) au site T17, ces résultats suggèrent une activation moindre de la CaMKII dans IC SAN. De fait, si l'expression de CaMKII était semblable dans les deux groupes, son niveau de phosphorylation était significativement réduit, indiquant une activation moindre. Pour tester la signification fonctionnelle de cette dernière diminution, nous avons perfusé un inhibiteur de la CaMKII, le KN93, sur le tissu SAN et analysé les mouvements de  $Ca^{2+}$ . Si le KN93 réduisait significativement la fréquence spontanée des transitoires  $[Ca^{2+}]_i$  dans les deux groupes, indiquant une certaine activation basale, son effet était proportionnellement plus importante dans les groupes IC, conduisant à une fréquence encore plus rapide.

Pour conclure, nous avons mis en évidence que la CaMKII est moins activé dans le SAN des souris IC. Cela conduit à une moindre phosphorylation du PLB et de RyR2, ce qui ralentit l'horloge  $Ca^{2+}$ . De plus, les niveaux d'expression de RyR2 et de NCX, deux éléments principaux de l'horloge  $Ca^{2+}$ , est diminué, ce qui altère davantage la fonction du nœud sinusal avec l'IC.

## Partie 2

Alors que toutes les souris soumises à la TAC ont montré une hypertrophie cardiaque et une fraction d'éjection déprimée, seulement quelques-uns des animaux ont présenté des signes d'insuffisance cardiaque congestive, et d'autres n'ont montré aucun signe de congestion (poids du poumon par rapport au poids corporel). Nous avons en parallèle du travail de la partie 1 aussi analysé ce groupe, nommé groupe hypertrophique (Hyp).

L'analyse in vivo du HR n'a montré aucune différence entre le groupe Hyp et le groupe IC, avant ou après l'inhibition d'ANS, présentant ainsi un dysfonctionnement du pacemaker cardiaque.

Les caractéristiques des transitoires  $[Ca^{2+}]_i$  et de sparks  $Ca^{2+}$  du groupe Hyp ont montré la même tendance que le groupe IC comparé au groupe de Sham. Les différences significatives observaient occasionnellement entre les deux groupes peuvent se référer aux différents degrés du dysfonctionnement de pacemaker cardiaque avec la sévérité pathologique.

Le niveau d'expression de la CaMKII était similaire entre les deux groupes, non différent groupe Sham, et le niveau de phosphorylation de la CaMKII était diminué de façon similaire entre les deux groupes TAC. Cependant, le niveau de phosphorylation de RyR2 et de PLB sur le site de PKA était significativement augmenté dans le groupe Hyp comparé aux groupes Sham et IC.

Nous proposons que le groupe Hyp est juste au milieu du chemin du groupe IC congestif. Considérant la fonction cardiaque, le groupe d'Hyp est sensiblement différent du groupe Sham et est plus semblable au groupe IC mais plus faiblement diminué. Le dysfonctionnement du pacemaker cardiaque s'est également produit dans ce groupe et la signalisation de CaMKII est également diminuée de manière significative dans le SAN de deux groupes TAC. Cependant, la voie de signalisation PKA est activée seulement dans le groupe Hyp.

## Partie 3

L'IC résulte de plusieurs pathologies qui imposent chroniquement un travail supplémentaire au cœur. Le diabète, une condition où la glycémie est élevée, peut être associé à l'IC. Puisque l'étiologie de l'IC au cours du diabète est très différente de celle après surcharge de pression comme la TAC, les voies de signalisation activées et ainsi les altérations cellulaires pourrait être différentes. Dans un travail collaboratif, nous avons analysé la signalisation  $Ca^{2+}$  intracellulaire des cellules du SAN de souris diabétiques de type 2 suite à une obésité (db/db, et leurs contrôles db/+).

Les souris souffrant de diabète et présentant une IC, ont montré aussi un dysfonctionnement de pacemaker cardiaque. Par contre, dans ce modèle, le HR était accélérée. En accord, les sparks  $Ca^{2+}$  sont plus fréquentes à l'état basal, montrant une accélération de l'horloge calcique, contrairement au modèle TAC. La stimulation beta-adrénergique par l'isoprotérenol (ISO, 20nM) augmentait encore plus cette libération diastolique de  $Ca^{2+}$  dans les SAN db/db IC. Une activation muscarinique par le Carbachol (500nM) avait l'effet opposé et diminuait la fréquence des transitoires  $[Ca^{2+}]_i$ , et aussi la fréquence des sparks  $Ca^{2+}$  dans les cellules SAN db/db, ramenant au niveau des souris db/+. Ainsi, le tonus parasympathique peut corriger le dysfonctionnement du SAN au cours de l'IC suite au diabète. Considérant que chez les patients IC, le tonus sympathique généralement plus activé et le tonus parasympathique est relativement inhibé, la conclusion de ces résultats fournit une perspective inspirante.

## Discussion

Le SAN est le principal pacemaker cardiaque. Il génère spontanément le signal électrique conduisant la contraction du cœur, qui pompe le sang dans tout le corps et soutient la vie. Il est maintenant largement admis que l'automatisme du SAN provient d'un système d'horloge couplé, composé d'une horloge membranaire et d'une horloge  $Ca^{2+}$ . De nombreuses conditions

pathologiques peuvent influencer la fonction SAN, comme l'hypertrophie et l'insuffisance cardiaque. L'insuffisance cardiaque est un trouble mortel et coûteux. Récemment, certaines études ont montré que l'insuffisance cardiaque réduit l'activité du pacemaker cardiaque par altération de l'horloge de voltage. L'horloge  $Ca^{2+}$  dans les cellules SAN du cœur défaillant est sous-étudié. Nous avons constaté que la CaMKII est moins activé dans le SAN des souris IC, bien que dans le ventricule c'est l'opposée. L'activation inférieure de cette kinase conduit à une diminution du taux basale de phosphorylation PLB et RyR2. De plus, l'altération dans les niveaux d'expression de ces deux protéines (augmentation du PLB et diminution du RyR), ralentie l'horloge  $Ca^{2+}$ . De plus, la partielle compensation qui peut proportionner l'activation de la voie de signalisation PKA que nous avons trouvé dans l'hypertrophie, n'est plus n'est plus trouvé dans l'IC plus avancée. En outre, la diminution de l'expression du NCX, qui est fondamental pour que le fonctionnement de l'horloge  $Ca^{2+}$ , en traduisant la libération du  $Ca^{2+}$  du SR en une dépolarisation de la membrane, va aussi dans le sens de ralentir l'automatisme du SAN. Tandis que dans IC induite par le diabète nous avons constaté que le taux intrinsèque de pacemaking est plus rapide que les contrôles, avec une augmentation de l'horloge  $Ca^{2+}$  évidente par une augmentation de la fréquence des sparks  $Ca^{2+}$ . Ces résultats opposés dans ce modèle, indiquent que l'étiologie de la dysfonction cardiaque est importante pour déterminer les altérations du pacemaker.

# Acknowledgement

My Ph.D. career is an impressive and amazing experience. And I would not have achieved it without the support and guidance I received from many people.

I would like to show my deepest gratitude to my supervisor, Dr. Ana Maria Gomez. It was she who opened the door for me to join the lab 4 years ago. And with her kind help, I was successful in applying for the Chinese scholarship and thus, I could have the chance to go aboard, to experience everything in France, to make all these life-changing events come true.

I also would like to express my great appreciation to Ana for her professional guidance, patience, constant encouragement and support. Her advice helped me all the way during my Ph.D. I also have learnt a lot from her in a broader sense other than only research. She is the best supervisor I could imagine.

I sincerely thank Dr. Jean-Pierre Benitah. He gave me a lot of valuable comments and suggestions for my project. We held many great discussions concerning the experiments. I really like those 'little courses' he gave on the white board in our office.

I am grateful for the contribution to my project by the authors in my paper. Special thanks to Susana Gomez for her help in the model building and monitor. I think Moran Davoodi and Yael Yaniv for doing the HRV analysis. To Dr. Yael Yaniv, also many thanks to her for giving the chance to visit her lab in Israel. Israel is so mysterious and attractive for me that I will never forget the travel there.

Many thanks to all my wonderful colleagues for offering precious help and letting my Ph.D. life enjoyable. And to Dr. Dawei Liu, I would like to show my special thanks. The first day I arrived in France, it was him who took me from the railway station and lead me to the lab.

I gratefully acknowledge the financial support of China Scholarship Council (CSC) for the past four years.

Finally, I would like to thank my parents. My mother Chunyan WANG and my father Qing XUE. Every time I feel down, I give a phone call to them and get the warmest comfort. Not only for these four years but for all the time and will be all lifetime. They are great parents.

# Content

|  |           |
|--|-----------|
| <b>Chapter 1 Introduction</b> .....  | <b>1</b>  |
| <b>1.1 Overview of heart function, action potentials and CICR</b> .....                | <b>1</b>  |
| 1.1.1 Heartbeat and electrocardiogram .....  | 1         |
| 1.1.2 Action potential .....   | 2         |
| 1.1.3 Calcium induced calcium release (CICR) .....                                     | 4         |
| <b>1.2 Sinoatrial node (SAN) automaticity</b> .....                                    | <b>6</b>  |
| 1.2.1 Voltage clock theory .....   | 8         |
| 1.2.1.1 HCN channels and funny current.....  | 9         |
| 1.2.1.2 L-type $\text{Ca}^{2+}$ Channel (LTCC).....                                    | 11        |
| 1.2.1.3 T-type $\text{Ca}^{2+}$ channel (TTCC) .....                                   | 12        |
| 1.2.1.4 Sodium Channel.....  | 12        |
| 1.2.1.5 Potassium Channels .....   | 13        |
| 1.2.1.6 TRP channels .....   | 14        |
| 1.2.1.7 Other channels .....   | 15        |
| 1.2.1.8 Voltage clock.....   | 15        |
| 1.2.2 $\text{Ca}^{2+}$ clock theory .....  | 16        |
| 1.2.2.1 RyR2 in $\text{Ca}^{2+}$ clock.....  | 16        |
| 1.2.2.2 $\text{Ca}^{2+}$ sparks and sarcoplasmic reticulum $\text{Ca}^{2+}$ load.....  | 16        |
| 1.2.2.3 Sodium-calcium exchanger (NCX).....  | 17        |
| 1.2.2.4 $\text{Ca}^{2+}$ clock .....   | 18        |
| 1.2.3 Coupled clock theory.....  | 18        |
| <b>1.3 Cardiac innervation and Autonomic regulation</b> .....                          | <b>20</b> |
| 1.3.1 Cardiac innervation.....   | 20        |
| 1.3.2 Sympathetic modulation .....   | 21        |
| 1.3.3 Parasympathetic modulation.....  | 23        |
| 1.3.4 Autonomic modulation on Heart rate variability (HRV) .....                       | 25        |
| <b>1.4 Heart failure and HF related pacemaker dysfunction</b> .....                    | <b>28</b> |
| 1.4.1 Overview of Heart failure .....  | 28        |
| 1.4.2 Ventricular dysfunction and Cardiac Hypertrophy (Hyp).....                       | 32        |
| 1.4.3 HF Induced $\text{Ca}^{2+}$ dysfunction in Cardiac myocyte.....                  | 36        |
| 1.4.4 HF induced SAN dysfunction.....  | 41        |
| 1.4.4.1 Voltage clock alteration and Ivabradine treatment .....                        | 41        |
| 1.4.4.2 $\text{Ca}^{2+}$ handling alteration .....                                     | 43        |
| <b>1.5 Objectives</b> .....  | <b>43</b> |
| <b>Chapter 2 Material and Methods</b> .....  | <b>45</b> |
| <b>2.1 Transverse Aortic Constriction</b> .....  | <b>45</b> |
| <b>2.2 Echocardiography and Doppler</b> .....  | <b>47</b> |
| <b>2.3 Telemetric ECG recording</b> .....  | <b>47</b> |
| 2.3.1 The transmitter implantation.....  | 48        |
| 2.3.2 ECG recordings.....  | 49        |
| 2.3.3 ECG analysis.....  | 49        |
| 2.3.4 HRV analysis based on ECG.....   | 51        |
| <b>2.4 SAN Preparation</b> .....   | <b>51</b> |
| 2.4.1 SAN dissection.....  | 51        |
| 2.4.2 Isolation of sinoatrial node myocytes .....                                      | 52        |
| <b>2.5 <math>\text{Ca}^{2+}</math> handling recording by confocal microscopy</b> ..... | <b>52</b> |
| 2.5.1 Principles on the confocal microscopy .....                                      | 52        |

|   |            |
|---|------------|
| 2.5.2 SAN tissue preparation recording .....  | 55         |
| 2.5.3 Single SAN Cell recording and Caffeine perfusion.....   | 55         |
| 2.5.4 Confocal microscope images analysis.....  | 55         |
| <b>2.6 Protein measurement .....</b>  | <b>56</b>  |
| 2.6.1 Protein extraction.....   | 56         |
| 2.6.2 Western Blot.....   | 57         |
| <b>2.7 Statistics .....</b>   | <b>60</b>  |
| <b>Chapter 3 Results .....</b>  | <b>61</b>  |
| 3.1 Heart failure induces sinus node dysfunction associated with reduced CaMKII signaling. ....                           | 61         |
| 3.2 The mysterious Hypertrophy group .....  | 84         |
| 3.3 Aberrant sinus node firing during $\beta$ -adrenergic stimulation leads to cardiac arrhythmias in diabetic mice ..... | 94         |
| <b>Chapter 4 Discussion .....</b>   | <b>108</b> |
| 4.1 TAC surgery outcomes-a real Troublemaker .....  | 108        |
| 4.2 The impaired SAN function .....   | 109        |
| 4.3 Different shapes different story .....  | 109        |
| 4.4 The less phosphorylated CaMKII.....   | 110        |
| 4.5 Opposite to the ventricles.....   | 110        |
| 4.6 Diabetes induced HF.....  | 111        |
| 4.7 Limitations and perspectives .....  | 111        |
| <b>References .....</b>   | <b>113</b> |

# Chapter 1 Introduction

## 1.1 Overview of heart function, action potentials and CICR

### 1.1.1 Heartbeat and electrocardiogram

The heart beats spontaneously to provide blood circulation. The human heart beats  $10^5$  times a day resulting in 2 billion heartbeats during a lifetime.

In 1791 Luigi Galvani discovered that electrical stimulation of a frog's heart lead to cardiac muscle contraction (De viribus Electricitatis in motu musculari Commentarius. Galvani.1791). Then, the idea that heart may be driven by electricity was raised. Based on the improvement of the instrumentation, mainly electrodes and galvanometers (to which Galvani's name is given), the recording electrical signals from heart became possible and that is the electrocardiogram (ECG).

Under normal physiological situation, the heart beat is initiated by the sinoatrial node (SAN) which is described as the primary pacemaker of the heart since more than 100 years ago [1]. The SAN can generate electrical impulse automatically and anticipates to atrioventricular (AV) node and Purkinje fibers network (PFN), which can also generate pacemaker activity. However, these two only drive the heart when the SAN or the heart is in pathological condition. For instance, AV node can become dominant during SAN block or heart failure, and PFN can also lead a viable rhythm during AV block. Therefore, this system can also maintain heartbeat under pathological situation (Fig.1).

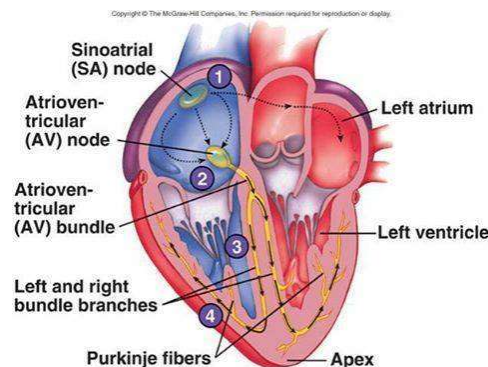


**Fig.1 Schematic diagram of the heart structure. (Picture is from MedicTests.com Facebook)**

SAN is located at the right atria near the entrance of the superior vena cava (SCV) and bordered by the crista terminalis (Fig.1). As the primary pacemaker, it initiates the electrical impulse, and spreads across the right and left atria and induce the atrial depolarization and contraction, which is the atrial systole. On the surface ECG, this process corresponds to the P wave (0.08s in human) (Fig.2). Then the impulse will reach to the AV node, and it will slow down because

of the conduction property of the AV node. This delay can make sure all the blood has been ejected to the ventricles before ventricular contraction. It corresponds to PR segment (0.04s in humans). While the PR intervals represent the duration from the beginning of atrial depolarization until ventricular depolarization. Then the AV node will pass the signal to His bundles into the left and right ventricles branches. Then, the signal passes to Purkinje fibers and go through both ventricles, initiating the ventricular depolarization and contraction. Thus, the blood will be pumped throughout the body. On the ECG, ventricular depolarization corresponds to the QRS complex (0.12s in human). Meanwhile the atrial repolarization occurs, and this process will be buried in the QRS complex. The ventricular repolarization is corresponding to the T wave.

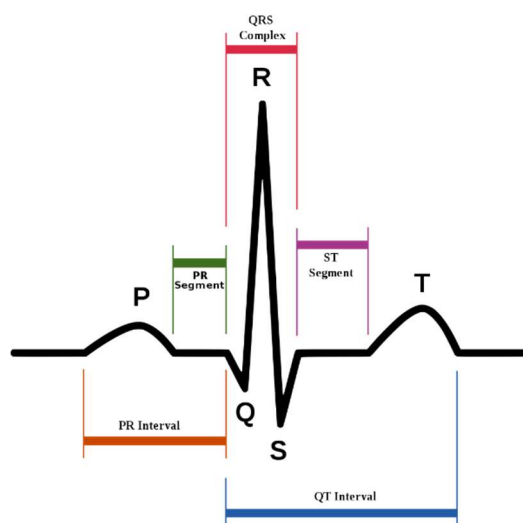


**Fig. 2 ECG of a heart in normal sinus rhythm.** The PR interval goes from the beginning of the P wave to the beginning of the QRS complex, while the QT interval is from the beginning of QRS complex until the end of T wave. The PR segment goes from the end of P wave until the beginning of Q wave, and the ST segment is between the end of S wave and the beginning of T wave. (Picture is from Wikipedia <http://en.wikipedia.org/wiki/Electrocardiography>)

## 1.1.2 Action potential

Nearly all cell membranes in animals, plants and fungi maintain a voltage difference between the exterior and interior of the cell, called the membrane potential. An action potential is a rapid rise and subsequent fall in membrane potential across a cellular membrane with a characteristic pattern. In 1939, A. L. HODGKIN & A. F. HUXLEY made the first direct recording of the electrical changes across the neuronal membrane that mediate the action potential [2]. The first recorded AP in cardiac muscle was performed by E. Coraboeuf\* and S. Weidman and published in the annals of the meeting of the Biology Society (*Coraboeuf E, Weidman S. Potentiel de repos et potentiel d'action du muscle cardiaque, mesures à l'aide de microelectrodes. CR Séances Soc Biol Fil 1949; 143: 1329-31. 3.*). And

in 1950, L. A. WOODBURY, J. W. WOODBURY, and H. H. HECHT reported the first action potential on single cardiac myocyte [3].

**\* Anecdote**

*When I began to write my long introduction part of my PhD thesis, I did not really know who really was Edouard Coraboeuf. Until my supervisor, Ana Maria Gomez, also the director of the Lab UMR-S1180 "Laboratoire de Signalisation et Physiopathologie Cardiovasculaire" mentioned in the comments that this lab is somehow the continuation of the one built by Edouard Coraboeuf. And in whose heritage, I am doing my thesis. Thus, to be honest I feel amazing and a bit honor for the career. Also, I would like to show my sincerely regards and acknowledgments to Edouard Coraboeuf and his pioneer work in the development of the cardiac electrophysiology.*

The cardiac AP morphology between cardiomyocytes varies dramatically in different regions of the heart. This is because the AP is result of multiple ion channels, pumps and exchangers that open and close generating both inward (depolarizing) and outward (repolarizing) currents at different and or overlapping times [4,5]. However, these components can be different from one tissue to another among the whole heart.

The AP of ventricular cells can be divided into four phases. The resting membrane potential is maintained by  $I_{K1}$  of the Kir2.1 potassium channel. After a ventricular myocyte is excited, the voltage dependent  $Na_v1.5$  sodium channels will be activated generating a rapid inward  $Na^+$  current ( $I_{Na}$ ) and lead to a rapid membrane depolarization constituting the upstroke of the AP (phase 0). This depolarization induces the inactivation of  $Na_v1.5$  channel and activation of voltage-dependent  $K^+$  channels ( $K_v4.3$  and  $K_v1.4$ ), which generates a rapid repolarization current ( $I_{to}$ ) (phase 1). Then, the voltage-dependent  $Ca^{2+}$  channels ( $Ca_v1.2$ ) are activated, producing an inward  $Ca^{2+}$  current ( $I_{Ca,L}$ ) slowing down the speed of repolarization. The activation of outward rectifying  $K^+$  currents ( $I_{Kur}$ ,  $I_{Kr}$  and  $I_{Ks}$  via  $K_v1.4$ ,  $K_v11.1$  and  $K_v7.1$ , respectively) and  $I_{Ca,L}$  at overlapping voltages, result in the plateau phase of AP (phase 2). Inactivation of  $Ca_v1.2$  induces the predominance of  $K^+$  currents and further membrane depolarization (phase 3). In the end, Kir2.1 is re-activated, which generates the  $I_{K1}$  current and makes the membrane potential back to the resting level (Fig.3 Left)

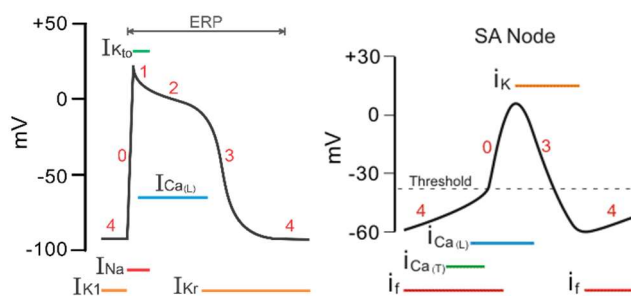


**Fig.3 Action potential in ventricular myocyte (Left) and in sinus node (Right).** *non-pacemaker cells have a true resting membrane potential (phase 4) that remains near the equilibrium potential for  $K^+$  ( $E_K$ ). The resting membrane potential is very negative during phase 4 (about -90 mV) because potassium channels are open ( $K^+$  conductance [ $g_{K^+}$ ] and  $K^+$  currents [ $I_{K1}$ ] are high). As shown in the figure, phase 4 is associated with  $K^+$  currents, in which positive potassium ions are leaving the cell and thereby making the membrane potential more negative inside. At the same time, fast sodium channels and (L-type) slow calcium channels are closed. SA nodal action potentials are divided into three phases. Phase 4 is the spontaneous depolarization (pacemaker potential) that triggers the action potential once the membrane potential reaches threshold between -40 and -30 mV. Phase 0 is the depolarization phase of the action potential. This is followed by phase 3 repolarization. Once the cell is completely repolarized at about -60 mV, the cycle is spontaneously repeated. (The picture is from Cardiovascular Physiology Concepts; Richard E. Klabunde, PhD)*

The morphology of AP in automatic cells, as SAN cells, is different from that of ventricular myocytes (Fig.3 Right). The SAN cells can spontaneously generate regular and cyclic AP. The SAN cell does not have real resting membrane potential. The most negative potential the SAN reaches is named maximum diastolic potential. The phase 4 includes the slow increase in membrane potential toward an excitation threshold, at which the action potential fires. Regarding the mechanisms of autonomic diastolic depolarization (DD), one important factor involved is the funny current ( $I_f$ ) carried by hyperpolarization-activated cyclic nucleotide-gated channels (HCN channels), which depolarizes the membrane. Other currents also contribute to the progression of depolarization, such as  $I_{Ca,T}$ ,  $I_{NCX}$  and  $I_{Ca,L}$  carried respectively by T-type  $Ca^{2+}$  channel ( $Ca_v3.1$ ,  $Ca_v3.2$ ), sodium-calcium exchanger (NCX), L-type  $Ca^{2+}$  channel ( $Ca_v1.2$ ,  $Ca_v1.3$ ). The phase 4 consists of two components, a linear component (the first two-thirds of DD) and a nonlinear, exponentially rising component (the last third of DD). The nonlinear component is proposed to occur along with the subsequent cytosolic  $Ca^{2+}$  increase induced by local  $Ca^{2+}$  release by SR and concomitant inward NCX activation. The rapid upstroke (phase 0, Figure 3) of SAN AP is much faster than diastolic depolarization, but still slower than that of ventricular myocytes as it's carried out by slow  $Ca^{2+}$  current in SAN instead of the fast  $Na^+$  current in ventricular myocytes. The initial repolarization phase (phase 1) in ventricular myocytes is completely absent, and the plateau of phase 2 is replaced by a slow velocity repolarization phase. In the end, the  $E_m$  is driven to maximum diastolic potential (MDP) by potassium channels. The AP of SAN has a relatively positive MDP of around -50mV due to the absence of  $I_{K1}$ .

### 1.1.3 Calcium induced calcium release (CICR)

Calcium induced calcium release (CICR) describes a biological process whereby 'a little amount' of calcium is able to activate calcium 'mass release' from intracellular  $Ca^{2+}$  stores (endoplasmic reticulum or sarcoplasmic reticulum). Bianchi and his co-workers first proposed, although without the direct evidence, that calcium ion itself might trigger the calcium release from SR [6,7]. Then, in

1968, Ford and Podolsky [8] and Endo et al. (PFOC. Intern. Congr. Physiol. Sci., 24th. 1968, vol. 7) first reported independently that calcium ion can induce a release of calcium.

CICR was firstly proposed as a mechanism in skeletal muscle in the 1970s [9]. Then in 1980s, Fabiato et Fabiato did a series of outstanding work to show CICR is also crucial for excitation-contraction coupling in cardiac muscle [10].

The CICR gives rise to a 'paradox of control' because the released calcium would be expected to trigger further release, leading to a regenerative, nearly all-or-none event. In 1992 Stern proposed the local control model theory to solve this paradox [11]. This model describes the whole event as the trigger for calcium release is the local calcium microdomain generated by influx through sarcolemmal calcium channels, and most of the gradation of release is due to statistical recruitment of localized release events. Only in one year, Cheng, Lederer & Cannell [12] discovered the localized, stochastic release events, named as the 'calcium sparks', the elementary events of cardiac excitation-contraction coupling. The whole cell calcium release could be viewed as the summation of these events. [13]. To be more detailed, a small group of RyR2 channels near the L-type  $\text{Ca}^{2+}$  channels form an autonomous  $\text{Ca}^{2+}$  release unit (CRU) in the microanatomical dyad structure [14]. Different CRUs are separated by several hundred nanometers. The activation of one or small amount of RyR2 inside one CRU will lead to rapid recruitment of RyR2 only in that CRU and form a  $\text{Ca}^{2+}$  spark. However, the adjacent CRUs are not usually activated because of the diffusion and buffering of  $\text{Ca}^{2+}$  outside the source dyad (Fig.4).

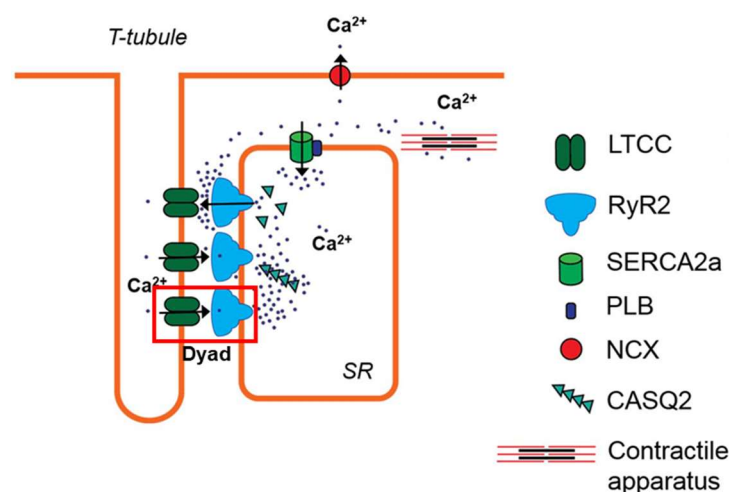


**Fig.4 Diagram of Dyad in cardiomyocytes.**  $\text{Ca}$  release unit is formed by a cluster of ryanodine receptors (RyR2) in the junctional sarcoplasmic reticulum (SR) and L-type  $\text{Ca}$  channels (LTCC) in the sarcolemma. During systole, inward  $\text{Ca}$  current through the LTCC activates RyR2 by the mechanism called  $\text{Ca}$ -induced  $\text{Ca}$  release (CICR). A global  $\text{Ca}$  transient causes activation of the contractile apparatus and thus myocyte contraction. During diastole, cytosolic  $\text{Ca}$  is pumped back into the SR by the  $\text{Ca}$ -ATPase (SERCA) and extruded from the cell by the  $\text{Na}$ - $\text{Ca}$  exchanger (NCX). (The picture is adapted from Nikolaienko, R [15])

However, the paradox of control was not really solved by this model. Inside one CRU, once the RyR2 is activated, a  $\text{Ca}^{2+}$  spark could progress independently of the trigger because of regenerative CICR within the dyad junction itself. Of course, this is not consistent with the actual situation. CICR is a process that can stop spontaneously at the right time.

To date, the mechanisms responsible for the control of SR release termination remain unclear. There are several potential mechanisms: (1) time-dependent inactivation and/or "adaptation" of the RyR2 channel; (2) stochastic attrition, all or most of the RyR2 channels in one CRU close at the same time to decrease the amount of the  $\text{Ca}^{2+}$  release and terminate the CICR; (3) allosteric coupling between RyR2s so that spontaneous closure of one RyR2 promotes closure of the others; (4)  $\text{Ca}^{2+}$ -dependent RyR2 gating changes, caused by the  $\text{Ca}^{2+}$  sensor of RyR2 in luminal side and also via an accessory protein such as calsequestrin (CSQ); (5) induction decay wherein a decreasing RyR2 release flux leads to local cytoplasmic  $\text{Ca}^{2+}$  levels becoming insufficient to maintain CICR [16].

## 1.2 Sinoatrial node (SAN) automaticity

This session serves to introduce SAN action potential and the generation of pacemaker activity.

In 1907, Keith, A., & Flack, M [1] firstly found an area at the junction of the superior cava vein with the right atrium. It was muscular but quite different from the surrounding musculature. They called it as sino-auricular node. Later on, in 1910, Lewis T, Oppenheimer BS, Oppenheimer A. began to call it as the pacemaker of the heart due to their brilliant work on the origin of the heart-beat in the dog [17].

Sinus node cells exhibit spontaneous diastolic depolarization, resulting in a positive "pacemaker potential," which triggers an action potential when a threshold potential is reached. The depolarizing pacemaker potential is the sum of individual ionic currents, each flowing through a unique ion channel type.

Diastolic depolarization during phase 4 of the sinus node action potential is the fundamental pacemaker potential and underlies sinus node automaticity [18]. It brings the membrane potential to a triggering threshold, thereby initiating the next heartbeat. The interaction of several individual membrane currents and intracellular currents, some under autonomic influence, execute this depolarization. In general terms, there are five main ionic currents which make up two key ionic systems, the membrane current or "voltage clock," and the "calcium clock." These two systems act synergistically in a coupled fashion to produce the sinus node action potential. [19]

The voltage clock is composed of time-dependent and voltage-dependent decay of the outward rectifier potassium current  $I_K$ , and voltage-dependent activation of at least three inward currents: the

$I_f$  "funny" current, the  $I_{CaL}$  L-type  $Ca^{2+}$  current, and the  $I_{CaT}$  T-type  $Ca^{2+}$  current.

The calcium clock including  $I_{NaCa}$  current is initiated by a  $Ca^{2+}$  handling mechanism, which is inherently linked with the voltage clock and has also an important contribution to automaticity. It involves ryanodine receptor-mediated calcium release from the sarcoplasmic reticulum resulting in sarcolemmal  $Na^+/Ca^{2+}$  exchange and has an important role in regulating sinus rate. The key ion channels and their temporal currents involved in producing the sinus node pacemaker action potential are depicted in Fig.5

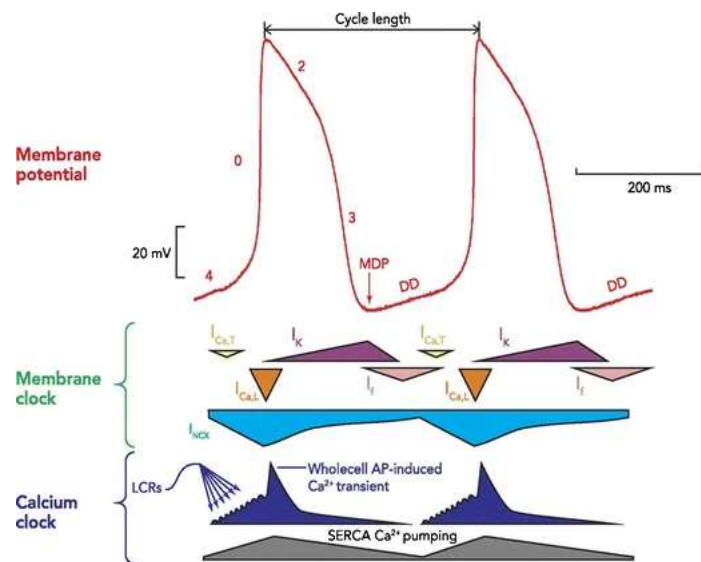


**Fig.5 Ionic currents involved in producing the sinus node pacemaker potential in a sinus node myocyte.** A typical action potential of spontaneously beating rabbit sinus node is shown on the top (red trace). The different phases are labeled, with phase 4 representing diastolic depolarization, the defining feature of pacemaking cells. The timing and magnitude of the components of the "voltage clock" is shown in the middle (green bracket). There is voltage-dependent decay of the outward rectifier  $K^+$  current  $I_K$  and voltage-dependent activation of inward currents:  $I_f$ ,  $I_{CaL}$ , and  $I_{CaT}$ . The timing and magnitude of the components of the

"Ca<sup>2+</sup> clock" are shown at the bottom (dark blue bracket). Ca<sup>2+</sup> entry into the cell via I<sub>CaL</sub> and I<sub>CaT</sub> results in spontaneous local Ca<sup>2+</sup> release (LCRs) from the sarcoplasmic reticulum through RyR2 channels. During phase 4, this rise in total intracellular calcium activates the NaCa exchanger NCX1 which generates the net inward I<sub>NCX</sub> (or I<sub>NaCa</sub>) current. Toward the end of diastole, activation of L-type Ca<sup>2+</sup> channels cause Ca<sup>2+</sup> induced Ca<sup>2+</sup> release from the SR via ryanodine receptors, resulting in the whole cell Ca<sup>2+</sup> transient. Cytoplasmic Ca<sup>2+</sup> is then removed by the SR Ca<sup>2+</sup> pump SERCA, and by the sarcolemmal sodium-calcium exchanger. MDP maximum diastolic potential, DD diastolic depolarization, I<sub>CaT</sub> T-type voltage-dependent Ca<sup>2+</sup> current, I<sub>CaL</sub> L-type voltage-dependent Ca<sup>2+</sup> current, I<sub>NCX</sub> sodium-calcium exchange current, I<sub>K</sub> delayed rectifier potassium current, I<sub>f</sub> funny current, SR sarcoplasmic reticulum, SERCA sarco-endoplasmic reticulum ATPase, LCRs local Ca<sup>2+</sup> releases.[20]

## 1.2.1 Voltage clock theory

Before introducing the voltage clock, we will simply discuss the ion channels involved in voltage clock.

AP's from the SAN were first recorded by microelectrodes by West in 1955 [21]. Further successful development of quantitative membrane excitation theory by Hodgkin and Huxley in 1952 (The Nobel Prize in 1963) and its application to heart in 1960 [22]. At that time, the search for the surface membrane cardiac pacemaker mechanism was initially and mainly studied, both experimentally and theoretically (from approx. 1950 to 1980), not in true pacemaker cells, that is, SANC, but rather in Purkinje fibers [23]. A "pure K<sup>+</sup> selective" I<sub>K2</sub> current redefined further as I<sub>f</sub>, a "funny" non-selective monovalent cation current activated by membrane hyperpolarization [24], was acclaimed as the true "pacemaker current". However, several early [25,26] and later studies [27] which specifically compared the contribution of different ion currents to the pacemaker activity, concluded that there is no single pacemaker current in the SAN. As the result, net membrane current is currently viewed as being spread among numerous components and subcomponents (Table 1) [23].

**Table 1.** Ion currents reported in sinoatrial node cells of various species [23]

| Group of currents   | Current   |
|---|---|
| Voltage-gated monovalent<br>Cation non-selective currents   | Hyperpolarization-activated, "funny" current, I <sub>f</sub><br>Sustained non-selective current I <sub>st</sub>             |
| Voltage-gated Ca <sup>2+</sup> currents<br>(I <sub>Ca</sub> = I <sub>CaL</sub> + I <sub>CaT</sub> ) | I <sub>CaL</sub> , High voltage-activated, L-type Ca current<br>I <sub>CaT</sub> , Low voltage-activated, T-type Ca current |

|   |  |
|---|--|
| Voltage-gated K <sup>+</sup> currents<br>(I <sub>4-AP</sub> = I <sub>to</sub> + I <sub>SUS</sub> and I <sub>K</sub> = I <sub>Kr</sub> + I <sub>Ks</sub> ) | I <sub>to</sub> , 4-AP sensitive transient K <sup>+</sup> current<br>I <sub>SUS</sub> , 4-AP sensitive sustained K <sup>+</sup> current<br>(the sustained part of initially discovered I <sub>to</sub> or I <sub>4-AP</sub> )<br>I <sub>Kr</sub> , the rapidly activating component of I <sub>K</sub> exhibiting strong inward rectification (mouse, rat, guinea pig, rabbit)<br>I <sub>Ks</sub> , the slowly activating component of I <sub>K</sub> exhibiting only weak rectification (guinea pig, pig)<br>I <sub>K1</sub> , inwardly rectifying K <sup>+</sup> current (mouse, rat, and monkey) |
| Voltage-gated Na <sup>+</sup> current   | I <sub>Na</sub> (absent in primary SAN/C)  |
| Background and ion transporter currents   | Background Na <sup>+</sup> current, I <sub>b,Na</sub><br>Background K <sup>+</sup> current, I <sub>KAch</sub><br>Na <sup>+</sup> /K <sup>+</sup> pump current, I <sub>NaK</sub> or I <sub>p</sub><br>Na <sup>+</sup> /Ca <sup>2+</sup> exchanger current, I <sub>NaCa</sub> or I <sub>NCX</sub><br>Cl <sup>-</sup> current, I <sub>Cl</sub><br>Present in one third of SAN/C   |

### 1.2.1.1 HCN channels and funny current

#### HCN channels

The hyperpolarization-activated cyclic nucleotide-gated (HCN) channel belongs to the superfamily of voltage-gated pore loop channels, expressed widely in nervous system and in heart. They are located on plasma membrane. As a voltage-gated channel, HCNs can sense the changes of the electrical membrane potential, be activated by membrane hyperpolarization (around -50/-65 mV) and generate a unique inward current, termed as the funny current, I<sub>f</sub>. The activation could be facilitated by direct interaction with cyclic adenosine monophosphate (cAMP), via binding with the C-terminus of the channel. Other regulators have also been described, including phosphatidylinositol 4,5-bisphosphate (PIP2), kinases and phosphatases.

Four members of this family (HCN 1-4) have been cloned so far. HCN1 channel shows fastest opening kinetics and the lowest sensitivity to cAMP. While HCN4 channel is the slowest activation isoform, and markedly sensitive to cAMP. HCN2 and HCN3 represent intermediate properties in between. All four HCN channel isoforms have been detected in the heart. In the SAN, HCN4 is the predominant isoform and accounts for 80% of I<sub>f</sub>, whereas the expression of HCN1 and HCN2 are also found and responsible for the remaining 20%. While HCN2 is the dominant ventricular isoform.

HCN4 channel is essential for the development of cardiac conduction system. For instance, global or heart-specific deletion of HCN4 channels will induce embryonic lethality. HCN4-deficient embryos had significantly slower heart rate, suppression of I<sub>f</sub> and AV block compared with wild type. On the other hand, temporally controlled deletion of HCN4, will lead to a reduction of I<sub>f</sub> (about 75%)

and a slight response to isoproterenol. HCN4 is also necessary for generating and maintaining a stable cardiac rhythm. Patient carrying HCN4 mutation L573X exhibits severe sinus bradycardia and intermittent episodes of atrial fibrillation, chronotropic incompetence during exercise.

### **I<sub>f</sub> current**

I<sub>f</sub> current, carried by HCN4, is activated upon membrane hyperpolarization at the end of the repolarization phases of an action potential. When I<sub>f</sub> is activated, it shifts the current flow from outward to inward, which reverses the action potential at maximum diastolic potential (MDP). It ends the repolarization process and initiates the first part of depolarization process until the activation of voltage-dependent Ca<sup>2+</sup> channels (TTCC) is achieved (~ -40mV).

The low activation voltage of I<sub>f</sub> may also protect SAN cells from hyperpolarizing, bradycardiac effect of surrounding atrial myocardium. Thus, it was also proposed that I<sub>f</sub> is responsible for a slower DD in the pacemaker range of < -65mV of subsidiary pacemaker cells rather than of SAN cells, due to its low activation voltage and slow activation kinetics. The activation of I<sub>f</sub> could be facilitated by direct interaction with cyclic adenosine monophosphate (cAMP), produced at the sarcolemma from adenosine triphosphate (ATP) by adenylate cyclases (ACs) in basal condition and during sympathetic/parasympathetic stimulation.

The physiological contribution of I<sub>f</sub> current in SAN pacemaker activity is still under debate. For instance, it is absent in some SAN cells from monkey and rat, although it is questioned that this could be artificial effect produced by dialysis of the intracellular medium with the pipette solution.

It is notable that blockade of I<sub>f</sub> only results in a modest prolongation of cycle length, for instance, Cs<sup>+</sup> (2mM) decreases beating rate of rabbit SAN cells by 30% and human SAN cells by 26%. Yet, this idea is challenged by DiFrancesco and his coworkers, who mentioned that Cs<sup>+</sup> does not fully block I<sub>f</sub> and the blockade is voltage dependent. Thus, the partially unblocked I<sub>f</sub> would still be able to drive the automaticity, and the membrane potential changes further unblock I<sub>f</sub>.

Ivabradine is also applied as a HCN4 blocker in later experiments. A low concentration of ivabradine (<3μM) specifically inhibits I<sub>f</sub> without suppressing I<sub>Ca,L</sub> or other membrane ion currents. Ivabradine slows automaticity by ~20% at concentration of 3μM in isolated rabbit SAN cells and reduces the heart rate in vivo in mice and conscious dogs, but still it does not block pacemaking. It is also noticeable that 3μM ivabradine also perturbs Ca<sup>2+</sup> clock with reduced SR Ca<sup>2+</sup> load, slowed intracellular Ca<sup>2+</sup> cycling kinetics, and prolonged the period of spontaneous LCRs occurrence during diastolic depolarization. A higher concentration of ivabradine (10μM) also suppresses I<sub>Ca,L</sub>. Therefore, these data again suggest that I<sub>f</sub> is probably not an absolute prerequisite for SAN automaticity.

### 1.2.1.2 L-type $\text{Ca}^{2+}$ Channel (LTCC)

In 1953, Paul Fatt and Bernard Katz discovered voltage gated calcium channels in crustacean muscle and in the Heart, calcium current was discovered in 1960s [28-30]. The voltage-dependent  $\text{Ca}^{2+}$  channels (VDCCs) are an important way for  $\text{Ca}^{2+}$  to entry in pacemaker cells in which the L- and T-type VDCCs have been consistently recorded in spontaneously active SAN and AVN cells [31,32].

The L-type calcium channel (also known as the dihydropyridine receptors in the EC field, or DHPR) is part of the high-voltage activated family of voltage-dependent calcium channel which is activated at around  $-40$  mV [30]. It has a slow kinetics of current decay, so that was named as L-type calcium current (L for long-lasting,  $I_{\text{CaL}}$ ). To date, there are 4 members identified in the L-type calcium channel family, they are named as  $\text{Ca}_v1.1\sim 1.4$  corresponding to  $\alpha1S$ ,  $\alpha1C$ ,  $\alpha1D$  and  $\alpha1F$  [32]. The  $\text{Ca}_v1.1$  is responsible for excitation-contraction coupling in skeletal muscle [33].  $\text{Ca}_v1.4$  is expressed in the retina, spinal cord, and immune cells [34]. These LTCCs play a role in cell secretion, neurohormones and neurotransmitters regulation, gene expression, mRNA stability, neuronal survival, ischemic-induced axonal injury, synaptic efficacy, and both activation and deactivation of other ion channels [35].

The  $\text{Ca}_v1.2$  is the major  $I_{\text{CaL}}$  in ventricular myocytes [36]. The  $\text{Ca}_v1.2$  knockout mice die during early embryonic development, probably due to the cardiovascular failure [37]. This type of LTCC is essential for excitation-contraction coupling (ECC) because it is the major trigger for  $\text{Ca}^{2+}$  release from the sarcoplasmic reticulum (SR, via the  $\text{Ca}^{2+}$ -induced  $\text{Ca}^{2+}$ -release mechanism, CICR) [38]. Some studies showed that in heart failure, the failing myocytes show a reduced SR  $\text{Ca}^{2+}$  release triggered by the LTCC [39]. While the  $I_{\text{Ca}}$  density is usually maintained in HF [40], the  $I_{\text{Ca}}$  efficacy to trigger  $\text{Ca}^{2+}$  release is usually decreased due to LTCC-RyR2 coupling efficiency decreasing [39], underlying the SR  $\text{Ca}^{2+}$  load and T-tubules density reduction in failing cells[41].

$\text{Ca}_v1.3$  produces currents endowed with a more negative activation threshold and faster kinetics compared to classical  $I_{\text{CaL}}$  [30].  $\text{Ca}_v1.3$  channels have also reduced sensitivity to DHPs [42]. Both the  $\text{Ca}_v1.2$  and  $\text{Ca}_v1.3$  are expressed in SAN [32]. Isolated SAN cells from  $\text{Ca}_v1.3$  gene inactivation mice showed a  $\sim 70\%$  reduction in  $I_{\text{Ca,L}}$  density, demonstrating the major contribution of  $\text{Ca}_v1.3$  to total  $I_{\text{Ca,L}}$  in mouse SAN cells and  $\text{Ca}_v1.2$ -mediated  $I_{\text{Ca,L}}$  accounts for the residual  $I_{\text{Ca,L}}$ [43]. In the past two decades, evidence accumulated showing that LTCC contribute directly to pacemaking [44,43]. The possible role for  $\text{Ca}_v1.2$  in pacemaking is controlling the  $\text{Ca}^{2+}$  dependent upstroke phase of action potential [43]. While the  $\text{Ca}_v1.3$  play a major role in the generation of cardiac pacemaker activity by contributing to diastolic depolarization in SAN pacemaker cells [44]. Recently, this "contributing to

diastolic depolarization" effect was proposed more precisely by *Mangoni M.E* and his colleagues. The Cav1.3-mediated  $I_{Ca,L}$  regulates the local  $[Ca^{2+}]_i$  release (LCR) of SAN pacemaker cells. For the first time, they demonstrated that Cav1.3 channels stimulate and synchronize RyR2-dependent  $[Ca^{2+}]_i$  release during normal SAN pacemaker activity. And since the LTCC also plays a key role in driving inward current in the diastolic depolarization phase, it is tempting to speculate that these channels constitute an unexplored functional bridge between 'Ca<sup>2+</sup> clock' and 'Voltage clock'[45].

### 1.2.1.3 T-type Ca<sup>2+</sup> channel (TTCC)

T-type Ca<sup>2+</sup> channel (TTCC) is also a voltage gated channel on sarcolemmal membrane as LTCC.

In 1975, Hagiwara et al. firstly revealed Ca<sup>2+</sup> currents with different properties with LTCC [46] . And these currents were subsequently characterized during 1980s [47,48]. Comparing with LTCC, these calcium currents activated at much more negative membrane potentials (~-70mV), inactivated rapidly. They were designated as T-type Ca<sup>2+</sup> currents for their 'Transient' openings [48].

There are three known types of T-type calcium channels, each associated with a specific  $\alpha 1$  subunit. They are Cav3.1 with  $\alpha 1G$ ; Cav3.2 with  $\alpha 1H$  and Cav3.3 with  $\alpha 1I$ . Cav3.1 is expressed in cardiac muscle, skeletal muscle and neurons, while Cav3.2 is expressed in cardiac muscle and neurons, and Cav3.3 is only expressed in neurons [49-52].

TTCC generates the  $I_{Ca,T}$  (Fig.5) so that takes part in the control of pace-making activity of the SA Node. However, the mechanism under the contribution of TTCC to SAN automaticity is not fully understood. The low activation voltage may indicate its involvement in initiation of diastolic depolarization and SAN automaticity. Moreover, a research suggested that  $I_{Ca,T}$  triggers Ca<sup>2+</sup> sparks from the SR, which in turn stimulate NCX activation and depolarize the pacemaker membrane potential to threshold in cat SAN cells [53,54].

### 1.2.1.4 Sodium Channel

The upstroke of SAN AP is relatively slower than in ventricle, as it is driven by Ca<sup>2+</sup> channels rather than Na<sup>+</sup> channels in ventricular cardiomyocytes. Most authors tend to attribute it to the lack of Na<sup>+</sup> channels in SAN cells. However, recent evidence showed the existence of Na<sup>+</sup> channels in SAN, although with heterogeneous distribution.

There are two sodium currents have been identified in SAN: the TTX-resistant isoform encoded by Nav1.5, and the TTX-sensitive neuronal isoforms (Nav1.1 in rat, Nav1.1 and Nav1.3 in mouse) [55,56].

Some studies have shown from the atrium to the SAN center, the  $\text{Na}_v1.5$  is substituted by  $\text{Na}_v1.1$  [57,58]. Although some recent study indicates that  $\text{Nav}1.5$ -mediated  $I_{\text{Na}}$  does not participate in the generation of automaticity but influences heart rate by contributing to impulse propagation within the SAN and from the SAN to the atrium [59].

However, the  $\text{Na}_v1.1$  is present throughout the SAN, while blockage of this current results in significant reduction of spontaneous pacemaking. It has also been reported that the TTX-sensitive sodium current accounts for spontaneous activity in the SAN cells from newborn rabbits [60-62].

### 1.2.1.5 Potassium Channels

To date, there are several types of  $\text{K}^+$  channels reported in SAN. They are inward rectifier  $\text{K}^+$  channel ( $I_{\text{K}1}$ ); voltage dependent  $\text{K}^+$  channels (including  $I_{\text{to}}$ ,  $I_{\text{sus}}$ ,  $I_{\text{Kr}}$ ,  $I_{\text{Ks}}$ ); ATP dependent  $\text{K}^+$  channel ( $I_{\text{KATP}}$ ), acetylcholine-activated  $\text{K}^+$  channel ( $I_{\text{KACH}}$ ), calcium-activated  $\text{K}^+$  channel ( $I_{\text{KCa}}$ ) [55,63].

Inward rectifier current ( $I_{\text{K}1}$ ) mainly expresses in ventricle and is responsible to maintain the resting membrane potential [64]. It has been reported that  $I_{\text{K}1}$  is absent in guinea pig, rabbit and pig SAN, but present in mouse, rat and monkey SAN [65]. However, a much lower density of  $I_{\text{K}1}$  was found in mouse and rat SAN than in ventricle [66,67].

The acetylcholine-activated  $\text{K}^+$  current ( $I_{\text{KACH}}$ ) has been described in SA node, atria and AV node [68-70]. Two subunits of the G-protein activated inwardly rectifying  $\text{K}^+$  channels (GIRK1 and GIRK4) which belong to the GIRK/Kir3 subfamily assemble as heterotetramers to form cardiac  $I_{\text{KACH}}$  channels [71].  $I_{\text{KACH}}$  is activated by muscarinic receptors via the G protein  $\beta\gamma$  subunit [72]. It is an outward current, can decrease the activity of the pacemaker and is required for normal recovery of resting heart rate after stress and  $\beta$ -stimulation [73]. A recent study showed that  $I_{\text{KACH}}$  could be the therapeutic target treating the sick sinus syndrome (SSS) induced by the  $\text{Ca}_v1.3$  knock-out (LTCC loss of function) in mouse [71]. Abolition or pharmacological inhibition of  $I_{\text{KACH}}$  strongly ameliorates SAN dysfunction, prevents tachycardia-bradycardia syndrome, and normalizes AV impulse conduction in a mouse model of human SSS [71].

The calcium-activated  $\text{K}^+$  channels are activated by elevation of cytosolic calcium and accounts for the membrane hyperpolarization [74,75]. Based on the channel conductance, calcium-activated  $\text{K}^+$  channels can be divided into three subfamilies:  $\text{B}_\text{K}$ ,  $\text{S}_\text{K}$  and  $\text{I}_\text{K}$ , which refer to "big", "small" and "intermediate" conductance, respectively [74,75]. The  $\text{B}_\text{K}$  channels ( $\text{K}_{\text{Ca}1.1}$ ) are expressed in central nervous system, smooth muscle, and the SAN [76,77]. Recently some studies demonstrated that the  $\text{B}_\text{K}$  channels are involved in the regulation of cardiac automaticity [78,79].  $\text{I}_\text{K}$  channels ( $\text{K}_{\text{Ca}3.1}$ ) also be

called as SK4[80] [81]) are primarily located in non-excitabile cells [81]. It is very similar to BK channels on structure. However, main differences between these two channels is the conductance, and the methods of modulation. It is known that IK channels are modulated by calmodulin, whereas BK channels are not. However, recent study showed that this channel regulates sinoatrial node firing rate and cardiac pacing in-vivo[82]. Small conductance calcium-activated potassium  $S_{K1}$  ( $K_{Ca2.1}$ ),  $S_{K2}$  ( $K_{Ca2.2}$ ) and  $S_{K3}$  ( $K_{Ca2.3}$ ) are identified in human and mouse atria and ventricles [83,84] and play a fundamental role in heart [75]. For example, genetic knock-out of  $S_{K2}$  channels leading to a prolongation of action potential duration especially in repolarization in atrial myocytes, and related to atrial fibrillation [85,86].

The delayed rectifier potassium currents,  $I_{Kr}$  and  $I_{Ks}$  are characterized by an increased positive slope at more positive membrane potential and slow deactivation kinetics [87].  $I_{Kr}$  is a "rapidly activating" delay rectifier  $K^+$  current, activated by depolarized membrane potentials from -50mV [88] while  $I_{Ks}$  is slower activated and faster deactivated than  $I_{Kr}$  [89]. Only  $I_{Kr}$  is recorded in mouse SAN, while both  $I_{Kr}$  and  $I_{Ks}$  exist in the rabbit and guinea pig SAN [90]. Besides, blockage of  $I_{Kr}$  by micromolar E-4031 decreased the pacemaking activity in SAN cells of rabbit and guinea pig [91,92] and in isolated rabbit right atrial preparations [93].

Other potassium channels including the transient outward current ( $I_{to}$ ) which is characterized by rapid activation and inactivation kinetics, and sensitivity to 4-AP; the sustained outward  $K^+$  current ( $I_{sus}$ ) is the sustained part of initially discovered  $I_{to}$  or  $I_{4-AP}$  [94] and the ATP-dependent  $K^+$  current ( $I_{KATP}$ ) is identified in rabbit and rat SAN which is activated by stretch or by low levels of intracellular ATP and decreases the pacemaker activity [95]

### 1.2.1.6 TRP channels

Two kinds of transient receptor potential (TRP) channels were found in SAN. They are TRPC (C is for canonical) and TRPM (M is for melastatin).

TRPC channels are nonselective cation channels that regulate ion homeostasis and intracellular  $Ca^{2+}$  signaling in numerous cell types [96]. The TRPC subfamily contains seven isoforms (TRPC1-7). Based on the sequence alignments and functional comparisons, these isoforms can be divided into three groups: TRPC1/4/5, TRPC3/6/7 and TRPC2 which is not expressed in human [97]. TRPC3/6/7 are activated by diacylglycerol (DAG), produced by PLC-mediated hydrolysis of phosphatidylinositol 4, 5-bisphosphate (PIP2). TRPC1/4/5 are activated by SR  $Ca^{2+}$  depletion or by stretch [98,99]. In SAN, TRPC1-4, 6 and 7 are detected, but not TRPC5 [100,101].

The stromal interaction molecule 1 (STIM1) is located in the SR acting as a  $\text{Ca}^{2+}$  sensor and oligomerized when SR  $\text{Ca}^{2+}$  is depleted, which in turn activates Orai1 and TRPC1/4/5 via direct binding [102,103]. STIM1 also indirectly activate TRPC3/6, but not TRPC7 [104]. Besides, it has also been suggested that Orai and TRPC form complexes that participate in SOCE [104] since it is observed that TRPCs are colocalized with STIM1 and Orai in lipid raft domains [105]. Activation of TRPCs promotes cardiac hypertrophy by  $\text{Ca}^{2+}$  influx and subsequent calcineurin activation [106,107]. TRPCs related SOCE is probably involved in modulation of heart rate rhythm [108].

TRPM4 and TRPM7 were detected in SAN, and both of them participate in SAN automaticity generation. TRPM4 is a  $\text{Ca}^{2+}$ -activated nonselective cation channel driving sodium and potassium inward current [109-111]. Pharmacological inhibition of TRPM4 reduces the automaticity associated with a reduction in diastolic depolarization slope in mouse or rat heart. TRPM7 is a divalent permeant channel [112]. Mice with global or SAN restricted TRPM7 deletion show sinus pauses and AVN block with slower diastolic depolarization and reduced HCN4 mRNA, suggesting that TRPM7 may influence SAN automaticity via regulation of HCN4 expression [112].

### 1.2.1.7 Other channels

The sustained inward current ( $I_{st}$ ) was identified in SAN of many species including mouse, rabbit, rat, guinea pig, and also in rabbit AVN [66,55,67]. It is activated at membrane potential of around -70mV, reaches to the peak around -50mV, and shows little inactivation during depolarization [113]. These characteristics indicate its role for the membrane depolarization and SAN automaticity generation. This current is carried mainly by  $\text{Na}^+$ , but unlike  $I_{Na}$ , this current is TTX-insensitive, can be blocked by DHP antagonists, facilitated by BAY K 8644 and inhibited by divalent cations. These characteristics also suggest that  $I_{st}$  might be mediated by a novel subtype of LTCC [55].

Other electrogenic molecules, for example, the  $\text{Na}^+ - \text{K}^+$  pump also exist on sarcolemmal membrane of SAN cells and plays a role in the maintenance of the ionic homeostasis and the normal SAN automaticity. The  $\text{Na}^+ - \text{K}^+$  pump extrudes three  $\text{Na}^+$  ions and brings in two  $\text{K}^+$  ions, which also influences the pacemaker activity of SAN cells [114].

### 1.2.1.8 Voltage clock

The ensemble of sarcolemmal electrogenic molecules forms a voltage membrane oscillator, known as voltage clock or voltage clock. According to voltage clock, the SAN action potential is predominantly generated by the funny current ( $I_f$ ), which is activated by membrane hyperpolarization.

It depolarizes the membrane, and then activates multiple voltage-gated ion channels. The first one is the TTCC which depolarizes the membrane further. TTCC inactivates rapidly, then LTCC will get involved [115,116]. LTCC will induce upstroke of the action potential while also initiating the CICR (Fig. 5). And during all the way, another current, the sodium-calcium exchanger current (NCX current, discussed later) takes part. Then, the membrane potential is repolarized to the maximum diastolic potential by  $K^+$  channels.

## 1.2.2 $Ca^{2+}$ clock theory

In the late 1980s, studies began to reveal on the role of  $Ca^{2+}$  in pacemaker function under normal physiologic conditions mainly based on improvement of confocal microscopy technology. It permitted detection of a more subtle form of spontaneous  $Ca^{2+}$  releases. Recent studies showed that sarcoplasmic reticulum (SR), as the major  $Ca^{2+}$  store, can spontaneously and rhythmically oscillate  $Ca^{2+}$  uptake and release (as the  $Ca^{2+}$  sparks). Thus, forming an additional oscillator mechanism in pacemaker cells, termed  $Ca^{2+}$ -clock.

### 1.2.2.1 RyR2 in $Ca^{2+}$ clock

In 1989, D S Rubenstein and S L Lipsius firstly found that application of ryanodine slowed the pacemaker activity. Under  $1\mu M$  of ryanodine, the cycle length increased 172% in the cat [117]. In 1996. Some studies illustrated that both ryanodine (RyR blocker) and cyclopiazonic acid (SERCA blocker) reduced pacemaker activity in guinea-pig SAN tissue [118] and proposed the 'possibility' that the calcium released from the SR might play a role in pacemaking through the regulation of sarcolemmal ionic currents, mainly RyR2. In single SAN cells, a concentration of  $3\mu M$  of ryanodine abolished activity in 50% of isolated-rabbit SAN cells [119]. More recent study (in 2012) on cardiac-specific knockout of RyR2 with acute ~50% loss of RyR2 protein was sufficient to cause bradycardia and arrhythmias [120]. And interestingly, the conclusion is also more convincing as the RyR2 'controls' the heart rate. These studies point to the idea that the SR  $Ca^{2+}$  release through RyR2 plays an important role in pacemaking.

### 1.2.2.2 $Ca^{2+}$ sparks and sarcoplasmic reticulum $Ca^{2+}$ load

$Ca^{2+}$  spark was firstly observed in ventricular cells by Cheng et al. in 1993 [12]. And in 2000 Huser et al. firstly suggested the  $Ca^{2+}$  sparks associating with the NCX currents precede the depolarization

of the membrane in both subsidiary pacemaker and normal pacemaker cells in the cat [53]. Interestingly, they found the  $\text{Ca}^{2+}$  sparks (or the local  $\text{Ca}^{2+}$  release, LCR) may be triggered by TTCC, since it happened around -60 mV, and this low voltage-activated  $\text{Ca}^{2+}$  release only happen in the pacemaker cells which may be the essential difference between the pacemaker with other kinds of cardiac myocytes.

Extensive work from the Lakatta laboratory indicates that in the basal state, such LCR's are frequent and powerful enough to initiate the SAN duty cycle and thereby sustain robust normal automaticity [121-125].

The following question could be why pacemaker cells can generate LCR automatically. A simple explanation could be there is higher  $\text{Ca}^{2+}$  concentration in pacemaker cells. However, this idea was proved not correct by direct measurements of  $[\text{Ca}^{2+}]_i$  in SAN cells in rabbit [126,123,127].

The sarcoplasmic reticulum (SR) is a membrane-bound structure found within myocyte (including cardiac myocyte) that is similar to the endoplasmic reticulum in other cells. The main function of the SR is to store calcium ions ( $\text{Ca}^{2+}$ ). Although the concentration of the  $\text{Ca}^{2+}$  is not the decisive factor for pacemaking, however to date, many studies have shown the SR  $\text{Ca}^{2+}$  load will influence the  $\text{Ca}^{2+}$  sparks frequency. On the SR there is one  $\text{Ca}^{2+}$  pump, called the sarco/endoplasmic reticulum  $\text{Ca}^{2+}$ -ATPase (SERCA), whose function is to transport calcium from the cytosol back to the sarcoplasmic reticulum to maintain the  $\text{Ca}^{2+}$  homeostasis in the cell. SERCA function could influence the SR  $\text{Ca}^{2+}$  load and then further influence the pacemaking.

### 1.2.2.3 Sodium-calcium exchanger (NCX)

Sodium-calcium exchanger (NCX) is a high-capacity, voltage-dependent,  $\text{Ca}^{2+}$ -dependent and time-independent electrogenic protein. It is one of the major electrogenic molecules that maintain  $\text{Ca}^{2+}$  homeostasis in SAN cells and can also contribute to diastolic depolarization in SAN cells [128]. NCX activity can be enhanced by the LCR during diastolic depolarization [53]. For each transport, it extrudes one  $\text{Ca}^{2+}$  from the cell and brings in 3  $\text{Na}^+$  inside the cell. Thus, NCX produces an inward current ( $I_{\text{NCX}}$ ) that depolarizes the membrane (Fig.5) [129]. Some studies suggest that there are crosstalk between RyR2-NCX-SERCA and this cross talk ensure the SAN function [130]. Meanwhile acute blockade of the NCX via inhibitor (KB-R7943), or via rapid substitution of  $\text{Na}^+$  by  $\text{Li}^+$  abolishes SAN cells beating [131,132]. These data indicate that  $I_{\text{NCX}}$  is attributed to elevated membrane potential and via RyR2-NCX-SERCA crosstalk contributing to SAN pacemaking.

To date, three kinds of NCX isoforms (NCX1-3) have been found. NCX1 is expressed widely in

mammalian tissues and considered as the cardiac isoform [133-135]. NCX2 is predominantly expressed in smooth muscles and brain, and NCX3 is mainly expressed in skeletal muscle.

The NCX1 genetic knock out results in lack of spontaneously heart beating and embryonic lethality [136]. The study in the incomplete NCX1 knockout mice suggested that NCX1 is critical for fight or flight reaction of SAN, but is not required for resting heart rate [137]. However, this result was challenged by Maltsev et al. [138]. They indicated that the local crosstalk between  $\text{Ca}^{2+}$  cycling proteins and NCX could compensate the low expression of NCX1. The lower NCX1 expression encourages CICR and in turn stabilizes the density of  $I_{\text{NCX}}$ . In their study, the mice selectively lacking NCX1 in cardiac pacemaking and conduction system, showed slower heart rate accompanied by severe arrhythmias. Thus, they suggested that NCX1 is critical for both SAN "fight or flight" reaction and maintenance of basal automaticity.

#### 1.2.2.4 $\text{Ca}^{2+}$ clock

The SR generates  $\text{Ca}^{2+}$  release (local  $\text{Ca}^{2+}$  release, LCR) via RyR2 rhythmically. The LCRs activate NCX, which generates depolarizing current and causes the slow increase in membrane potential toward an excitation threshold for action potential firing, resulting in pacemaking (Fig.5). Then the cytosolic  $\text{Ca}^{2+}$  is extruded by NCX or pumped back into SR by SERCA (sarcoplasmic/endoplasmic reticulum  $\text{Ca}^{2+}$ -ATPase) to complete the  $\text{Ca}^{2+}$  cycle. In this process, the amount of  $\text{Ca}^{2+}$  extruded by NCX should quantitatively match the  $\text{Ca}^{2+}$  entry through the currents on the membrane including  $I_f$ , TTCC and LTCC. The  $\text{Ca}^{2+}$  transferred by SERCA needs to match the  $\text{Ca}^{2+}$  released by RyR2.

### 1.2.3 Coupled clock theory

For more than 50 years, the identities and the relative roles of the control mechanisms within heart pacemaker cells that ignite the AP have been debated. The predominant theory, named "M-clock" for voltage clock advocated that the ensemble of surface membrane ion channels was sufficient to ignite spontaneous AP [139]. In the late 1980s, some studies began to infer the role of  $\text{Ca}^{2+}$  in pacemaking function under normal physiologic conditions [140,117,141]. The related theory was later named as  $\text{Ca}^{2+}$ -clock. To date, a more comprehensive theory is that to ignite an AP, the  $\text{Ca}^{2+}$ -clock communicates with the M-clock via multiple  $\text{Ca}^{2+}$  and voltage-dependent mechanisms. This theory is the so-called "Coupled clock theory": the SR rhythmically discharges local diastolic  $\text{Ca}^{2+}$  releases (LCRs) beneath the cell surface membrane; LCRs activate an inward  $\text{Na}^+/\text{Ca}^{2+}$  exchange (NCX) current which depolarizes the membrane potential and also provoke the other membrane

currents (M clock). In this way the ensemble of the two clocks work together to generate an AP [139].

The two clocks can influence each other. For example, the LCR  $Ca^{2+}$  signal is regulated by the phosphorylation status of M-clock proteins, T-type  $Ca^{2+}$  channels. The  $Ca^{2+}$  ions entering cells through TTCC could enhance the  $I_{NCX}$ , and also, some studies suggest the TTCC also related to the  $Ca^{2+}$  sparks generation [53,54]. And in turn, LCR signals affect  $Ca^{2+}$ -dependent electrogenic processes for example, also through the  $I_{NCX}$ , to reach the threshold for voltage-dependent  $Ca^{2+}$  fluxes (such as L-type  $Ca^{2+}$  channels). Therefore, the LCR  $Ca^{2+}$  signal can be 'sensed' by M-clock proteins. This kind of cross talk can have more profound effect on the modulation mechanism. For example, the crosstalk determines cell  $Ca^{2+}$  which, in turn, activates adenylyl cyclase (AC)-dependent protein kinase A (PKA) and  $Ca^{2+}$ /calmodulin-dependent protein kinase II (CaMKII) [142-145]. The following phosphorylation signaling cascades can act on both SR (phospholamban and RyR2) and M-clock proteins (such as L type  $Ca^{2+}$  channels and  $K^+$  channels) (Fig.6).

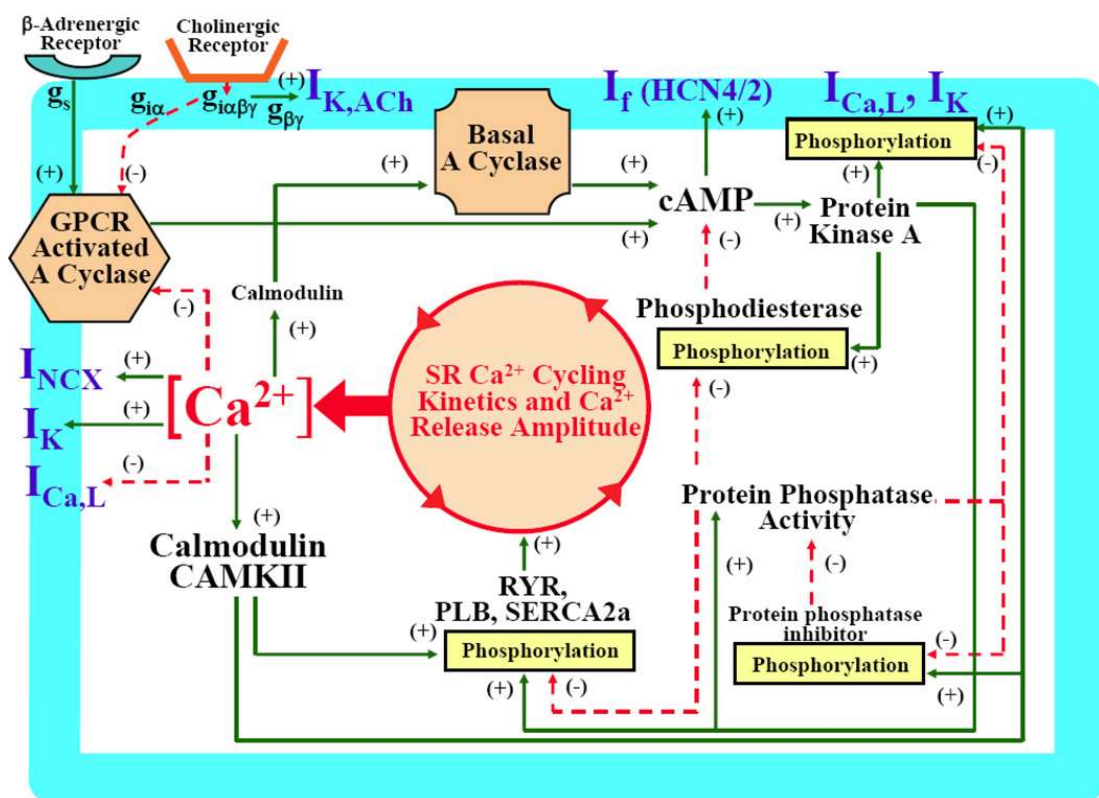


**Fig. 6 Schematic illustration of the interplay of  $Ca^{2+}$ .** Basal  $Ca^{2+}$ -activated AC, cAMP, PDE activity and PKA and CaMKII activity, cast in the context of sarcoplasmic reticulum  $Ca^{2+}$  cycling, L-type  $Ca^{2+}$  channels, and other ion channels. Spontaneous but rhythmic local submembrane  $Ca^{2+}$  releases during the later DD activate  $I_{NCX}$  causing the DD to increase exponentially to achieve the threshold for  $I_{CaL}$  activation and the generation of the next AP [146].

Moreover, some recent studies indicated that the LCR periods vary among individual LCRs occurring within each spontaneous AP cycle [147]. This variability is very similar to the action

potential beating interval variability (AP BIV) among different cycles [148,149]. Based on the coupled-clock theory, the stochasticity of LCR  $\text{Ca}^{2+}$  signal depends on stochastic RyR2 activation [148] and the cell  $\text{Ca}^{2+}$  balance that in turn is determined, in part, by stochastic sarcolemmal ion channel openings and closings. The occurrence of an AP synchronizes global stochastic RyR2 activation, and therefore synchronizes subsequent generation of LCRs by the RyR2s during the diastolic depolarization phase [139].

The BIV will influence the heart rate variability (HRV). HRV is believed to be determined by the autonomic nerve system, but these results show that an intrinsic rhythm exists in the SAN pacemaker due to the coupled clock. However, as shown in the Fig.6, the whole SAN and the coupled clock are under the control of autonomic modulation, the G-protein coupled  $\beta$ -adrenergic and the cholinergic receptor pathway. So maybe the BIV is just the HRV under the ANS modulation on the more microscopic, the intracellular dimension.

## **1.3 Cardiac innervation and Autonomic regulation**

### **1.3.1 Cardiac innervation**

In 1794, Scarpa published the first paper concerning the cardiac innervation. Now it has been more than 200 years. The intracardiac nervous system (ICNS) modulates several domains of cardiac physiology, including the rhythm of the heart, the conduction system and coronary circulation [150,151]. The ICNS is a neural network located in the heart that acts as an integration site for the regulation of the autonomic efferent cardiac output. This intrinsic system is believed to be a short cardio cardiac feedback control loop within the cardiac regulation hierarchy, adapting an appropriate response to vascular impedance and body metabolic demands. This hierarchy includes neural networks located not only in the heart, but also in intrathoracic extracardiac ganglia and in the central nervous system [152].

Based on the different morphology, neurochemistry, and function, ICNS can be divided into several subpopulations, resulting in the forming of the intracardiac ganglia (ICG) by complex array of neurons. Each ICG is composed by 200 to 1000 intracardiac neurons in humans, acting as a major local integration center of the ICNS [153,154]. Groups of ICG are typically associated with interconnecting nerves forming ganglionated plexi (GP). The GP are gathered in the atria, the sinoatrial (SA) and atrioventricular (AV) nodes, the interventricular septum, and both ventricles. Each group of ICG contains efferent, sensory, and local circuit neurons that control multiple cardiac properties. The interconnections between individual ganglia, alongside the interactions between

neurons within ICG, provide an anatomical and functional basis of the complex nervous network of the heart, also called its “little brain” [152].

The ICG neural network comprises a heterogeneous population of neurons made up of autonomic (parasympathetic and sympathetic) efferent neurons, local circuit neurons, and afferent neurons[155] (Fig. 7). Within the ICG, the autonomous efferent neurons can be activated by local or chemical stimuli, subsequently transmitting this information to local circuit neurons and/or autonomous efferent neurons in order to convey an appropriate modulatory response. The autonomic efferent neurons can still receive sympathetic and parasympathetic pre-ganglionic information from the higher neuronal hierarchy[156]. In addition, circulating catecholamines may also exert direct effects on ICNS affecting the cardiac motor output to the heart [152,157].

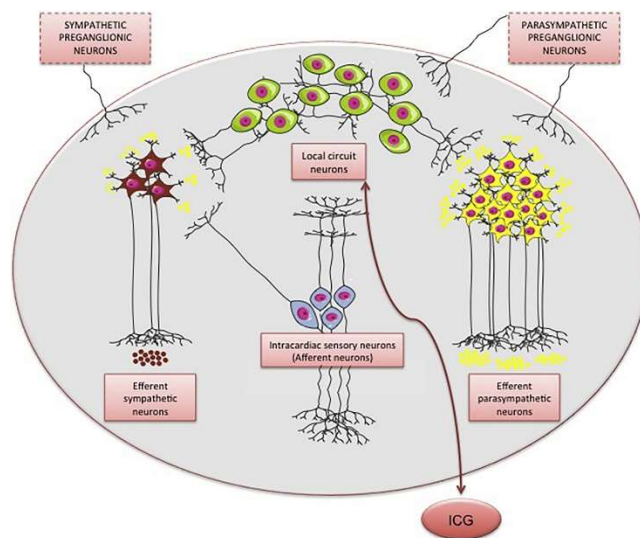


**Fig. 7. Schematic drawing of an ICG, showing the different intracardiac neurons (autonomic efferent neurons, local circuit neurons and afferent neurons) and their projections [152].**

The SAN is strongly influenced by the autonomic nervous system. There are a variety of neurotransmitters [catecholamines such as norepinephrine (NE) and epinephrine, ACh, histamine, serotonin (5-HT)], and neuropeptides [158]. These substances bind to a G-protein-coupled-receptor (for example the  $\alpha$ - and  $\beta$ -adrenergic receptors and M2-receptor) leading to a conformational change in its cytoplasmic domains, separating its subunits ( $G\alpha$  and  $G\beta\gamma$ ), which results in activation [159-161]. For the SAN, the most important  $G\alpha$  isoforms are  $G\alpha_s$ ,  $G\alpha_i/o$ , and  $G\alpha_q/11$  [162]. And while the  $G\alpha$  subunits initiate the primary signaling cascades,  $G\beta\gamma$  subunits may also be involved [161].

### 1.3.2 Sympathetic modulation

Catecholamines (Norepinephrine, NE, and Epinephrine, E) are released from sympathetic neurons of the ANS [158]. NE and E bind to  $\alpha$ - and  $\beta$ -adrenergic receptors (AR). There are four

subtypes of  $\beta$ -AR:  $\beta_1/2/3$ -AR are expressed in the heart while  $\beta_1$ -AR is the most abundant in the heart (75–80%); and  $\beta_4$ -AR have not yet been thoroughly characterized [163].

The adenylyl cyclase (AC) in mammalian consists of nine isoforms [164]. AC5 and AC6 are the major isoforms in the heart activated by  $\beta$ -AR stimulation [165], while AC5 is predominantly expressed in mature adult ventricle and AC6 is mainly in fetal ventricle. Meanwhile, AC1 and AC8 are activated by  $\text{Ca}^{2+}/\text{CaM}$  [166] indicating that basal  $\text{Ca}^{2+}$  cycling regulates  $\text{Ca}^{2+}$ -activated AC-cAMP pathway resulting in rhythmic LCRs and driving the generation of rhythmic action potential [144].

$\beta_1$ -AR are coupled with  $G_s$  proteins, and can initiate the stimulatory AC/cAMP/PKA cascade (Fig. 8), which has been proved to be essential for the increase in HR during adrenergic stimulation in rabbit SAN myocytes [167]. The increasing of the HR by  $\beta_1$ -AR stimulation in the SAN is through  $G_{\text{as}}$ -activation of AC (mainly AC5/6), leading to an increase in cAMP. The cAMP, when binding to the cyclic nucleotide-binding domain (CNBD) of HCN channels, can enhance channel activity [168]. Recently, some studies show that through Epac (exchange protein directly activated by cAMP), there is a link between  $\beta$ -AR/cAMP signaling and CaMKII activation, and is independent of PKA [169]. PKA, which is also known as cAMP-dependent protein kinase, can also be directly activated by cAMP [170].

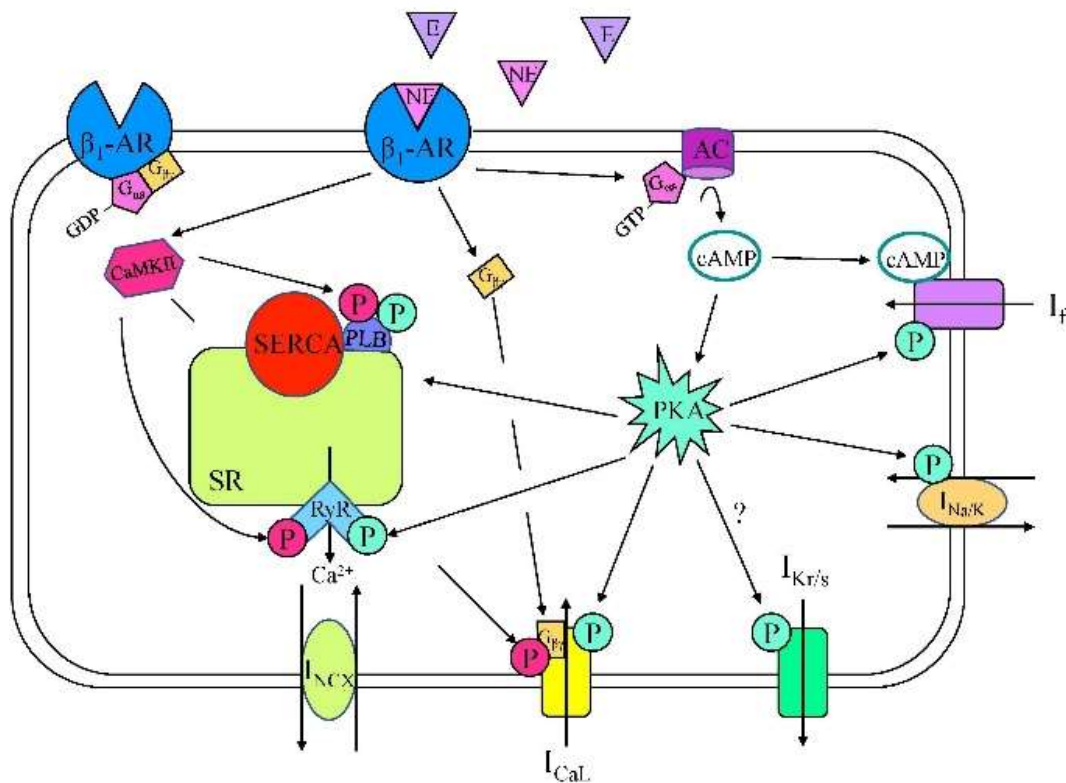


**Fig. 8 The  $\beta_1$ -AR sympathetic modulation.**  $\beta_1$ -adrenergic receptor (AR) signaling cascades in a sinoatrial node myocyte. AC, adenylyl cyclase;  $\text{Ca}^{2+}$ , calcium; CaMKII,  $\text{Ca}^{2+}$ /calmodulin-dependent protein kinase; cAMP, cyclic adenosine monophosphate; E, epinephrine; GDP, guanosine diphosphate; GTP, guanosine triphosphate;  $I_{\text{CaL}}$ , long-lasting (L-type)  $\text{Ca}^{2+}$  current;  $I_f$ , “funny” current;  $I_{\text{Kr/s}}$ , rapid/slow delayed rectifier  $\text{K}^+$  current;  $I_{\text{Na/K}}$ ,  $\text{Na}^+$ - $\text{K}^+$  ATPase current;  $I_{\text{NCX}}$ ,  $\text{Na}^+$ - $\text{Ca}^{2+}$  exchanger current; PLB, phospholamban; RyR2, ryanodine receptor, SERCA, sarco/endoplasmic reticulum  $\text{Ca}^{2+}$ -ATPase; SR, sarcoplasmic reticulum. (adapted from Eilidh A MacDonald et al)

[162])

PKA can also increase  $I_f$  by a phosphorylation-driven shift of its voltage-dependence of activation, as shown in mouse SAN myocytes [171]. PKA also phosphorylates many other coupled-clock components that enhance the automaticity. For example, PKA phosphorylates the  $\alpha 1$  subunit of LTCC, purified from bovine hearts, increases their open probability, so that increase the current [172]. Besides, it has been shown that the  $G_{\alpha s}$ -subunit can directly stimulate LTCC [173]. However, on the other hand, the TTCC is not affected by  $\beta 1$ -AR stimulation in rabbit SAN myocytes [174].

PKA also phosphorylates the phospholamban (PLB) on PLB- Ser<sup>16</sup> site [175]. PLB is a SR protein and can inhibit SERCA function. After phosphorylation, the inhibitory function will be dismissed and causing more rapid  $Ca^{2+}$  re-uptake into the SR, which increases SR  $Ca^{2+}$  content [162]. Thus, PKA could increase the SERCA function by phosphorylating PLB and enhancing the pacemaking activity. As well, PKA phosphorylates RyR2 at RyR2-S2808 site and plays an important role in regulation of SR  $Ca^{2+}$  release during  $\beta$ -adrenergic receptor stimulation or in heart failure [176-178]. Studies in different models including the mouse [179], guinea pig [180], and dog [181] have all demonstrated that blockade of RyR2 with ryanodine diminishes the chronotropic response to  $\beta 1$ -AR stimulation, indicating a critical role for  $Ca^{2+}$  release from the SR.

CaMKII is also a kinase which can phosphorylate PLB, RyR2 and LTCC at different sites than PKA [182,183]. Basal levels of CaMKII-dependent phosphorylation of RyR2, PLB, and LTCC are present in rabbit (but not mouse) SAN myocytes [184-186], suggesting a species-dependence of the role that CaMKII plays in the maintenance of basal HR. In both mouse and rabbit, CaMKII is important under physiological stress, with CaMKII levels increased by sympathetic stimulation [185]. For instance, when CaMKII is inhibited, mice are less responsive to  $\beta 1$ -AR stimulation [179].

Further, the  $\beta 1$ -AR stimulation has some other targets, including the Delayed-rectifier  $K^+$  channels [187],  $Na^+$ - $K^+$  ATPase [188] and NCX [125]. Finally, while sympathetic stimulation in the SAN primarily acts through  $\beta 1$ -AR, automaticity may also be affected by activation of  $\beta 2$ -,  $\beta 3$ -, and  $\alpha 1$ -AR.

### **1.3.3 Parasympathetic modulation**

The parasympathetic modulation of the ANS counterbalances sympathetic effects. Parasympathetic neurons release Acetylcholine (ACh), which binds to muscarinic receptors in the sarcolemma [189]. There are five muscarinic subtypes that have been identified, and within mammalian heart the  $M_2$  receptor plays a prominent role while other muscarinic receptor subtypes localize in the human heart ( $M_1$ ,  $M_3$  and  $M_5$ ) [189].

In the SAN, ACh activation of M<sub>2</sub>R leads to decreased HR as it is coupled to Gi-proteins (Fig. 9) [190]. In rabbit SAN, the decrease of HR is associated with a negative shift of maximum diastolic potential (MDP), a decrease in spontaneous diastolic depolarization (SDD) rate, and many M<sub>2</sub>R-mediated pathways including the activation of I<sub>KACH</sub>, inhibition of I<sub>f</sub>, and inhibition of Ca<sup>2+</sup>-clock components [191]. After ACh binding M<sub>2</sub>R, the G<sub>βγ</sub> subunit will activate G-protein regulated K (GIRK) channels. GIRK<sub>1</sub> and GIRK<sub>4</sub> are both expressed in the heart and form the channel I<sub>KACH</sub> [192].

I<sub>KACH</sub> is the fastest-muscarinic pathway, with the response occurring in less than 2 s in rabbit SAN cells, and no cytosolic components are required for current activation [191]. And causes a negative shift of MDP with the efflux of K<sup>+</sup>, slows the HR [193]. Interestingly, the basal HR of GIRK<sub>4</sub> knockout mice is similar to control, but GIRK<sub>4</sub> is indispensable for the generation of I<sub>KACH</sub>, which accounts for approximately half of the HR reduction provoked by vagal stimulation [194].

The slower effect causing decreased HR upon M<sub>2</sub>R stimulation are based on the second messenger cascades. The activated G<sub>αi</sub> subunit reduces AC activity, leading to the opposite effect than G<sub>αs</sub> including the decrease of cAMP levels, fewer active HCN channels (due to a negative shift in the voltage dependence of activation of I<sub>f</sub>), and a reduction in the SDD slope [191,195]. Activation of M<sub>2</sub>R with carbachol in rabbit SAN has been proved to have a dose-dependent effect via Gi-dependent pathway [196] and dependent upon cAMP/PKA phosphorylation both in single rabbit SAN cells and in a computational rabbit SAN cell model [197,198]. As shown in Fig.9, it is the negative chronotropic and is opposite than the positive one induced by G<sub>αs</sub> subunits (the sympathetic stimulation). Briefly, the phosphorylation level of the PLB, RyR2, LTCC will decrease. And combined with the activity decrease of CaMKII, the phosphorylation level will further decrease on the CaMKII phosphorylation site. Thus, leading to a suppression of the Ca<sup>2+</sup> cycling and Ca<sup>2+</sup> clock.

Further, the activation of M<sub>2</sub>R also coupled with NO synthesis, mediated by endothelial NO synthase (eNOS) [199]. NO generation activates GC receptors, causing an increase in cGMP levels, PDE2 activation, decrease in cAMP, reduced L-type Ca<sup>2+</sup> channel phosphorylation, and ultimately decreased I<sub>CaL</sub> [200].

To conclude, the combination of the direct effects of M<sub>2</sub>R stimulation, including a more negative MDP due to I<sub>KACH</sub> activation and a slower SDD due to reduced I<sub>f</sub> and Ca<sup>2+</sup> cycling, along with indirect NO/cGMP-mediated effects, leads to a decrease in HR in response to ACh release [162].

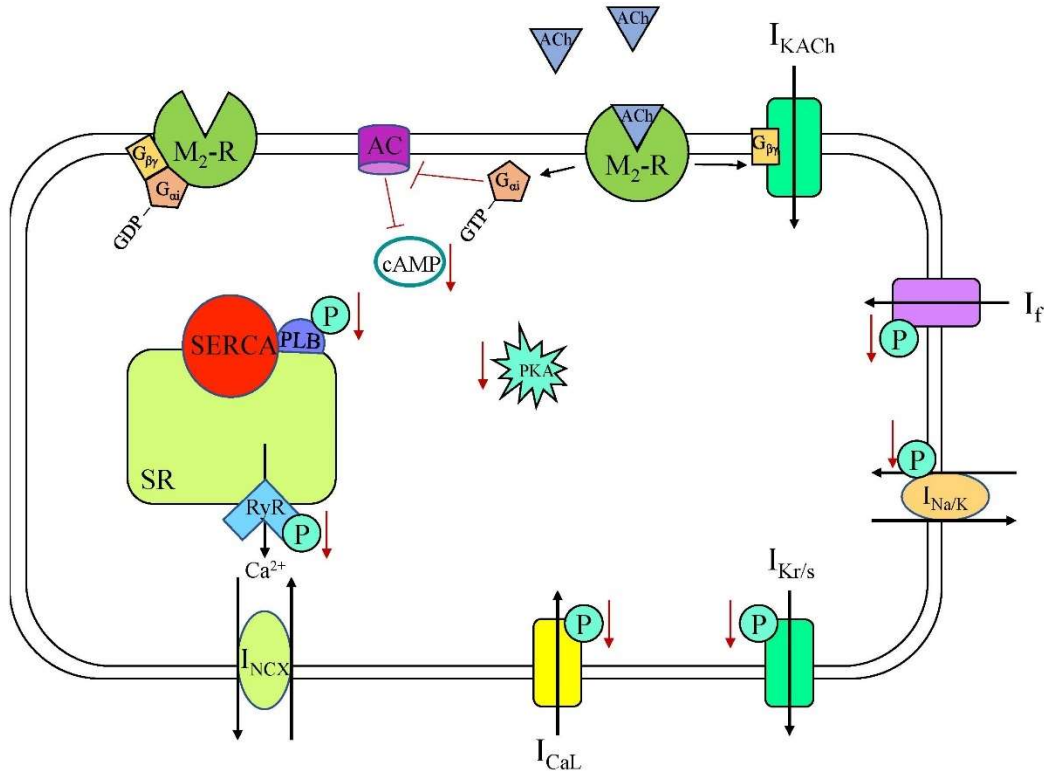


**Fig.9 Muscarinic acetylcholine receptor ( $M_2$ -R) signaling cascade in a sinoatrial node myocyte.** AC, adenylyl cyclase; ACh, acetylcholine; cAMP, cyclic adenosine monophosphate;  $I_{CaL}$ , long-lasting (L-type)  $Ca^{2+}$  current;  $I_f$ , "funny" current;  $I_{KACh}$ , acetylcholine-activated  $K^+$  current;  $I_{Kr/s}$ , rapid/slow delayed rectifier  $K^+$  current;  $I_{Na/K}$ ,  $Na^+$ - $K^+$  ATPase current;  $I_{NCX}$ ,  $Na^+$ - $Ca^{2+}$  exchanger current; P, phosphorylation; PKA, phosphokinase A; PLB, phospholamban; RyR, ryanodine receptor, SERCA, sarco/endoplasmic reticulum  $Ca^{2+}$ -ATPase; SR, sarcoplasmic reticulum.[162]

It is also worth to note that sympathetic and vagal activations induce shifts in the leading pacemaker site, which could be explained by the regional densities of adrenergic and muscarinic receptors within SAN [55]. The ratio between vagal and sympathetic input differs among species and causes different basal heart rates in mammals, which are inversely correlated with the body weight, although the intrinsic properties of pacemaker cells in different species also account [201]. For example, in mice, the sympathetic tone is dominant, while dogs and humans show vagal predominance. The ratio between vagal and sympathetic input could also be influenced. For instance, long-term endurance training increases parasympathetic activity and decreases sympathetic activity in human heart at rest, termed cardiovascular adaptation. This enhanced vagal tone could also explain the bradycardia observed in the trained athlete, although the local factors should also be considered, such as downregulation of HCN4 channel [202].

### 1.3.4 Autonomic modulation on Heart rate variability (HRV)

Alterations of the heart rate is easily measured clinically from ECG recordings and is used to

quantify cardiac autonomic modulations as HRV [203]. HRV reflects the variation of the interbeat intervals of the heart (RR-intervals) and is considered to reflect the organism's capacity to adapt to changes of endogenous and exogenous influences to match the needs of blood supply [204]. Therefore, the interest concerning the analysis of HRV keeps increasing in various fields of research. In 1963, the clinical use of HRV was described for the first time [205]. Then it became a strong and important factor in the death cases after heart failure during the 90s. Nowadays, HRV can be used as a biomarker [206] for assessing the integrity of the interactivity of the cerebral and cardiovascular systems and autonomic regulation of the myocardium, respectively [207,208]. The central autonomic network affects the autonomic neural activity and remotely regulates oscillations of heart rate [209]. Thus, HRV is viewed as "a window into autonomic control of HR" [210] and also considered as a measure of neurocardiac function that reflects interactions between heart, brain and autonomic nervous system dynamics [211].

There are two main methods to analyze the HRV, the time domain and frequency domain methods [212]. The time domain method utilizes either statistical or geometric approaches and rely on a continuous electrocardiographic (ECG) record, which allows the calculation either of heart rate at any point in time or the intervals between successive normal beats. Descriptive time domain variables are the mean normal-to-normal (NN) interval, mean heart rate, and the range for a given time interval. In addition, the Standard Deviation of the NN interval (SDNN) is one of the most widely used time domain indices of HRV and quantifies the total variability that arises from both periodic and random sources. The Root Mean Sum of Squared Successive Differences (RMSSD) and the proportion of NN differences exceeding 50 milliseconds (pNN50), (which in mice considering the high HR they have, pNN5 or pNN6 is commonly used) rank among the most commonly used time domain measures of short-term variation and signify high frequency variations in heart rate of mainly parasympathetic origin [213]. These measures are highly correlated and have been found, among others, to signal risk for coronary lesions unstable angina pectoris [214]. SDNN, SDNN index and RMSSD have proven useful in clinical research [215].

It should also be noted that the total variance of HRV increases with the length of analyzed recording[216]. Thus, on arbitrarily selected ECGs, SDNN is not a well-defined statistical quantity because of its dependence on the length of the recording period. In practice, it is inappropriate to compare SDNN measures obtained from recordings of different durations. On the contrary, durations of the recordings used to determine SDNN values (and likewise other HRV measures) should be standardized. Short-term 5-minute recordings and nominal 24-hour long-term recordings appear to be appropriate options [217].

Frequency domain methods divides the total variance of a continuous series of beats into frequency components. Power spectral density analysis provides the basic information of how power distributes as a function of frequency. In this way, oscillatory components hidden in the variability signal can be detected [213].

Three main spectral components can be distinguished in a spectrum calculated from short-term recordings of 2 to 5 minutes [218,219]: Very Low Frequency (VLF), Low Frequency (LF), and High Frequency (HF) components. The distribution of the power and the central frequency of LF and HF are not fixed but may vary in relation to changes in autonomic modulations of the heart period [220,221]. The physiological explanation of the VLF component is less well defined, and the existence of a specific physiological process attributable to these heart period changes might even be questioned. VLF assessed by means of short-term recordings ( $\leq 5$  minutes) is not a reliable measure and should be avoided when the PSD of short-term ECGs is interpreted [217].

Measurement of VLF, LF, and HF power components is usually made in absolute values of power (milliseconds squared). LF and HF may also be measured in normalized units [220,221] which represent the relative value of each power component in proportion to the total power minus the VLF component. The representation of LF and HF in normalized units emphasizes the controlled and balanced behavior of the two branches of the autonomic nervous system. Moreover, normalization tends to minimize the effect of the changes in total power on the values of LF and HF components. Nevertheless, normalized units should always be quoted with absolute values of the LF and HF power in order to describe the overall distribution of power in spectral components [217].

Spectral analysis also may be used to analyze the sequence of NN intervals of the entire 24-hour period. The result then includes an ULF component, in addition to VLF, LF and HF components. The slope of the 24-hour spectrum can also be assessed on a log-log scale by linear fitting of the spectral values. Selected frequency domain measures are outlined in Table 2 [222].

**Table 2:** Summary of heart rate variability measures in the *PhysioZoo software* [222]

| Measures           | Units              | Definition   |
|--------------------|--------------------|--|
| <b>Time domain</b> |                    |  |
| AVNN               | [ms]               | Average NN interval duration   |
| SDNN               | [ms]               | Standard deviation of NN interval duration   |
| RMSSD              | [ms]               | The square root of the mean of the sum of the squares of differences between adjacent NN intervals |
| pNN5               | [%]                | Percent of NN interval differences greater than 5 milliseconds                                     |
| <b>Frequency</b>   |                    |  |
| Total power        | [ms <sup>2</sup> ] | Total power  |
| VLF                | [ms <sup>2</sup> ] | Power in the very low frequency band   |
| LF                 | [ms <sup>2</sup> ] | Power in the low frequency band  |
| HF                 | [ms <sup>2</sup> ] | Power in the high frequency band   |
| VLF norm           | [%]                | Low frequency power in normalized units $LF / (Total\ power) \times 100$                           |
| LF norm            | [%]                | Low frequency power in normalized units $LF / (Total\ power - VLF) \times 100$                     |
| HF norm            | [%]                | High frequency power in normalized units: $HF / (Total\ power - VLF) \times 100$                   |
| LF/HF              | [n.u]              | Low frequency band to high frequency band power ratio (LF/HF)                                      |

In heart failure, markedly reduced HRV has been demonstrated which coincides with the severity of HF as well as being an independent marker of sympatho-excitation [217]. There is strong evidence that sympathetic efferent neuronal activity is increased in CHF [223]. Such sympathetic activation in HF can also trigger malignant arrhythmias. An average SDNN < 50 ms for more than four weeks in a row is associated with a three-fold increase in mortality risk [224]. Moreover, a reduced VLF power is a powerful and independent risk predictor of mortality in these patients [225]. Some studies [226] suggest that short-term HRV recordings should be routine in chronic heart failure (CHF) patients.

## 1.4 Heart failure and HF related pacemaker dysfunction

### 1.4.1 Overview of Heart failure

Heart failure (HF) is a condition when the heart is unable to pump sufficiently to maintain blood flow to meet the body's need, first at effort and then also at rest. When there are body fluids retention is known as congestive heart failure (CHF) and congestive cardiac failure (CCF). The clinical syndrome of heart failure is the final pathway for myriad diseases that affect the heart. It is a costly and deadly disorder. In 2015 heart failure affected about 40 million people globally [227]. Overall around 2% of adults have heart failure [228] and in those over the age of 65, this increases to 6–10% [229,230]. Above 75 years old rates are greater than 10% [228]. In the USA, the total medical costs for patients

with HF are expected to rise from US\$20.9 billion in 2012 to \$53.1 billion by 2030 [231].

CHF develops when the ventricles cannot pump enough blood volume to the body. Eventually, blood and other fluids can back up inside the lungs, abdomen, liver, lower body and cause the congestion. (Fig. 10)

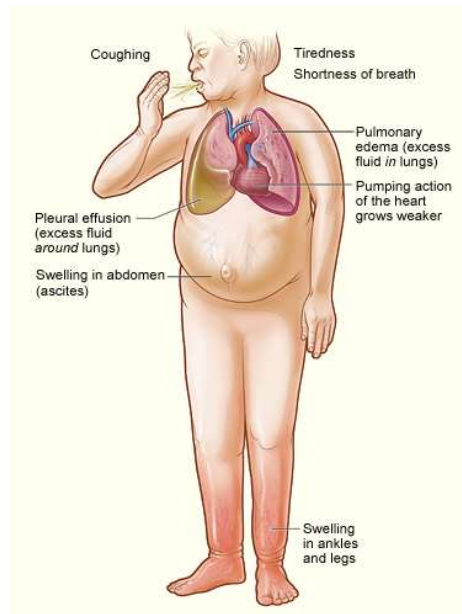


**Fig. 10 Signs and symptoms of severe heart failure (Picture is from Wikipedia [https://en.wikipedia.org/wiki/Heart\\_failure](https://en.wikipedia.org/wiki/Heart_failure))**

Left-sided CHF is the most common type of CHF. There are two kinds of left-sided heart failure: **1. Systolic heart failure** occurs when the left ventricle fails to contract normally. This reduces the level of force available to push blood into circulation. Without this force, the heart cannot pump properly. **2. Diastolic failure**, or diastolic dysfunction, happens when the muscle in the left ventricle becomes stiff. Because it can no longer relax properly, the heart cannot quite fill with blood between beats. Left-sided heart failure affects the transportation of oxygen-rich blood from the lungs to the rest of the body, causing retention of blood, and therefore congestion in the lungs. This congestion affects breathing and thus causes increased fatigue and reduced oxygenation in the blood. Other clinical manifestations of heart failure include enlargement of the heart, due to compensation by the left ventricle.

Right-sided heart failure often results from pulmonary heart diseases like pulmonary hypertension and pulmonary artery stenosis but can also result from left-sided heart failure. Physical observations include peripheral edema, ascites, and liver enlargement, while increased pressure in the jugular vein will be present as a marker of fluid retention. Right-sided heart failure thus leads to congested systemic capillaries generating excess fluid accumulation in the body (edema) as well as potential Nocturia (frequent nighttime urination). In increasingly severe cases, ascites and liver

enlargement may develop with subsequent complications [232].

It is possible to have left-sided and right-sided CHF at the same time. Usually, the disease starts in the left side and then extend to the right when left untreated.

There are a variety of tests used to diagnose heart conditions: Electrocardiogram (EKG or ECG) records heart's electrical activity. Echocardiogram to record the heart's structure and motion and test for the blood flow, muscle damage, or a heart muscle that does not contract normally. MRI takes both still and moving pictures\_of heart with more resolution than echocardiography. Stress tests show how well heart performs under different levels of stress. Blood tests can check for neurohumoral factors. For example, the level of biomarkers such as BNP, a hormone that rises with heart failure. Cardiac catheterization can show blockages of the coronary arteries [233].

### **Different stages of HF**

The American College of Cardiology and the American Heart Association have published a guideline for the evaluation and management of chronic heart failure [234]. It defined four stages of heart failure according to the evolution and progression of the HF: Patients with stage **A** heart failure are at high risk for the development of heart failure but have no apparent structural abnormality of the heart. Patients with stage **B** heart failure have a structural abnormality of the heart but have no symptoms of heart failure or would be considered to have New York Heart Association (NYHA) class I symptoms. Patients with stage C heart failure have known structural heart disease and current or previous symptoms of heart failure. Their symptoms may be classified as NYHA class I, II, III, or IV. Patients with stage **D** heart failure have end-stage symptoms of heart failure that are refractory to standard treatment, all such patients would be considered to have NYHA class IV symptoms. [235].

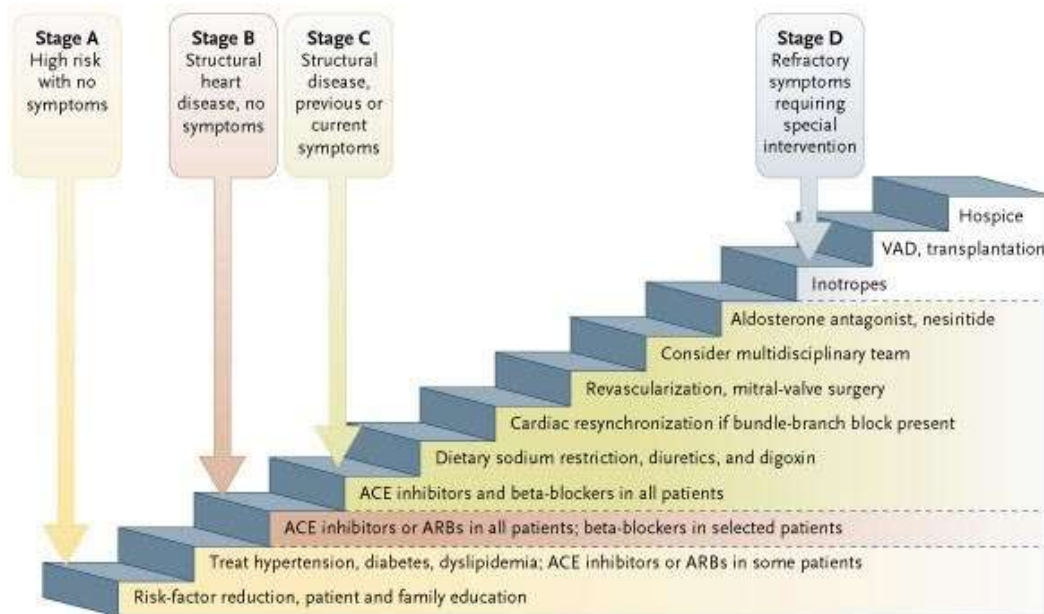


**Figure 11. Stages of Heart Failure and Treatment Options for Systolic Heart Failure.** Patients with stage A heart failure are at high risk for heart failure but do not have structural heart disease or symptoms of heart failure. This group includes patients with hypertension, diabetes, coronary artery disease, previous exposure to cardiotoxic drugs, or a family history of cardiomyopathy. Patients with stage B heart failure have structural heart disease but have no symptoms of heart failure. This group includes patients with left ventricular hypertrophy, previous myocardial infarction, left ventricular systolic dysfunction, or valvular heart disease, all of whom would be considered to have New York Heart Association (NYHA) class I symptoms. Patients with stage C heart failure have known structural heart disease and current or previous symptoms of heart failure. Their symptoms may be classified as NYHA class I, II, III, or IV. Patients with stage D heart failure have refractory symptoms of heart failure at rest despite maximal medical therapy, are hospitalized, and require specialized interventions or hospice care. All such patients would be considered to have NYHA class IV symptoms. ACE denotes angiotensin-converting enzyme, ARB angiotensin-receptor blocker, and VAD ventricular assist device. [236]

The goal of treatment in stage A is to prevent remodeling. The goals of therapy for patients with heart failure (in stage B-D) and a low ejection fraction are to improve survival, slow the progression of disease, alleviate symptoms, and minimize risk factors.

Modifications of lifestyle can be helpful, for example less sodium intake and regularly scheduled exercise. Application of ACE inhibitors, or Beta-blockers can improve in survival, the rate of hospitalization, symptoms, cardiac performance, neurohormonal levels. Such beneficial effects were associated with so-called reverse remodeling, in which the therapy promoted a return to a more normal ventricular size and shape [237-240]. The reverse-remodeling process is a mechanism through which a variety of treatments palliate the heart-failure syndrome.

Cardiac resynchronization therapy is an innovative, pacemaker-based approach to the treatment of patients with heart failure who have a wide QRS complex on 12-lead electrocardiography. The purpose of resynchronization is to provide electromechanical coordination and improved ventricular

synchrony in symptomatic patients who have severe systolic dysfunction and clinically significant intraventricular conduction defects, particularly left bundle-branch block.

A percutaneous, three-lead, biventricular pacemaker system is used; one lead is placed in the right atrium, one is placed in the right ventricle, and a third is passed through the right atrium, through the coronary sinus, and into a cardiac vein on the lateral wall of the left ventricle. This left ventricular lead constitutes the key difference between resynchronization therapy and standard dual-chamber pacing. Beneficial effects include reverse remodeling, resulting in decreased heart size and ventricular volumes, improved ejection fraction, and decreased mitral regurgitation. Clinical improvements in exercise tolerance, quality of life, and the rate of hospitalization have been documented [241-243]. To date, however, resynchronization therapy has not been shown to enhance survival.

Finally, the role of mechanical devices that serve to support patients who are awaiting heart transplantation or are definitive therapy for end-stage (stage D) heart failure continues to evolve, and such devices offer great hope to many patients who are not eligible for cardiac transplantation [244].

It is noticeable that it is estimated that 20 to 50 percent of patients with heart failure have preserved systolic function or a normal left ventricular ejection fraction. Although such hearts contract normally, relaxation (diastole) is abnormal. Mortality among these patients may be as high as that among patients with systolic heart failure, and the rates of hospitalization in the two groups are equal [245]. Unfortunately, unlike heart failure due to systolic dysfunction, diastolic heart failure has been studied in few clinical trials, so there is little evidence to guide the care of patients with this condition. And furthermore, although substantial efforts have been made to treat HF patients, the large epidemiologic surveys have not documented any meaningful change in overall death rates. (Death seems to have been delayed, however, and occurs a longer time after major cardiac events such as a myocardial infarction.) Symptomatic heart failure continues to confer a worse prognosis than most cancers in this country, with one-year mortality of approximately 45 percent. So, more investigation needs to be taken in the field.

### **1.4.2 Ventricular dysfunction and Cardiac Hypertrophy (Hyp)**

The heart must continuously pump blood to meet the body needs. Mammalian cardiomyocytes generally exit the cell cycle soon after birth, so most cardiomyocytes are terminally differentiated in adults and do not proliferate under physiological conditions. However,

cardiac tissue exhibits plasticity to adapt to the changes of systematic demand, the heart is equipped with multiple complex biological systems. The processes of growth (hypertrophy), angiogenesis, and metabolic plasticity are critically involved in maintenance of cardiac homeostasis.

Cardiac hypertrophy is classified as physiological when it is associated with normal cardiac function or as pathological when associated with cardiac dysfunction. Primary triggering events of cardiac hypertrophy are mechanical stress and neurohumoral stimulation, and these contribute for the modulation of various cellular responses including gene expression, protein synthesis, sarcomere assembly, cell metabolism, leading to the development and progression of cardiac hypertrophy [246-248]. Accumulating evidence indicates that pathological and physiological hypertrophy differs in the signaling pathways. Physiological hypertrophy of the heart occurs in response to normal growth of children or during pregnancy, as well as in athletes. Pathological hypertrophy is induced by factors such as prolonged and abnormal hemodynamic stress, due to hypertension, myocardial infarction [249].

### **Physiological Hypertrophy**

Normal physiological enlargement of the heart mainly occurs through hypertrophy of cardiomyocytes in response to growth of the body, exercise or pregnancy, and the enlarged cardiomyocytes receive adequate nourishment due to corresponding expansion of the capillary network. For example, there is a linear relationship between the increase of body weight and cardiac weight. The increase of cardiac weight during growth is largely attributable to enlargement of cardiomyocytes, and there is an almost 3-fold increase of cardiomyocyte diameter in humans during development from infants to adults [249].

Physiological hypertrophy is characterized with normal or enhanced contractile function coupled with normal architecture and organization of cardiac structure [250]. Negative cardiac remodeling including fibrosis does not predominantly develop and is generally not considered to be a risk factor for heart failure and even beneficial in healthy individuals.

Physiological cardiac hypertrophy develops through finite signals from growth hormones and mechanical forces. Within a physiological range, growth hormones such as insulin, insulin-like growth factor1 and thyroid hormone, and mechanical forces induce physiological cardiac hypertrophy via the activation of several signaling pathways such as PI3K (phosphoinositide 3-kinase), Akt, AMP-activated protein kinase and mTOR (mammalian target of rapamycin) pathways [246,251-255].

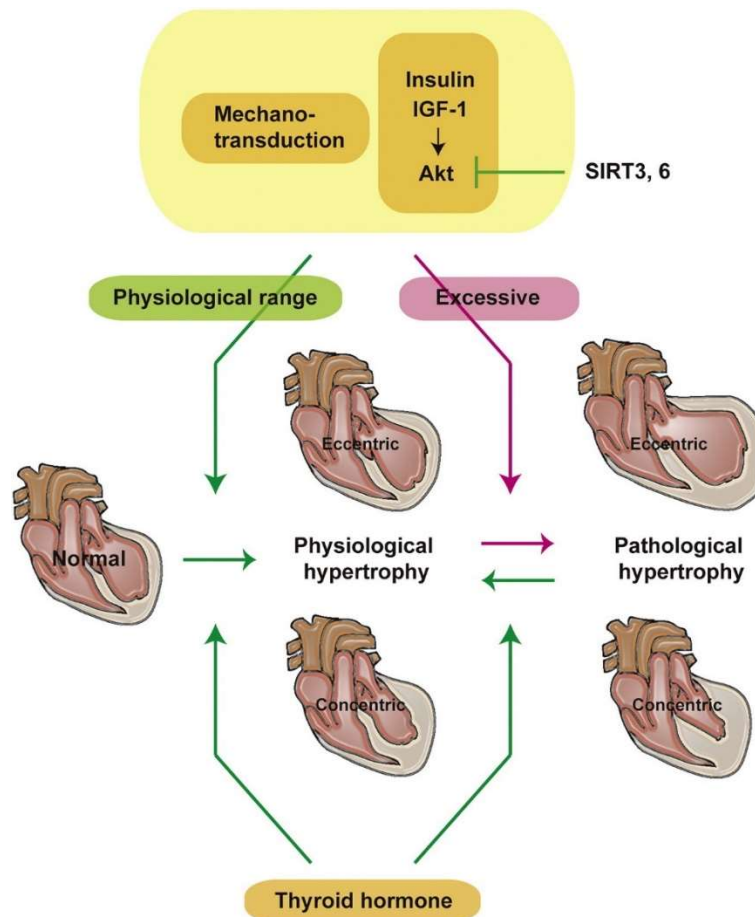


**Fig. 12. Geometry of the heart and signaling pathways contributing mainly for physiological cardiac hypertrophy.** Cardiac hypertrophy can also be classified as eccentric or concentric hypertrophy based on the geometry of the heart. Mechanotransduction and Insulin/IGF-1/Akt signaling induce physiological hypertrophy, but excessive activation of these pathways promotes pathological hypertrophy. Thyroid hormone induces physiological hypertrophy and has the potential to ameliorate pathological hypertrophy. SIRT3 and SIRT6 suppresses Akt, thereby inhibit hypertrophic responses [249].

### Pathological hypertrophy

Enlargement of the heart in response to hypertensive stress, myocardial injury, or excessive neurohumoral activation is associated with cardiac dysfunction and is described as “pathological hypertrophy” [256]. In the pathological setting, cardiomyocyte growth exceeds the capacity of the capillaries to adequately supply nutrients and oxygen, leading to cardiac hypoxia and remodeling [257,258] and is an independent risk factor for cardiac events.

The heart initially undergoes a compensatory response to the additional load or cardiac insult by increasing in size and mass to normalize wall stress and allow normal cardiovascular function at rest [259] (as a consequence of MI, the heart undergoes regional hypertrophy) and this is described as the adaptive phase. However, sustained pressure overload promotes the transition from the adaptive to maladaptive phase, which is characterized by a reduced ejection fraction and left ventricular dilation. Ventricular wall stress is proportional to both the left ventricular (LV) cavity radius and LV pressure, while it is inversely proportional to LV wall thickness [260,261]. However, LV hypertrophy

has been reported as an independent risk factor for adverse cardiovascular events, such as heart failure and arrhythmia.

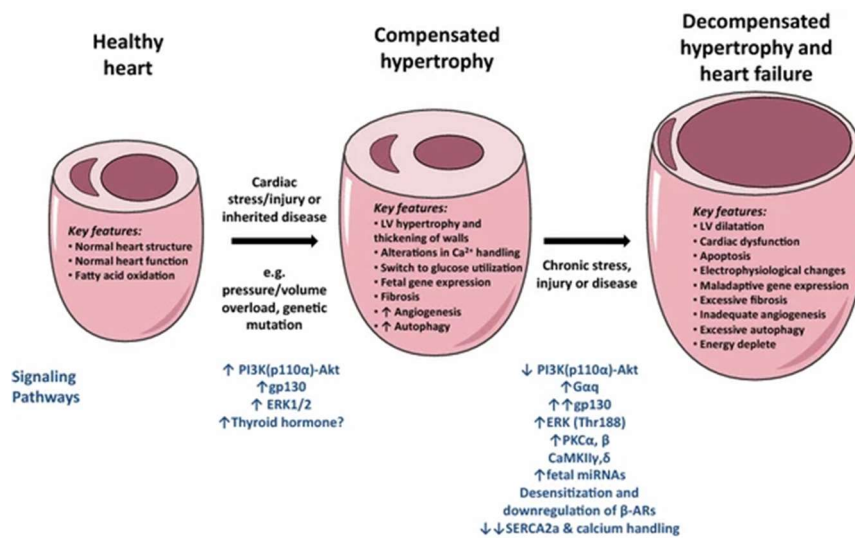


**Fig. 13 Processes and main signaling pathways involved in cardiac remodeling.** A schematic displaying the morphological, molecular, and biochemical changes and altered signaling pathways associated with the transition from compensated hypertrophy to decompensated hypertrophy and heart failure.  $\beta$ -AR  $\beta$ -adrenergic receptors, CaMK calcium-/ calmodulin-dependent protein kinase, ERK extracellular signal-regulated kinase, gp130 glycoprotein 130, LV left ventricular, PI3K phosphoinositide 3-kinase, PKC protein kinase C, SERCA2a sarco/endoplasmic reticulum  $Ca^{2+}$ -ATPase [262]

Pathological cardiac hypertrophy is usually associated with increased rates of myocytes death and fibrotic remodeling, which would promote systolic and diastolic dysfunction, generally predisposing to the development of heart failure. The activation of mechano-transduction and neurohormonal mechanisms are the initial step that drives pathological hypertrophy preceding heart failure. Proteins acting as mechano-transducers are crucial for physiological hypertrophy and dysregulation of this system promotes pathological hypertrophy [246]. Adrenergic nervous system and renin-angiotensin system are extensively studied neurohormonal mechanisms, initially activated upon stress to increase contractility and survival in the early phase and become pathological in the chronic phase. The  $\beta$ -adrenergic receptor blockers, angiotensin-converting enzyme inhibitors and angiotensin receptor blockers are well accepted to reduce left ventricular mass and contribute for favorable clinical outcome in patients with heart failure. Different signaling members are proposed to mediate cardiac hypertrophy, and several molecules are reported to be involved in pathogenic signaling pathways.

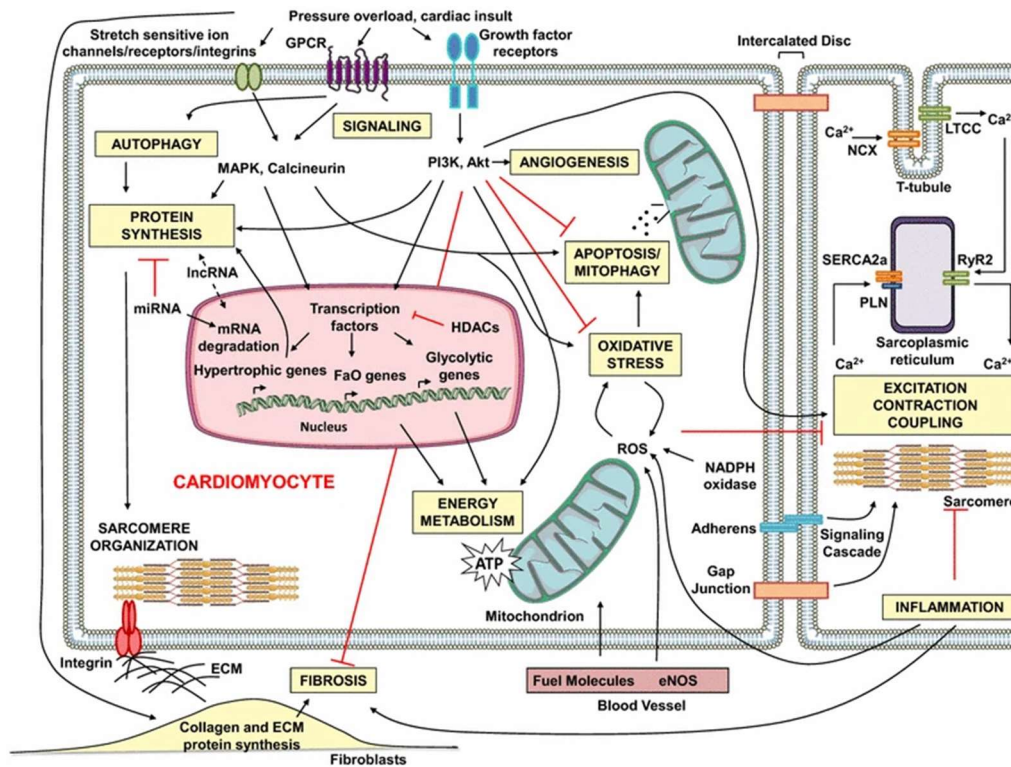


**Fig.14 Overview of cellular processes that contribute to remodeling in cardiac hypertrophy.** ECM extracellular matrix, eNOS endothelial nitric oxide synthase, FaO fatty acid oxidation, GPCR G protein-coupled receptor, HDAC histone deacetylase, IncRNA long noncoding RNA, LTCC L-type  $Ca^{2+}$  channels, miRNA microRNA, NADPH nicotinamide-adenine dinucleotide phosphate, NCX  $Na^+/Ca^{2+}$  exchanger, PLN phospholamban, ROS reactive oxygen species, RyR2 type 2 ryanodine receptors, SERCA2a sarco/endoplasmic reticulum  $Ca^{2+}$ -ATPase [262]

Besides, Cardiac dysfunction is also associated with a complex spectrum of pathophysiological changes, including capillary rarefaction, metabolic derangement, sarcomere disorganization, altered calcium handling, inflammation, cellular senescence, cell death and fibrosis. Due to such complexity, no simple therapeutic approach is adequate for the management of this condition.

It is also noticeable that there is some overlap between the mechanisms of physiological and pathological cardiac hypertrophy, since there is evidence for a central role of Akt signaling or mechano-transduction in physiological hypertrophy, while neurohormonal factors or continuously overloaded biomechanical stress induce multiple signaling pathways, including Akt, in pathological hypertrophy.

### 1.4.3 HF Induced $Ca^{2+}$ dysfunction in Cardiac myocyte

The mechanisms that underlie in HF have been investigated from a broad of perspectives during the few decades [263]. These mechanisms are listed in Table 3 (Adapted from Geoffrey W. Cho et.al [264]). In this study, we mainly focus on  $Ca^{2+}$  dysfunction.

**Table 3** Summary of current hypotheses explaining HF progression

| <b>Hypothesis</b>                          | <b>Description</b>  |
|--|---|
| Impaired EC coupling                       | Alterations in Ca <sup>2+</sup> -handling and cardiomyocyte ultrastructure lead to impaired Ca <sup>2+</sup> cycling that impinge on both systolic and diastolic function. Ca <sup>2+</sup> overload might trigger mitochondrial dysfunction and cell death |
| Mitochondrial dysfunction                  | Reduced mitochondrial function, increased ROS production and diminished ATP production  |
| Increased cell death                       | Necrosis, apoptosis and autophagy contribute to progressive reduction and remodeling in cardiomyocytes in failing hearts  |
| Alterations in sarcomeric proteins         | Switch in myosin, actin, troponin, tropomyosin, and titin isoforms  |
| Adrenergic system                          | Increased adrenergic signaling in HF  |
| Renin-angiotensin aldosterone axis         | Increased activity of this axis leads to maladaptive hypertension and HF development  |
| Epigenetic modification and noncoding RNAs | Modifications in gene expression associated with cardiac remodeling and HF progression  |
| Innate immunity                            | Increased inflammation in HF patients related to left ventricular remodeling and dysfunction  |
| Reactive oxygen species                    | Activation of unfolded protein response, apoptosis and senescence   |
| Nitric oxide (NO)                          | NO insensitivity. Increased ROS leads to peroxynitrite formation and deficient NO-cGMP-PKG activity. Impairment in LV function and endothelial dysfunction  |
| Changes in autophagic flux                 | Increased autophagic activity correlates with hypertrophic and HF progression   |

(Adapted from Geoffrey W. Cho et.al [264])

Ventricular cardiac myocytes have no automaticity, but they are excitable, being their AP triggered by the electrical impulse generated by pacemaker cells. The impulse travels rapidly via membrane invaginations termed the transverse tubular (t-tubule) network. T-tubules dive into the cell, terminating close to the sarcoplasmic reticulum (SR) to form structures, termed dyads, which are situated at the Z-line regions of the sarcomere [265]. Membrane depolarization within the t-tubule triggers Ca<sup>2+</sup> entry (CICR) from the SR through the type 2 ryanodine receptor (RyR2) mainly through L-type Ca<sup>2+</sup> channels (LTCC). Ca<sup>2+</sup> binding onto the sarcomere relieves actin from troponin C-dependent inhibition, activating cross-bridge cycling and myocyte contraction. Subsequently, Ca<sup>2+</sup> is pumped back into the SR by the SR Ca<sup>2+</sup> ATPase 2a (SERCA2a) [266]. It is generally accepted that alterations in Ca<sup>2+</sup>-handling proteins, coupled with remodeling of the t-tubule architecture, contribute to HF pathogenesis, promoting impaired contraction and reductions in cardiac output [39,264] (Fig. 15).

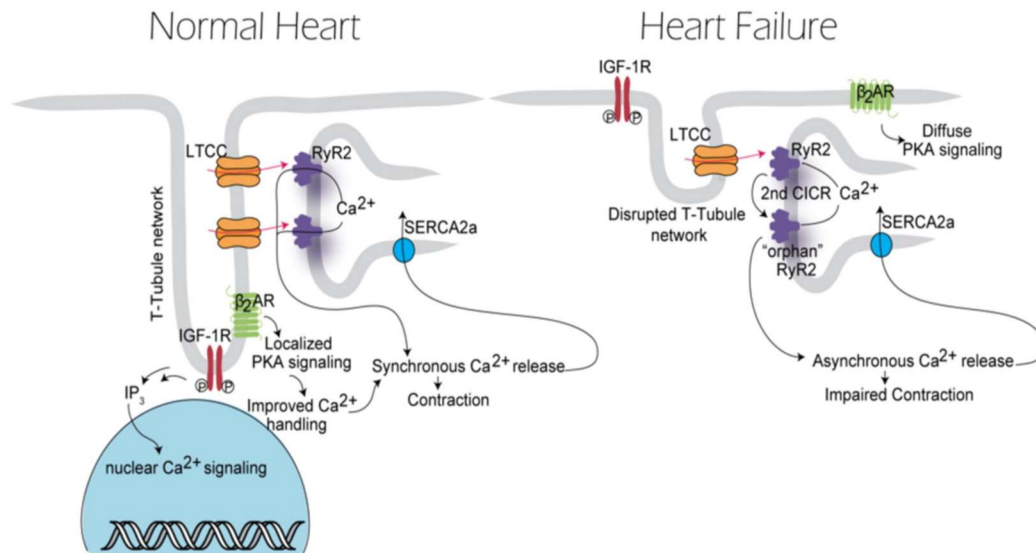


**Fig. 15. Disruption of t-tubule network in HF.** In failing cardiomyocytes, there is progressive deterioration of t-tubule architecture, impeding the normal propagation of action potentials into the cardiomyocyte core. It has been proposed that “orphan” RyR2 are located outside the junctional cleft, triggering a second wave of CICR that perturbs synchronicity during systole and diastole. As these orphan RyR2 are located distant from the dyads, they are activated late, contributing to impaired contractile performance. Distorted t-tubule architecture may also impair signaling elicited by catecholamines and growth factors. [264]

The intracellular calcium  $[Ca^{2+}]_i$  homeostasis or  $[Ca^{2+}]_i$  cycling is an essential mediator of cardiac contractile function, and remodeling of  $[Ca^{2+}]_i$  cycling is one important factor contributing to the mechanical and electrical ventricular dysfunction characteristic of HF [267]. Over the years, numerous studies, using human and experimental models of heart failure, have highlighted the alteration in intracellular  $Ca^{2+}$  handling in HF. These include down regulation of the SERCA2 $\alpha$  pump, or an increase in the PLB/SERCA ratio [268-270]. Seminal functional analyses in human ventricles manifested a decrease in the amplitude of the  $[Ca^{2+}]_i$  transient, and maintained  $I_{Ca}$  density. Thus, a defect in the EC coupling efficiency is evidenced as contributor to contractile dysfunction in HF [39].

A hallmark of failing cardiomyocytes is altered EC-coupling, including reduced  $Ca^{2+}$  transients ( $Ca^{2+}$  released from SR stores during excitation), as well as delayed onset and decay of those transients. Together, these changes culminate in reduced force of contraction, delayed onset of contraction, and slowed relaxation [271]. Alterations in  $Ca^{2+}$  handling have been ascribed to impaired function of the RyR2, SERCA2a,  $Na^+-Ca^{2+}$  exchanger (NCX), and transient receptor potential cation (TRPC) channels [264].

## RyR2

Number of factors can modulate RyR2 function [272] including cytosolic and SR  $Ca^{2+}$  load, ATP,  $Mg^{2+}$  concentrations, oxidation, as well as the PKA-dependent and CaMKII-dependent hyperphosphorylation of RyR2 (at S2808 and S2814 respectively) [176,273]. These events increase SR  $Ca^{2+}$  leak, which consequently depletes SR  $Ca^{2+}$  stores partially and diminishes  $Ca^{2+}$  transients after membrane

depolarization and thus, contribute to reduced contractility in failing hearts. More recently, this  $\text{Ca}^{2+}$  leak has been associated with mitochondrial  $\text{Ca}^{2+}$  overload and dysfunction [274]. The RyR2-mediated  $\text{Ca}^{2+}$  leak induces: 1)  $\text{Ca}^{2+}$  redistribution from SR to cytosol, reducing the electrochemical gradient and diminishing systolic contractile performance; 2) an increase in basal, cytosolic  $\text{Ca}^{2+}$  concentration impairing diastolic function; 3) spontaneous  $\text{Ca}^{2+}$  release events ("sparks"); 4) membrane depolarization through the forward mode of NCX ( $\text{Ca}^{2+}$  out/ $\text{Na}^+$  in), triggering delayed afterdepolarizations; and 5) excessive energy consumption to restore  $\text{Ca}^{2+}$  gradients[264].

### **SERCA**

SERCA2a drives the process of ATP-dependent re-uptake of  $\text{Ca}^{2+}$  into the SR after mechanical contraction. In mouse and rat, SERCA2a activity accounts for  $\approx 93\%$  of  $\text{Ca}^{2+}$  removal from the cytosol [266] while in human and rabbit, it represents closer to 74% of  $\text{Ca}^{2+}$  removal [266]. SERCA can be inhibited by several small proteins, including phospholamban (PLB) [275] and sarcolipin [276]. PLB is phosphorylated by PKA or CaMKII at different site releasing SERCA from PLB-mediated inhibition [277] while the dephosphorylation is mediated by protein phosphatase 1 [278]. Reduced SERCA activity plus increased SR  $\text{Ca}^{2+}$  leak synergize to promote systolic and diastolic dysfunction. Supporting this hypothesis, cardiomyocyte-restricted silencing of SERCA2a triggers HF [279]. Conversely, SERCA2a over-expression improves myocardial contractility in both human and animal models of HF [280].

### **NCX**

NCX is a bidirectional, electrogenic cation cotransporter that exchanges a single  $\text{Ca}^{2+}$  ion for three  $\text{Na}^+$  ions. Some study showed that NCX activity is up-regulated in failing heart [281] leading to competition between NCX with SERCA for  $\text{Ca}^{2+}$ . More  $\text{Ca}^{2+}$  therefore extruded, resulting in a lower SR  $\text{Ca}^{2+}$  load and a subsequent decrease in SR  $\text{Ca}^{2+}$  release during ECC [282]. However, on the other hand, due to reduced  $\text{Na}^+/\text{K}^+$  ATPase, and possibly increased TRPC channel function in failing hearts [283,284], cytosolic  $\text{Na}^+$  concentrations are elevated.  $\text{Na}^+$  accumulation diminishes the transmembrane  $\text{Na}^+$  gradient, suppressing NCX-dependent  $\text{Ca}^{2+}$  extrusion. This can culminate in arrhythmia or even cell death due to  $\text{Ca}^{2+}$  overload.

### **TRPC channels**

TRPC channels participate in store operated  $\text{Ca}^{2+}$  entry (SOCE), serving to refill depleted SR  $\text{Ca}^{2+}$  stores. TRPC channel expression increases during pathological hypertrophy and HF [284], possibly as an adaptive mechanism to compensate for SR  $\text{Ca}^{2+}$  leak and consequent  $\text{Ca}^{2+}$  depletion. TRPC channels conduct  $\text{Ca}^{2+}$  and  $\text{Na}^+$  [285], and their activation can contribute to  $\text{Ca}^{2+}$  and  $\text{Na}^+$  overload

in failing cardiomyocytes. Inhibition of TRPC subfamilies represses both pressure overload- and angiotensin II-induced cardiac hypertrophy [286]. Furthermore, TRPC channels are implicated in ventricular pathological remodeling, increases in RyR2 leak [287] and increases ischemia/reperfusion (I/R)-induced apoptosis [288], referring to a deleterious role of TRPC channels in HF.

### **T-tubule network**

Recently, it has been proposed that t-tubule network remodeling is a progressive process that commences early and contributes to HF pathogenesis [289]. Intricately organized dyads along the myocyte promote coordinated  $\text{Ca}^{2+}$  release responses and synchronous activation of the sarcomeres. The t-tubule remodeling generates "orphan RyR2s", which refers to the SR  $\text{Ca}^{2+}$ -release channels localized relatively distant from the dyad. Activation of these isolated RyR2s can generate a second wave of  $\text{Ca}^{2+}$  release triggered by delayed arrival of  $\text{Ca}^{2+}$  diffusing from normal RyR2 channels localized appropriately at the dyad. This, in turn, elicits asynchronicity in EC coupling, perturbing both systolic and diastolic function and promoting arrhythmia [290].

Disruption of the t-tubule architecture may also disrupt cell signaling. In HF,  $\beta_2$ -adrenergic receptors are redistributed from deep within the t-tubules to the cell surface, disrupting localized  $\beta_2$ -adrenergic signaling [291]. In addition, the remodeling of T-tubule network can also influence the IGF-1 (insulin-like growth factor-1) signaling in cardiomyocytes [292] which requires the precise organization of the t-tubule network in cardiac myocyte. IGF-1 is notable for its anti-apoptotic and pro-survival effects in cardiomyocytes and has been proposed as a therapeutic approach for HF [293,294].

### **Mitochondrial $\text{Ca}^{2+}$**

In addition to their vital role as fuel burning sources of energy, mitochondria function as sinks for intracellular  $\text{Ca}^{2+}$ . Indeed, mitochondrial  $\text{Ca}^{2+}$  is required for normal functioning of metabolic enzymes, serving as a cofactor for several of them. In HF, however, elevated cytosolic  $\text{Ca}^{2+}$  facilitates accumulation of  $\text{Ca}^{2+}$  within mitochondria, which promotes ROS generation, impairs mitochondrial function, and can activate cell death pathways. ROS generation induced by mitochondrial  $\text{Ca}^{2+}$  overload may increase RyR2 oxidation, thereby exacerbating cytosolic  $\text{Ca}^{2+}$  accumulation and mitochondrial  $\text{Ca}^{2+}$  overload [274,264].

### **HFrEF vs. HFpEF**

It is noticeable that most of the information above is due to the research on the HFrEF (Heart

failure with a reduced ejection fraction). In contrast with the considerable literature on HFrEF, the alterations in  $\text{Ca}^{2+}$  handling associated with HFpEF (preserved ejection fraction) are poorly defined. A major limitation to investigation of cardiomyocyte  $\text{Ca}^{2+}$  homeostasis in HFpEF is limited availability of cardiac tissue from HFpEF patients, as this HF population rarely undergoes cardiac transplantation. Complicating the lack of studies from human tissue is the paucity of animal models that recapitulate the complex clinical progression of HFpEF [295].

Therapies which target cardiomyocyte  $\text{Ca}^{2+}$  handling mechanisms are effective in HFrEF, where cardiac dysfunction is intrinsic to the cardiomyocyte. Cardiac dysfunction in HFpEF is complex and in many cases extrinsic to the cardiomyocyte. Pharmacological treatment of HFpEF is largely ineffective. However, unfortunately, half of all heart failure patients are diagnosed with HFpEF [295]. There are still many more mysteries waiting to be unveiled.

#### **1.4.4 HF induced SAN dysfunction**

Patients with HF exhibit significant remodeling of the SAN function characterized by a decrease in the intrinsic heart rate [296-299], prolonged corrected SAN recovery time and sinoatrial conduction time, and a caudal shift of the leading pacemaker site [300,301].

Fibrosis is common in HF SAN. In a rabbit model, the study revealed that the SAN in HF exhibited an automaticity exit block, SAN-PV conduction block, and severe fibrosis[302]. Therefore, the abnormal conduction may be attributed to increased fibrosis in SAN [303].

The increase in left ventricular end diastolic pressure in HF causes an increase in the intra-atrial pressure and atrial stretch, which not only results in atrial electrical remodeling but also induces atrial dilation [304,305]. Stretch of the SAN increases heart rate, however, dilation of RA is unusual in HF [306,307]. It is unclear why HF on the left side of the heart causes dysfunction in the SAN located on the right side of the heart [303]. More blood retention in the right atrium, may cause chronic stretching, as well as the neurohormonal activation may play a critical role [300,308].

##### **1.4.4.1 Voltage clock alteration and Ivabradine treatment**

Previously, it has been shown that the decreased intrinsic heart rate and prolonged corrected SAN recovery time were at least due to remodeling of components of the voltage clock. HF impairs the voltage clock by downregulation of  $I_f$  in the SAN of rabbit [309] and downregulation of the corresponding hyperpolarization-activated (HCN) channel subunits, HCN4 and HCN2, both on mRNA and protein level in the SAN of dogs [310]. In addition, TTX-sensitive neuronal  $\text{Na}^+$  channels,  $\text{Na}_v1.1$

and  $\text{Na}_v1.6$ , are downregulated in SAN tissue of HF rats [311]. Although the center of the node contains few or no  $\text{Na}^+$  channels. The effects of tetrodotoxin (an  $\text{I}_{\text{Na}}$  inhibitor) on reducing the SAN pacemaker rate and action potential amplitude are more prominent in the SAN in HF, thus suggesting that impaired  $\text{I}_{\text{Na}}$  also causes SAN dysfunction in HF [312,308]. Finally, HF upregulates  $\text{I}_{\text{Ks}}$  in HF SAN cells of rabbit [309], but since  $\text{I}_{\text{Ks}}$  plays a limited role in pacemaker activity without adrenergic stimulation [187], this change in voltage clock is hardly involved in the increase in intrinsic cycle length during HF [309].

Although the intrinsic HR is decreased in the research, on the clinical situation, the patients show an elevated resting heart rate. The elevated resting heart rate is an independent predictor of cardiovascular morbidity and mortality in both the general population and in patients with HF, irrespective of underlying ejection fraction [313-316]. Patients with HF in particular are prone to higher resting heart rates due to compensatory neurohumoral activation resulting in increased sympathetic activity [317]. This drives an increase in oxygen demand, reduced ventricular efficiency and consequently worsens HF [318]. Higher discharge heart rates in patients with HF are associated with increased mortality and hospital readmission [319]. A meta-analysis of patients with HF indicated that for every 5 beats per minute (bpm) reduction in heart rate achieved, an 18% reduction in all-cause mortality is observed [320,321].

Ivabradine (Procoralan, Servier Laboratories Ltd, France and Corlanor, Amgen Inc., USA) is a selective  $\text{I}_f$  ('funny') channel inhibiting drug, which acts on the sinoatrial node, resulting in a reduction in heart rate. Ivabradine enters the  $\text{I}_f$  channel and binds to its intracellular side, subsequently disrupting the mixed sodium and potassium ion current flow through the channel. This prolongs the slow spontaneous phase of diastolic depolarization, and thereby reduces HR. Experimental studies of ivabradine have demonstrated independent reduction of heart rate without any effects on blood pressure, myocardial contractility and relaxation, ventricular repolarization or myocardial conduction [322-324]. The activity of ivabradine is therefore dependent on the opening (during repolarization) and closing (in depolarization) of the  $\text{I}_f$  channels, with greater potency seen with faster heart rates. At higher concentrations, the activity of ivabradine saturates, preventing adverse reductions in the HR [325,326].

Moreover, in animal models and human hearts with severe ischemic cardiomyopathy, HCN channels reappear in greater numbers and increasing amplitude in ventricular myocytes. In mouse models at least thin increase in HCN channels expression has been associated with enhanced likelihood of automaticity and the development of spontaneous action potentials which may give rise to arrhythmia, independent of sympathetic mediated tachycardia [327-330]. Ivabradine block of

these channels may lead to a reduction in rates of sudden cardiac death, and it remains a potential area of focus for future research [331-334].

Finally, we could possibly raise a paradox of ivabradine. Since HF impairs the voltage clock by downregulation of  $I_f$  in the SAN of rabbit [309], Ivabradine further block the  $I_f$  current without influence other possible mechanisms [322-324], it should be so toxic to patients other than an effective treatment.

#### 1.4.4.2 $Ca^{2+}$ handling alteration

SAN dysfunction in HF is also associated with suppression of rhythmic spontaneous sarcoplasmic reticulum  $Ca^{2+}$  release ( $Ca^{2+}$  clock), resulting in unresponsiveness and superior shift of the SAN to isoproterenol and caffeine [335].

Yanni *et al* [303] reported that the expression of RyR2 and RyR3, inositol 1,4,5-trisphosphate (IP3) receptors, calsequestrin 2 (SR  $Ca^{2+}$ -binding protein) and plasma membrane  $Ca^{2+}$ -ATPase 1 are significantly increased in the SAN but not in atrial tissue during HF. While other group showed HF SANs had a lower protein expression of RyR2, which may cause RyR2 dysfunction [312].

Some groups have shown that oxidized calmodulin kinase II (ox-CaMKII) can be a biomarker for SAN dysfunction in humans and dogs, which triggered SAN cell apoptosis [336]. A CaMKII inhibitor was shown to improve cardiac function and suppress arrhythmias [337]. Stabilization of the ryanodine receptor (RyR) decreases intracellular  $Ca^{2+}$  leakage and improves diastolic and systolic function, and is a potential treatment strategy for HF [338-340]. While actually a similar CaMKII expression level has been found by other group [312]

Finally, different groups found that SERCA function decreased in HF SAN [301], this may due to the less phosphorylation level of PLB which in turn increased the inhibition of SERCA function [312]. And interestingly, this group tested the PLB-T17 phosphorylation, which is believed as a CaMKII site and found there is less phosphorylation on PLB-T17 site. This result again contradicts for those results that showed activated CaMKII can be a biomarker [337,336].

In all, up to date, little is known about the SAN  $Ca^{2+}$  handling under HF and there is no consensus between the existing results. This may be due to the different used models (mouse, rabbit or canine) and the different way to induce the HF (rapid pacing or TAC).

## 1.5 Objectives

SAN is the primary pacemaker of the mammalian heart and is predominantly responsible for cardiac function. Many pathology conditions such as heart failure, can influence the SAN function.

Ca<sup>2+</sup> handling plays a key role in regulating the function of SAN. The aim of this study was to analyze how the intrinsic pacemaker cell function is altered under heart failure and the relationship between the function alteration and the changing of Ca<sup>2+</sup> handling in SAN. Further, the research will also explore the possible mechanism underlying the changing of the Ca<sup>2+</sup> handling. And the connection between these mechanisms and the existing research on the membrane-clock, to provide more comprehensive understanding on heart failure induced pacemaker dysfunction as well as to provide promising clinical perspectives.

# Chapter 2 Material and Methods

## 2.1 Transverse Aortic Constriction

(TAC, Performed by Susana Gomez)

The study of underlying pathophysiological mechanisms and potential therapeutic approaches for heart failure require appropriate animal models. These animal models should reliably display phenotypic features and allow for the measurement of endpoints relevant to clinical heart failure [341,342].

The murine transverse aortic constriction (TAC) model developed by Rockman et al. [343] is widely used to characterize the impact of genetic or pharmacologic interventions on cardiac remodeling in mice. In this study, 10 weeks old of male C57BL/6J mice were used.

Animal study was approved by the French Ministry (Ministere de l'Education Nationale, de l'Enseignement superieur et de la Recherche) no. B9201901.

Briefly, animals need to be anesthetized and ventilated. The aorta arch is then exposed via a left thoracotomy with a longitudinal cut made in the proximal portion of the sternum. A constriction of the transverse aortic arch is created using a 6/7-0 ligature between the brachiocephalic and left carotid arteries (Fig. 16), then a small piece of a blunt needle is located parallel to the transverse aorta in order to possibly obtain a constriction of a standard diameter. After two knots, the needle is then removed. Aortic banding does not allow a sufficient enlargement of the aorta lumen and a restriction of the cardiac output is produced, thus increasing afterload. TAC mimics human aortic stenosis.

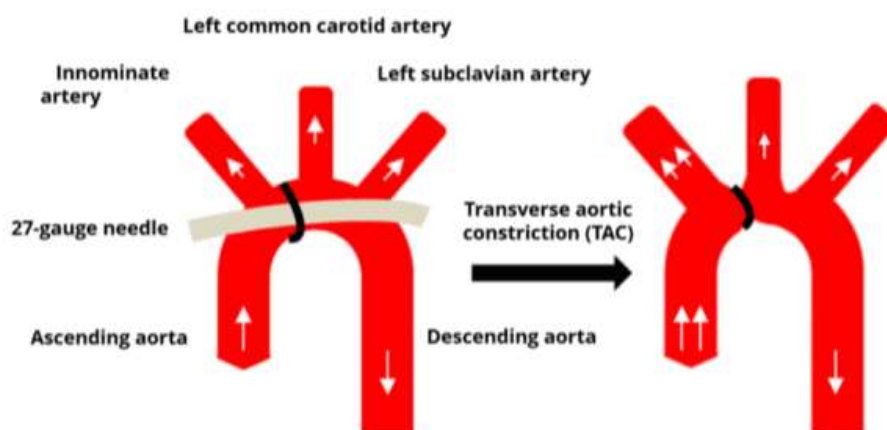


**Fig.16 Schematic diagram of the transvers aortic constriction (TAC) surgery** [344]

TAC initially leads to compensated hypertrophy of the heart, which often is associated with a

temporary enhancement of cardiac contractility. Over time, however, the response to the chronic hemodynamic overload becomes maladaptive, resulting in cardiac dilatation and heart failure [345]. Generally, cardiac hypertrophy is developed in mice within 1–2 weeks, and cardiac dilatation and congestive heart failure after 6–8 weeks [346].

However, published mouse TAC studies report varying profiles for the degree and time course of progression for hypertrophy and cardiac dysfunction, attributed partly to variation in protocol factors prominently including the severity of aortic constriction but also including size and strain of experimental animals, timing for hemodynamic and morphometric assessments and overall study duration [347,348]. Beyond these protocol-based sources of variability, an intrinsic limitation of the mouse TAC model, for example, banding the aorta require opening the thoracic cavity and mechanically ventilating the lungs. Ventilation results in compensatory physiological responses both at the whole-body level as well as down to the cellular level. These compensatory mechanisms can confound study results and can increase fatality during recovery. Moreover, the inter-individual variation in the response to pressure overload also exist even when employing a standard severity of aortic stenosis and controlling for animal strain, gender and age [349,347,350]

The cardiac phenotype of this model has been described as compensated hypertrophy (left ventricular [LV] hypertrophy, or LVH) in some studies [343,351,352] and as HF in others [353,354]. This may be a critical distinction as the presence of HF may be associated with differential activation of signaling pathways [355,356] and differential response to pharmacologic interventions [357,358]. Furthermore, variability in a model will affect the sample size required to detect the influence of genetic or pharmacologic interventions on LV structure or function and is particularly important when small subsets are selected for assessment of different hemodynamic, biochemical, or genetic parameters [359].

Thus, in this study, the HF was defined as lung/body weight > Mean value + 2SD than in sham-operated mice with remaining mice characterized as compensated LVH [360].

Male C57BL/6J mice, 7 to 10 weeks old and 19 to 26 g body weight are used in this protocol. Maintain the mice for one week after arrival in the animal facility on a 12h/12h light/dark cycle, in standard cages, with food and water available *ad libitum*.

The mouse was firstly anesthetized by Isoflurane gas and then placed in a supine position atop at heating pad (37 °C) to maintain body temperature. A rubber band is placed over the front teeth of the animal to extend the neck. Hair clippers are used to shave the fur from the neckline to mid chest level.

A single dose of a mixture of ketamine (90 mg/kg) and xylazine (8 mg/kg) diluted in saline solution (0.9% NaCl) was injected intra-peritoneally. Then a 5 mm upper partial sternotomy was performed under a surgical microscope and the sternum retracted using a chest retractor. Fine tip 45° angled forceps are used to gently separate the thymus and fat tissue from the aortic arch. Following identification of the transverse aorta, a small piece of a 4.0 silk suture is placed between the innominate and left carotid arteries. Two loose knots were tied around the transverse aorta and a blunted 0.385 OD gauge needle (Fig.16) placed parallel to the transverse aorta. The first knot is quickly tied against the needle, followed by the second and the needle promptly removed to yield a constriction of 0.38 mm in diameter. In sham control mice, the entire procedure is identical except for the aorta ligation.

Then, the chest retractor was removed, and the sternum closed using a 6/0 monofilament polypropylene suture with an interrupted suture pattern. The skin is closed using a 6/0 monofilament polypropylene suture with an interrupted suture pattern. The animals were then administered 0.03 µg/mg Buprenorphine s.c. and allowed to recover on a heating pad until fully awake.

## **2.2 Echocardiography and Doppler**

(Echo, Performed by Susana Gomez)

Transthoracic echocardiography was performed using an echocardiograph (Vivid 9, GE Healthcare) equipped with a 15-MHz linear transducer, under 2% isoflurane gas anesthesia in 0.8 L/min 100% O<sub>2</sub>. The thickness of the left ventricular anterior and posterior walls were measured in short and long axis at papillary muscle level using two-dimensional-guided (2D) M-mode echocardiography during systole and diastole, and contractile parameters such as fractional shortening (FS %) or ejection fraction (EF %) were calculated from these measurements. For anatomical parameter, the whole heart weight is always normalized to body weight or tibia length. The left ventricular mass is an echocardiography-based left ventricular mass estimation calculated by a most commonly used Penn formula for rodents: LV mass (Penn) = 1.04 ([LVIDd + LVPWd + IVSd]<sup>3</sup> - [LVIDd]<sup>3</sup>).

Echocardiographic examinations were performed in a blinded fashion.

The data analysis and statistic were performed by Jianbin XUE

## **2.3 Telemetric ECG recording**

In order to analyze the basal electrocardiogram (ECG) and arrhythmia we used a telemetry method, which allows us to record ECG in awake animals and avoids the effects of anesthesia.

### 2.3.1 The transmitter implantation

(Performed by Susana Gomez)

The electrocardiogram (ECG) is a graphical, accurate and composite record of the electrical activity generated by the heart (see Introduction), recorded through the electrodes on the body surface. ECG is used to depict the electrical function of the heart.

While it is possible to measure ECG in humans in awake conditions, for animal recordings, mostly rodents, it needs anesthesia to immobilize the animal. This may perturb the ECG. Thus, we have used a telemetry system, which implant the transmitter (7 ETA-F10) subcutaneously in the animal during surgery. After one-week recovery, the ECG can be recorded in awake animals. As it transmits the data to receiving equipment without contact, the data can be continuous monitored in the cage when mice are placed over the receiver. The telemetry monitoring system normally has 3 electrodes or 5 electrodes, including one electrical ground or 2 electrodes like in our case.

Before the surgery, sterilization of ECG transmitters was needed. The transmitters were soaked by Actril® cold sterilant for a minimum of 5.5 hours at room temperature. They were thoroughly rinsed in sterile saline at least 3 times until no residues left, detected by detector strips provided by Actril manufacturer. The sterile transmitters were then soaked in sterile saline for minimum of 5.5 hours up to 48 hours. If the transmitters will not be reused after 48 hours, it should be air dried at room temperature and stored at dry place. After dry storage, re-sterilization might be necessary. During the subcutaneous implantation of ECG transmitter, the mouse was placed in an isoflurane (2.5%) inhalation apparatus for anesthesia induction. Then, the animal was placed on a warm pad fitted with a device to provide a continuous flow of 1.5% isoflurane in 0.5 L/min oxygen for maintenance during surgery. On the abdomen (Figure 17) or on the dorsum of the mouse, a midline incision was made in the skin to free a subcutaneous pocket for placing the transmitter. The ECG electrodes were positioned as shown in Figure 26. The electrode with white sheath was placed on the upper right chest, and the one with red sheath was placed on the left side of the abdomen below the diaphragm. If the transmitter was placed on the abdomen, a blunt scissor was used to detach the skin from the muscle from the incision until the final electrode sites. Then, the electrodes were anchored to the underlying muscle/peritoneal tissue by suture to make a good electrical contact.

When the transmitter was placed on the dorsum, two incisions on the position where the electrodes should be placed were cut, and two tunnels from the dorsal incision until each electrode incision were made. And then, the electrodes were pulled through the tunnels and anchored. The incision was closed by suture. During the surgery, tissue was maintained wet by the sterile saline.

Betadine was applied to the wound. Post-operative analgesia was provided in the drinking water (0.5 ml of Ibuprofene syrup for 100 ml of water) for 24 hours.

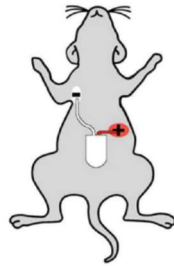


**Fig. 17 Telemetry implantation on the abdomen of the mouse with proper positive and negative electrode sites.** (Adpated from McCauley and Wehrens, 2010 [361])

### 2.3.2 ECG recordings

At least one week after surgery, to allow recovery, basal and challenged ECGs were recorded. Basal ECGs were recorded during day and night time. The animals were kept in a cycle of 12 hours light (from 8 to 20h) and 12 hours dark. We analyzed separately day time (rest time for mice, because they are nocturnal) and night time (activity period). The first hour of each light change was discarded.

We also analyzed ECG response to sympathetic stimulation. We injected isoprenaline (ISO, Sigma, 1 mg/kg i.p., in sterilized saline solution, freshly prepared). ECG was continuously monitored and analyzed when the RR intervals reached the maximal effect. At least two hours later (HR had already regained basal levels), Propranolol plus Atropine mixed solution (Sigma, 2mg/kg each), which inhibit the autonomic nerve system, was injected and data analyzed as before. The ECGs were recorded at least two hours after injection for full response. Data was collected and analyzed with ECG AUTO software (EMKA Technologies).

At the end of the experiments, mice were sacrificed, and the ECG transmitters were extracted for reuse. Upon extraction, all possible attached tissue and sutures were gently removed. Then, the transmitters were rinsed with water. Attached tissues rests were dissolved in a 1% (w/v) solution of Terg-A-Zyne® for a minimum of 4 and maximum of 72 hours at room temperature. After thorough rinse, the transmitters were air dried at room temperature and stored in a dry place.

### 2.3.3 ECG analysis

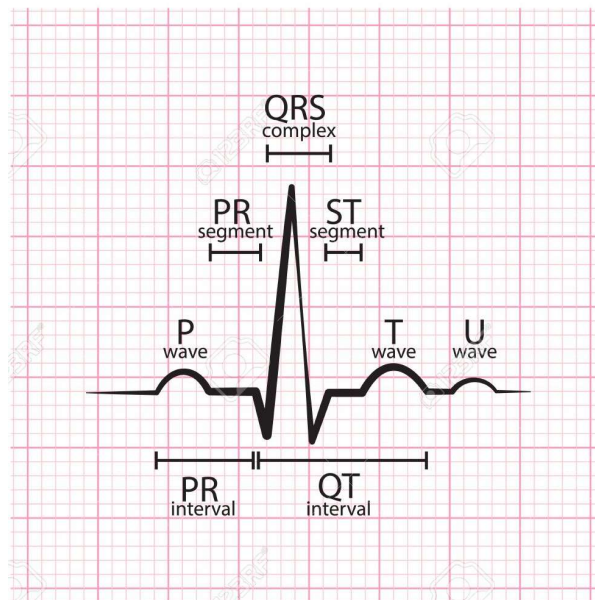


**Fig.18 A normal human ECG waveform.** The PR interval goes from the beginning of the P wave to the beginning of the QRS complex, while the QT interval is from the beginning of QRS complex until the end of T wave. The PR segment goes from the end of P wave until the beginning of Q wave, and the ST segment is between the end of S wave and the beginning of T wave. (the picture is from [https://fr.123rf.com/photo\\_55067903\\_ecg-normal-%C3%A9lectrocardiogramme-onde-p-segment-de-pr-l-intervalle-pr-qrs-intervalle-qt-le-segment-st.html](https://fr.123rf.com/photo_55067903_ecg-normal-%C3%A9lectrocardiogramme-onde-p-segment-de-pr-l-intervalle-pr-qrs-intervalle-qt-le-segment-st.html) image ID: 55067903)

The ECG waveform is shown in Fig. 18. The electrical activity is initiated from SAN as mentioned previously. It spreads across both right and left atrium and induces the atria depolarization. This process corresponds to P wave on ECG. Then the impulse goes through the AV node, which corresponds to PR segment, a flat line following the P wave. The PR interval represents the duration from the beginning of atrial depolarization until ventricular depolarization. After that, the impulse travels to His bundle, bundle branches and Purkinje fibers, inducing ventricular depolarization. On the ECG, it is represented by QRS complex. Meanwhile, the atrial repolarization occurs, although it is buried in QRS complex. The Q wave depicts the septum depolarization, from left to right. When the depolarization travels throughout the ventricles, the R wave and S wave show up. Then another flat line, ST segment (Fig. 18), indicates no large electrical vector, while ventricle is contracting. The ventricle repolarization represented by T wave. As the epicardial cells repolarize before the endocardial cells, the T wave reflects positively.

For ECG analysis, all the recordings were analyzed firstly with ECG-auto (EMKA tech. version 3.3.0.5). Heart rate and RR interval (RR, duration of adjacent R waves), P, PR interval and QT interval were quantified. The preliminary data was further statistically analyzed by Origin 9.0 (Microcal)

### **2.3.4 HRV analysis based on ECG**

(Physiozoo platform was performed by Moran Davoodi)

Briefly, the analysis was performed with Physiozoo platform [362]. Each RR signal was cut into 10-20 minutes, non-overlapping window and then was sent to analysis. Any extracted window was also checked to have less than 10% outliers which we have defined to be less or more than  $2 \times \text{std}$  of the 10 min window. Every window was also cut into windows of 3 minutes in order to average the results.

## **2.4 SAN Preparation**

Most of the analyses presented in this thesis were taken from isolated SAN preparation. In some experiments, after dissection, single SAN cardiomyocytes were obtained by enzymatic method (see below).

### **2.4.1 SAN dissection**

The mice were anaesthetized by i.p. injection of around 100 mg/kg Na pentobarbital (Ceva Sante Animale) with 0.1ml50U/ml heparin (Sigma) to avoid blood coagulation. When the mouse lost consciousness and failed to respond to leg pinch, we opened its chest extracted the heart into oxygenated Tyrode solution (NaCl 140 mM, KCl 5.4 mM,  $\text{CaCl}_2$  1.8 mM,  $\text{MgCl}_2$  1 mM, HEPES 5 mM, and glucose 5.5 mM, pH 7.4, titrated with NaOH). Tyrode solution is widely used as a physiological bathing medium to reproduce the extracellular environment in vivo. It mimics the ionic composition and pH of blood. For SAN dissection, heparin (50 U/ml) was also added into tyrode solution as anticoagulant.

The heart was fixed onto a homemade silicon dish in posterior position under binocular lenses. Ventricles were separated from atriums and then divided left and right ventricle, frozen in liquid nitrogen then stored in  $-80^\circ\text{C}$  for further use. The right atrium was fixed with pins, and SAN was exposed between superior vena cava and inferior vena cava. Then the tissue was moved and pinned down to the bottom of the homemade dish for confocal microscope recording as shown in Fig. 19. It was bathed with  $37^\circ\text{C}$  Tyrode solution during all the procedures. The body weight, heart weight, lung weight and tibia length were measured along the way of SAN preparation.

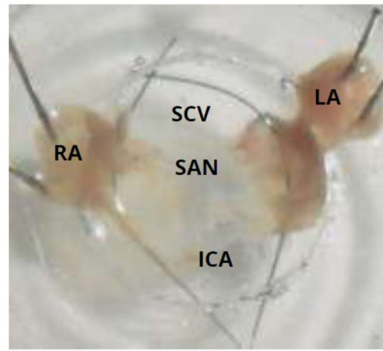


**Fig. 19 Photograph of typical preparation and SAN location on a homemade dish.** SAN, sinoatrial node; SCV, superior vena cava; RA, right atrium; ICA, inferior vena cava; LA, left atrium.

## 2.4.2 Isolation of sinoatrial node myocytes

SAN tissue were cut into strips and transferred into a "low- $\text{Ca}^{2+}$ -low- $\text{Mg}^{2+}$ " solution containing (in mM/L) 140 NaCl, 5.4 KCl, 0.5  $\text{MgCl}_2$ , 0.2  $\text{CaCl}_2$ , 1.2  $\text{KH}_2\text{PO}_4$ , 50 taurine, and 5.5 D-glucose; 1 mg/mL BSA; and 5 HEPES-NaOH, adjusted to pH 6.9 with NaOH. Tissue was digested by Liberase TH (229 U/mL; Roche Diagnostics), elastase (1.9 U/mL; Boehringer Mannheim), and 200  $\mu\text{M}$   $\text{CaCl}_2$ . Digestion was carried out for 9–13 minutes at 37°C, under manual mechanical agitation. Tissue strips were then washed and transferred into a modified Kraftbruehe (KB) medium containing (in mM/L) 70 L-glutamic acid, 20 KCl, 80 KOH, 10 ( $\pm$ )D- $\beta$ -OH-butyric acid, 10  $\text{KH}_2\text{PO}_4$ , and 10 taurine; 1 mg/mL BSA; and 10 HEPES-KOH, adjusted to pH 7.4 with KOH. Single SAN myocytes were then isolated by agitation in KB solution at 37 °C. Cellular automaticity was restored by readapting the cells to a physiological extracellular  $\text{Ca}^{2+}$  concentration by addition of a solution containing (in mM/L) 10 NaCl, 1.8  $\text{CaCl}_2$ , and normal Tyrode's solution containing BSA (1 mg/mL). The final cell storage solution contained (in mM/L) 100 NaCl, 35 KCl, 1.3  $\text{CaCl}_2$ , 0.7  $\text{MgCl}_2$ , 14 L-glutamic acid, 2 ( $\pm$ )D- $\beta$ -OH-butyric acid, 2  $\text{KH}_2\text{PO}_4$ , and 2 taurine; and 1 mg/ml BSA (pH 7.4).

## 2.5 $\text{Ca}^{2+}$ handling recording by confocal microscopy

### 2.5.1 Principles on the confocal microscopy

Intracellular  $\text{Ca}^{2+}$  was analyzed by confocal microscopy in SAN cells isolated or within the tissue loaded with the fluorescence calcium dye Fluo-4.

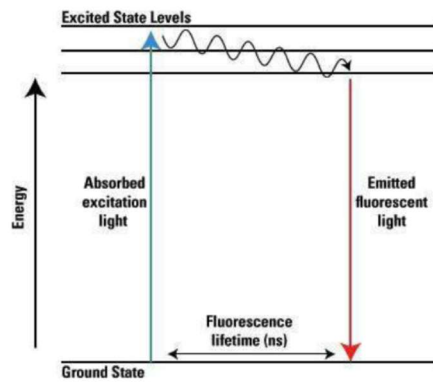


**Fig.20 Jablonski energy diagram of fluorescence.** (Adapted from <https://www.thermofisher.com>)

To visualize the  $\text{Ca}^{2+}$  dynamics in SAN cells, the SAN was loaded with fluorescence  $\text{Ca}^{2+}$  dye Fluo-4. Fluorescence is the property that have some molecules of emitting light when illuminated. They absorb energy and emit energy in the form of photons. During the excitation, the electrons of the molecule go into an excited electronic state (Fig.20), and then returns to the ground state losing the energy by emitting light (fluorescence, Fig.20). While in the excited state, there is some energy dissipation due to molecular vibrations. Thereby the emitted light has lower energy than the absorbed energy, and thus the emitted light has longer wavelength than the exciting light. Thus, the emitted fluorescence can be distinguished from the excitation light. The excitation and emission of molecule is cyclical, which means it can be excited repeatedly until irreversibly damaged.

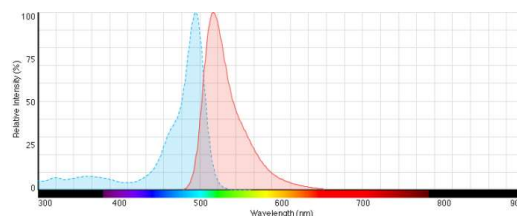


**Fig.21 Fluorescent excitation (blue) and emission (red) spectra of Fluo-4.** (Adapted from <https://www.thermofisher.com/order/catalog/product/F14201>)

Fluo-4 is a calcium indicator used to analyze the spatial dynamics of  $\text{Ca}^{2+}$  ions. It displays high sensitivity to  $\text{Ca}^{2+}$  and large fluorescence increase upon excitation (Fig.21). Fluo-4 is excited at peak 488 nm (Fig.21), and the fluorescence is emitted between 500 and 650nm. The Fluo-4 AM (acetomethyl ester) is a cell permeable form. The AM ester helps the Fluo-4 pass through the lipid membrane and enter the cell. Once inside the cell, esterases in the cytosol cleave the AM residue and release the active Fluo-4. Fluo-4 is only fluorescence when bound to  $\text{Ca}^{2+}$ .

In this work, we dissolved Fluo-4 AM in DMSO with 20% Pluronic acid. Pluronic acid was used to prevent aggregation of Fluo-4 AM and help uptake by the cell. Fluo-4 AM was loaded to the SAN tissue at concentration of  $30\mu\text{M}$  (diluted by Tyrode solution) for 1h at  $37^\circ\text{C}$  on a rocking device. After Fluo-4 AM incubation, the SAN tissue was loaded with Tyrode solution contained Blebbistatin ( $5\mu\text{M}$ ,

Sigma) 10 mins before recording to avoid contraction artifacts. To evaluate  $\text{Ca}^{2+}$  dynamics in SAN cells, the SAN tissue was detected under confocal microscopy after Fluo-4 AM loading. Confocal microscopy is one of the fluorescence microscopies with a pinhole to eliminate out-of-focus light away from the focal plane, which provides possibility for high-quality images recording of fixed or living cells and tissues.

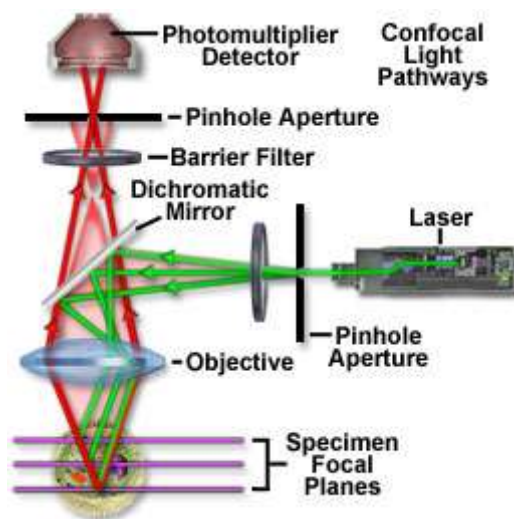


**Fig. 22 The diagram of a confocal microscopy.**

(Adapted from <http://www.olympusconfocal.com/theory/>)

A confocal microscope contains laser for excitation source, the beam splitter, the detector pinhole with variable aperture, and the detector (Fig.22). The laser emitted by the laser excitation source passes through the excitation filter, and it is reflected by the beam splitter mirror with a scanning head to scan across the specimen. It directs to a point of fluorophore-labeled specimen, and scans across the specimen. The labeled specimen then emits fluorescence, which passes back through the beam splitter mirror and toward the pinhole aperture (termed detector pinhole aperture in Fig.22) to eliminate fluorescence outside the focal plane. The mirror is set to match the spectral excitation and emission characteristics of the fluorophore and scan the specimen at a given speed. The pinhole aperture is positioned in front of the detector to select the emitted fluorescence from the focal plane of the specimen, and excludes lights emitted from the above and below planes (termed out-of-focus light rays, Fig.22). Thus, the emitted fluorescence becomes confocal through this pinhole aperture, and then detected by the detector. Only a small fraction of the out-of-focus fluorescence emission is delivered through the pinhole aperture, most of this extraneous light is not detected and does not contribute to the resulting image. The confocal microscope equipped with a resonant scanning mirror can generate the necessary speed of 8000 Hz for ultrafast time line scan imaging.

## 2.5.2 SAN tissue preparation recording

In this work, SAN tissues were recorded under a resonant scanning confocal microscope (Leica SP5) equipped with a  $\times 40$  water immersion objective and a white laser that we tuned to 500 nm, and from different regions of the SAN as basal condition. To visualize the response of each compound, SAN perfused with the compound (such as ISO 20nM, KN-93 3 $\mu$ M) Then the same SAN cells recorded in the basal conditions were recorded again in the presence of the compound. Both line-scan images and 2D images are captured, at a scanning speed of 8000 Hz. In order to get better signal to noise, 4-line average were used on line-scan, thus the final speed was 0.25 ms per line. A small window of only one cell was used in the 2 D images to optimize the time between 2 consecutives images. All the recordings are performed at 37°C. The fluorescent emission is collected above 510 nm.

## 2.5.3 Single SAN Cell recording and Caffeine perfusion

Fresh SAN cells were incubated for 30 min at room temperature with 7  $\mu$ M of Fluo-4 AM. The Fluo-4 Ca<sup>2+</sup> signal was recorded with a laser scanning confocal microscope (Leica SP5) equipped with a  $\times 20$  water immersion objective. Fluo-4 was excited at 490 nm with a white light laser, and emission was collected at  $>510$  nm. For SR Ca<sup>2+</sup> load estimation, SAN cells were rapidly perfused with 10 mM caffeine. The amplitude of the caffeine-evoked [Ca<sup>2+</sup>]<sub>i</sub> transients was used to assess the SR Ca<sup>2+</sup> load.

## 2.5.4 Confocal microscope images analysis

Line-scan images were quantified by IDL (8.5) with homemade programs, and statistically analyzed by Origin 9.0 (Microcal). Characteristics of [Ca<sup>2+</sup>]<sub>i</sub> transients, including time to peak (ms), amplitude (maximum value of F/F<sub>0</sub>, where F is the fluorescence signal and F<sub>0</sub> the fluorescence on diastolic period) and decay time constant (tau, time constant obtained by fitting the descending portion of the fluorescence trace to a single exponential function, in ms), were quantified. Characteristics of [Ca<sup>2+</sup>]<sub>i</sub> sparks during diastolic periods were also quantified (Fig. 23), including spark frequency (number of sparks/s/100 $\mu$ m), width at half maximum (W50,  $\mu$ m), time to peak (ms), duration at half maximum (D50, ms) and peak amplitude (F/F<sub>0</sub>).

Global calcium transients of 2D images were quantified using a Region of Interest (ROI) covering the whole cell and further analyzed by Origin (9.0), while the mean cycle length (duration between the peaks of two transients) was measured.

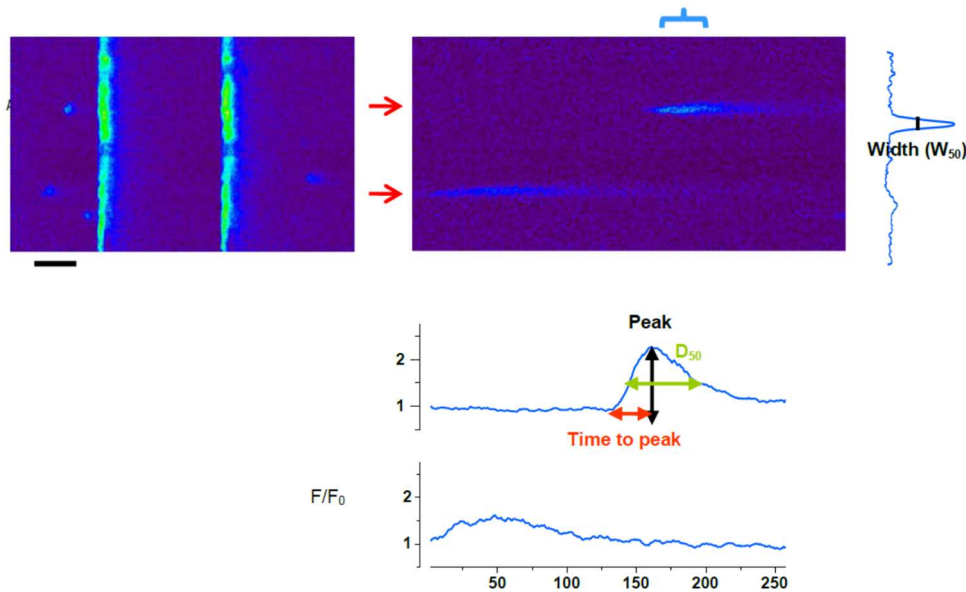


**Fig. 23  $\text{Ca}^{2+}$  spark characteristics.** The up-left image shows a line-scan image recorded by confocal microscope. The up-right image corresponds the 250ms depicting in the up-left image, while the linear trace on its right shows the spatial profile in the blue bracket indicating the  $W_{50}$  of the spark. The down-right image presents the time profile of two sparks, and the peak (black arrow),  $D_{50}$  (green arrow) and time to peak (red arrow) of the upper spark. (Picture is from YueYi Wang 2016. NNT: 2016SACLS156)

## 2.6 Protein measurement

To measure the channel expression, we extracted protein from SAN and performed Western Blot.

### 2.6.1 Protein extraction

Protein extraction is the sample preparation step for Western Blot. In this step, the protein is brought into solution by breaking the tissue or cells, such as homogenization. Lysis and extraction buffer are also used to efficiently lyse cells or tissue, increase protein solubilization, and avoid protein degradation. In this work, we used RIPA buffer. RIPA buffer (radioimmunoprecipitation assay buffer) is a lysis buffer, commonly used for whole cell extracts and membrane-bound proteins. RIPA buffer contains Tris HCl pH=8 (50 mM), NaCl (150 mM), phosphatase inhibitor (Tablet PhosSTOP, Roche (1 for 5 ml)), protease inhibitor (Tablet Complete, EDTA free, Roche (1 for 5 ml)), Triton X100(1%), DOC (sodium deoxycholate acid, 0.5%), SDS(0.1%). Tris HCl acts as buffer providing an ionic environment similar to that of the cell in vivo and maintaining the protein stability. NaCl maintains or increases the strength of the ionic medium and detergents, to dissolve the cell membranes and concomitantly facilitates the release of proteins. Phosphatase inhibitor and protease inhibitor are used to avoid the

protein degradation. DOC, SDS and Triton X-100 are detergents, which are used to lyse cells, solubilize proteins and lipids, etc. DOC and SDS could denature and solubilize the protein, and Triton X100 facilitates lysis.

To extract protein, the intact SAN tissue samples were placed into Bertin tubes with 4-5 beads and RIPA buffer (50µl for each sample), and homogenized Bertin homogenizer (6500rpm x 10sec, 2 cycles). Then the samples were centrifuged at 4°C 3000 rpm for 1 minute to eliminate bubbles. The lysates were taken and put into a new EP tube. The samples can be used immediately, or frozen at -80°C for later use.

The concentration of cell/tissue lysate protein could be measured by many methods, such as BCA assay, Lowry protein assay, etc. In this work, we used BCA assay. BCA assay is a high precision method, which detects the color change of the sample solution from green to purple in proportion to protein concentration and compares to protein standards. The peptide bonds of protein reduce the cupric ions ( $\text{Cu}^{2+}$ ) to cuprous ions ( $\text{Cu}^+$ ) in an alkaline environment at a higher temperature (37 to 60°C). Then two BCA molecules chelate one  $\text{Cu}^+$  forming an intense purple complex, which has a strong linear absorbance at 562nm with the increase of protein concentration.

The protein concentration of the sample is determined by comparing this absorbance with a standard curve of absorbance from varying bovine serum albumin (BSA).

In this work, we used 96-well flat-bottom plate to perform the BCA. Different BSA concentrations were used to make absorbance curve (30, 25, 20, 15, 10, 5, 2.5, 1.25 µg). Each sample (2 µl) was mixed with 98 µl  $\text{H}_2\text{O}$  and 100 µl smart BCA solution (contains 98 µl solution A and 2 µl solution B, iNtRON Biotechnology). Samples were performed in triplicate. The plate was then wrapped with aluminum, incubated at 60°C for 20 min, and read by TECAN instrument.

The protein concentration was calculated by comparing the absorbance with the standard curve, and 10-15µg of total protein was used for Western Blot. Generally, around 40mg protein in total was extracted from one SAN.

## **2.6.2 Western Blot**

Before running the gel, the lysate protein was loaded with loading buffer. Loading buffer contains anionic denaturing detergent SDS to denature proteins and make them negatively charged. SDS removes the secondary and tertiary structure, which facilitates the protein separation by molecular weight and the following binding with antibody. Meanwhile, the proteins are negatively charged via attachment to the SDS, with equal charge-densities per unit length as SDS binds to the

majority of proteins at a constant ratio of 1.4mg SDS/gm protein.  $\beta$ -mercaptoethanol and dithiothreitol (DTT) are reducing agents used to break disulphide bonds. Glycerol is added to the loading buffer to increase the density of the sample, making the sample easier to load and maintaining at the bottom of the well. A small anionic dye molecule (e.g. Bromophenol blue) is also used to track the migration of protein. Since it is anionic and small, it migrates faster than proteins to provide a migration front and monitor the running progress. Loading buffer also contains Tris-HCl pH=6.8, which is the same as stacking gel buffer. In this thesis, we used the loading buffer produced by Sigma. Boiling/heating is also useful to denature the protein. The temperature and heating duration depends on the protein, which will describe later.

Then, the anionic protein is fractionated on SDS-PAGE (Sodium Dodecyl Sulfate PolyAcrylamide Gel Electrophoresis) gel. The gel is a sieving electrophoresis matrix formed by three-dimensional networks of long hydrocarbons crosslinked by methylene groups. The gel is made of acrylamide, bis-acrylamide, denaturant (such as SDS), a buffer with adjusted pH, and TEMED and APS to initiate polymerization. During electrophoresis, proteins move through the pores of the gel, and are separated based on the molecular weight. Larger molecules pass through at slower speeds and migrate less than smaller molecules. The pore size of a gel is determined by the percentages of acrylamide and cross-linker (bis-acrylamide). A lower percentage gel provides bigger pore size and is better for resolving higher molecular weight molecules. Normally, a conventional gel is formed by two sections, the running gel on the bottom and the stacking gel on the top. The stacking gel has a lower acrylamide concentration to ensure the proteins enter the gel. The stacking gel also is prepared with low pH buffer to provide a lower ionic strength, which lines the proteins up at the starting line. The running gel has a higher acrylamide concentration and higher pH to separate the proteins.

In this study we use the prepared gel. We employ two kinds of gel, one is 4%-20% Tris-Glycine Gel (Invitrogen Novex Wedgewell) the other is 3%-8% Tris-Acetate Gel (Invitrogen NuPAGE). These two gels need different running buffer. The buffer for the first one is TG-SDS (Tris-Glycine-SDS buffer, Euromedex), the other is Tris-Acetate SDS Running Buffer (Novex).

The purposed proteins were separated into two groups according to the molecular weight. The first group called as the large protein, contains RyR2, HCN4, SERCA and NCX. For this group, the samples were heated at 50 °C for 10 mins, and then were loaded onto the 3%-8% gel. The running condition was 200V for 40 mins. The second group called as small proteins contains CaMKII, PPP1C and PLB. All the samples were heated at 95 °C for 10 mins, and were loaded onto 4%-20% gel. The running condition was 150V for 60 mins.

After running the gel, the proteins were transferred from the gel to a nitrocellulose (NC) or

polyvinylidene difluoride (PVDF) membrane. This step uses an electric current to pull proteins from the gel into the membrane. When an electric field is applied across the gel, the negative charged proteins migrate from the negative electrode and towards the positive electrode, hence from the gel to the membrane. The proteins bind to the membrane through the non-specific hydrophobic interactions. In this thesis, NC membrane (iBlot 2 NC Mini Stacks, Invitrogen) was used. The procedures were taken following the instruction book of the kit.

Then, to avoid the hydrophobic binding between the membrane and the antibodies, the membrane was blocked by BSA or non-fat dry milk in TBS solution, with a low concentration of detergent (such as Tween 20 or Triton X-100) to prevent unspecific protein-protein interaction. In this work, the membranes were incubated in 2% BSA solution (in TTBS), agitated at 20 rpm for 1h.

Finally, the membrane was incubated with the primary antibody which binds to the specific protein, and then the labeled secondary antibody which binds to the first antibody. Both antibodies were diluted in 2% BSA TTBS solution. Through the second antibody, the specific protein is detected. The second antibody is commonly labeled with horseradish peroxidase (HRP). HRP is an enzyme which oxidizes the chromogenic, fluorogenic, and chemiluminescent substrates that produces colored, fluorimetric or luminescent derivatives, respectively. In this work, the membrane was incubated with the primary antibody overnight at 4°C, 20 rpm. The next morning, the first antibody was collected for reuse (it can be used 3 times) and frozen at -20°C. The membrane was washed with TTBS (at 70 rpm, 3x 10 min), and incubated with the secondary antibody for 1h at 20 rpm, and after, washed in TTBS as previously (at 70 rpm, 3x 10 min). The first antibody used in this study were shown in table 4:

**Table 4: List of primary antibodies used for Western Blot**

| <b>Protein</b>         | <b>Host</b> | <b>Dilution</b> | <b>Code</b> | <b>Source</b>     |
|------------------------|-------------|-----------------|-------------|-------------------|
| <i>RyR2 total</i>      | mouse       | 1/1000          | MA3-916     | Thermo Scientific |
| <i>RyR2 P-Ser2808</i>  | rabbit      | 1/2000          | A010-30AP   | Badrilla          |
| <i>RyR2 P-Ser2814</i>  | rabbit      | 1/2000          | A010-31AP   | Badrilla          |
| <i>CaMKII P-Thr286</i> | rabbit      | 1/2000          | MA1-047     | Thermo Scientific |
| <i>CaMKII (pan)</i>    | rabbit      | 1/1000          | 3362S       | Cell signaling    |
| <i>SERCA2a</i>         | mouse       | 1/500           | SC-376235   | Santa Cruz        |
| <i>PLB total</i>       | rabbit      | 1/5000          | 8495S       | Cell Signaling    |
| <i>PLB P-Ser16</i>     | rabbit      | 1/5000          | A010-12     | Badrilla          |
| <i>PLB P-Thr17</i>     | rabbit      | 1/5000          | A010-13     | Badrilla          |
| <i>PPP1Cα+β HRP</i>    | Rabbit      | 1/5000          | EP1511Y     | abcam             |
| <i>HCN4</i>            | Rabbit      | 1/200           | APC-052     | Alomone labs      |
| <i>NCX</i>             | mouse       | 1/1000          | R3F1        | Swant             |
| <i>β-actin HRP</i>     | mouse       | 1/20000         | SC-47778    | Santa Cruz        |

To visualize the protein, the membrane was loaded with the substrate (PICO, PICO+, DURA or

Femto Luminata Western Substrates, Millipore and Thermo Scientific) depending on the quantity of the proteins. PICO was used for high signals, and Femto was used for the lowest signals. In this study we firstly use PICO for SERCA, PICO+ for  $\beta$ -Actin and NCX, Dura for all the others. If the signal is bad, the stronger one will be applied.

After 3 minutes incubation at room temperature, the membrane was exposed and visualized by the iBright FL1000 (Invitrogen) appropriately. After saving the images, the membrane was rinsed and washed with TTBS for around 5 minutes and sealed to clean plastic sheet. Membranes can be stored at 4°C and reused for re-blotting of other proteins.

To re-blot the protein, we rinsed the membrane with 1x Re-blot Plus Strong solution (Millipore, 10x, in water), (it should be another one) followed by blocking, first/second antibody incubation, and so on.

The Western Blot images were quantified with Image J, and further statistically analyzed by Origin (9.0).

## 2.7 Statistics

One-way ANOVA was used for multiple comparisons. T test was used when data was normally distributed. The non-parametric Mann-Whitney test was used for non-normally distributed data. An unpaired  $t$  test was used to compare 2 independent groups. A paired  $t$  test was used to compare measurements made in the same mice or in the same cells under 2 different conditions. The  $t$  tests were two-tailed and a value of  $P < 0.05$  was considered significant. Results are expressed as mean  $\pm$  SEM. The Graph Pad Prism 7 Software and the Origin 9 (Microcal) software were used.

# Chapter 3 Results

During my Ph.D. career, I mainly focused on the  $\text{Ca}^{2+}$  handling in the primary pacemaker-the sinus node (SAN) in heart failure mouse model. The first manuscript constitutes the main part of the work. However, some of the data I have obtained in my work were not included in the manuscript and they are under the second part of the result, called the 'mysterious hypertrophy group. And the reason why that part was not included is also discussed in the second part. Then during the time spend in the lab, I also participated in a collaborative project concerning the pacemaker function in heart failure due to type 2 diabetes, using the db/db mouse model. Since the diabetes can also induce heart failure and in this work, after evaluating the cardiac function of the db/db mice we have used, they were under heart failure condition. So, I also add this manuscript in my thesis as the third part of the result. In this paper my work was concentrated into the  $[\text{Ca}^{2+}]_i$  handling in SAN cells. The other experiments were done in Denmark.

## **3.1 Heart failure induces sinus node dysfunction associated with reduced CaMKII signaling.**

# Heart failure induces sinus node dysfunction associated with reduced CaMKII signaling

Jian-Bin XUE<sup>1</sup>, Moran Davoodi<sup>2</sup>, Susana Gómez<sup>1</sup>, Yael Yaniv<sup>2</sup>, Jean-Pierre Benitah<sup>1</sup>, Ana María Gómez<sup>1</sup>.

<sup>1</sup>Signaling and Cardiovascular Pathology, UMR-S 1180, Université Paris-Saclay, Inserm, 92296 Châtenay-Malabry, France.

<sup>2</sup>Biomedical engineering, Technion institute, Haifa, Israel.

## *Correspondance*

*Ana María Gómez or Jean-Pierre Benitah*

*5 Rue Jean Baptiste Michel*

*Faculté de Pharmacie, Université Paris-Saclay*

*92296 Châtenay-Malabry, France*

*ana-maria.gomez@inserm.fr*

*Tel: +33 146 83 57 18*

*jean-pierre.benitah@inserm.fr*

*Tel: +33 146 83 57 66*

## **Abstract**

Dysfunction of the sinoatrial node (SAN), the natural heart pacemaker, commonly occurs with heart failure (HF). While SAN spontaneous activity relies on various ion currents in the plasma membrane (voltage clock), intracellular  $\text{Ca}^{2+}$  ( $[\text{Ca}^{2+}]_i$ ) release via Ryanodine Receptor 2 (RyR2) ( $\text{Ca}^{2+}$  clock) plays an important synergetic role. Whereas remodeling of voltage clock components has been revealed in HF, less is known about possible alterations of  $\text{Ca}^{2+}$  clock. Here, we analyzed  $[\text{Ca}^{2+}]_i$  handling in SAN from a mouse HF model after transverse aortic constriction (TAC) and compared to sham operated animals. ECG data from awake animals showed heart rate slower in HF mice upon autonomic nervous system blockade, indicating intrinsic sinus node dysfunction. Confocal microscopy analyses of SAN cells within the whole tissue showed slower and less frequent  $[\text{Ca}^{2+}]_i$  transients in the HF group. This was correlated with fewer and smaller spontaneous  $\text{Ca}^{2+}$  sparks in HF SAN cells, associated with less RyR2 protein expression level and reduced phosphorylation level of this protein at the CaMKII site. Moreover, the phosphorylation level of PLB at the CaMKII site was also decreased in HF, which could lead to the reduced sarco/endoplasmic reticulum  $\text{Ca}^{2+}$ -ATPase (SERCA) function and lower sarcoplasmic reticulum  $\text{Ca}^{2+}$  content, which further depressed the coupling between the clocks. The inhibition of CaMKII with KN93 slowed  $[\text{Ca}^{2+}]_i$  transient rate in both SAN groups, but this effect was smaller in HF SAN, consistent with less CaMKII activation. In conclusion, our data uncover that the intrinsic pacemaker dysfunction in HF could be due to an alteration in coupled clock function by a mechanism involving reduced CaMKII activation.

## **Key words**

Heart failure; Sinus node;  $\text{Ca}^{2+}$  handling; CaMKII; Coupled clock

## ***Introduction***

Heart failure (HF), the condition where the heart cannot optimally pump blood to the body, first during exercise and then at rest [1], is a serious disease with death rates over 50% at 5 years after diagnosis [2]. Although death among HF patients is mainly the consequence of pump failure or ventricular arrhythmias, severe bradyarrhythmias also cause sudden cardiac death (SCD) in HF patients [3-6], suggesting Sinoatrial node (SAN) dysfunction in HF [7]. Indeed, in HF patients, as well as in experimental animal models, decrease in the intrinsic heart rate and SAN dysfunction is common [8,7,9-14]. Improving SAN function could potentially prevent the progression of HF [15]. In addition, chronotropic incompetence, an abnormal HR response to exercise which might reflect both an imbalance autonomic nervous system sinus node dysfunction per se [16], have been reported during the HF process [17-20].

Although SAN dysfunction is a hallmark of HF, the mechanisms and underlying pathophysiological influences of HR abnormalities in HF are incompletely understood. The SAN function, the primary heart pacemaker, is accomplished by the automatic generation of action potentials (APs). Multiple studies showed that the spontaneous diastolic depolarization in SAN occurs because of a synergistic interaction ("coupled clock" [5]) between the voltage clock mediated by voltage sensitive membrane ion currents [21,22], and  $Ca^{2+}$  clock mediated by rhythmic spontaneous sarcoplasmic reticulum (SR)  $Ca^{2+}$  release and  $Na^+/Ca^{2+}$  exchanger (NCX) current activation [23]. Most of the studies about understanding the mechanisms of SAN dysfunction in HF, have focused on the hyperpolarization-activated (HCN) channel subunits, which carry the  $I_f$  current, as well as other ion channel alterations (for review see [24]). However, less is known about the  $Ca^{2+}$  handling alteration in diseased SAN. The  $Ca^{2+}$  clock is initiated by spontaneous  $Ca^{2+}$  release from the SR through the  $Ca^{2+}$  release channel, the ryanodine receptor (RyR2) [25]. This  $Ca^{2+}$  is extruded by the NCX in the outer membrane, generating an inward (depolarizing) current, as it exchanges 3  $Na^+$  by each  $Ca^{2+}$  [26]. The propensity of RyR2 to release  $Ca^{2+}$  is modulated by the amount of  $Ca^{2+}$  stored in the SR, which also depends on the Sarco-Endoplasmic Reticulum ATPase (SERCA) activity [27,28]. Moreover, the spontaneous  $Ca^{2+}$  release activity also determines the degree of coupling of the clock system.[29].

The elements involved in the  $Ca^{2+}$  clock (RyR2, SERCA) are also expressed in ventricular cardiomyocytes, where they have a key role in excitation-contraction coupling, and they have been shown to be altered in heart failure (HF) [27,30]. In fact, failing hearts show a decrease in SERCA function that may be due to diminished expression, or increase in phospholamban (PLB) expression (its natural inhibitor) or a decrease in phospholamban phosphorylation [31,32]. This may bring to a reduction in the amount of  $Ca^{2+}$  stored in the SR, which may be sufficient of contribute to the decrease in the amount of  $Ca^{2+}$  released to activate contraction [33], although less efficacious EC coupling due to transverse tubule remodeling also plays a role [34]. However, the function of these  $Ca^{2+}$  handling elements, and in fine whether the  $Ca^{2+}$  clock may be involved in SAN dysfunction during HF, is largely unknown but recognized as pivotal [24].

Here we used an experimental model of HF in the mouse by transverse aortic constriction (TAC).

By Holter telemetry we analyzed basal ECG and after pharmacologic challenge. The HF mice showed slower heart rate when the autonomic nervous system was blocked, and the dissected SAN showed slower spontaneous  $[Ca^{2+}]_i$  transients as well as less frequent and smaller  $Ca^{2+}$  sparks. This was correlated with less activation of the CaMKII and less phosphorylation of its targets, the RyR2 and PLB. Thus, our results show that in HF, the  $Ca^{2+}$ /CaMKII signaling is depressed in the SAN and this may contribute to impair the coupled clock function.

## **Methods**

### **Heart Failure Model**

Animal study was approved by the French Ministry (Ministere de l'Education Nationale, de l'Enseignement superieur et de la Recherche no. B9201901). Congestive Heart failure was induced by transverse aortic constriction (TAC) under anesthesia (intraperitoneal injection of ketamine 90 mg/kg and xylazine 8 mg/kg) in C57BL/6J male mice (8 weeks of age). After thoracotomy, the aortic arch was constricted between the brachiocephalic and the left carotid arteries with a thread (4.0 Prolene suture) around a blunt needle ( $\varnothing$  0.385 mm) [35]. The knots were tied against the needle before removing it, leaving a region of stenosis which reduced the vascular diameter. Sham-operated mice underwent the same procedure without aortic ligation and served as controls. Cardiac contractile function was assessed 8 weeks after the surgery by transthoracic echocardiography, performed in a blinded fashion using an echocardiograph (Vivid 9, GE Healthcare) equipped with a 15-MHz linear transducer, under 2% isoflurane gas anesthesia in 0.8 L/min 100% O<sub>2</sub>. The thickness of the left ventricular anterior and posterior walls was measured in short and long axis at papillary muscle level using two-dimensional-guided (2D). M-mode echocardiography measurements during systole and diastole were used to calculate parameters such as fractional shortening (FS %), ejection fraction (EF %) or left ventricular mass, calculated using the Penn formula for rodents: LV mass (Penn) = 1.04 ([LVIDd + LVPWd + IVSd]<sup>3</sup> - [LVIDd]<sup>3</sup>). After euthanasia under sodium pentobarbital (100 mg/kg, i.p.) anesthesia, body, heart and lung weights (BW, HW and LW, respectively) were measured, as well as tibia length (TL). Only mice with a LW/TL greater than that of Sham+2SD enrolled in the HF group [36].

### **ECG recording**

To monitor ECGs in awake, free moving mice, the sterilized DSI transmitters (7 ETA-F10) were subcutaneous implanted according to the manufacturer's recommendation [37] after Isoflurane (2.5%) inhalation anesthesia using MINERVE workstation (0901128). The mice were placed on a warm pad (37°C), continuously receiving 1.5% isoflurane inhalation. After at least 7 days recovery period, ECG were recorded for 24 hours. For sympathetic and autonomic challenges, ECG were recorded at baseline during 20 min and 5 min after Propranolol plus Atropine mixed solution (2mg/kg each) challenge. Data was collected with ECG AUTO software (EMKA Technologies). Heart rate variability was analyzed using PhysioZoo platform [38].

### **In vitro intact SAN cell recording**

Mice were anesthetized by sodium pentobarbital (100 mg/kg, i.p.). The hearts were quickly removed from the animal and placed in Tyrode solution (NaCl 140 mM, KCl 5.4 mM, CaCl<sub>2</sub> 1.8 mM, MgCl<sub>2</sub> 1 mM, HEPES 5 mM, and glucose 5.5 mM, pH 7.4, titrated with NaOH), oxygenated to saturation and maintained at 37°C. SAN and some surrounding atrial tissue were dissected and pinned down with the endocardial side up in homemade optical chambers bathed with Tyrode solution as previously described [39]. The tissue was loaded with 30- $\mu$ M fluo-4 AM (Invitrogen) during 60 minutes at 37°C. Images were recorded at 37°C with a resonant scanning confocal microscope Leica SP5, equipped with a white laser fitted to 500 nm. Excitation was collected at > 510 nm. Two-dimensional and X-Time images were recorded from the primary pacemaker region which is located in between the superior and inferior -vena cava and bounded by the crista terminalis. The cytosolic Ca<sup>2+</sup> variation was analyzed by dividing the peak fluorescence intensity (F) by the average resting fluorescence intensity (F<sub>0</sub>) after background subtraction. The time constant of decay (ms), which was calculated by fitting the decay portion of the fluorescence trace to a mono-exponential function. Analysis was made in IDL software (Exelis Visual Inc.) by homemade routines.

### **Isolation of sinoatrial node myocytes**

For cell isolation, SAN tissue strips were transferred into a “low-Ca<sup>2+</sup>–low-Mg<sup>2+</sup>” solution containing (in mM) 140 NaCl, 5.4 KCl, 0.5 MgCl<sub>2</sub>, 0.2 CaCl<sub>2</sub>, 1.2 KH<sub>2</sub>PO<sub>4</sub>, 50 taurine, and 5.5 D-glucose; 1 mg/mL BSA; and 5 HEPES-NaOH, adjusted to pH 6.9 with NaOH. Tissue was digested by Liberase TH (229 U/mL; Roche Diagnostics), elastase (1.9 U/mL; Boehringer Mannheim) during 15–20 minutes at 37°C, under manual mechanical agitation. Tissue strips were then washed and transferred into a modified Kraftbruehe (KB) medium containing (in mM) 70 L-glutamic acid, 20 KCl, 80 KOH, 10 ( $\pm$ )D- $\beta$ -OH-butyric acid, 10 KH<sub>2</sub>PO<sub>4</sub>, and 10 taurine; 1 mg/mL BSA; and 10 Hepes-KOH, adjusted to pH 7.4 with KOH. Single SAN myocytes were then isolated by agitation in KB solution at 37 °C. Cellular automaticity was restored by readapting the cells to a physiological extracellular Ca<sup>2+</sup> concentration by addition of 10 mM NaCl and 1.8 mM CaCl<sub>2</sub> to the Tyrode’s solution. The final cell storage solution contained (in mM/L) 100 NaCl, 35 KCl, 1.3 CaCl<sub>2</sub>, 0.7 MgCl<sub>2</sub>, 14 L-glutamic acid, 2 ( $\pm$ )D- $\beta$ -OH-butyric acid, 2 KH<sub>2</sub>PO<sub>4</sub>, and 2 taurine; and 1 mg/ml BSA (pH 7.4).

To image Ca<sup>2+</sup> on isolated SAN cells, they were loaded with 7  $\mu$ M Fluo-4/AM for 30 min at room temperature and viewed with confocal microscopy (see above). The amplitude of the 10 mM caffeine-evoked [Ca<sup>2+</sup>]<sub>i</sub> transients was used as an index of the SR Ca<sup>2+</sup> load.

### **Western blot**

SAN dissected from Sham and TAC mice were lysed by Bertin homogenizer with RIPA lysis buffer, run on 4%–20% or 3%–8% discontinuous gradient polyacrylamide gels depending on the M.W of the proteins, and transferred to NC membranes. NC membranes were incubated with blocking buffer of TBS with Tween-20 (1%) and BSA (3%). Membranes were then incubated with primary antibodies (listed in supplementary Table 1) diluted in 3% BSA TBST overnight at 4°C, followed by the secondary antibodies. Antigen complexes were visualized with iBright FL1000 (Invitrogen by Thermo Fisher Scientific) and quantified with Image J (NIH).

## Statistics

Analysis were conducted on n cells from N mice, using Graph Pad Prism 7 and the Origin 9 (Microcal) softwares. When conditions of parametric tests were meet, statistical comparisons between two groups were analyzed using Student's t-test (paired or unpaired for 2 dependent or independent groups, respectively) and using One- or two-way ANOVA for multiple comparisons, and results expressed as mean  $\pm$  SEM. The non-parametric Mann-Whitney test was used for WB and Ca<sup>2+</sup> spark parameters and presented as box (with median and 25-75% range) and whisker (Min-Max). A value of  $p < 0.05$  was considered significant.

## Results

### ***TAC induced congestive heart failure showed signs of SAN dysfunction.***

Since HF is frequently associated abnormalities of the pacemaker system, we first analyzed ECG in the pressure overload induced mouse model. 8-weeks after TAC, mice showed signs of congestive heart failure (HF group), characterized by increased Heart weight (HW)/Tibia length (TL), Lung weight (LW) /TL and left ventricle (LV) mass and reduced ejection fraction (EF) and fraction shortening (FS) compared to Sham animals (Table 1). Holter telemetric ECG recorded during 24 h in freely moving mice, as exemplified in fig. 1a (upper panels), showed at baseline longer QT and PR intervals but normal RR interval in HF group I (Table 2). However, the intrinsic heart rate, or the heart rate free of autonomic nervous system (ANS) influences, appeared altered (fig. 1a bottom panels). After ANS inhibition, the HR slowdown is greater in HF group compared with Sham group (fig. 1b). To reveal the SAN and ANS contributions, we conducted analysis of the HR variability, in the time- and frequency-domain, before and after propranolol and atropine injection (Table 3). At baseline, we observed a reduction of pNN5, reflecting a reduced parasympathetic activity in HF group, whereas the total autonomic variability (SDNN) and vagally mediated short-term HRV (RMSS) were not modified compared with sham group. The decreased of the time-domain HRV indices following ANS blockade in Sham group, is prevented in HF group excepted for SDNN, implying on reduced pacemaker function. In addition, at baseline, the HRV related to baroreceptor activity and the respiratory cycle, as gauged by Low Frequency (LFreq) and High Frequency (HFreq) respectively, showed no change in HF group. However, we observed an increased Very Low Frequency (VLFreq), which denotes an enhanced SAN spectral contribution to HRV in HF group [40]. After ANS blockade, the LFreq reduction and HFreq increase observed in HF group was less than those observed in Sham group, whereas VLFreq reduction was greater.

Taken together, these results indicate that our TAC induced congestive HF mouse model showed SAN dysfunction.

### ***Ca<sup>2+</sup> handling is depressed in sinoatrial node preparations from HF mice.***

SAN automaticity is dependent on synergetic interplay of voltage- and calcium-dependent mechanisms. Even if we observed a downregulation of protein expression level of HCN4 (fig.1 c) in HF group, as consistently observed [24], little is known on rhythmic spontaneous sarcoplasmic reticulum Ca<sup>2+</sup> release in HF SAN dysfunction. We thus recorded *ex vivo* the spontaneous [Ca<sup>2+</sup>]<sub>i</sub>

transients of Fluo-4AM-loaded SAN cells within the intact tissue (from 5 Sham and 7 HF mice) by confocal microscopy [39]. Fig. 1d shows representative line scan confocal images and corresponding fluorescent traces of SAN cells from a Sham and a HF mouse. The spontaneous  $[Ca^{2+}]_i$  transient rate, measured between consecutive spontaneous  $[Ca^{2+}]_i$  transients at their maximal upstroke, was lower in HF than in Sham cells (fig. 1 e), consistent with the decrease in intrinsic HR after ANS blockade in-vivo (fig. 1 a, b).

The  $Ca^{2+}$  handling dynamics were also altered in HF group as shown in fig. 2a. While the time to peak showed no difference between two groups (fig. 2 b), in HF SAN cells the  $[Ca^{2+}]_i$  transients peak (F/F0) was lower (fig. 2 c) and decay time (fig. 2d) longer than in Sham SAN cells. The latter being mainly dependent on the  $Ca^{2+}$  extrusion by NCX and SERCA function controlled by phospholamban (PLB), we compared their protein expression levels by Western blot in dissected SAN tissues from Sham and HF mice. The protein expression level of NCX was decreased in HF group (fig. 3 a). Whereas SERCA expression level was maintained in HF group (fig. 3 b), the total PLB level was higher than in Sham group (fig. 3 c), leading to an increase in the ratio of PLB over SERCA (fig. 3 d). In addition, the phosphorylation status of PLB, which relieved its inhibitory effect on SERCA, is altered. Whereas the levels of S16 PKA-dependent phosphorylation were not significantly modified (fig. 3 e), the PLB phosphorylation levels at the T17 CaMKII site were decreased in HF group (fig.3 f). Those changes on PLB might reduce SERCA function contributed to the prolonged decay of the spontaneous SAN  $[Ca^{2+}]_i$  transients in HF group. Indeed, estimation of SR  $Ca^{2+}$  content by rapid caffeine application on isolated SAN cells showed smaller amplitude of the caffeine-evoked  $[Ca^{2+}]_i$  transient in HF than in Sham SAN cells (fig. 4), indicating reduced SR  $Ca^{2+}$  load related to reduced SERCA function. As one might notice in displayed examples in fig.4a, isolated SAN cells from HF group show lower frequency, lower amplitude and longer duration of spontaneous  $[Ca^{2+}]_i$  transients as in intact SAN tissues.

To further analyze SAN  $Ca^{2+}$  dynamics, and the degree of  $Ca^{2+}$  clock coupling, we analyzed diastolic  $Ca^{2+}$  release events during the diastolic phase that were observed as  $Ca^{2+}$  sparks (fig. 5 a). We observed a lower  $Ca^{2+}$  sparks frequency in HF group (fig. 5 b). While the sparks width maintained in HF group (fig. 5 c), the amplitude was weaker (fig. 5 d), and the duration was shorter (fig. 5 e) in HF group. Meanwhile, the time to peak of the sparks was also shorter in HF group. (fig. 5 f), which may refer to a shorter opening time of the RyR2 channels. Moreover, the mass of the  $Ca^{2+}$  sparks, calculated as the amplitude  $\times$  width  $\times$  duration, was smaller in the HF cells, indicating that less  $Ca^{2+}$  is released from each  $Ca^{2+}$  spark in HF group (fig. 5 g).

The less frequent and smaller SAN cells  $Ca^{2+}$  sparks in HF group might also indicate an alteration in the RyR2. We thus evaluated RyR2 protein expression level as well as its phosphorylation status by Western blots in intact SAN tissues. We found that the total RyR2 expression was lower in SAN from HF mice compared to Sham mice (fig. 6 a). Although RyR2 phosphorylation level at S2808, supposedly PKA site, was similar in both groups (fig. 6 b), the phosphorylation level at S2814, CaMKII site was unequivocally decreased in HF group (fig. 6 c).

### ***CaMKII signaling is decreased in HF group***

We were surprised to find that a reduction of RyR2- S2814 phosphorylation in SAN from HF mice, since it classically augmented in the ventricles [41-43]. Indeed, in the ventricles of the same mice we observed an increase of the phosphorylation level at S2814 CaMKII site in the HF ventricles compared with Sham ventricles (fig. 6 d), indicating a different regulation during HF of the SAN with respect to the ventricles within the same heart. We next analyzed whether these lower phosphorylation level might be related to higher phosphatase expression or to less CaMKII expression and/or activity in SAN intact HF tissue. We found that the total expression level of phosphatases (fig. 6 e) and CaMKII (fig. 6 f) were not different between Sham and HF SANs. However, the CaMKII phosphorylation level, indicator of its activity, is reduced in the SAN from HF mice compared with Sham mice (fig. 6 f), to opposite of what we observed in ventricles (fig. 6 g), suggesting that the CaMKII signaling is differently modulated in HF SAN and ventricles.

To test the functional effect of this HF SAN CaMKII alterations, we next analyzed the selective CaMKII inhibitor effect, KN93, on spontaneous SAN  $[Ca^{2+}]_i$  transients in cells from both groups (fig. 7 a). The reduction of spontaneous  $[Ca^{2+}]_i$  transient rate by KN93 was smaller in HF SAN cells (fig. 7 b), whereas its inactive derivative, KN92, failed to affect the  $[Ca^{2+}]_i$  transient rate in either group (fig. 7 c).

## ***Discussion***

The sinus node dysfunction has been observed in patients with heart failure [7] as well as in different animal models. However, the underlying mechanism is still not clear. In addition of the impairment of the voltage clock due to HCN4 downregulation, our study uncovers the alteration of SAN  $Ca^{2+}$  clock under HF condition. We observe an over-all functional decrease of SAN  $Ca^{2+}$  homeostasis in HF mice, with altered  $Ca^{2+}$  transients dynamics and decreased  $Ca^{2+}$  sparks frequency and mass. We found that SERCA, RyR2 and NCX were downregulated, whereas PLB was upregulated, in association with a decrease of CaMKII activity, at opposite of HF ventricle.

Only few and somewhat controversial studies evaluated SAN  $Ca^{2+}$  clock function in HF. In intact dog SAN tissues after 2-week rapid pacing induced HF, reduced SR  $Ca^{2+}$  release has been suggested [44], consistent with our results. On the other hand, isolated SAN cardiomyocytes from volume and pressure overload HF rabbit model showed preserved  $Ca^{2+}$  transient characteristics and SR  $Ca^{2+}$  content [45]. However, the latter study reported slower  $Ca^{2+}$  transient decay due to reduced SERCA activity, as we observed in our model. Differences might be related to the used HF model and/or preparation. Nevertheless, both studies showed, at baseline or during  $\beta$ -adrenergic stimulation, reduced late diastolic  $[Ca^{2+}]_i$  elevation in HF SAN, consistent with the decrease in  $Ca^{2+}$  sparks occurrence and mass reported herein. In the SAN,  $Ca^{2+}$  sparks are considered as the initiating event of  $Ca^{2+}$  clock [22]. Our kinetic studies on SAN  $Ca^{2+}$  sparks showed that both the peak and duration of  $Ca^{2+}$  sparks decreased in the HF group. This resulted in smaller  $Ca^{2+}$  sparks and in decreased  $Ca^{2+}$  released by  $Ca^{2+}$  spark during diastolic phase. Together with the decreasing in  $Ca^{2+}$  spark frequency, it might explain the HF induced  $Ca^{2+}$  clock malfunction. In addition, the reduction of NCX channel expression level could affect the membrane depolarization and slow down the  $Ca^{2+}$

clock. Thus, our results show an impairment in the  $\text{Ca}^{2+}$  clock, which may amplify the decrease in membrane clock [46]. Together, the coupled-clock function is reduced, and results in decreasing of the intrinsic sinus automaticity, which may be compensated on HR by the increased sympathetic activation in HF.

There are two possible reasons for the decrease in  $\text{Ca}^{2+}$  sparks. First, the decreased SR  $\text{Ca}^{2+}$  load in HF SAN, which could be related to diminished SERCA function. We found that while the SERCA protein expression level was similar in HF and Sham SAN, there was an up-regulation and decreased phosphorylation level at PLB-T17 site of PLB. This may inhibit the  $\text{Ca}^{2+}$  SERCA reuptake, consistent with prolongation in the  $[\text{Ca}^{2+}]_i$  transients decay time. Second, the decreased RyR2 channel expression and phosphorylation level at RyR-S2814 might further alter the regulation of the  $\text{Ca}^{2+}$  clock. Of note, both effects on PLB and RyR2 with similar protein expression of CaMKII and SERCA has been in SANs from rabbits with HF [47].

Our results pointed out an alteration of the CaMKII signaling as a contributing mechanism in the SAN dysfunction in HF. It has been well documented that CaMKII-dependent phosphorylation of RyR2 and PLB affected SAN  $\text{Ca}^{2+}$  clock [48-51]. Based on measurement of CaMKII autophosphorylation and phosphorylation of the CaMKII targets (RyR2-S2814 and PLB-T17), our results suggested that reduced CaMKII activation might participate to HF SAN dysfunction. Although PKA might also mediated phosphorylation of the Thr17 CaMKII site on PLB [52] or phosphorylation of the Ser2815 CaMKII site on RyR2 [53] we did not observe PKA-dependent phosphorylation of these targets, suggesting a CaMKII specificity. Indeed, this Ser/Thr kinase is initially activated by the  $\text{Ca}^{2+}$ /Calmodulin complex, thus reduction of autonomous activity of CaMKII was consistent with reduced  $\text{Ca}^{2+}$  handling. Lower CaMKII contribution to SAN activity in HF was further emphasized using CaMKII inhibitor KN93. Although the CaMKII role to maintain basal SAN activity is controversial in mice [54,55], our results were consistent with CaMKII critical role during physiopathological stress. Moreover, CaMKII dysfunction might also participate to voltage-clock perturbation in HF. The transcription factor myocyte enhancer factor 2 (MEF2) activation through CaMKII phosphorylation of histone deacetylases (HDACs) is a common end point for cardiac hypertrophic signaling pathways [56] Now, it is known that the HCN4 expression is in part controlled through the HDAC MEF2 system [57]. Likewise, RyR2 promoter contains a consensus MEF2 site [58]. Altogether this suggested a vicious circle, in which  $\text{Ca}^{2+}$  clock malfunction begets CaMKII dysfunction that in turn worsens voltage- and  $\text{Ca}^{2+}$ - clocks, as the mechanism responsive for SAN dysfunction in HF.

Further, we denoted that CaMKII was affected in opposite way in SAN and ventricles. Likewise, HF differentially modulated HCN4 [59], as well as microRNA [60] in SAN and ventricles. This HF related difference was also observed between SAN and ectopic pacemaker cardiomyocytes of pulmonary veins [61]. The challenge is now to understand the molecular basis of these differences.

In summary, our study, for the first time, comprehensively revealed a defect in SAN  $\text{Ca}^{2+}$  handling in TAC-induced heart failure mouse model, which contributes to the intrinsic pacemaker dysfunction in HF by the mechanism that includes depression in the CaMKII signaling pathway.

## Acknowledgements

This work was funded by Inserm, University Paris-Saclay, ANR (ANR-19-CE-0031-01 to AMG), and PHC Maimonide to AMG, Israel Ministry of Science to Yael Yaniv and Jian-Bin XUE was a fellow from the CSC.

## References

1. Del Buono MG, Arena R, Borlaug BA, Carbone S, Canada JM, Kirkman DL, Garten R, Rodriguez-Miguel P, Guazzi M, Lavie CJ, Abbate A (2019) Exercise Intolerance in Patients With Heart Failure. *JACC State-of-the-Art Review* 73 (17):2209-2225. doi:10.1016/j.jacc.2019.01.072 *J* Journal of the American College of Cardiology
2. Kannel WB (2000) Incidence and epidemiology of heart failure. *Heart Fail Rev* 5 (2):167-173. doi:10.1023/A:1009884820941
3. Uretsky BF, Sheahan RG (1997) Primary prevention of sudden cardiac death in heart failure: will the solution be shocking? *J Am Coll Cardiol* 30 (7):1589-1597. doi:10.1016/s0735-1097(97)00361-6
4. Luu M, Stevenson WG, Stevenson LW, Baron K, Walden J (1989) Diverse mechanisms of unexpected cardiac arrest in advanced heart failure. *Circulation* 80 (6):1675-1680. doi:10.1161/01.cir.80.6.1675
5. Faggiano P, d'Aloia A, Gualeni A, Gardini A, Giordano A (2001) Mechanisms and immediate outcome of in-hospital cardiac arrest in patients with advanced heart failure secondary to ischemic or idiopathic dilated cardiomyopathy. *Am J Cardiol* 87 (5):655-657, A610-651. doi:10.1016/s0002-9149(00)01450-8
6. Stevenson WG, Stevenson LW, Middlekauff HR, Saxon LA (1993) Sudden death prevention in patients with advanced ventricular dysfunction. *Circulation* 88 (6):2953-2961. doi:10.1161/01.cir.88.6.2953
7. Sanders P, Kistler PM, Morton JB, Spence SJ, Kalman JM (2004) Remodeling of sinus node function in patients with congestive heart failure: reduction in sinus node reserve. *Circulation* 110 (8):897-903. doi:10.1161/01.CIR.0000139336.69955.AB
8. Janse MJ (2004) Electrophysiological changes in heart failure and their relationship to arrhythmogenesis. *Cardiovasc Res* 61 (2):208-217. doi:10.1016/j.cardiores.2003.11.018
9. Opthof T, Coronel R, Rademaker HME, Vermeulen JT, Wilms-Schopman FJG, Janse MJ (2000) Changes in Sinus Node Function in a Rabbit Model of Heart Failure With Ventricular Arrhythmias and Sudden Death. *Circulation* 101 (25):2975-2980. doi:10.1161/01.CIR.101.25.2975
10. Verkerk AO, Wilders R, Coronel R, Ravesloot JH, Verheijck EE (2003) Ionic remodeling of sinoatrial node cells by heart failure. *Circulation* 108 (6):760-766. doi:10.1161/01.CIR.0000083719.51661.B9
11. Du Y, Huang X, Wang T, Han K, Zhang J, Xi Y, Wu G, Ma A (2007) Downregulation of neuronal sodium channel subunits Nav1.1 and Nav1.6 in the sinoatrial node from volume-overloaded heart failure rat. *Pflugers Arch* 454 (3):451-459. doi:10.1007/s00424-007-0216-4
12. Jose AD, Taylor RR (1969) Autonomic blockade by propranolol and atropine to study intrinsic myocardial function in man. *J Clin Invest* 48 (11):2019-2031. doi:10.1172/JCI106167
13. Vatner SF, Higgins CB, Braunwald E (1974) Sympathetic and parasympathetic components of reflex tachycardia induced by hypotension in conscious dogs with and without heart failure. *Cardiovasc Res* 8 (2):153-161. doi:10.1093/cvr/8.2.153
14. Jose AD, Collison D (1970) The normal range and determinants of the intrinsic heart rate in man. *Cardiovasc Res* 4 (2):160-167. doi:10.1093/cvr/4.2.160
15. Alboni P, Menozzi C, Brignole M, Paparella N, Gaggioli G, Lolli G, Cappato R (1997) Effects of permanent pacemaker and oral theophylline in sick sinus syndrome the THEOPACE study: a randomized controlled trial. *Circulation* 96 (1):260-266. doi:10.1161/01.cir.96.1.260
16. Zweerink A, van der Lingen ACJ, Handoko ML, van Rossum AC, Allaart CP (2018) Chronotropic Incompetence in Chronic Heart Failure. *Circ Heart Fail* 11 (8):e004969. doi:10.1161/CIRCHEARTFAILURE.118.004969

17. Higginbotham MB, Morris KG, Conn EH, Coleman RE, Cobb FR (1983) Determinants of variable exercise performance among patients with severe left ventricular dysfunction. *Am J Cardiol* 51 (1):52-60. doi:10.1016/s0002-9149(83)80010-1
18. Weber KT, Kinasewitz GT, Janicki JS, Fishman AP (1982) Oxygen utilization and ventilation during exercise in patients with chronic cardiac failure. *Circulation* 65 (6):1213-1223. doi:10.1161/01.cir.65.6.1213
19. Brubaker PH, Joo KC, Stewart KP, Fray B, Moore B, Kitzman DW (2006) Chronotropic incompetence and its contribution to exercise intolerance in older heart failure patients. *J Cardiopulm Rehabil* 26 (2):86-89. doi:10.1097/00008483-200603000-00007
20. Benes J, Kotrc M, Borlaug BA, Lefflerova K, Jarolim P, Bendlova B, Jabor A, Kautzner J, Melenovsky V (2013) Resting heart rate and heart rate reserve in advanced heart failure have distinct pathophysiologic correlates and prognostic impact: a prospective pilot study. *JACC Heart Fail* 1 (3):259-266. doi:10.1016/j.jchf.2013.03.008
21. Maltsev VA, Vinogradova TM, Lakatta EG (2006) The emergence of a general theory of the initiation and strength of the heartbeat. *J Pharmacol Sci* 100 (5):338-369. doi:10.1254/jphs.cr0060018
22. Yaniv Y, Lakatta EG, Maltsev VA (2015) From two competing oscillators to one coupled-clock pacemaker cell system. *Front Physiol* 6:28. doi:10.3389/fphys.2015.00028
23. Lakatta EG, DiFrancesco D (2009) What keeps us ticking: a funny current, a calcium clock, or both? *J Mol Cell Cardiol* 47 (2):157-170. doi:10.1016/j.yjmcc.2009.03.022
24. Dobrzynski H, Boyett MR, Anderson RH (2007) New insights into pacemaker activity: promoting understanding of sick sinus syndrome. *Circulation* 115 (14):1921-1932. doi:10.1161/CIRCULATIONAHA.106.616011
25. Lakatta EG, Maltsev VA, Vinogradova TM (2010) A coupled SYSTEM of intracellular Ca<sup>2+</sup> clocks and surface membrane voltage clocks controls the timekeeping mechanism of the heart's pacemaker. *Circ Res* 106 (4):659-673. doi:10.1161/CIRCRESAHA.109.206078
26. Bogdanov KY, Vinogradova TM, Lakatta EG (2001) Sinoatrial nodal cell ryanodine receptor and Na<sup>(+)</sup>-Ca<sup>(2+)</sup> exchanger: molecular partners in pacemaker regulation. *Circ Res* 88 (12):1254-1258. doi:10.1161/hh1201.092095
27. Lipskaia L, Chemaly ER, Hadri L, Lompre AM, Hajjar RJ (2010) Sarcoplasmic reticulum Ca<sup>(2+)</sup> ATPase as a therapeutic target for heart failure. *Expert Opin Biol Ther* 10 (1):29-41. doi:10.1517/14712590903321462
28. Logantha SJR, Stokke MK, Atkinson AJ, Kharche SR, Parveen S, Saeed Y, Sjaastad I, Sejersted OM, Dobrzynski H (2016) Ca<sup>2+</sup>-Clock-Dependent Pacemaking in the Sinus Node Is Impaired in Mice with a Cardiac Specific Reduction in SERCA2 Abundance. *Circ Res* 117 (197). doi:10.3389/fphys.2016.00197
29. Yaniv Y, Sirenko S, Ziman BD, Spurgeon HA, Maltsev VA, Lakatta EG (2013) New evidence for coupled clock regulation of the normal automaticity of sinoatrial nodal pacemaker cells: bradycardic effects of ivabradine are linked to suppression of intracellular Ca<sup>(2+)</sup> cycling. *J Mol Cell Cardiol* 62:80-89. doi:10.1016/j.yjmcc.2013.04.026
30. Gomez AM, Valdivia HH, Cheng H, Lederer MR, Santana LF, Cannell MB, McCune SA, Altschuld RA, Lederer WJ (1997) Defective excitation-contraction coupling in experimental cardiac hypertrophy and heart failure. *Science* 276 (5313):800-806. doi:10.1126/science.276.5313.800
31. Chen Y, Escoubet B, Prunier F, Amour J, Simonides WS, Vivien B, Lenoir C, Heimbürger M, Choqueux C, Gellen B, Riou B, Michel JB, Franz WM, Mercadier JJ (2004) Constitutive cardiac overexpression of sarcoplasmic/endoplasmic reticulum Ca<sup>2+</sup>-ATPase delays myocardial failure after myocardial infarction in rats at a cost of increased acute arrhythmias. *Circulation* 109 (15):1898-1903. doi:10.1161/01.CIR.0000124230.60028.42
32. Prunier F, Chen Y, Gellen B, Heimbürger M, Choqueux C, Escoubet B, Michel JB, Mercadier JJ (2005) Left ventricular SERCA2a gene down-regulation does not parallel ANP gene up-regulation during post-MI remodelling in rats. *Eur J Heart Fail* 7 (5):739-747. doi:10.1016/j.ejheart.2004.10.007
33. Eisner DA, Caldwell JL, Kistamas K, Trafford AW (2017) Calcium and Excitation-Contraction Coupling in the Heart. *Circ Res* 121 (2):181-195. doi:10.1161/CIRCRESAHA.117.310230
34. Guo A, Zhang C, Wei S, Chen B, Song LS (2013) Emerging mechanisms of T-tubule remodelling in heart failure. *Cardiovasc Res* 98 (2):204-215. doi:10.1093/cvr/cvt020
35. Furihata T, Kinugawa S, Takada S, Fukushima A, Takahashi M, Homma T, Masaki Y, Tsuda M, Matsumoto J, Mizushima W, Matsushima S, Yokota T, Tsutsui H (2016) The experimental model of transition from compensated cardiac hypertrophy to failure created by transverse aortic constriction in mice. *Int J Cardiol Heart Vasc* 11:24-28. doi:10.1016/j.ijcha.2016.03.007
36. Vinet L, Rouet-Benzineb P, Marniquet X, Pellegrin N, Mangin L, Louedec L, Samuel JL, Mercadier JJ (2008) Chronic doxycycline exposure accelerates left ventricular hypertrophy and progression to heart failure in mice

- after thoracic aorta constriction. *Am J Physiol Heart Circ Physiol* 295 (1):H352-360.  
doi:10.1152/ajpheart.01101.2007
37. Cesarovic N, Jirkof P, Rettich A, Arras M (2011) Implantation of radiotelemetry transmitters yielding data on ECG, heart rate, core body temperature and activity in free-moving laboratory mice. *J Vis Exp* (57).  
doi:10.3791/3260
38. Behar JA, Rosenberg AA, Weiser-Bitoun I, Shemla O, Alexandrovich A, Konyukhov E, Yaniv Y (2018) PhysioZoo: A Novel Open Access Platform for Heart Rate Variability Analysis of Mammalian Electrocardiographic Data. *Front Physiol* 9:1390. doi:10.3389/fphys.2018.01390
39. Wang YY, Mesirca P, Marques-Sule E, Zahradnikova A, Jr., Villejoubert O, D'Ocon P, Ruiz C, Domingo D, Zorio E, Mangoni ME, Benitah JP, Gomez AM (2017) RyR2R420Q catecholaminergic polymorphic ventricular tachycardia mutation induces bradycardia by disturbing the coupled clock pacemaker mechanism. *JCI Insight* 2 (8). doi:10.1172/jci.insight.91872
40. Rosenberg AA, Weiser-Bitoun I, Billman GE, Yaniv Y (2020) Signatures of the autonomic nervous system and the heart's pacemaker cells in canine electrocardiograms and their applications to humans. *Sci Rep* 10 (1):9971. doi:10.1038/s41598-020-66709-z
41. Curran J, Brown KH, Santiago DJ, Pogwizd S, Bers DM, Shannon TR (2010) Spontaneous Ca waves in ventricular myocytes from failing hearts depend on Ca<sup>2+</sup>-calmodulin-dependent protein kinase II. *J Mol Cell Cardiol* 49 (1):25-32. doi:10.1016/j.yjmcc.2010.03.013
42. Anderson ME, Brown JH, Bers DM (2011) CaMKII in myocardial hypertrophy and heart failure. *J Mol Cell Cardiol* 51 (4):468-473. doi:10.1016/j.yjmcc.2011.01.012
43. Swaminathan PD, Purohit A, Hund TJ, Anderson ME (2012) Calmodulin-dependent protein kinase II: linking heart failure and arrhythmias. *Circ Res* 110 (12):1661-1677. doi:10.1161/CIRCRESAHA.111.243956
44. Shinohara T, Park HW, Han S, Shen MJ, Maruyama M, Kim D, Chen PS, Lin SF (2010) Ca<sup>2+</sup> clock malfunction in a canine model of pacing-induced heart failure. *J Mol Cell Cardiol* 49 (6):H1805-1811. doi:10.1152/ajpheart.00723.2010
45. Verkerk AO, van Borren MM, van Ginneken AC, Wilders R (2015) Ca<sup>2+</sup> cycling properties are conserved despite bradycardic effects of heart failure in sinoatrial node cells. *Front Physiol* 6:18. doi:10.3389/fphys.2015.00018
46. Zicha S, Fernandez-Velasco M, Lonardo G, L'Heureux N, Nattel S (2005) Sinus node dysfunction and hyperpolarization-activated (HCN) channel subunit remodeling in a canine heart failure model. *Cardiovasc Res* 66 (3):472-481. doi:10.1016/j.cardiores.2005.02.011
47. Chang SL, Chuang HL, Chen YC, Kao YH, Lin YK, Yeh YH, Chen SA, Chen YJ (2017) Heart failure modulates electropharmacological characteristics of sinoatrial nodes. *Exp Ther Med* 13 (2):771-779. doi:10.3892/etm.2016.4015
48. Vinogradova TM, Zhou YY, Bogdanov KY, Yang D, Kuschel M, Cheng H, Xiao RP (2000) Sinoatrial node pacemaker activity requires Ca<sup>2+</sup>/calmodulin-dependent protein kinase II activation. *Circ Res* 87 (9):760-767. doi:10.1161/01.res.87.9.760
49. Li Y, Sirenko S, Riordon DR, Yang D, Spurgeon H, Lakatta EG, Vinogradova TM (2016) CaMKII-dependent phosphorylation regulates basal cardiac pacemaker function via modulation of local Ca<sup>2+</sup> releases. *Am J Physiol Heart Circ Physiol* 311 (3):H532-544. doi:10.1152/ajpheart.00765.2015
50. Luo M, Guan X, Luczak ED, Lang D, Kutschke W, Gao Z, Yang J, Glynn P, Sossalla S, Swaminathan PD, Weiss RM, Yang B, Rokita AG, Maier LS, Efimov IR, Hund TJ, Anderson ME (2013) Diabetes increases mortality after myocardial infarction by oxidizing CaMKII. *J Clin Invest* 123 (3):1262-1274. doi:10.1172/JCI65268
51. Wu Y, Anderson ME (2014) CaMKII in sinoatrial node physiology and dysfunction. *Front Pharmacol* 5:48. doi:10.3389/fphar.2014.00048
52. Said M, Mundina-Weilenmann C, Vittone L, Mattiazzi A (2002) The relative relevance of phosphorylation of the Thr(17) residue of phospholamban is different at different levels of beta-adrenergic stimulation. *Pflugers Arch* 444 (6):801-809. doi:10.1007/s00424-002-0885-y
53. Ferrero P, Said M, Sanchez G, Vittone L, Valverde C, Donoso P, Mattiazzi A, Mundina-Weilenmann C (2007) Ca<sup>2+</sup>/calmodulin kinase II increases ryanodine binding and Ca<sup>2+</sup>-induced sarcoplasmic reticulum Ca<sup>2+</sup> release kinetics during beta-adrenergic stimulation. *J Mol Cell Cardiol* 43 (3):281-291. doi:10.1016/j.yjmcc.2007.05.022
54. Zhang R, Khoo MS, Wu Y, Yang Y, Grueter CE, Ni G, Price EE, Jr., Thiel W, Guatimosim S, Song LS, Madu EC, Shah AN, Vishnivetskaya TA, Atkinson JB, Gurevich VV, Salama G, Lederer WJ, Colbran RJ, Anderson ME (2005) Calmodulin kinase II inhibition protects against structural heart disease. *Nat Med* 11 (4):409-417. doi:10.1038/nm1215

55. Wu Y, Gao Z, Chen B, Koval OM, Singh MV, Guan X, Hund TJ, Kutschke W, Sarma S, Grumbach IM, Wehrens XH, Mohler PJ, Song LS, Anderson ME (2009) Calmodulin kinase II is required for fight or flight sinoatrial node physiology. *Proc Natl Acad Sci U S A* 106 (14):5972-5977. doi:10.1073/pnas.0806422106
56. Backs J, Olson EN (2006) Control of cardiac growth by histone acetylation/deacetylation. *Circ Res* 98 (1):15-24. doi:10.1161/01.RES.0000197782.21444.8f
57. Vedantham V, Evangelista M, Huang Y, Srivastava D (2013) Spatiotemporal regulation of an Hcn4 enhancer defines a role for Mef2c and HDACs in cardiac electrical patterning. *Dev Biol* 373 (1):149-162. doi:10.1016/j.ydbio.2012.10.017
58. Nishida K, Otsu K, Hori M, Kuzuya T, Tada M (1996) Cloning and characterization of the 5'-upstream regulatory region of the Ca(2+)-release channel gene of cardiac sarcoplasmic reticulum. *Eur J Biochem* 240 (2):408-415. doi:10.1111/j.1432-1033.1996.0408h.x
59. Kuwabara Y, Kuwahara K, Takano M, Kinoshita H, Arai Y, Yasuno S, Nakagawa Y, Igata S, Usami S, Minami T, Yamada Y, Nakao K, Yamada C, Shibata J, Nishikimi T, Ueshima K, Nakao K (2013) Increased expression of HCN channels in the ventricular myocardium contributes to enhanced arrhythmicity in mouse failing hearts. *J Am Heart Assoc* 2 (3):e000150. doi:10.1161/JAHA.113.000150
60. Yanni J, D'Souza A, Wang Y, Li N, Hansen BJ, Zakharkin SO, Smith M, Hayward C, Whitson BA, Mohler PJ, Janssen PML, Zeef L, Choudhury M, Zi M, Cai X, Logantha S, Nakao S, Atkinson A, Petkova M, Doris U, Ariyaratnam J, Cartwright EJ, Griffiths-Jones S, Hart G, Fedorov VV, O'ceandy D, Dobrzynski H, Boyett MR (2020) Silencing miR-370-3p rescues funny current and sinus node function in heart failure. *Sci Rep* 10 (1):11279. doi:10.1038/s41598-020-67790-0
61. Chan CS, Lin YK, Chen YC, Lu YY, Chen SA, Chen YJ (2019) Heart Failure Differentially Modulates Natural (Sinoatrial Node) and Ectopic (Pulmonary Veins) Pacemakers: Mechanism and Therapeutic Implication for Atrial Fibrillation. *Int J Mol Sci* 20 (13). doi:10.3390/ijms20133224

## Tables

**Table 1. Macroscopic parameters of mice**

|                               | <b>Sham</b><br>(n=12) | <b>HF</b><br>(n=12) |
|-------------------------------|-----------------------|---------------------|
| <b>Body parameters</b>        |                       |                     |
| Lung Weight/Tibia Length      | 9.52±0.25             | 15.41±1.52 *        |
| Heart Weight/Tibia Length     | 9.80±0.19             | 16.78±1.05 *        |
| <b>Echocardiographic data</b> |                       |                     |
| FS, %                         | 27.62±1.00            | 13.62±0.91*         |
| EF, %                         | 60.38±1.62            | 33.94±2.03*         |
| IVSd, mm                      | 0.64±0.03             | 0.65±0.03           |
| IVSs, mm                      | 0.92±0.03             | 0.81±0.04 *         |
| LVIDd, mm                     | 3.76±0.11             | 4.44±0.15 *         |
| LVIDs, mm                     | 2.73±0.10             | 3.83±0.14 *         |
| LVPWd, mm                     | 0.68±0.04             | 0.78±0.08           |
| LVPWs, mm                     | 0.84±0.03             | 0.86±0.08           |
| LV mass, mg                   | 81.60±5.97            | 124.95±18.99 *      |
| Heart Rate, (beats/min)       | 470±10                | 486±11              |

Abbreviations: FS, Fractional Shortening; EF, Ejection Fraction; IVSd, Interventricular septal thickness at end-diastole; IVSs, Interventricular septal thickness at end-systole; LVIDd, Left ventricular internal dimension at end-diastole; LVIDs, Left ventricular internal dimension at end-systole; LVPWd, left ventricular posterior wall thickness at end-diastole; LVPWs, left ventricular posterior wall thickness at end-systole. One-way ANOVA followed by Bonferroni test were used. All the values are mean ± SEM. \*, p<0.05 versus Sham group

**Table 2 Baseline ECG parameters in conscious mice**

| parameters | Sham (N=7) |                    | HF (N=5) |                    |
|------------|------------|--------------------|----------|--------------------|
|            | Day        | Night              | Day      | Night              |
| RR, ms     | 120±4      | 108±4 <sup>#</sup> | 123±5    | 106±3 <sup>#</sup> |
| PR, ms     | 38±0.5     | 36±0.4             | 41±1.6*  | 37±1.6             |
| QRS, ms    | 8.6±0.17   | 8.7±0.12           | 9.0±0.30 | 9.0±0.32           |
| QT, ms     | 42±0.5     | 41±0.5             | 51±3.2*  | 47±2.8             |

Two-way repeated ANOVA followed by Bonferroni test was used. #, p<0.05 versus the same group in the day period. \*, p<0.05 versus Sham in the same period.

**Table 3. Heart-rate variability parameters in conscious Sham and TAC mice during the daytime**

| Parameters                | Sham (n=7) |                        | HF (n=5)              |                         |
|---------------------------|------------|------------------------|-----------------------|-------------------------|
|                           | Basal      | ANS inhibition         | Basal                 | ANS inhibition          |
| Time domain parameters    |            |                        |                       |                         |
| SDNN (ms)                 | 8.83±0.95  | 2±0.25 <sup>#</sup>    | 6.89±1.18             | 3.9±1.14                |
| RMSSD (ms)                | 5.03±0.64  | 2.4±0.34 <sup>#</sup>  | 3.38±0.99             | 3.95±1.33               |
| pNN5 (%)                  | 22.5±5.2   | 0.35±0.18 <sup>#</sup> | 3.52±1.2 <sup>*</sup> | 1.49±1.25               |
| Frequency parameters      |            |                        |                       |                         |
| VLFreq/Total (n.u)        | 58.5±1.0   | 48.2±6.1               | 64.6±1.9              | 37.9±2.4 <sup>#</sup>   |
| LFreq Normalization (n.u) | 66.2±4.3   | 27.4±5.2 <sup>#</sup>  | 76.3±2.5              | 53.4±11.2 <sup>#*</sup> |
| HFreq Normalization (n.u) | 33.8±4.3   | 72.6±5.2 <sup>#</sup>  | 23.7±2.5              | 46.6±11.2 <sup>#*</sup> |
| LFreq/HFfreq (n.u)        | 2.79±0.43  | 0.43±0.11 <sup>#</sup> | 3.61±0.53             | 0.82±0.21               |

Abbreviations: SDNN: Standard deviation of the number of pairs of successive NN (Normal to Normal RR intervals); RMSSD: Root mean square of the successive differences; PNN5: The proportion of the number of pairs of successive NN (R-R) intervals that differ by more than 5 ms divided by the total number of NN (R-R) intervals. In frequency parameters, the measures shown are the normalized power (NORM) for each band (Very Low Frequency, VLFreq; Low Frequency, LFreq; and High Frequency, HFreq) and the ratio of LFreq to Hfreq. Two -way repeated ANOVA followed by Bonferroni test were used. All the values are mean ± SEM. \*, p<0.05 versus Sham group. #, p<0.05 versus the same group under basal condition.

## Figure and Legends

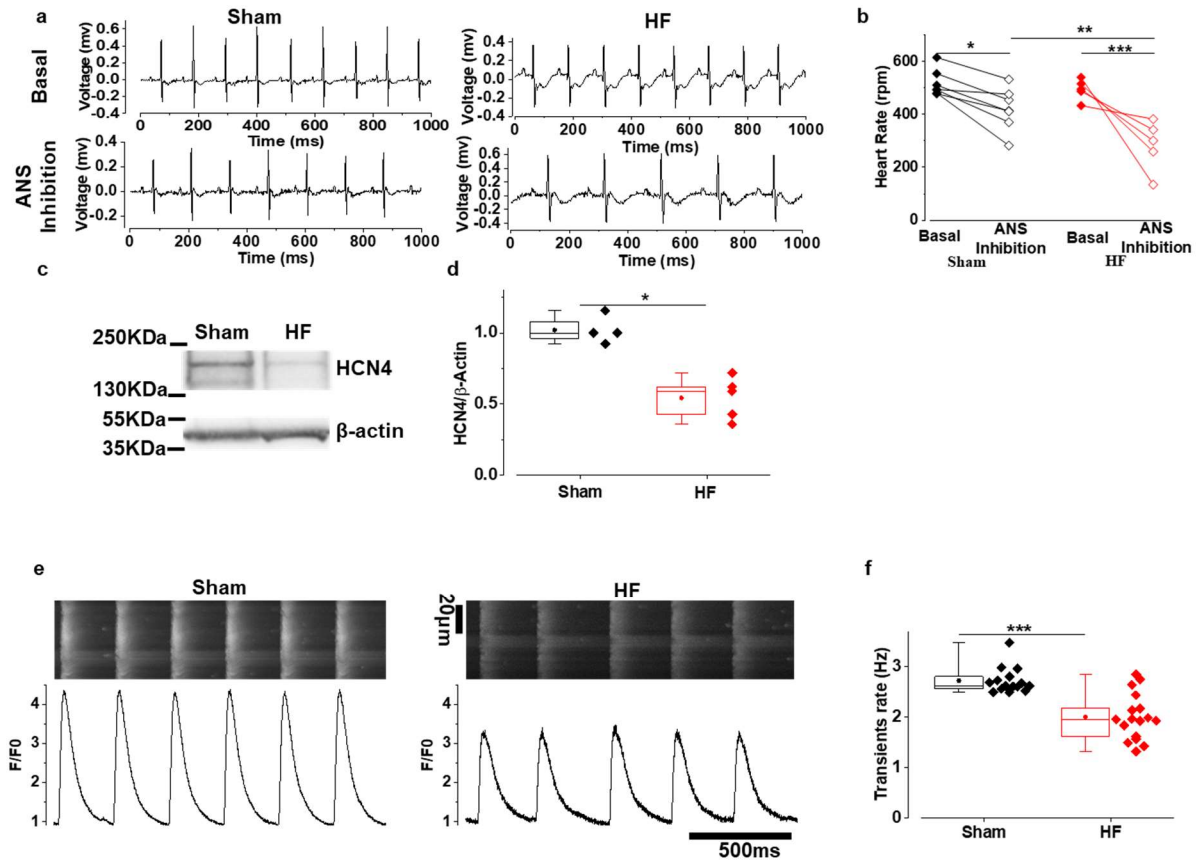


**Figure 1. The intrinsic Heart rate and the SAN cells firing rate are lower in HF mice** **a**, Representative examples of telemetric ECG traces (daytime) under basal and after atropine and propranolol injection (2mg/kg respectively, i.p) from Sham-operated and transverse aortic constriction-induced heart failure (HF) mice. **b**, Quantification of Heart rate (HR) under basal condition and upon ANS inhibition in the same mice. **c and d**, Representative Western Blot and quantification of HCN4 protein expression levels. **e**, Examples of line scan images (0.25 ms per line) and corresponding fluorescence traces of Fluo-4, AM loaded SAN intact tissues. **f**, Quantification of spontaneous SAN  $[Ca^{2+}]_i$  transients rate from Sham and HF mice. The Two-way repeated ANOVA followed by Bonferroni test was used in **b**, \* $p < 0.05$ , \*\* $p < 0.01$  and \*\*\* $p < 0.001$ . The non-parametric Mann-Whitney test was used in **d** and **f**, \* $p < 0.05$  and \*\*\* $p < 0.001$ .

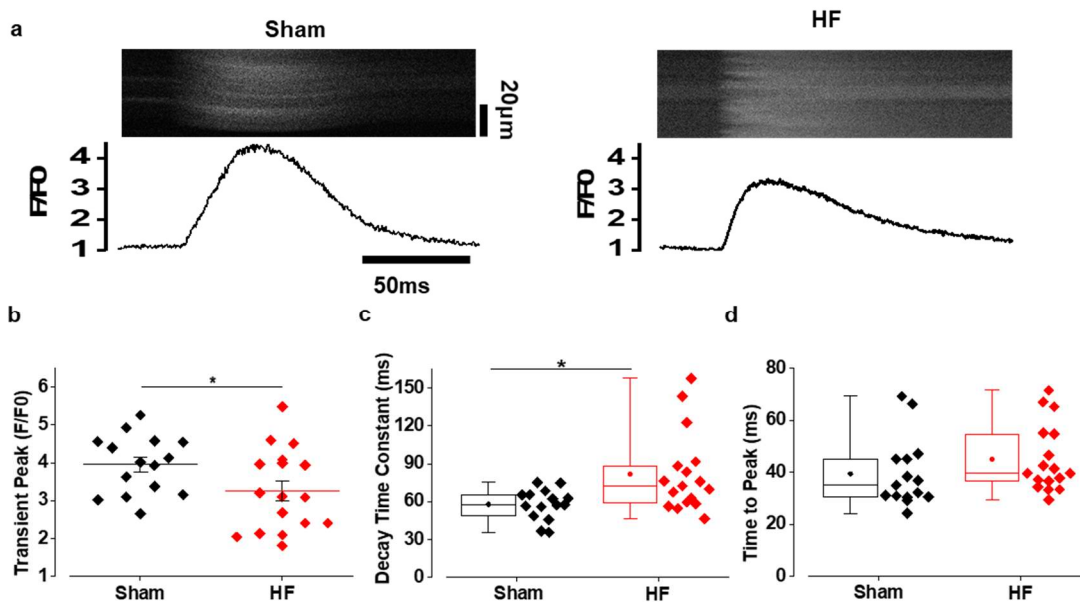


**Figure 2. The  $[Ca^{2+}]_i$  transient characteristics are altered in HF SAN cells.** **a**, Representative examples of line scan images (0.25 ms per line) and corresponding fluorescence traces of Fluo-4, AM loaded single cells from intact Sham and HF SAN tissues; **b**, Averaged amplitude of the  $[Ca^{2+}]_i$  transient measured as peak F/F0, where F is the maximum fluorescence and F0 the fluorescence during diastolic periods. **c and d**, Analyses of the  $[Ca^{2+}]_i$  transients kinetics (decay time constant and the time to peak, respectively). Decay time constant was obtained by fitting the descendent portion of the fluorescence trace to a single exponential function. The two-sample t-test was used in b, while the non-parametric Mann-Whitney test was used in c and d. \*p < 0.05.

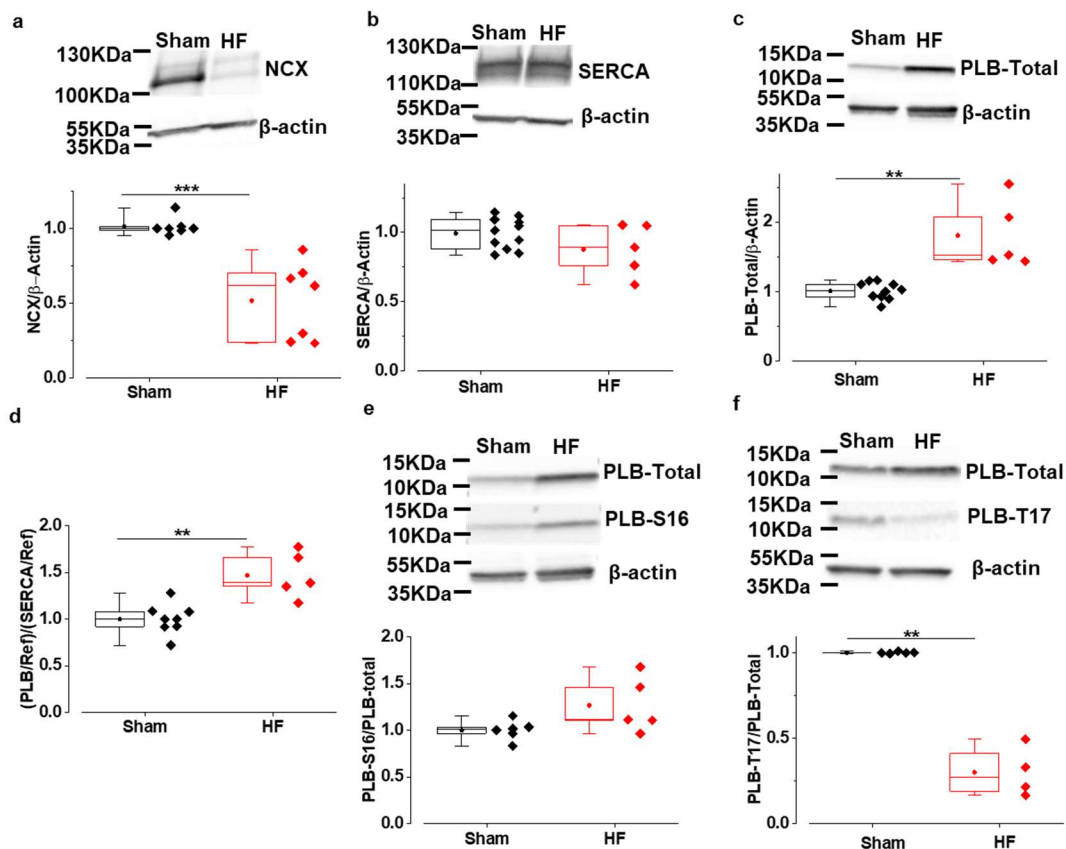


**Figure 3. NCX protein expression level decreased while total and phosphorylated PLB increased.** **a to c**, Representative Western Blots and quantification of protein expression levels of the Na<sup>+</sup>/Ca<sup>2+</sup> exchanger (NCX, **a**), the sarco/endoplasmic reticulum Ca<sup>2+</sup>-ATPase (SERCA, **b**) and the phospholamban (PLB, **c**) in SAN tissues from sham and HF mice. **d**, Calculated PLB over SERCA ratio for each studied sample. **e and f**. Representative Western Blots and quantification of phosphorylated PLB-S16 (**e**) and PLB-T17 (**f**) normalized by PLB-total. The non-parametric Mann-Whitney test was used. \*\*p<0.01 and \*\*\*p<0.001

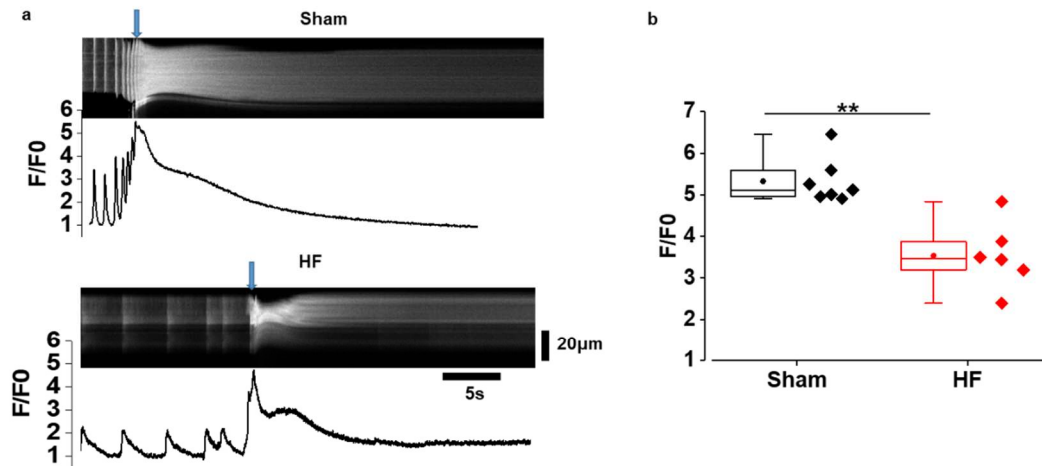


**Figure 4. SR Ca<sup>2+</sup> load decreased in isolated cells of HF SAN.** **a**, Line scan images (0.25 ms per line) of isolated SAN cardiomyocytes from Sham and HF mice before and during the Caffeine perfusion, the arrows indicate the time when caffeine is applied; **b**, Quantification of the caffeine-induced F/F0 as an index of the SR Ca<sup>2+</sup> load. The non-parametric Mann-Whitney test was used. \*\*p<0.01.

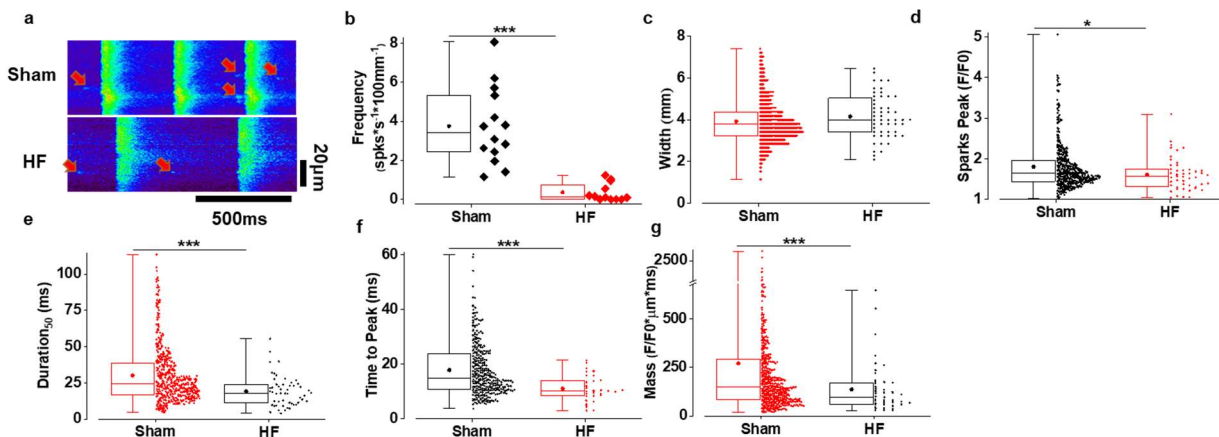


**Figure 5. Ca<sup>2+</sup> sparks are less frequent and smaller in HF SAN.** **a**. Representative line scan images (0.25 ms per line) of spontaneous beating cells from intact SAN; Arrows indicate Ca<sup>2+</sup> sparks.

**b.** Quantification of  $\text{Ca}^{2+}$  spark frequency (number of sparks/s/100 $\mu\text{m}$ ) in Sham and HF SAN; **c to g.** Analysis of  $\text{Ca}^{2+}$  spark characteristics (width in **c**, amplitude in **d**, half duration time in **e**; time to peak in **f**, and mass in **g**). For each  $\text{Ca}^{2+}$  spark the mass was calculated as amplitude  $\times$  width  $\times$  duration. The non-parametric Mann-Whitney test was used. \* $p < 0.05$  and \*\*\* $p < 0.001$ .

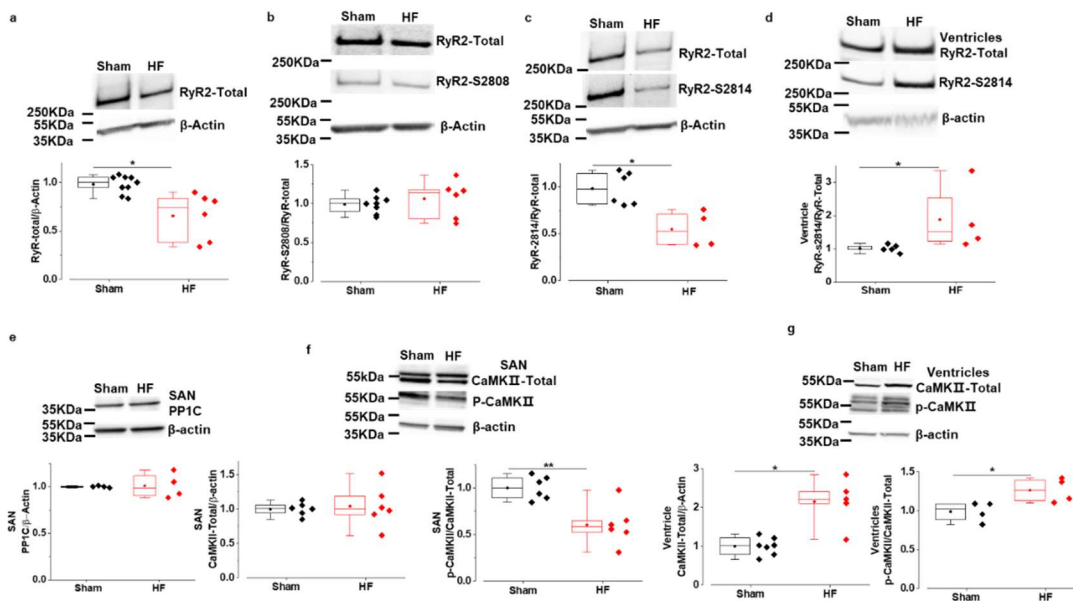


**Figure 6. RyR2 expression level and phosphorylation level decreased while CaMKII activation level decreased in HF SAN. a-c,** Representative Western Blots and quantification of RyR2-Total (**a**); RyR2-S2808 (**b**) and RyR2-S2814 (**c**) normalized to RyR2-total in SAN tissues from Sham and HF mice. **d,** Same as **c** but in left ventricles from the same mice. **e,** Representative Western Blots and quantification of PP1C in SAN. **F and g,** Representative Western Blots and quantification of total and phosphorylated CaMKII (normalized by CaMKII-total) in SAN tissues (**f**) and ventricles (**g**) from sham and HF mice. The non-parametric Mann-Whitney test was used; \* $p < 0.05$  and \*\* $p < 0.01$ .

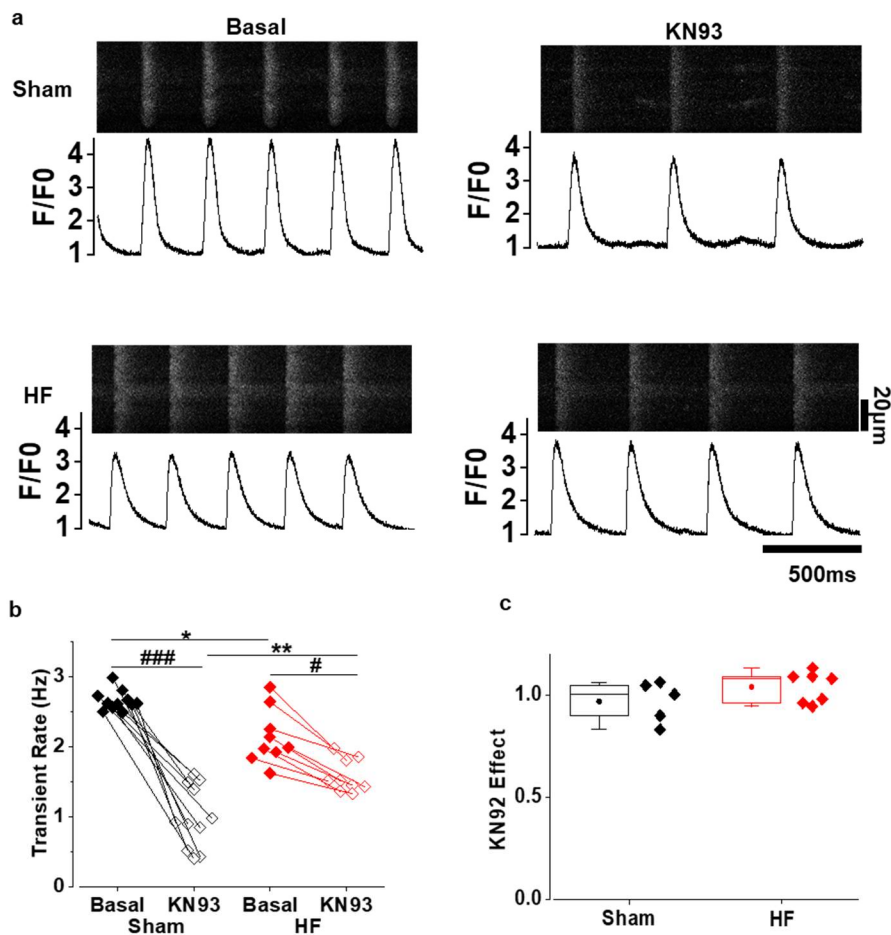


**Figure 7. The CaMKII inhibition by KN93 showed less effect in HF SAN tissue.** **a**, Superimposed line scan images (0.25 ms per line) and corresponding fluorescence traces, before and after 3-µM KN93 perfusion in the SAN preparation. **b**, Calculated spontaneous  $[Ca^{2+}]_i$  transients rate before and after KN93 perfusion. **c**, Normalized effect of KN92, the inactive analogue of KN93, on the  $[Ca^{2+}]_i$  transients rate. The Two-way repeated ANOVA followed by Bonferroni test was used in **b**, while the non-parametric Mann-Whitney test was used in **c**. \* $p < 0.05$ , \*\* $p < 0.01$  vs. Sham, # $p < 0.05$ , ### $p < 0.001$ .

## Supplemental material

**Supplemental Table 1: List of primary antibodies used for Western blot**

| <b>Protein</b>          | <b>Host</b> | <b>Dilution</b> | <b>Code</b> | <b>Source</b>     |
|-------------------------|-------------|-----------------|-------------|-------------------|
| <i>RyR2 total</i>       | mouse       | 1/1000          | MA3-916     | Thermo Scientific |
| <i>RyR2 P-Ser2808</i>   | rabbit      | 1/2000          | A010-30AP   | Badrilla          |
| <i>RyR2 P-Ser2814</i>   | rabbit      | 1/2000          | A010-31AP   | Badrilla          |
| <i>CaMK II P-Thr286</i> | rabbit      | 1/2000          | MA1-047     | Thermo Scientific |
| <i>CaMK II (pan)</i>    | rabbit      | 1/1000          | 3362S       | Cell signaling    |
| <i>SERCA</i>            | mouse       | 1/500           | SC-376235   | Santa Cruz        |
| <i>PLB total</i>        | rabbit      | 1/5000          | 8495S       | Cell Signaling    |
| <i>PLB P-Ser16</i>      | rabbit      | 1/5000          | A010-12     | Badrilla          |
| <i>PLB P-Thr17</i>      | rabbit      | 1/5000          | A010-13     | Badrilla          |
| <i>PPP1Ca+β HRP</i>     | Rabbit      | 1/5000          | EP1511Y     | abcam             |
| <i>HCN4</i>             | Rabbit      | 1/200           | APC-052     | Alomone labs      |
| <i>NCX</i>              | mouse       | 1/1000          | R3F1        | Swant             |
| <i>β-actin HRP</i>      | mouse       | 1/20000         | SC-47778    | Santa Cruz        |



## 3.2 The mysterious Hypertrophy group

In my work that is explained in the manuscript above, we divided the animals into two groups: Those who were subjected to TAC surgery to induce heart failure, and those with Sham operation to use as controls. To verify that TAC surgery worked, we measured the Ejection fraction by M mode echocardiography before sacrifice. On sacrifice, we measured body, heart, and lung weight, and tibia length.

Along with the experiments, we found that the KN93 had no effect on TAC group. However, there is a tendency on increasing the transient rate which confused us. When we reviewed our data, especially the body parameters of different mice, we observed that the severity of illness was different from mouse to mouse. We tried to divide the mice based on the ejection fraction. However, one of my colleagues (many thanks to Crozatier Bertrand) pointed out that even in the compensated hypertrophy, the EF also decreased. It is easy to understand because the surgery 'constricted' the aorta. The EF of compensated hypertrophy mice may decrease less than non-compensated one. Then we decided to divide the mice based on Lung weight (the pulmonary edema) which is a notable sign for congestive heart failure (This standard is from Mercadier Jean-Jacques, many thanks to him.)

While all TAC mice showed cardiac hypertrophy and depressed ejection fraction, some animals presented signs of congestive heart failure, which are included in the manuscript above, and other with no signs of congestion (no increased lung to body weight). We named this group hypertrophy group (Hyp) and did the experiments.

### ***3.2.1 Body parameters and HRV analysis***

In the body parameters we observed the Lung Weight was similar than Sham group while the Heart weight increased significantly, showing the cardiac hypertrophy. However, compared to HF group, this group shows less hypertrophy. (Table 3.2.1)

To evaluate the cardiac function, the results showed that the EF and FS are also decreased in Hyp group compared to Sham. Similarly, these two parameters are still less decreased compared to HF group. The mice in this group also showed a longer QT interval compared to Sham (data not shown). In all, although significant, this group showed a milder cardiac function decrease compared to HF group, so the results in this group are displayed in the middle of Sham and HF (Table 5).

**Table 5. Body parameters and Echocardiographic Data**

| Groups                        | Sham       | Hyp                     | HF                        |
|-------------------------------|------------|-------------------------|---------------------------|
| <b>Body parameters</b>        |            |                         |                           |
| Lung Weight/Tibia Length      | 9.52±0.25  | 9.71±0.21               | 15.41±1.52 <sup>a,b</sup> |
| Heart Weight/Tibia Length     | 9.80±0.19  | 13.50±0.50 <sup>a</sup> | 16.78±1.05 <sup>a,b</sup> |
| <b>Echocardiographic data</b> |            |                         |                           |
| FS, %                         | 27.62±1.00 | 19.01±0.76 <sup>a</sup> | 13.62±0.91 <sup>a,b</sup> |
| EF, %                         | 60.38±1.62 | 45.20±1.45 <sup>a</sup> | 33.94±2.03 <sup>a,b</sup> |
| IVSd, mm                      | 0.64±0.03  | 0.66±0.03               | 0.65±0.03                 |
| IVSs, mm                      | 0.92±0.03  | 0.88±0.04               | 0.81±0.04                 |
| LVIDd, mm                     | 3.76±0.11  | 4.20±0.08 <sup>a</sup>  | 4.44±0.15 <sup>a</sup>    |
| LVIDs, mm                     | 2.73±0.10  | 3.41±0.09 <sup>a</sup>  | 3.83±0.14 <sup>a,b</sup>  |
| LVPWd, mm                     | 0.68±0.04  | 0.68±0.04               | 0.78±0.08                 |
| LVPWs, mm                     | 0.84±0.03  | 0.82±0.04               | 0.86±0.08                 |
| LV mass, mg                   | 81.60±5.97 | 100.63±6.82             | 124.95±18.99 <sup>a</sup> |
| Heart Rate, (beats/min)       | 470±10     | 474±9                   | 486±11                    |

*Abbreviations: FS, Fraction Shortening; EF, Ejection Fraction; IVSd, Interventricular septal thickness at end-diastole; IVSs, Interventricular septal thickness at end-systole; LVIDd, Left ventricular internal dimension at end-diastole; LVIDs, Left ventricular internal dimension at end-systole; LVPWd, left ventricular posterior wall thickness at end-diastole; LVPWs, left ventricular posterior wall thickness at end-systole. One-way ANOVA followed by Bonferroni test were used. All the values are mean ± SEM. a, p<0.05 versus Sham group; b, p<0.05 versus Hyp group. N=12 in each group*

In HRV analysis, we meet the first striking point for Hyp group. While all the other parameters keep the same tendency than HF group, the PNN5 of Hyp showed no difference in basal condition compared to Sham (Table 6). However, after the ANS blockade, in Sham group PNN5 decreased significantly but in Hyp PNN5 was maintained compared to basal condition. This is really amazing, while SDNN, RMSSD and PNN5 describe the variability of the heart rate, and the pNN5 is correlated with the RMSSD and high frequency power and PNN5 is closely correlated with PNS activity. Meanwhile, in Hyp group, the RMSSD in ANS inhibition did not decrease significantly either.

**Table 6.** Heart-rate variability parameters in conscious Sham and TAC mice during the daytime

| Parameters | SHAM (n=7) | Hypertrophy (n=5) | Failure (n=5) |
|------------|------------|-------------------|---------------|
|------------|------------|-------------------|---------------|

|                               | Control   | ANS blockade | Control   | ANS blockade | Control     | ANS blockade  |
|-------------------------------|-----------|--------------|-----------|--------------|-------------|---------------|
| <b>Time domain parameters</b> |           |              |           |              |             |               |
| SDNN (ms)                     | 8.83±0.95 | 2±0.25#      | 7.8±0.9   | 3.1±0.6 #    | 6.89±1.18   | 3.9±1.14 #    |
| RMSSD (ms)                    | 5.03±0.64 | 2.4±0.34#    | 4.76±0.56 | 3.56±0.62    | 3.38±0.99   | 3.95±1.33     |
| pNN5 (%)                      | 22.5±5.2  | 0.35±0.18#   | 20.9±4.15 | 18.1±2.4*    | 3.52±1.2*\$ | 1.49±1.25\$   |
| <b>Frequency parameters</b>   |           |              |           |              |             |               |
| VLF/Total (%)                 | 58.5±1.0  | 48.2±6.1     | 59.4±1.7  | 32.6±3.7 #   | 64.6±1.9*   | 37.9±2.4 #    |
| LF Norm (%)                   | 66.2±4.3  | 27.4±5.2#    | 68.3±3.1  | 37.0±3.0 #   | 76.3±2.5    | 53.4±11.2 #*  |
| HF Norm (%)                   | 33.8±4.3  | 72.6±5.2#    | 31.7±3.1  | 63.0±3.0 #   | 23.7±2.5    | 46.6±11.2 # * |
| LF/HF (n.u)                   | 2.79±0.43 | 0.43±0.11#   | 2.78±0.37 | 0.65±0.12 #  | 3.61±0.53   | 0.82±0.21 #   |

*Abbreviations: SDNN: Standard deviation of The number of pairs of successive NN (Normal to Normal RR intervals); RMSSD: Root mean square of the successive differences-used for a good snapshot of the Autonomic Nervous System's Parasympathetic branch; PNN5: The proportion of The number of pairs of successive NN (R-R) intervals that differ by more than 5 ms divided by the total number of NN (R-R) intervals. Two-way ANOVA followed by Bonferroni test were used. All the values are mean ± SEM. \*, p<0.05 versus Sham group. #, p<0.05 versus the same group under basal condition.*

In ECG analysis, there was no difference between TAC group and Sham group, or no difference in between the two TAC groups (Fig.24). The intrinsic HR decreased to the same extend in the two TAC groups, and is significant slower than Sham group, revealing that the two TAC groups both showed SAN dysfunction.

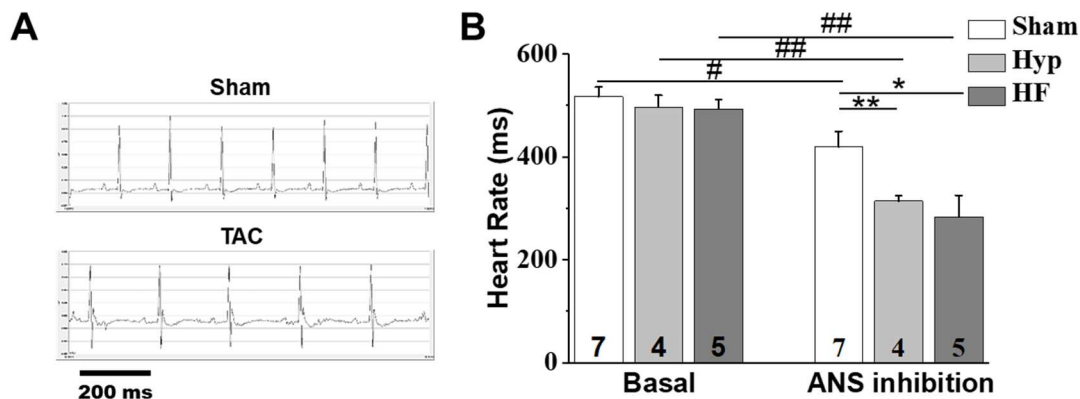


**Fig.24 Heart rate is lower in TAC mice under autonomic nerve system (ANS) blockade. A, Representative examples of ECG traces after atropine and propranolol injection. B, Heart rate (HR) under basal (day) and ANS inhibition situations. \*p<0.05, \*\*p<0.01 vs Sham; # p<0.05, ##p<0.01 vs. the same group. N indicates the number of mice**

### 3.2.2 Ca<sup>2+</sup> transients and Ca<sup>2+</sup> sparks

We also analyzed  $Ca^{2+}$  handling in this group. Fig.25 shows spontaneous  $[Ca^{2+}]_i$  transients. The  $Ca^{2+}$  transient rate is slower in hyp than in HF and the time to peak is longer than the other two groups. For the half time of duration (D50) the Hyp group is longer than it in Sham group, while no difference comparing with HF because of the slightly increase in HF group. And for the transient peak and the decay time, the Hyp group showed no different than the other two groups, but in average intermediate between Sham and HF (Fig.25).

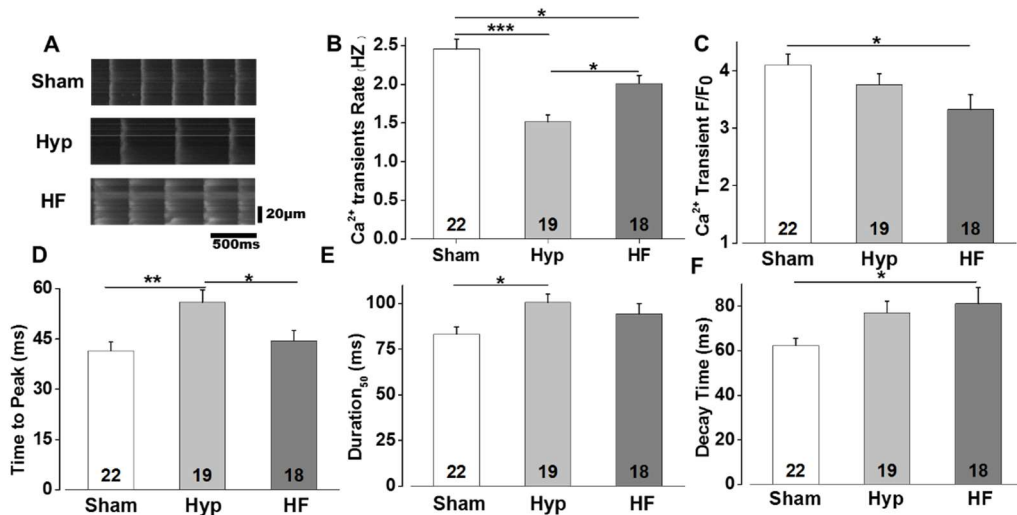


**Fig.25  $[Ca^{2+}]_i$  transients rate is slower and characteristics are significantly altered in SAN cells from TAC mice .** **A.** Line scan images (0.25 ms per line) over the calculated fluorescence traces. **B.** Spontaneous  $[Ca^{2+}]_i$  transients rate. **C.** Amplitude of the  $[Ca^{2+}]_i$  transient measured as peak  $F/F_0$ , where  $F$  is the maximum fluorescence and  $F_0$  the fluorescence during diastolic periods. **D.** Analyses of the  $[Ca^{2+}]_i$  transients kinetics, showed longer time to peak in Hyp group. **E.** longer duration at half maximum in Hyp group comparing with Sham and **F.** prolonged decay time in HF cells while only a tendency in Hyp group compared to Sham. Decay time constant was obtained by fitting the descendent portion of the fluorescence trace to a single exponential function. \* $p < 0.05$ , \*\* $p < 0.01$ , \*\*\* $p < 0.001$ .  $N$  indicates the number of cells from at least 5 different intact SAN preparations.

As we found slower  $[Ca^{2+}]_i$  transient spontaneous activity, we analyzed diastolic  $Ca^{2+}$  release.  $Ca^{2+}$  sparks frequency in the Hyp group showed a decrease compared to Sam group, but this decrease was less marked than in HF (Fig.26). There was significantly difference between each of the two groups and the 50% duration of the sparks also showed the similar change. The mass of the sparks also showed the same tendency but there was no significant difference between Hyp and HF group. The peak of the sparks decreased in the two TAC groups comparing with sham while the width was maintained in three groups.

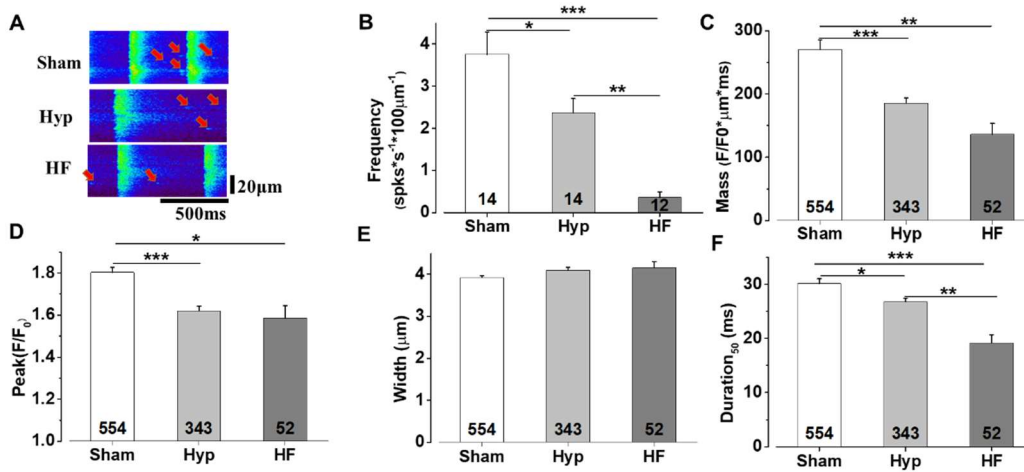


**Fig.26 Ca<sup>2+</sup> Sparks frequency and characteristics are significantly altered in TAC SAN** **A.** Line scan images (0.25 ms per line) and arrows point to Ca<sup>2+</sup> sparks. **B.** Ca<sup>2+</sup> spark frequency (number of sparks/s/100μm) were significantly decreased in TAC SAN. **C.** Ca<sup>2+</sup> spark mass (amplitude(**D**) × width(**E**) × duration(**F**), indicating the Ca<sup>2+</sup> release in each spark) is smaller in TAC SAN cells \**p*<0.05, \*\**p*<0.01, \*\*\**p*<0.001. *N* in **B** indicates the number of cells from SAN preparation. *N* in **C-F** indicates the number of sparks.

### 3.2.3 RyR2 expression and phosphorylation level

The protein expression level of RyR2 showed a continuously decreasing tendency between the three groups and was significantly different between HF and Sham (Fig.27 A, B). The RyR2 phosphorylation level at S2808 site (the PKA site) in Hyp group was obviously higher in Hyp group compared to Sham, while only showed a tendency to increase in HF group compared to TAC (Fig.26C). The RyR2 phosphorylation level at S2814 site, the two TAC groups decreased to the same level, which was significantly lower than sham group (Fig.26D).

Interestingly, there was the opposite tendency in SAN than in ventricles (Fig.27 F-H). The RyR2 expression level in Ventricles showed a continuously increasing from Sham to Hyp then to HF other than decreasing in SAN. And the phosphorylation level on S-2814 in TAC group increased to the same level other than decreased in SAN.

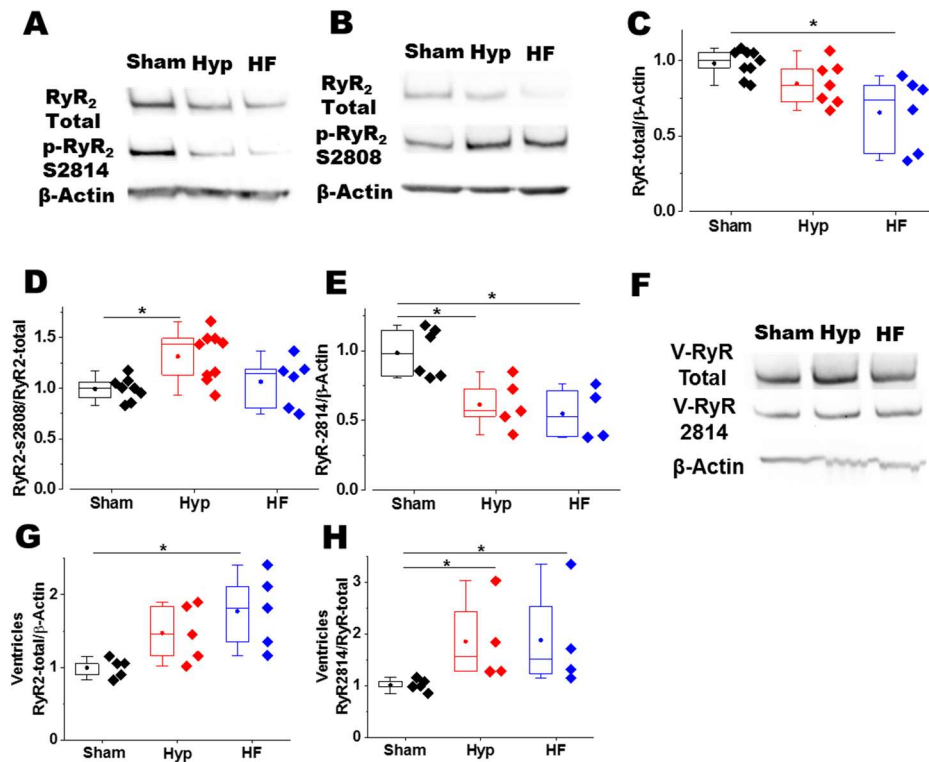


**Fig.27 RyR2 expression and phosphorylation level were altered in TAC SAN and showed opposite tendency than it in ventricles. A-B** Examples of Western Blot obtained for total or phosphorylated RyR2 and  $\beta$ -Actin from SAN tissue. **C** Quantification of Total RyR2 expression in SAN, **D** and phosphorylated RyR2-S2808 normalized by RyR2-total, **E** and RyR2-S2814 normalized by RyR2-Total are altered in SAN. **F**, Examples of Western Blot obtained for total and phosphorylated RyR2-S2814 and  $\beta$ -Actin from Ventricles. **G-H** Quantification of RyR2-total and RyR2-S2814 normalized by RyR2-total in ventricles. \* $p < 0.05$ , \*\* $p < 0.01$  vs Sham

### 3.2.4 SERCA function was more inhibited by PLB while NCX expression level decreased in HF group

The SERCA expression level maintained in three groups (Fig.28 A, B). The PLB expression level showed a continuously increasing in the three groups resulting in the PLB/SERCA ratio showed the same increasing way (Fig.28 C-F). The phosphorylation level of PLB-s16, the PKA site showed the same changing pattern with RyR2 PKA site. There was a significant increasing in Hyp group while there was no difference between Sham and HF group. However, the PLB-T17 site phosphorylation level showed a continuously decreasing in the three groups. This pattern is also different than it in RyR2 CaMKII site.

Thus, the SERCA function can be more inhibited in HF group by more and less phosphorylated PLB, and this can contribute to the  $[Ca^{2+}]_i$  transient prolongation. But  $[Ca^{2+}]_i$  transient decay also depends on  $Ca^{2+}$  extrusion through the NCX. Fig.5 J&K show that NCX expression is reduced in TAC group, which, together with the PLB increased expression can lead to prolonged  $[Ca^{2+}]_i$  transients.

On the other hand, the decrease in SERCA activity could lead to a lower SR  $Ca^{2+}$  load. We estimated

SR  $Ca^{2+}$  content by rapid caffeine application in isolated SAN cells. Fig. 28 I shows the amplitude of the caffeine-evoked  $[Ca^{2+}]_i$  transient and shows that the SR  $Ca^{2+}$  load is smaller in TAC than in Sham SAN cells and there was no difference between the two TAC groups.

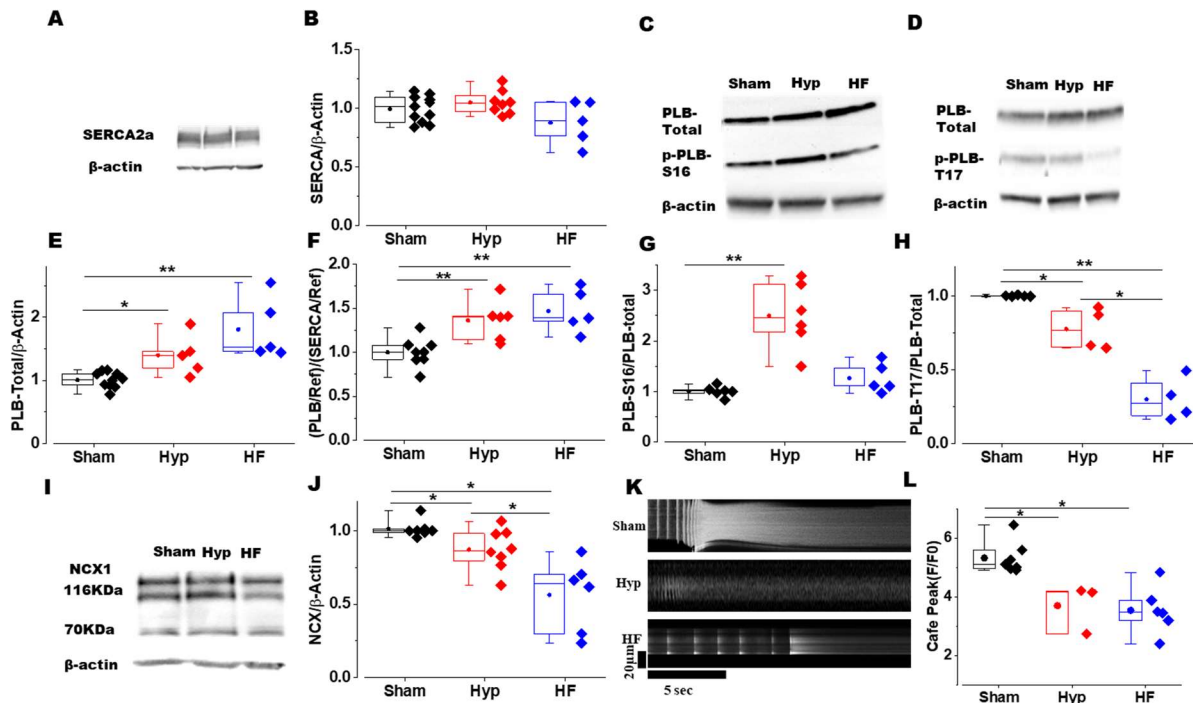


**Fig.28 SERCA function was inhibited by PLB leading to a lower SR  $Ca^{2+}$  load in HF SAN while NCX protein expression level also decreased. A, Representative Western Blot B, and quantification of SERCA. C, D, Representative Western Blot of PLB-Total, PLB-S16 and PLB-T17. E, quantification of PLB-total F, the PLB over SERCA ratio. G, Quantification of PLB-S16 normalized by PLB-total H, PLB-T17 normalized by PLB-Total. I, Representative Western Blot J, and quantification of NCX. K, Line scan images (0.25 ms per line) over the single SAN cell before and during the Caffeine perfusion and L, the quantification of the F/F<sub>0</sub> after caffeine arrived indicating the SR  $Ca^{2+}$  load. Each spot in L indicates the different cells from SAN preparation. Each spot in WB results indicates one single SAN preparation. \*p < 0.05, \*\*p < 0.01, \*\*\*p < 0.001.**

### 3.2.5 CaMKII expression and phosphorylation level

The CaMKII expression level in SAN showed a tendency on increasing in Hyp group, but no significance between the three groups (Fig.29 A, B). The phosphorylation level of CaMKII showed an obviously decreasing in the two TAC groups (Fig.29 C). However, in ventricles, the CaMKII expression level showed a continuously increasing between the three groups (Fig. 29 D, E), and for the phosphorylation level, the two TAC group both increased significantly than sham (Fig.29 F).

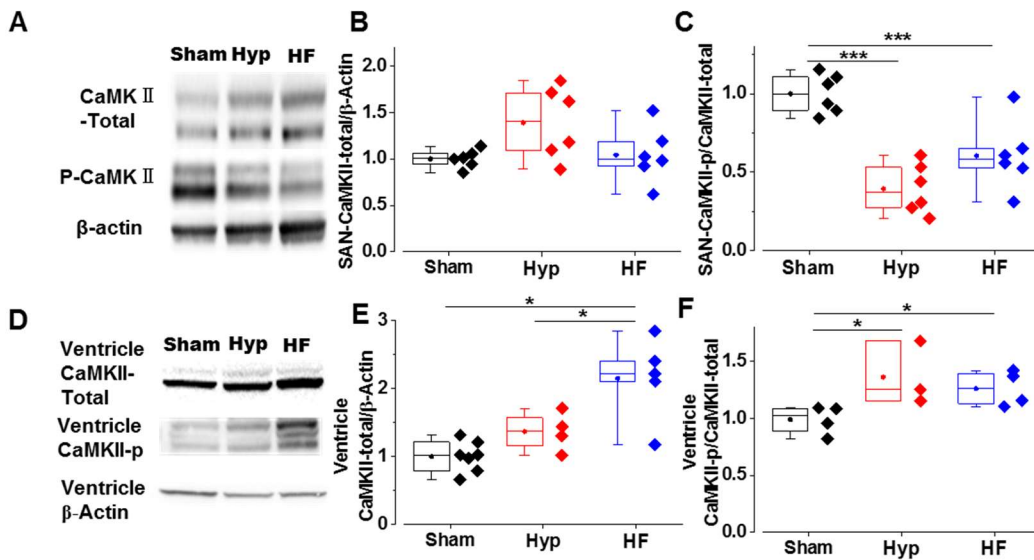


**Fig.29 CaMKII activation level decreased in TAC SAN.** **A-C.** Representative Western Blot and quantification of SAN CaMKII-total and phosphorylation CaMKII normalized by CaMKII-total; **D-E,** Representative Western Blot, and quantification of left ventricles CaMKII-total and phosphorylation CaMKII normalized by CaMKII-total. Each spot indicates one single SAN preparation. \*p < 0.05, \*\*p < 0.01 vs Sham.

### 3.2.6 KN93 perfusion effect in TAC group

After the KN93 perfusion, we found the second unexplained result. KN93 is an inhibitor of CaMKII, and KN93 decreased the  $[Ca^{2+}]_i$  transients' rate significantly in Sham and HF group. However, it increased the rate obviously in Hyp group. And the KN93 decreased the Peak in Sham and Hyp group. For other parameters including the duration, time to peak and Decay time constant, the KN93 did not show significant effect on the three groups.

KN93 did not influence the frequency of the  $Ca^{2+}$  sparks. But their frequency showed a tendency on increasing in Hyp group. However, the mass of the  $Ca^{2+}$  sparks in Hyp group decreased significantly comparing with basal condition in this group. The duration and the peak both decreased in Hyp group after KN93 perfusion. This is the third mysterious result we cannot explain yet.

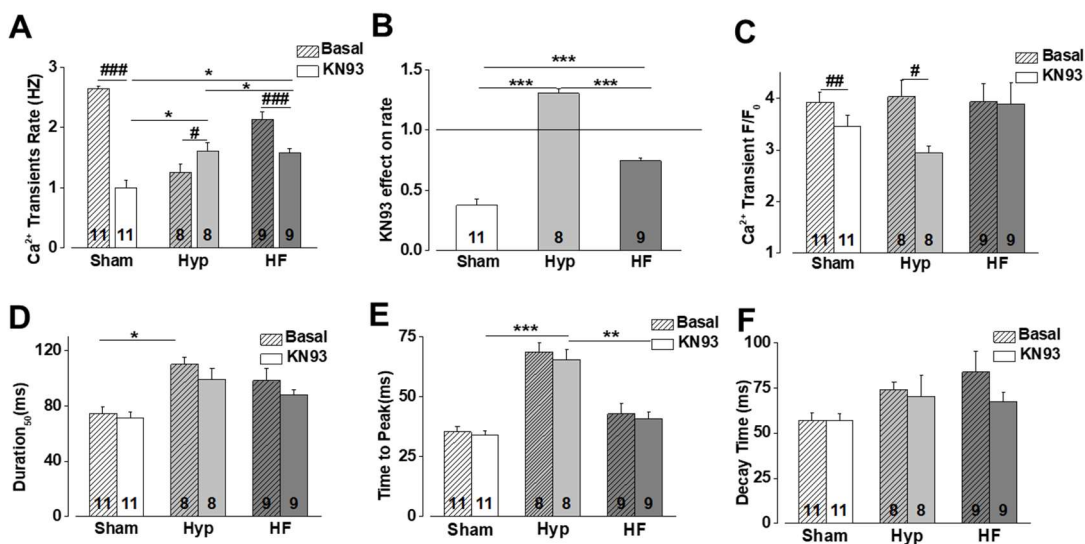


**Fig.30**  $[Ca^{2+}]_i$  transients rate in sinoatrial node (SAN) is higher and characteristics are significantly altered in SAN cells from TAC mice after pharmacologically blocking CaMKII by KN93. **A.** Spontaneous  $[Ca^{2+}]_i$  transients rate after perfusing KN93. **B.** KN93 effect on transient rate. KN93 decreased the rate when below 1.0 and accelerate it when above 1.0. **C.** Amplitude of the  $[Ca^{2+}]_i$  transient measured as peak  $F/F_0$ , where  $F$  is the maximum fluorescence and  $F_0$  the fluorescence during diastolic periods. **D.** Analyses of the  $[Ca^{2+}]_i$  transients kinetics, showed longer time to peak, longer duration at half maximum and  $F$ , prolonged decay time in TAC cells compared to Sham. Decay time constant was obtained by fitting the descendent portion of the fluorescence trace to a single exponential function. \* $p < 0.05$ , \*\* $p < 0.01$ , \*\*\* $p < 0.001$  vs sham or Hyp. # $p < 0.05$ , ## $p < 0.01$ , ### $p < 0.001$  vs. the same group before KN93 perfusion.

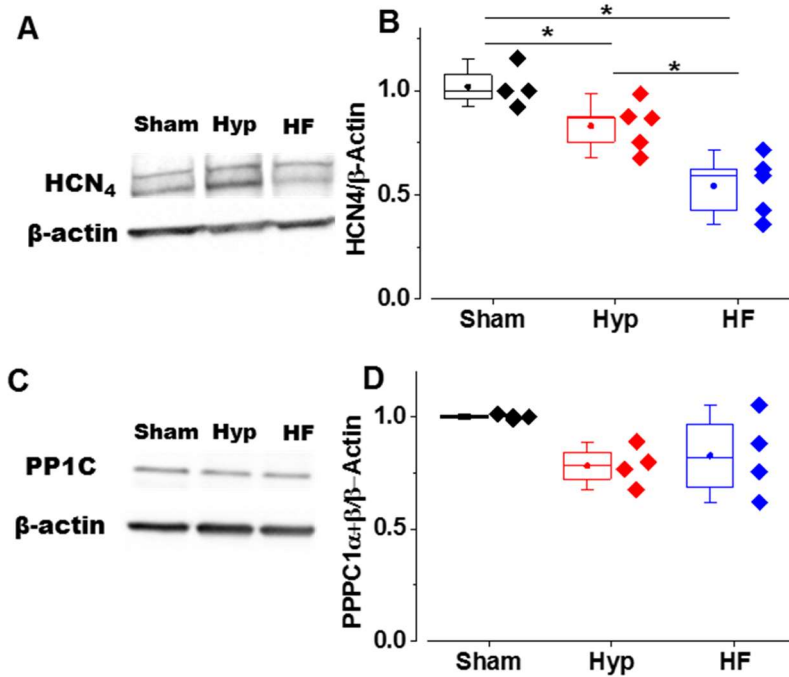


**Fig.31** The HCN4 protein expression level decreased in TAC group while the PP1C maintained in the three groups. **A** Representative of Western blot of HCN4 and **B**, the quantification of HCN4 expression level. **C**, Representative of Western blot of PP1C and **D**, the quantification of PP1C. \* $p < 0.05$ . N indicates the number of SAN preparation

### 3.2.7 conclusion for this part

We were tempted to think that the Hyp group is just in the middle of the way to congestive HF group. Considering for the cardiac function, the Hyp group is significantly different than sham group and is more similar to HF group but milder. However, this is not so consistent. In one side, although the time after TAC was similar, the TAC surgery may have different outcomes. Some animals may develop congestive heart failure while others not. We may think that if we wait longer, all the mice in the Hyp group could be finally developing HF, but we cannot be sure of that, as some TAC animals showed signs of congestive HF at only 3 weeks after surgery and others did not at even 12 weeks. Although we cannot disregard that longer time will be needed to develop congestion in some animals. Moreover, some parameters in Hyp group showed different or even opposite tendency than

it in Sham and HF. For example, the PNN5 was maintained in Hyp group after ANS inhibition. And KN93 perfusion increased the transients' rate in Hyp while decreased the rate in both Sham and HF group.

### **3.3 Aberrant sinus node firing during $\beta$ -adrenergic stimulation leads to cardiac arrhythmias in diabetic mice**

Heart failure arises as a consequence to several pathologies that impose chronically an extra work to the heart. Diabetes mellitus, a condition where blood glucose is elevated, when maintained can develop heart failure. When the primary disease is different, the cellular alteration in the heart can be different, as the signaling pathways are different in, for example hypertension, after myocardial infarction or diabetes. During my Ph.D. I participated in a collaborative work. Although I am not a main author, I performed the  $[Ca^{2+}]_i$  handling analyses in SAN from diabetic model, and think that this part can add to my work of SAN dysfunction in HF.

**Manuscript:**



# Aberrant sinus node firing during $\beta$ -adrenergic stimulation leads to cardiac arrhythmias in diabetic mice

Anniek F. Lubberding<sup>1</sup> | Laetitia Pereira<sup>2</sup> | Jianbin Xue<sup>2</sup> | Lisa A. Gottlieb<sup>1</sup> | Vladimir V. Matchkov<sup>3</sup> | Ana M. Gomez<sup>2</sup> | Morten B. Thomsen<sup>1</sup>

<sup>1</sup>Department of Biomedical Sciences, Faculty of Health and Medical Sciences, University of Copenhagen, Copenhagen, Denmark

<sup>2</sup>Université Paris-Saclay, Inserm, UMR-S 1180, Châtenay-Malabry, France

<sup>3</sup>Department of Biomedicine, Aarhus University, Aarhus, Denmark

## Correspondence

Morten B. Thomsen, Department of Biomedical Sciences, University of Copenhagen, Blegdamsvej 3B, Panum Building, 12.5.36, DK-2200 Copenhagen N, Denmark.  
Email: mbthom@sund.ku.dk

## Funding information

Agence Nationale de la Recherche, Grant/Award Number: ANR-13-BSV1-0023-01; Chinese Scholarship Council; Carlsberg Foundation; Laboratory of Excellence LERMIT, Grant/Award Number: ANR-11-IDEX-0003-02

## Abstract

**Aim:** Cardiovascular complications, including cardiac arrhythmias, result in high morbidity and mortality in patients with type-2 diabetes mellitus (T2DM). Clinical and experimental data suggest electrophysiological impairment of the natural pacemaker of the diabetic heart. The present study examined sinoatrial node (SAN) arrhythmias in a mouse model of T2DM and physiologically probed their underlying cause.

**Methods:** Electrocardiograms were obtained from conscious diabetic db/db and lean control db/+ mice. In vivo SAN function was probed through pharmacological autonomic modulation with isoprenaline, atropine and carbachol. Blood pressure stability and heart rate variability (HRV) were evaluated. Intrinsic SAN function was evaluated through ex vivo imaging of spontaneous  $\text{Ca}^{2+}$  transients in isolated SAN preparations.

**Results:** While lean control mice showed constant RR intervals during isoprenaline challenge, the diabetic mice experienced SAN arrhythmias with large RR fluctuations in a dose-dependent manner. These arrhythmias were completely abolished by atropine pre-treatment, while carbachol pretreatment significantly increased SAN arrhythmia frequency in the diabetic mice. Blood pressure and HRV were comparable in db/db and db/+ mice, suggesting that neither augmented baroreceptor feedback nor autonomic neuropathy is a likely arrhythmia mechanism. Cycle length response to isoprenaline was comparable in isolated SAN preparations from db/db and db/+ mice; however,  $\text{Ca}^{2+}$  spark frequency was significantly increased in db/db mice compared to db/+ at baseline and after isoprenaline.

**Conclusion:** Our results demonstrate a dysfunction of cardiac pacemaking in an animal model of T2DM upon challenge with a  $\beta$ -adrenergic agonist. Ex vivo, higher  $\text{Ca}^{2+}$  spark frequency is present in diabetic mice, which may be directly linked to in vivo arrhythmias.

## KEYWORDS

autonomic nervous system, baroreflex, calcium, electrophysiology, isoprenaline, type-2 diabetes

## 1 | INTRODUCTION

Patients with diabetes, most of whom suffer from type-2 diabetes mellitus (T2DM), experience a higher incidence of cardiac arrhythmias. Diabetes<sup>1-3</sup> and poor glycaemic control<sup>2</sup> have been identified as independent risk factors for the development of atrial fibrillation, a disease characterized by electrical and structural remodelling, fibrosis, and conduction slowing in the atria. Hyperglycaemia alone can contribute to the process of remodelling in atrial fibrillation.<sup>4</sup> Additionally, stress hyperglycaemia poses an increased risk of arrhythmia and death after myocardial infarction.<sup>5</sup>

Diabetes has also been linked to other arrhythmias, such as atrioventricular block<sup>6</sup> and sick sinus syndrome.<sup>7</sup> Additionally, whereas an elevated resting heart rate is considered common among patients with diabetes, analyses of the population of bradycardic patients requiring an electronic pacemaker report a statistically significant overrepresentation of people with diabetes.<sup>8,9</sup> This altered basal heart rate may contribute to the increased cardiovascular mortality in people with diabetes.<sup>10-12</sup>

Animal studies have also identified alterations in basal heart rate in rodent models of T1DM and T2DM, finding both increased and decreased heart rates in conscious animals, as well as in whole heart and sinoatrial node (SAN) preparations.<sup>13</sup> The db/db mouse, a commonly used mouse model of obesity-induced T2DM because of leptin receptor deficiency, has been reported to exhibit both increased<sup>14</sup> and decreased<sup>15,16</sup> heart rate in vivo. In our hands, anaesthetized db/db mice and heterozygote, non-obese, normoglycaemic db/+ control mice have comparable heart rates.<sup>17</sup> The mouse model also has a contractile remodelling primarily based on reduced L-type Ca<sup>2+</sup> current<sup>18</sup> (reviewed in<sup>19</sup>), a current that also has critical control over heart rate.<sup>20</sup>

Recently, we reported SAN dysfunction unmasked by sympathetic stimulation in the anaesthetized db/db mouse.<sup>17</sup>

$\beta$ -Adrenergic stimulation with isoprenaline caused arrhythmias emanating from the SAN in these mice; however, the pathophysiological mechanism underlying the arrhythmias remains unclear. The typical arrhythmia was characterized by a sudden prolongation of the PP interval lasting 5-10 beats before picking up pace and returning to normal rate. Interestingly, the arrhythmias occurred 7-10 minutes after the peak of the chronotropic response by isoprenaline.

We identified three potential mechanisms for these characteristic arrhythmias: (a) A sudden increase in total peripheral vascular resistance would cause a surge in central blood pressure, increase cardiac afterload and cause a compensatory decrease in heart rate and stroke volume as part of the baroreceptor reflex. (b) An autonomic remodelling underlying periods of poor heart rate control resulting in episodes of SAN slowing. Cardiac autonomic neuropathy (CAN) is a frequent clinical finding in hyperglycaemic pathologies and contributes to resting tachycardia in diabetic patients.<sup>21,22</sup> (c) An intrinsic SAN defect may be present secondary to electrophysiological remodelling of the SAN cells potentially causing impaired response to the autonomic nervous system.

To confirm our previous report of SAN arrhythmias in db/db mice and to solidify the finding, we hypothesized that conscious db/db mouse have SAN arrhythmias upon challenge with isoprenaline in a dose-dependent manner. Secondly, we aimed to identify the underlying cause of arrhythmias in db/db mice via functional, physiological tests probing each of the three potential mechanisms outlined above.

## 2 | RESULTS

Higher body weights and hyperglycaemia were confirmed in the db/db mice at 9 weeks of age and remained high over the course of the experimental period (Figure 1). RR, PR, QRS and QT intervals at baseline were comparable in db/db and

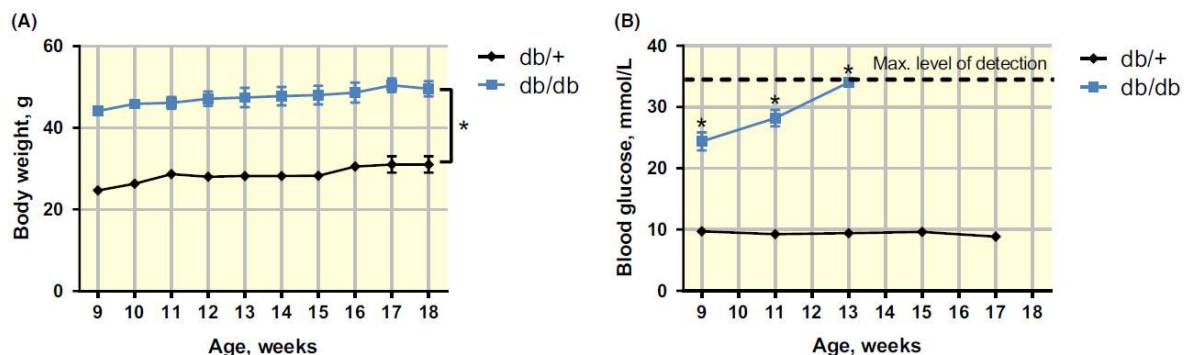


**FIGURE 1** Body weight and non-fasting blood glucose in diabetic db/db and lean db/+ controls. Body weight (g) (A) and non-fasting blood glucose (mmol/L) (B) were significantly elevated in diabetic db/db mice (n = 9-15) throughout the experimental period, compared with lean db/+ mice (n = 6-12). Note that the glucometer had a maximum detection level of 33 mmol/L. \* $P < .05$ , mixed model ANOVA followed by post-hoc Bonferroni test

db/+ mice (Table 1), although there was a tendency of slower heart rate in db/db mice (RR interval, Table 1;  $P = .057$ ).

## 2.1 | $\beta$ -Adrenergic stimulation causes SAN arrhythmias in diabetic mice

To evaluate the effect of  $\beta$ -adrenergic stimulation in the conscious db/db mouse, mice were challenged with different doses of isoprenaline (2, 20, 200, and 2000  $\mu\text{g}/\text{kg}$ ) in a random crossover design. Isoprenaline injections caused an acute, moderate shortening of the RR interval. While RR interval was constant after isoprenaline in the 10 minute analysis window in the db/+ mice, isoprenaline challenge provoked large, characteristic fluctuations of RR intervals in the db/db mice (Figure 2A-D). The large RR fluctuations emanated from the SAN, as P waves were preserved and PR interval remained constant (Figure 2D). These SAN arrhythmias occurred in a dose-dependent manner in the db/db mice reaching an apparent maximum at 200  $\mu\text{g}/\text{kg}$  isoprenaline ( $0.64 \pm 0.10 \text{ min}^{-1}$  in db/db mice vs  $0.05 \pm 0.02 \text{ min}^{-1}$  in db/+;  $P < .05$ ; Figure 2E). The arrhythmia occurrence was not heart rate dependent: isoprenaline at doses of 20  $\mu\text{g}/\text{kg}$  and above increased heart rate in both db/+ and db/db mice (Figure 2F). This chronotropic effect was comparable in the two groups.

## 2.2 | Parasympathetic involvement in arrhythmias

Next, we evaluated the influence of parasympathetic modulation on the presence of these SAN-associated arrhythmias. Blocking of the muscarinic receptor by means of atropine did not significantly affect mean RR interval in either group of mice (Figure 3A). Neither did subsequent isoprenaline administration. Nevertheless, atropine did prevent all isoprenaline-induced arrhythmias in the db/db mice (Figure 3E,G). As parasympathetic block abolished all SAN arrhythmias, we simulated parasympathetic stimulation by carbachol administration in separate experiments using the same mice. Carbachol significantly increased RR intervals similarly in the db/+ and

db/db mice ( $216 \pm 44\%$  and  $260 \pm 39\%$  increases, respectively;  $P > .05$ ; Figure 3B). Subsequent isoprenaline administration significantly shortened the RR interval similarly in both groups of mice (Figure 3B). Carbachol alone did not elicit the SAN-related arrhythmias in the mice, but combined with subsequent isoprenaline, it produced SAN-associated arrhythmias in all nine db/db mice and two of six db/+ mice ( $P = .01$ ; Fisher's Exact test; Figure 3D,F). The db/db mice experienced a significantly higher incidence of arrhythmias after carbachol and isoprenaline in comparison to the db/+ mice (db/+ :  $16 \pm 15$  vs db/db:  $80 \pm 23$  per 10 minutes,  $P < .05$ ; Figure 3G). Thus, the parasympathetic nervous system has an important modulating role in the development of these arrhythmias, but is not in itself sufficient to trigger the arrhythmias.

## 2.3 | Probing the underlying cause

As the activity of the autonomic nervous system is in constant feedback with peripheral blood pressure, we next sought to establish whether peripheral changes in blood pressure preceded the SAN fluctuations. If the SAN arrhythmias are secondary to a baroreceptor-mediated response to sudden surges in central blood pressure, we would be able to identify this in simultaneous recordings of electrocardiogram (ECG) and blood pressure. Comparable to the observations in ECG-only telemetry, RR interval shortened in response to isoprenaline (Figure 4A). Isoprenaline also induced a small, yet non-significant, change in blood pressure ( $16 \pm 5\%$  and  $15 \pm 4\%$  decrease in systolic and diastolic blood pressure, respectively;  $P = .36$  and  $=.44$ , respectively; Figure 4B). We observed the characteristic SAN arrhythmias in the db/db mice and none of these RR fluctuations was preceded by a change in blood pressure (Figure 4C).

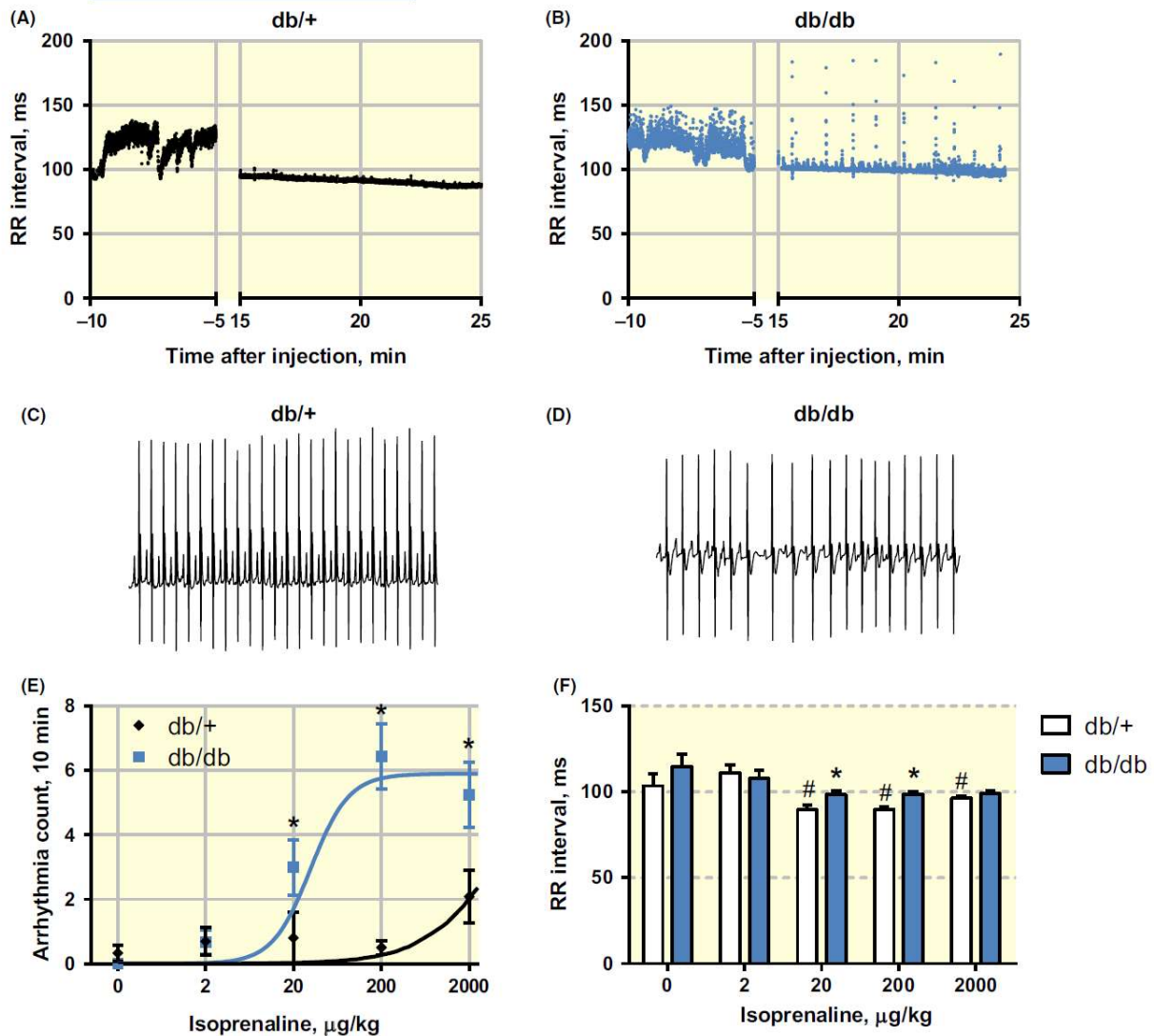
Cardiac autonomic neuropathy is frequently associated with hyperglycaemic circumstances. We used analysis of heart rate variability (HRV) to identify potential remodelling of the cardiac sympathetic and parasympathetic nerves. We observed no differences in standard deviation of RR intervals (SDRR) or root mean square of successive differences (RMSSD) in db/db and db/+ mice, irrespective of time of day (Table 2). There was a significantly larger proportion of beats with a beat-to-beat difference exceeding 6 ms (pNN6) in db/db mice during the dark period, which is compatible with their higher RR interval in that period. In addition, we observed no differences in relative fractions of low frequency (LF) or high frequency (HF), between db/db and db/+, irrespective to the time of day (Table 2). This suggests the absence of sympathetic or parasympathetic remodelling and neuropathy. Thus, it appears that of the three potential mechanisms we suggested, neither sudden increases in blood pressure nor neuropathy is underlying the SAN-associated arrhythmias.

To probe the electrophysiological remodelling in the SAN itself, we recorded cellular  $\text{Ca}^{2+}$  transients in multicellular,

**TABLE 1** Baseline electrocardiogram (ECG) parameters in conscious control (db/+) and diabetic (db/db) mice

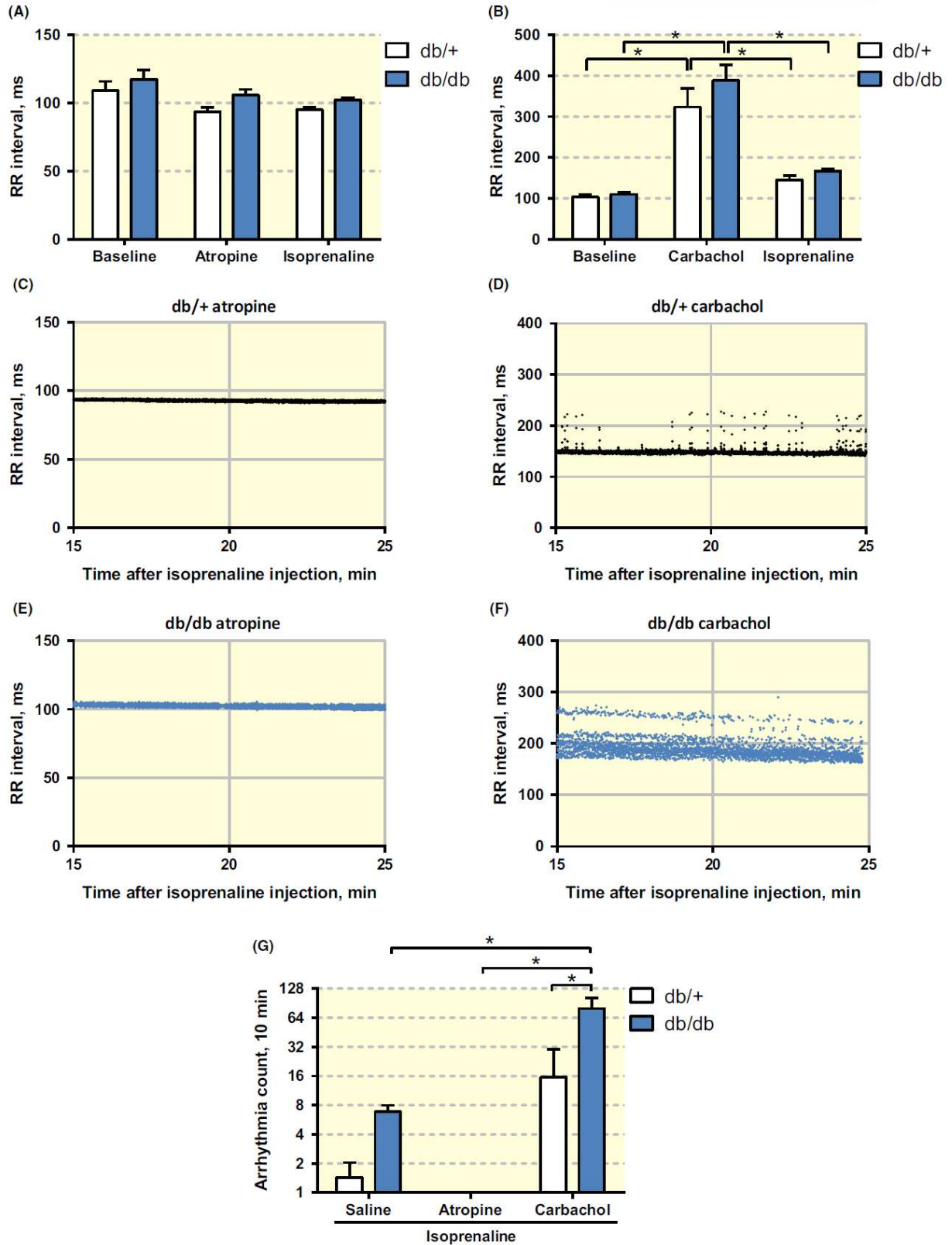
|         | db/+         | db/db        |
|---------|--------------|--------------|
| RR, ms  | $106 \pm 3$  | $113 \pm 2$  |
| PR, ms  | $33 \pm 1$   | $33 \pm 1$   |
| QRS, ms | $11 \pm 0.2$ | $11 \pm 0.2$ |
| QT, ms  | $48 \pm 1$   | $50 \pm 1$   |
| n, mice | 12           | 15           |

Note: Data from multiple baseline recordings prior to the experiments illustrated in Figures 2 and 3.



**FIGURE 2** RR fluctuations upon  $\beta$ -adrenergic stimulation in db/db mice. A and B, Representative RR interval tachograms 15–25 min after isoprenaline challenge (200  $\mu\text{g}/\text{kg}$ ) in a db/+ (A) and db/db (B) mouse, showing RR fluctuations in the diabetic db/db mouse. The break in the axis from –5 to 15 minutes includes a brief period of anaesthesia in association with drug administration, see Section 4. C and D, Raw electrocardiogram traces from the same mice. Note the presence of P waves and preservation of regular PR interval duration during the arrhythmias. E, Arrhythmia count between 15 and 25 min after injection of saline and different doses of isoprenaline (2, 20, 200, 2000  $\mu\text{g}/\text{kg}$ ) in db/db ( $n = 9$ ) and db/+ ( $n = 12$ ) mice. The db/db mice exhibit SA node-related arrhythmias in a dose-dependent manner. The plotted curves are for illustrative purposes only. F, RR interval between 15 and 20 min after injection of saline and different doses of isoprenaline (2, 20, 200, 2000  $\mu\text{g}/\text{kg}$ ) in db/db ( $n = 9$ ) and db/+ ( $n = 12$ ) mice. No differences were found between groups at any dose of isoprenaline. \* $P < .05$  compared with 0  $\mu\text{g}/\text{kg}$  (ie saline) of same genotype; # $P < .05$  compared with 2  $\mu\text{g}/\text{kg}$  of same genotype, mixed model ANOVA followed by post-hoc Bonferroni test

**FIGURE 3** The effect of parasympathetic modulation on arrhythmia occurrence. A, Mean RR interval at baseline, after atropine (1 mg/kg) and after subsequent isoprenaline (200  $\mu\text{g}/\text{kg}$ ) administration 30 min later in db/db ( $n = 8$ ) and db/+ ( $n = 7$ ) mice. B, Mean RR interval at baseline, after carbachol (0.5 mg/kg) and after subsequent isoprenaline (200  $\mu\text{g}/\text{kg}$ ) administration 30 min later in db/db ( $n = 9$ ) and db/+ ( $n = 6$ ) mice. C–F, Exemplary RR interval tachograms of 15–25 min after isoprenaline injection preceded by atropine (C, E) or carbachol (D, F). G, Quantification of arrhythmias after isoprenaline preceded by saline, atropine and carbachol in db/db ( $n = 7$ ) and db/+ ( $n = 6$ ) mice. Note the log scale of the y-axis. \* $P < .05$ , mixed model ANOVA followed by post-hoc Bonferroni test



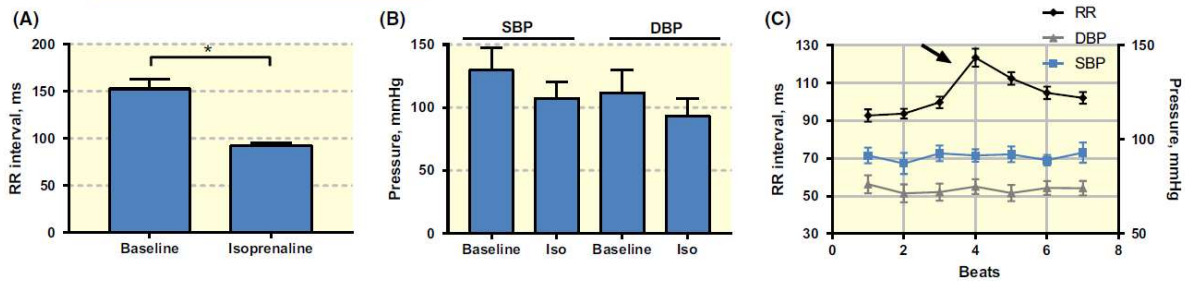


**FIGURE 4** Blood pressure stability prior to arrhythmic events. A, Mean RR interval and (B) systolic blood pressure (SBP) and diastolic blood pressure (DBP) after saline and isoprenaline (200  $\mu\text{g}/\text{kg}$ ) in db/db mice ( $n = 4$ ). C, Mean SBP, DBP and RR interval of five arrhythmic events in db/db mice. The arrhythmias were aligned with the fourth beat having the longest RR interval. Stable BP is observed prior to the arrhythmia

ex vivo preparations of the SAN from db/db and db/+ mice. Recordings of spontaneous  $\text{Ca}^{2+}$  transients in the SAN region allowed us to quantify the spontaneous cycle length of the node before and during pharmacological autonomic stimulation (Figure 5A). Basal SAN cycle length in the ex vivo preparation was considerably longer than in vivo (eg Figure 2F), and preparations from db/db mice were significantly faster than db/+ preparations (Figure 5B). Cycle length significantly shortened after isoprenaline in both db/db and db/+ SAN preparations, but to a lesser extent in the db/db SAN cells (Figure 5B). The  $\text{Ca}^{2+}$  transient amplitude and decay time was comparable in db/db and db/+ SAN preparations and was not changed by isoprenaline (data not shown). In SAN preparations, isoprenaline is known to elicit a positive chronotropic response and does not change the  $\text{Ca}^{2+}$  transient amplitude or duration (compare 23,24). We did not observe fluctuations in cycle length in any of the ex vivo recordings. However, SAN preparations from db/db mice

showed a significantly higher frequency of  $\text{Ca}^{2+}$  sparks in the diastolic periods, indicating spontaneous  $\text{Ca}^{2+}$  leak through the ryanodine receptors, both at basal conditions and during isoprenaline (Figure 5C), suggestive of intrinsic SAN dysfunction. In another batch of experiments, we pre-treated the preparations with either carbachol or atropine to mimic the in vivo experiments illustrated in Figure 3. Carbachol doubled cycle length, (by 114% and 81% in db/+ and db/db preparations, respectively), whereas atropine did not significantly change the spontaneous cycle length of the SAN preparations (by  $-20\%$  and  $-37\%$  in db/+ and db/db preparations respectively). Atropine pre-treatment of db/db preparations reduced spark frequency, both alone and after co-treatment with isoprenaline (Figure 5D), which corroborates the in vivo data. In apparent disagreement with our in vivo results, carbachol pre-treatment of db/db preparations had comparable results to atropine: In addition to its negative chronotropic effect, carbachol reduced spark frequency before and after co-treatment with isoprenaline (Figure 5D).

**TABLE 2** Heart rate variability parameters in conscious control (db/+) and diabetic (db/db) mice

|             | Light period |             | Dark period |               |
|-------------|--------------|-------------|-------------|---------------|
|             | db/+         | db/db       | db/+        | db/db         |
| RR, ms      | $138 \pm 6$  | $133 \pm 4$ | $113 \pm 2$ | $125 \pm 3^*$ |
| SDRR, ms    | $21 \pm 1$   | $19 \pm 1$  | $19 \pm 1$  | $22 \pm 2$    |
| RMSSD, ms   | $9 \pm 2$    | $8 \pm 1$   | $7 \pm 1$   | $7 \pm 1$     |
| pNN6, %     | $36 \pm 6$   | $38 \pm 6$  | $19 \pm 2$  | $29 \pm 4^*$  |
| LF Power, % | $34 \pm 5$   | $30 \pm 4$  | $35 \pm 6$  | $29 \pm 5$    |
| HF Power, % | $66 \pm 5$   | $70 \pm 4$  | $65 \pm 6$  | $70 \pm 5$    |
| n, mice     | 6            | 5           | 6           | 5             |

Note: Data from conscious, undisturbed and freely roaming mice. LF Power was determined between 0.15 and 1.5 Hz; HF Power between 1.5 and 5.0 Hz. HRV analysis was performed according to.<sup>34</sup> Two-way ANOVA followed by post-hoc Bonferroni test where appropriate.

Abbreviations: HRV, heart rate variability; pNN6, percentage of consecutive RR intervals differing by more than 6 ms; RMSSD, root mean square of the successive differences of RR interval; SDRR, standard deviation of RR intervals.

\* $P < .05$  vs db/+ in same period of day.

### 3 | DISCUSSION

Diabetes has been linked to a variety of cardiac arrhythmias, including atrial fibrillation,<sup>1-3</sup> AV node block<sup>6</sup> and sick sinus syndrome.<sup>7</sup> Additionally, patients with diabetes are known to experience resting tachycardia, but are also over-represented in patients with bradycardia requiring a pacemaker.<sup>8,9</sup> These data suggest that diabetes might affect the electrophysiology of the natural pacemaker of the heart. As altered resting heart rate may contribute to the increased cardiovascular mortality observed in diabetic patients, it is key to understand the pathophysiological cause of impaired cardiac pacemaking in these patients.

In the present study, we show that conscious db/db mice experience SAN-related arrhythmias upon sympathetic stimulation and that these are modulated by the parasympathetic nervous system. We proposed three possible mechanisms: (a) peripheral blood pressure surges leading to instant, intense parasympathetic feedback resulting in episodes of slow heart rates. (b) Neuropathy of the autonomic fibres and (c) intrinsic SAN

dysfunction causing an exaggerated response to autonomic control. By physiologically probing the mechanism behind these arrhythmias, we find that peripheral blood pressure surges and cardiac neuropathy are not likely candidates to be involved in the development of these arrhythmias, but that ex vivo SAN preparations show changes in intracellular  $\text{Ca}^{2+}$  homeostasis that may set the stage for cardiac arrhythmias.

### 3.1 | Stable blood pressure prior to SAN-related arrhythmias

Db/db mice develop hypertension and show disrupted blood pressure circadian rhythm and blunted baroreceptor sensitivity.<sup>14,16</sup> We confirm a moderate hypertension at baseline in db/db mice (Figure 4B). Isoprenaline not only affects heart rate, but also mediates vasodilation through its  $\beta_2$ -receptor activity.<sup>25</sup> As such, we hypothesized that changes in peripheral BP could be preceding the SAN-related arrhythmias. We observed a moderate decrease in BP upon isoprenaline administration as expected, but also falsified the hypothesis: SAN arrhythmias were not preceded by blood pressure fluctuations (Figure 4C).

### 3.2 | CAN as a possible cause to SAN arrhythmias

Cardiac autonomic neuropathy is a long-term complication of diabetes, characterized by demyelination and axonal degeneration of the autonomic nerve fibres innervating the heart and vasculature. Upon CAN progression, it manifests as resting tachycardia, orthostatic hypotension and exercise intolerance.<sup>26</sup> Resting tachycardia is a common feature of CAN and thought to be caused by damage to parasympathetic fibres occurring earlier than to sympathetic fibres. CAN is diagnosed on the finding of reduced HRV, which is an independent risk factor for sudden death in patients with diabetes.<sup>27</sup>

To understand the complex nature and consequences of CAN, its progression has been investigated in a variety of animal models (reviewed in<sup>13</sup>). While studies reported a decrease in HRV, some reported neuropathy of all autonomic nerve fibres,<sup>28,29</sup> some of only sympathetic fibres<sup>30,31</sup> and some no neuropathy at all, but rather an increase in cholinergic nerve density.<sup>32</sup> Heart rate variability analysis on the db/db mouse using telemetry has both shown unchanged HRV at 8-9 weeks of age<sup>16</sup> and reduced HRV at 12 weeks of age<sup>14</sup>

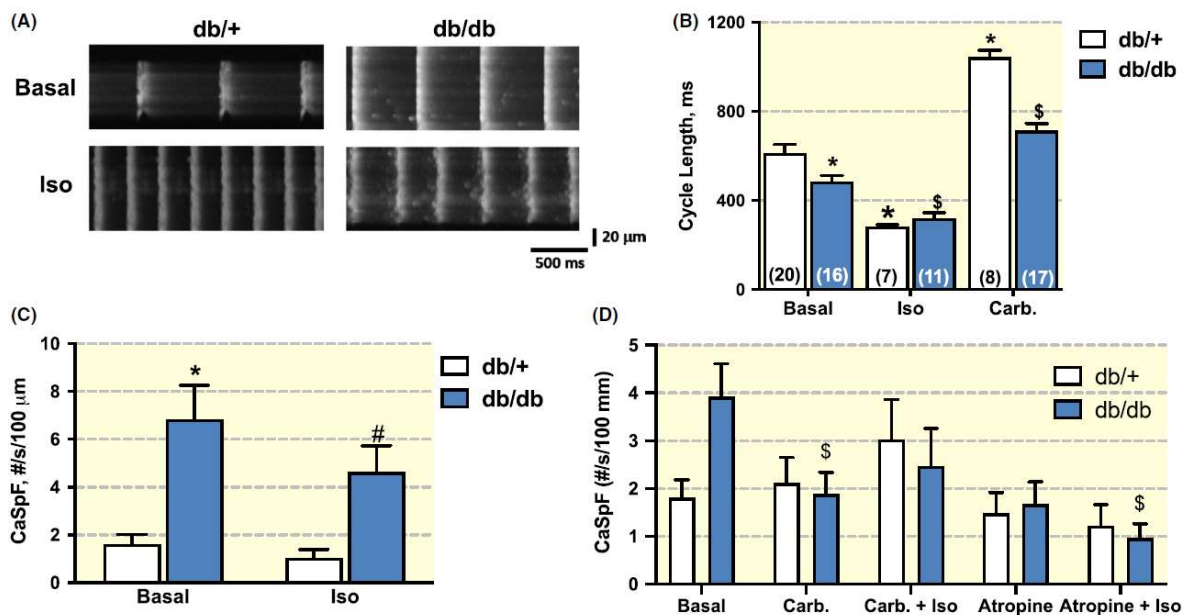


**FIGURE 5** The effect of sympathetic and parasympathetic stimulation on isolated sinus node tissue. A, Representative examples of line scan images of spontaneous  $\text{Ca}^{2+}$  transients in cells from isolated sinoatrial node (SAN) tissue from db/+ and db/db mice in basal condition and during 20 nmol/L isoprenaline. B, Mean cycle length in SAN preparations before and after superfusion with isoprenaline. The number of cells within the tissue is stated inside each bar for each group. C, Mean  $\text{Ca}^{2+}$  spark frequency (CaSpF, represented as number of spark events per second per 100  $\mu\text{m}$ ) measured in the same preparations as used for panel B. D, Calcium-spark frequency in SAN preparations from db/+ and db/db mice during basal conditions and with either carbachol or atropine pre-treatment followed by isoprenaline stimulation. \* $P < .05$  in comparison to baseline db/+. # $P < .05$  in comparison to isoprenaline-treated db/+ preparations. \$ $P < .05$  in comparison to baseline db/db. Mixed model ANOVA followed by post-hoc Bonferroni test. Results obtained from preparations from  $N = 9$  db/+ and  $N = 8$  db/db mice

in two separate studies; however, few studies have directly investigated the presence of CAN in the db/db mouse. An early report showed lower noradrenaline concentration in db/db hearts and a reduction in sympathetic nerves.<sup>33</sup> We previously reported a 29% reduction in synaptophysin expression in right atrial tissue indicative of relative denervation of the SAN in atria from db/db mice.<sup>17</sup>

In the present study, we used HRV analysis, a functional measure of cardiac frequency control, for indications of the presence of CAN. In the time domain, no differences in RR variability were found, but we did find a higher pNN6 in the db/db mice (Table 2). pNN6 is a measure of the percentage of normal consecutive RR intervals differing by >6 ms, and evaluates the parasympathetic modulation of heart rate.<sup>34</sup> The higher pNN6 is likely influenced by the longer RR interval found in these mice at the same time of day. In the frequency domain, the HF component represents predominantly parasympathetic control, while the LF component is considered to be influenced by a mixture of parasympathetic and sympathetic control.<sup>34</sup> We did not observe differences in HF or LF power (Table 2) between conscious db/db and db/+ mice to substantiate the suggestion of larger parasympathetic modulation by pNN6. Thus, in the present study, we cannot identify solid signs of CAN in the db/db mice, and we conclude that CAN does not contribute to the substrate for SAN-related arrhythmias in the diabetic mice.

### 3.3 | Intrinsic SAN dysfunction in the diabetic db/db heart

Krishnaswamy and colleagues observed indications of intrinsic SAN dysfunction in T1DM Akita mice.<sup>35</sup> They found increased SAN-recovery time, reduction in conduction velocity in the SAN area and reduced heart rate responsiveness to the parasympathetic agonist carbachol. Insulin treatment normalized these abnormalities. The present study used the T2DM db/db mouse which is characterized by hyperinsulinaemia evident until at least 14 weeks of age,<sup>16</sup> meaning different mechanisms are likely involved in the SAN dysfunction in the T1DM Akita and db/db mice.

Streptozotocin-induced T1DM mice also show prolonged SAN-recovery time,<sup>36</sup> in line with our previous report of prolonged SAN-recovery time in db/db mice.<sup>17</sup> Howarth et al have provided evidence of SAN dysfunction in streptozotocin-induced T1DM rats. They observed reduced resting heart rates in isolated hearts of the T1DM rats, increased action potential duration in the SAN area<sup>37</sup> and increased SAN conduction time.<sup>38</sup> Recently, SANs of these streptozotocin-induced T1DM rats were reported to exhibit different mRNA expression profiles than control SANs.<sup>39</sup> Differences were found in several proteins related to the pacemaker function

of the SAN, including the hyperpolarization-activated cycle nucleotide-gated channel 4, inositol 1,4,5-triphosphate (IP<sub>3</sub>) receptors and the Na<sup>+</sup>/Ca<sup>2+</sup> exchanger.

Diabetic hyperglycaemia has also been shown to increase Ca<sup>2+</sup>/calmodulin-dependent protein kinase II (CaMKII) activation in the hearts of mice, rats and humans.<sup>40</sup> The activation of CaMKII was linked to spontaneous SR Ca<sup>2+</sup> release and an increased incidence of ventricular arrhythmias. Additionally, increased oxidized CaMKII was found specifically in SAN cells of mice with streptozotocin-induced T1DM along with increased SAN cell apoptosis.<sup>36</sup> This was associated with doubled mortality after myocardial infarction.

In the present study, we find a higher number of spontaneous Ca<sup>2+</sup> sparks in SAN preparations from the db/db mice, both at baseline and upon isoprenaline exposure. This increased spark frequency was reduced by the parasympathetic modulators, also after co-treatment with isoprenaline, preventing the higher spark frequency seen with isoprenaline alone (Figure 5). The atropine findings *in vivo* and *ex vivo* appear to act in concert, suggesting that SAN arrhythmias are triggered when both sympathetic and parasympathetic discharges to the SAN are relatively high. The large increase in carbachol-induced SAN arrhythmias *in vivo* is not paralleled by a carbachol-induced increase in Ca<sup>2+</sup> spark frequency *ex vivo*, suggesting that non-cardiac muscarinic effects are important for precipitating the arrhythmia. Nevertheless, the data indicate altered Ca<sup>2+</sup> handling in diabetic SAN leading to electrophysiological changes of pacemaker firing.

### 3.4 | Proposed mechanism

Based on our obtained results with isoprenaline, atropine and carbachol in conscious mice and our testing of the three proposed mechanisms, we speculate that the diabetic SAN undergoes substantial electrophysiological remodelling that serves as a substrate for arrhythmias upon augmented autonomic regulation. Upon pharmacological sympathetic stimulation, RR intervals shorten and the mouse increases its endogenous parasympathetic drive to compensate. After 7-10 minutes of continuous adrenergic and muscarinic activation, the Ca<sup>2+</sup> handling of the SAN of the diabetic mouse becomes aberrant resulting in SAN-related cardiac arrhythmias.

### 3.5 | Limitations

The altered Ca<sup>2+</sup> handling found *ex vivo* in the diabetic SAN is not directly linked to the SAN arrhythmias in the present study. We did not obtain functional data of true autonomic firing, but rather used a marker based on heart rate. In light of potential

intrinsic SAN dysfunction, such a marker might be a false positive signal. In fact, HRV analysis has received criticism, as it is highly dependent on heart rate, and might therefore be unsuitable for measuring autonomic nerve activity without comparable heart rates.<sup>41</sup> The present study was performed using the db/db mouse, a leptin receptor-deficient mouse presenting with high circulating leptin levels. Leptin has been shown to affect cardiac metabolism, to have anti-hypertrophic properties and to increase sympathetic tone, as reviewed in.<sup>42</sup> Any direct involvement of increased leptin levels on the SAN phenotype cannot be ruled out. Additionally, the db/db mouse is obese, hyperglycaemic and diabetic; which one of these alterations is the driving force behind the SAN arrhythmias remains unclear. Finally, caution must be exerted when extrapolating the results of the present study to patients with diabetes.

### 3.6 | Conclusion and clinical implications

Upon pharmacological  $\beta$ -adrenergic stimulation, conscious diabetic mice exhibit SAN-related arrhythmias in a dose-dependent manner. The parasympathetic nervous system is involved in the development of these arrhythmias, as atropine fully abolished the arrhythmias, while carbachol increased their incidence significantly. Of the three proposed mechanisms, remodelling of intracellular  $\text{Ca}^{2+}$  handling is the most likely cause of the cardiac arrhythmias. Intrinsic SAN dysfunction could be a contributing factor in the altered heart rate control and increased mortality seen in patients with diabetes, especially in the setting of stress and increased sympathetic drive.

## 4 | MATERIALS AND METHODS

### 4.1 | Animals

Experiments were performed according to the European Union legislation for the protection of animals used for scientific purposes (Directive 2010/63/EU) and according to national and local animal care guidelines. The study was conducted using 27 male leptin receptor-deficient db/db mice (BKS(D)-Lepr db/JOrlRj) and 21 lean control heterozygote db/+ mice (BKS(D)-Lepr db/JOrlRj Control) purchased at Janvier Labs (France) at 9-19 weeks of age. Mice had access to ad libitum water and standard chow and were housed in a 12-hour light-dark schedule at a constant ambient temperature of 22°C.

### 4.2 | Implantation of telemetric devices

Nineteen db/db and 12 db/+ mice were used for recording ECG and blood pressure in conscious mice. For

implantation of the ECG telemetric devices (ETA-F10; DataSciences International) mice of 8-9 weeks of age were anaesthetized using 2% isoflurane in 100%  $\text{O}_2$ . Body temperature was monitored throughout the surgery and kept at  $37 \pm 0.5^\circ\text{C}$ . A subcutaneous pocket was created in the mid-dorsal region and the telemetric device was placed inside. The electrode leads were tunnelled subcutaneously to the right shoulder joint (negative lead) and under the left armpit (positive lead) and secured using non-absorbable suture (Ethicon), creating a lead-II ECG with a high signal-to-noise ratio.<sup>43</sup> In a subset of db/db mice, blood pressure in the abdominal aorta was recorded simultaneously with the ECG (HD-X11; DataSciences International) as previously described.<sup>44</sup> A mixture of lidocain (0.4 mg/kg) and bupivacaine (1.0 mg/kg) in the pocket and an s.c. injection of carprofen (10 mg/kg) were administered for post-operative analgesia. Mice were allowed to recover for >7 days prior to start of experimentation.

### 4.3 | Recording ECG and blood pressure from conscious mice

On experimental days, mice were weighed and on every second experimental day, their non-fasting blood glucose was measured using a Contour Next glucometer (Bayer) with an upper limit of 33 mmol/L. The pharmacological ECG telemetry study was conducted in two sequential experimental protocols, using a random cross-over design, with 1 week between experiments. First, mice were challenged with saline or altering doses of isoprenaline (2, 20, 200 and 2000  $\mu\text{g}/\text{kg}$ ) in a random cross-over design. Based on the results of these studies, 200  $\mu\text{g}/\text{kg}$  isoprenaline was chosen for subsequent testing. In the second block, mice received saline, atropine (1 mg/kg), or carbachol (0.5 mg/kg) 30 minutes prior to isoprenaline (200  $\mu\text{g}/\text{kg}$ ). Drugs were purchased from Sigma Aldrich (Denmark) and injected intraperitoneally.

Because of the location of the telemetric device and its leads, restraint by the scruff was impossible. Injections were therefore performed after <3 minutes of isoflurane anaesthesia (2% in 100%  $\text{O}_2$ ). In a pilot experiment ( $n = 5$  mice), the effects of isoflurane on ECG parameters were found to last no longer than  $8.2 \pm 1.0$  minutes (range: 6-11 minutes, RR interval being the most sensitive parameter). Therefore, analysis of drug effect was performed over a 10-minute period starting 15 minutes after injection.

In the pharmacological studies, ECG was recorded continuously at 2 kHz from 30 minutes before first injection until 30 minutes after last injection. For HRV analysis, ECGs were recorded continuously for 24 hours in 5 db/db and 6 db/+ mice of 12-14 weeks of age. The mice were not disturbed for the duration of the recordings. The ECG signal from the

telemetric device was acquired by a receiver (RPC-1) underneath the cage, converted by an Analog Output Adapter (Option R08; Data Science International), recorded through a Powerlab 8/30 (ADInstruments) and stored for offline analysis with LabChart 7 (AD Instruments).

#### 4.4 | Ex vivo recordings of SAN activity

Hearts from anaesthetized db/db ( $n = 8$ ) and db/+ ( $n = 9$ ) mice were quickly excised and placed in Tyrode solution (140 mmol/L NaCl, 5.4 mmol/L KCl, 1 mmol/L  $MgCl_2$ , 1.8 mmol/L  $CaCl_2$ , 5.5 mmol/L glucose and 5 mmol/L of 4-(2-hydroxyethyl)-1-piperazineethanesulfonic acid (HEPES)) at 37°C, pH 7.4, and a constant oxygenation with 100%  $O_2$ . The SAN and surrounding right atrial tissue was identified and pinned to the bottom of a custom-made optical chamber, as previously detailed.<sup>24,45</sup> The endocardial side of the preparation was facing upwards. The tissue was loaded with 30  $\mu$ mol/L fluo-4 AM (Invitrogen) for 60 minutes at 37°C. Images were recorded with a resonant scanning confocal microscope (Leica SP5), equipped with a white laser fitted to 500 nm. Excitation was collected at >510 nm. Two-dimensional images were recorded from several locations in the pacemaker region from each preparation at baseline and during perfusion with isoprenaline (20 nmol/L), carbachol (500 nmol/L) and/or atropine (500 nmol/L). Analysis was made in IDL software (Exelis Visual) and homemade routines.

#### 4.5 | Data analysis

ECG and blood pressure were analysed using LabChart 7 (AD Instruments). For measurement of ECG parameters, complexes within selected periods were aligned to the R peak, movement-related noise and inaccurate R peak detection were omitted, and the selection was combined into an averaged ECG. Parameters were subsequently measured manually. The end of the QRS complex was considered the change in slope after negative S deflection. The first positive deflection after S was defined as the J wave. The last negative deflection was defined as the T wave, the end of which was measured by the tangent method as described previously.<sup>46</sup> For analysis of baseline ECG parameters, 10 minutes baseline traces of every experiment (dose dependency of isoprenaline and autonomic block experiments) were analysed and averaged for the individual mouse before mean calculation within the groups.

Sinoatrial node arrhythmias were quantified in a 10-minute period (15–25 minutes after drug administration). RR intervals were obtained and plotted over time. The SAN arrhythmias were characterized by progressive beat-to-beat

lengthening and subsequent progressive shortening of the RR interval without changes in the other intervals (eg PR and QRS) or morphology of the waves and complexes (eg P wave and QRS complex), such that RR fluctuations originated from fluctuating SA nodal function. The frequency of such RR fluctuations was determined essentially by outlier analysis: One arrhythmia was counted when the RR interval was longer than the 10-minute average RR plus 10 SDs. In the experiments using carbachol, the fluctuations were frequent, giving a high SD, such that this method was ineffective. To quantify the arrhythmias in these experiments, the 10-minute RR interval files were analysed comparing all RR interval with a moving average of the three previous RR intervals. One arrhythmia was counted when the RR interval was longer than the 3-beat average plus 10 SDs.

Heart rate variability was analysed according to Thireau et al.<sup>34</sup> For time domain analysis, RR interval time series were exported of the 12-hour light and 12-hour dark periods. MATLAB (MathWorks) was subsequently used to calculate the time domain parameters mean RR interval, SDRR, RMSSD and the percentage of successive intervals differing more than 6 ms (pNN6). Frequency domain analysis was carried out using Labchart 7 (AD Instruments) to generate spectral analysis of the LF and HF components.

#### 4.6 | Statistics

ECG analyses were performed in a blinded manner, where the investigator was not aware of the preceding drug treatment. Data are presented as mean  $\pm$  SEM. Variables tested between the two types of mice were performed by a two-tailed Student's *t* test. A mixed model ANOVA followed by a Bonferroni post-hoc test was used to compare the two types of mice across different doses or drugs. To compare the occurrence of arrhythmias a Fisher's exact test was used.  $P < .05$  were considered statistically significant.

#### ACKNOWLEDGEMENTS

The study was supported by the Carlsberg Foundation (to MBT), ANR-13-BSV1-0023-01 (to AMG), the Laboratory of Excellence LERMIT ANR-11-IDEX-0003-02 (to LP) and the Chinese Scholarship Council (to JX).

#### CONFLICT OF INTEREST

The authors have no conflict of interest.

#### DATA AVAILABILITY STATEMENT

The data that support the findings of this study are available from the corresponding author upon reasonable request.

## ORCID

Anniek F. Lubberding  <https://orcid.org/0000-0002-6691-8581>

Vladimir V. Matchkov  <https://orcid.org/0000-0002-3303-1095>

Morten B. Thomsen  <https://orcid.org/0000-0002-2469-6458>

## REFERENCES

- Movahed M-R, Hashemzadeh M, Mazen JM. Diabetes mellitus is a strong, independent risk for atrial fibrillation and flutter in addition to other cardiovascular disease. *Int J Cardiol.* 2005;105:315-318.
- Dublin S, Glazer NL, Smith NL, et al. Diabetes mellitus, glycemic control, and risk of atrial fibrillation. *J Gen Intern Med.* 2010;25:853-858.
- Pallisgaard JL, Schjerning A-M, Lindhardt TB, et al. Risk of atrial fibrillation in diabetes mellitus: a nationwide cohort study. *Eur J Prev Cardiol.* 2016;23:621-627.
- Zhang Q, Liu T, Ng CY, Li G. Diabetes mellitus and atrial remodeling: mechanisms and potential upstream therapies. *Cardiovasc Ther.* 2014;32:233-241.
- Capes SE, Hunt D, Malmberg K, Gerstein HC. Stress hyperglycaemia and increased risk of death after myocardial infarction in patients with and without diabetes: a systematic overview. *Lancet.* 2000;355:773-778.
- Movahed M-R, Hashemzadeh M, Jamal MM. Increased prevalence of third-degree atrioventricular block in patients with type II diabetes mellitus. *Chest.* 2005;128:2611-2614.
- Wasada T, Katsumori K, Hasumi S, et al. Association of sick sinus syndrome with hyperinsulinemia and insulin resistance in patients with non-insulin-dependent diabetes mellitus: report of four cases. *Intern Med.* 1995;34:1174-1177.
- Hasslacher C, Wahl P. Diabetes prevalence in patients with bradycardiac arrhythmias. *Acta Diabetol Lat.* 1977;14:229-234.
- Podlaha R, Falk A. The prevalence of diabetes mellitus and other risk factors of atherosclerosis in bradycardia requiring pacemaker treatment. *Horm Metab Res Suppl.* 1992;26:84-87.
- Linnemann B, Janka HU. Prolonged QTc interval and elevated heart rate identify the type 2 diabetic patient at high risk for cardiovascular death. The Bremen Diabetes Study. *Exp Clin Endocrinol diabetes.* 2003;111:215-222.
- Hillis GS, Woodward M, Rodgers A, et al. Resting heart rate and the risk of death and cardiovascular complications in patients with type 2 diabetes mellitus. *Diabetologia.* 2012;55:1283-1290.
- Asaad N, El-Menyar A, AlHabib KF, et al. Initial heart rate and cardiovascular outcomes in patients presenting with acute coronary syndrome. *Acute Card Care.* 2014;16:49-56.
- Stables CL, Glasser RL, Feldman EL. Diabetic cardiac autonomic neuropathy: insights from animal models. *Auton Neurosci.* 2013;177:74-80.
- da Costa Goncalves AC, Tank J, Diedrich André, et al. Diabetic hypertensive leptin receptor-deficient db/db mice develop cardioregulatory autonomic dysfunction. *Hypertension.* 2009;53(2):387-392.
- Semeniuk LM, Kryski AJ, Severson DL. Echocardiographic assessment of cardiac function in diabetic db/db and transgenic db/db-hGLUT4 mice. *Am J Physiol Heart Circ Physiol.* 2002;283:H976-H982.
- Senador D, Kanakamedala K, Irigoyen MC, Morris M, Elased KM. Cardiovascular and autonomic phenotype of db/db diabetic mice. *Exp Physiol.* 2009;94:648-658.
- Soltysinska E, Speerschneider T, Winther SV, Thomsen MB. Sinoatrial node dysfunction induces cardiac arrhythmias in diabetic mice. *Cardiovasc Diabetol.* 2014;13:122.
- Pereira L, Matthes J, Schuster I, et al. Mechanisms of  $[Ca^{2+}]_i$  transient decrease in cardiomyopathy of db/db type 2 diabetic mice. *Diabetes.* 2006;55:608-615.
- Pereira L, Ruiz-Hurtado G, Rueda A, Mercadier JJ, Benitah JP, Gómez AM. Calcium signaling in diabetic cardiomyocytes. *Cell Calcium.* 2014;56:372-380.
- Linscheid N, Logantha SJRJ, Poulsen PC, et al. Quantitative proteomics and single-nucleus transcriptomics of the sinus node elucidates the foundation of cardiac pacemaking. *Nat Commun.* 2019;1-19.
- Ewing DJ, Campbell IW, Clarke BF. Heart rate changes in diabetes mellitus. *Lancet.* 1981;1:183-186.
- Balcioğlu AS, Müderrisoğlu H. Diabetes and cardiac autonomic neuropathy: clinical manifestations, cardiovascular consequences, diagnosis and treatment. *World J Diabetes.* 2015;6:80-91.
- Grubb S, Aistrup GL, Koivumäki JT, et al. Preservation of cardiac function by prolonged action potentials in mice deficient of KChIP2. *Am J Physiol Heart Circ Physiol.* 2015;309:H481-H489.
- Neco P, Torrente AG, Mesirca P, et al. Paradoxical effect of increased diastolic  $Ca^{2+}$  release and decreased sinoatrial node activity in a mouse model of catecholaminergic polymorphic ventricular tachycardia. *Circulation.* 2012;126:392-401.
- Richardson PD, Withrington PG. The vasodilator actions of isoprenaline, histamine, prostaglandin E<sub>2</sub>, glucagon and secretin on the hepatic arterial vascular bed of the dog. *Br J Pharmacol.* 1976;57:581-588.
- Vinik AI, Ziegler D. Diabetic cardiovascular autonomic neuropathy. *Circulation.* 2007;115:387-397.
- Kataoka M, Ito C, Sasaki H, Yamane K, Kohno N. Low heart rate variability is a risk factor for sudden cardiac death in type 2 diabetes. *Diabetes Res Clin Pract.* 2004;64:51-58.
- Sanyal SN, Wada T, Yamabe M, et al. Synaptic degradation of cardiac autonomic nerves in streptozotocin-induced diabetic rats. *Pathophysiol Off J Int Soc Pathophysiol.* 2012;19:299-307.
- Xuan Y-L, Wang YE, Xue M, et al. In rats the duration of diabetes influences its impact on cardiac autonomic innervations and electrophysiology. *Auton Neurosci Basic Clin.* 2015;189:31-36.
- Kellogg AP, Converso K, Wiggins T, Stevens M, Pop-Busui R. Effects of cyclooxygenase-2 gene inactivation on cardiac autonomic and left ventricular function in experimental diabetes. *Am J Physiol Heart Circ Physiol.* 2009;296:H453-H461.
- Wang YE, Xuan Y-L, Hu H-S, et al. Risk of ventricular arrhythmias after myocardial infarction with diabetes associated with sympathetic neural remodeling in rabbits. *Cardiology.* 2012;121:1-9.
- Mabe AM, Hoover DB. Remodeling of cardiac cholinergic innervation and control of heart rate in mice with streptozotocin-induced diabetes. *Auton Neurosci.* 2011;162:24-31.
- Tessari F, Travagli RA, Zannoni R, Prosdocimi M. Effects of long-term diabetes and treatment with gangliosides on cardiac sympathetic innervation: a biochemical and functional study in mice. *J Diabet Complications.* 1988;2:34-37.
- Thireau J, Zhang BL, Poisson D, Babuty D. Heart rate variability in mice: a theoretical and practical guide. *Exp Physiol.* 2008;93:83-94.

35. Krishnaswamy PS, Egom EE, Moghtadaei M, et al. Altered parasympathetic nervous system regulation of the sinoatrial node in Akita diabetic mice. *J Mol Cell Cardiol.* 2015;82:125-135.
36. Luo M, Guan X, Luczak ED, et al. Diabetes increases mortality after myocardial infarction by oxidizing CaMKII. *J Clin Invest.* 2013;123:1262-1274.
37. Howarth CF, Al-Sharhan R, Al-Hammadi A, Qureshi MA. Effects of streptozotocin-induced diabetes on action potentials in the sinoatrial node compared with other regions of the rat heart. *Mol Cell Biochem.* 2007;300:39-46.
38. Howarth FC, Nowotny N, Zilahi E, El Haj MA, Lei M. Altered expression of gap junction connexin proteins may partly underlie heart rhythm disturbances in the streptozotocin-induced diabetic rat heart. *Mol Cell Biochem.* 2007;305:145-151.
39. Ferdous Z, Qureshi MA, Jayaprakash P, et al. Different profile of mRNA expression in sinoatrial node from streptozotocin-induced diabetic rat. *PLoS ONE.* 2016;11:e0153934.
40. Erickson JR, Pereira L, Wang L, et al. Diabetic hyperglycaemia activates CaMKII and arrhythmias by O-linked glycosylation. *Nature.* 2013;502:372-376.
41. Monfredi O, Lyashkov AE, Johnsen A-B, et al. Biophysical characterization of the underappreciated and important relationship between heart rate variability and heart rate. *Hypertension.* 2014;64:1334-1343.
42. Sweeney G. Cardiovascular effects of leptin. *Nat Rev Cardiol.* 2010;7:22-29.
43. Gottlieb LA, Lubberding A, Larsen AP, Thomsen MB. Circadian rhythm in QT interval is preserved in mice deficient of potassium channel interacting protein 2. *Chronobiol Int.* 2017;34:45-56.
44. Schepelmann M, Yarova PL, Lopez-Fernandez I, et al. The vascular Ca<sup>2+</sup>-sensing receptor regulates blood vessel tone and blood pressure. *Am J Physiol Cell Physiol.* 2016;310:C193-204.
45. Wang YY, Mesirca P, Marqués-Sulé E, et al. RyR2R420Q catecholaminergic polymorphic ventricular tachycardia mutation induces bradycardia by disturbing the coupled clock pacemaker mechanism. *JCI insight.* 2017;2:e91872. <https://doi.org/10.1172/jci.insight.91872>
46. Speerschneider T, Thomsen MB. Physiology and analysis of the electrocardiographic T wave in mice. *Acta Physiol (Oxf).* 2013;209:262-271.

**How to cite this article:** Lubberding AF, Pereira L, Xue J, et al. Aberrant sinus node firing during  $\beta$ -adrenergic stimulation leads to cardiac arrhythmias in diabetic mice. *Acta Physiol.* 2020;229:e13444. <https://doi.org/10.1111/apha.13444>

### **Discussion for this part**

The mice suffering the diabetes induced HF, showed pacemaker dysfunction as well. The intrinsic beating rate is faster than WT mice. While the  $\text{Ca}^{2+}$  sparks are more frequent under the basal condition referring to more  $\text{Ca}^{2+}$  leak during the diastolic phase and may result in more arrhythmias. ISO will further increase the  $\text{Ca}^{2+}$  leak in db/db HF SANs. However, after applying ISO, the rate was also significantly increased and Thus, decreased the diastolic time interval leading to a shorter period of time to observe the sparks. So that although on calculation, the frequency of Sparks did not really increase comparing to the basal condition in db/db group. Carbachol decreased the intrinsic rate and sparks frequency in db/db SAN cells significantly, leading both back to the normal level comparing to these in WT mice under the basal condition. Thus, the parasympathetic tone can rectify the dysfunction of SAN under the diabetes induced HF. Considering that in HF patients, the sympathetic tone usually more activated and the parasympathetic tone is relatively inhibited, the finding in this paper provides an inspiring perspective.

# Chapter 4 Discussion

SAN is the primary pacemaker of the heart. It spontaneously generates the electrical signal leading the contraction of the heart, which further pumps blood throughout the body and sustains life. Recently it is widely accepted that the automaticity of the pacemaker is originated from the "coupled-clock" system. This system is consisted by the "voltage clock," and the " $\text{Ca}^{2+}$  clock." Many pathological conditions can influence SAN function, such as hypertrophy and heart failure. Heart failure is a deadly and costly disorder. Recently, some studies showed that Heart failure reduces pacemaker activity of SAN cells through an increase in intrinsic cycle length by impairing the components of voltage clock. The  $\text{Ca}^{2+}$  cycling in the SAN cells from the failing heart is understudied. And the few existing studies did not get consistent results. The aim of this study was to analyze the  $\text{Ca}^{2+}$  handling in SAN using the HF mice model induced by different pathology situation, including transverse aortic constriction (TAC) surgery and diabetes. We have found the CaMKII is less activated in TAC HF SAN other than more phosphorylated observed in ventricles. The lower activation of this kinase leads to lower phosphorylation of PLB and RyR2. Together with the change on the expression level of these two factors, the  $\text{Ca}^{2+}$  clock is impaired in HF sinus node. Further, the decreasing of NCX current links the  $\text{Ca}^{2+}$  clock with voltage clock. So that for the first time we determined the coupled-clock system was impaired in TAC HF SAN. While in Diabetes induced HF we found the intrinsic pacemaking rate is faster than WT and more frequent  $\text{Ca}^{2+}$  sparks were found. These opposite findings within this model may refer to a completely different mechanism than in TAC induced HF.

## 4.1 TAC surgery outcomes-a real Troublemaker

TAC initially leads to compensated hypertrophy of the heart, which is often associated with a temporary enhancement of cardiac contractility. Over time, however, the response to the chronic hemodynamic overload becomes maladaptive, resulting in cardiac dilatation and heart failure. However, published mouse TAC studies report varying profiles for the degree and time course of progression for hypertrophy and cardiac dysfunction. The cardiac phenotype of this model has been described as compensated hypertrophy (left ventricular [LV] hypertrophy, or LVH) in some studies [343,351,352] and as HF in others [353,354]. This may be a critical distinction as the presence of HF may be associated with differential activation of signaling pathways [355,356] and differential response to pharmacologic interventions [357,358]. Furthermore, variability in a model will affect the sample size required to detect the influence of genetic or pharmacologic interventions on LV structure or function and is particularly important when small subsets are selected for assessment of different hemodynamic, biochemical, or genetic parameters.

This standard has some limitation. When the lung shows obvious edema, it should be class 3 or 4 (end stage) of heart failure. So that we may lost the samples on the milder situation of heart failure and making the situation more limited and more extreme. While mixing those class 1 or 2 mice into the hypertrophy group which may lead to the overlap of compensated with non-compensated ones, making the situation more complicated. Reflecting on the results, we cannot explain why KN93 accelerate the pacemaking rate in Hypertrophy group SAN preparation.

## **4.2 The impaired SAN function**

It is now known that HF causes dysfunction of the SAN demonstrating as an increase in intrinsic cycle length [300,363,364]. In our study, we found the same conclusion both in-vivo and in SAN preparation. And the increase in cycle length also happened in Hyp group but to a more extend comparing with HF group. Like discussed before, this group may be mild HF. However, this result shows at the first stage of the pathology, the SAN pacemaking decreased and then recovered a bit when it became severe HF. And the studies showed that this CL increase is mainly due to the impaired voltage clock components. In our study, both HCN4 and NCX decreased in the hyp group and HF group. If the hyp group only contains compensate hypertrophy mice, that could mean the changes on the voltage clock components is not caused by heart failure, but the cardiac hypertrophy or maybe more essential, caused by the pressure overload induced by TAC.

## **4.3 Different shapes different story**

When taken Hyp group into consideration, there are several changing patterns the results may show.

The continuously changing from sham to Hyp then to HF, which is typically showed in RyR2, PLB, NCX and HCN4 expression level. This type of alteration indicates the changes might happen along the pathology process. However, this process may be the severity of the HF (if the Hyp group only contains mild HF), or along the cardiac hypertrophy (if the Hyp group is the mix of HF and compensate hypertrophy).

However, the  $[Ca^{2+}]_i$  transient rate in the Hyp group is much slower than the other two groups. This result indicates that although the components expression level keeps a continuously changing pattern, the modulation level maybe not. The evidence lied into the phosphorylation level of RyR2 and PLB on the PKA site. We found an obvious increasing in Hyp group, revealing the PKA may be more activated in the Hyp group.

This is very critical. Some studies showed that the PKA played a key role in the process from the hypertrophy to HF, while others debated for this conclusion. They think the CaMKII is more important.

However, in our study we found both are important. While CaMKII seem to play a role all the way, because it showed no difference in between the two TAC groups and significantly different between the TAC and Sham. The PKA may have more influence in the first stage of the pathology. Perhaps, whether PKA can show a prominent effect depending on the pathological stage of the mouse when it was sacrificed. The different outputs of the TAC model undoubtedly had a huge impact on the accurate location of the disease course, which led to different results observed in different groups.

Another question will follow. Comparing with HF group, Hyp group showed more HCN4 and NCX, higher phosphorylation level of PLB on both sites, and less PLB as well as higher phosphorylation level on RyR2-S2808 site. It supposed that the Hyp group should have faster  $[Ca^{2+}]_i$  transient rate. However, the result is just opposite. The automaticity of the SAN is not only related to the factors we investigated in this study, but also influenced by other components including LTCC and potassium channels, which may need further investigation.

#### **4.4 The less phosphorylated CaMKII**

In our study the changing of CaMKII showed obvious difference between the Sham and TAC group and no difference was found in the two TAC groups. However, opposite than the situation in the ventricles [273], in our experiment, the CaMKII is less activated in SAN. This is also one of the most interesting results in our study. To date, it is widely accepted that in ventricles under the HF, the CaMKII is more activated demonstrating as more CaMKII expression level while higher phosphorylation level of CaMKII [336,273]. In our results, in order to verify our model, we also conducted the WB in left ventricles and found the Results consistent with published literature.

And since the changing of CaMKII in SAN showed no difference between the TAC groups, it seems that the CaMKII decreased the activity from the beginning stage of the pathology and did not, like PKA, recover in the end stage. This change also leads to the same changing pattern on RyR2-S2814 site.

However, on the PLB CaMKII site, it did not really follow this pattern and may be due to the influence of phosphatase (PP1C). Another reason could be CaMKII has many kinds of activation style. Some studies showed that after the TAC, in the SAN the oxidized CaMKII is higher. More evidence begins to emerge that ox-CaMKII participate in cardiovascular and pulmonary diseases.

#### **4.5 Opposite to the ventricles**

The less phosphorylated CaMKII leads to less phosphorylation levels on RyR2 and PLB which is also opposite to the ventricles. Also, in our study we found there is more RyR2 expression in HF ventricles while in SAN it is less. Thus, in SAN, it tends to decrease the pace making to slow down the

heart rate, while in ventricles it tends to enhance the contractility. Considering that the Ivabradine is a very promising treatment on clinical trial. And Ivabradine can block the HCN4 channels to decrease the HR without influence the contractility. And it showed to be good for HF patients. So that both the SAN and the ventricles are doing the right things to counteract HF. We now tend to call the changes in SAN under HF as the dysfunction, however, we may need to think twice if it is really a 'bad guy'. The heart is a syncytium, but different part chooses different strategies to treat one situation- the heart failure. Who is the commander to ask the ventricle for activating CaMKII and SAN to depress it? This will lead to a contradiction. Maybe slowing the heart rate can allow enough time to the ventricles to fill and recover from the previous contraction and contract more vigorously

## 4.6 Diabetes induced HF

Diabetes will also induce heart failure. Our model, the db/db mice, is a well described model, which present a decrease in ejection fraction at the age we have used them[365]. Thus, they were already under the heart failure condition. In this work, we found that the HRV during the daytime was maintained in db/db HF group and the HRV increased during the night. This is contrary to our pressure overload model, the TAC, where the HRV was decreased in the all the time and we only showed the situation during daytime.

The main difference is that in db/db model, the  $Ca^{2+}$  transients rate was increased comparing with the wildtype. While the TAC mice showed slower  $Ca^{2+}$  transients rate. This result shows that induced by different ways, the HF was may produce different consequences for the pacemaker.

## 4.7 Limitations and perspectives

There are some limitations in this study.

Firstly, the different outcomes of TAC are still confusing. Whether the Hyp group is 'pure' will critically influence the conclusion we may have. And the HF mice we have in this study can only represent the stage 3 or 4 HF. During the project, we also noticed that some dying mice which could hardly move and have severe respiration problems. This kind of mice showed almost totally different results than any other group. However, the sample size is too small, and the situation is quite extreme. But these samples may represent patients who are terminally ill and need to be rescued. It is also very meaningful. And, if not distinguished, it will have a huge impact on other experimental data.

Then, we only investigated the HCN4 channel expression level, for representing the voltage clock components as well as the voltage clock changes. Although this part is not the main topic of this study, the other components of the voltage clock is well worth to notice, such as LTCC and potassium

channels.

Another limitation is that we only investigated the protein expression level of RyR2, PLB, NCX, CaMKII and HCN4. The CaMKII $\delta_c$  containing an 11 amino acid nuclear localization sequence and localized in the nucleus. It can mediate the gene translation. Since we have already noticed the CaMKII phosphorylation level decreased, we should also check the mRNA level of RyR2, PLB, NCX and HCN4 by qPCR.

The db/db HF model showed opposite phenotype than TAC induced HF. This may infer us that only one or two models can not include all the possible situations concerning the heart failure.

Finally, I would like to show one of my thinking. About 400 year ago, people still believed that the earth is the center of the universe, while the Sun is always there. Nowadays we tend to think the calcium is the center of the cardiac modulation while the oxygen is always there.

# References

1. Keith A, Flack M (1907) The Form and Nature of the Muscular Connections between the Primary Divisions of the Vertebrate Heart. *J Anat Physiol* 41 (Pt 3):172-189
2. Hodgkin AL, Huxley AF (1939) Action Potentials Recorded from Inside a Nerve Fibre. *Nature* 144 (3651):710-711. doi:10.1038/144710a0
3. Woodbury LA, Woodbury JW, Hecht HH (1950) Membrane resting and action potentials of single cardiac muscle fibers. *Circulation* 1 (2):264-266. doi:10.1161/01.cir.1.2.264
4. Fozzard HA, Gibbons WR (1973) Action potential and contraction of heart muscle. *Am J Cardiol* 31 (2):182-192. doi:10.1016/0002-9149(73)91031-x
5. Shih HT (1994) Anatomy of the action potential in the heart. *Tex Heart Inst J* 21 (1):30-41
6. Bianchi CP, Bolton TC (1966) Effect of thiocyanate on radiocalcium uptake during potassium contracture of frog sartorius muscle. *J Pharmacol Exp Ther* 151 (3):456-463
7. Isaacson A, Sandow A (1967) Quinine and caffeine effects on  $^{45}\text{Ca}$  movements in frog sartorius muscle. *J Gen Physiol* 50 (8):2109-2128. doi:10.1085/jgp.50.8.2109
8. Ford L, Podolsky R Force development and calcium movements in skinned muscle fibers. In: Federation Proceedings, 1968. vol 2. FEDERATION AMER SOC EXP BIOL 9650 ROCKVILLE PIKE, BETHESDA, MD 20814-3998, pp 375-&
9. Endo M (1977) Calcium release from the sarcoplasmic reticulum. *Physiol Rev* 57 (1):71-108. doi:10.1152/physrev.1977.57.1.71
10. Fabiato A (1983) Calcium-induced release of calcium from the cardiac sarcoplasmic reticulum. *Am J Physiol* 245 (1):C1-14. doi:10.1152/ajpcell.1983.245.1.C1
11. Stern MD (1992) Theory of excitation-contraction coupling in cardiac muscle. *Biophys J* 63 (2):497-517. doi:10.1016/S0006-3495(92)81615-6
12. Cheng H, Lederer WJ, Cannell MB (1993) Calcium sparks: elementary events underlying excitation-contraction coupling in heart muscle. *Science* 262 (5134):740-744. doi:10.1126/science.8235594
13. Song LS, Stern MD, Lakatta EG, Cheng H (1997) Partial depletion of sarcoplasmic reticulum calcium does not prevent calcium sparks in rat ventricular myocytes. *J Physiol* 505 ( Pt 3):665-675. doi:10.1111/j.1469-7793.1997.665ba.x
14. Franzini-Armstrong C, Protasi F, Ramesh V (1998) Comparative ultrastructure of  $\text{Ca}^{2+}$  release units in skeletal and cardiac muscle. *Ann N Y Acad Sci* 853:20-30. doi:10.1111/j.1749-6632.1998.tb08253.x
15. Nikolaienko R, Bovo E, Zima AV (2018) Redox Dependent Modifications of Ryanodine Receptor: Basic Mechanisms and Implications in Heart Diseases. *Front Physiol* 9:1775. doi:10.3389/fphys.2018.01775
16. Cannell MB, Kong CHT (2017) Quenching the spark: Termination of CICR in the submicroscopic space of the dyad. *J Gen Physiol* 149 (9):837-845. doi:10.1085/jgp.201711807
17. Lewis T (1910) The site of origin of the mammalian heart beat : the pacemaker in the dog. *Heart* 2:147-169
18. Bozler E (1943) THE INITIATION OF IMPULSES IN CARDIAC MUSCLE. *American Journal of Physiology-Legacy Content* 138 (2):273-282. doi:10.1152/ajplegacy.1943.138.2.273
19. Maltsev VA, Lakatta EG (2008) Dynamic interactions of an intracellular  $\text{Ca}^{2+}$  clock and membrane ion channel clock underlie robust initiation and regulation of cardiac pacemaker function. *Cardiovasc Res* 77 (2):274-284. doi:10.1093/cvr/cvm058
20. Monfredi O, Maltsev VA, Lakatta EG (2013) Modern concepts concerning the origin of the heartbeat. *Physiology (Bethesda)* 28 (2):74-92. doi:10.1152/physiol.00054.2012
21. West TC (1955) Ultramicroelectrode recording from the cardiac pacemaker. *J Pharmacol Exp Ther* 115 (3):283-290
22. Noble D (1960) Cardiac action and pacemaker potentials based on the Hodgkin-Huxley equations. *Nature* 188:495-497. doi:10.1038/188495b0
23. Maltsev VA, Vinogradova TM, Lakatta EG (2006) The emergence of a general theory of the initiation and strength of the heartbeat. *J Pharmacol Sci* 100 (5):338-369. doi:10.1254/jphs.cr0060018
24. DiFrancesco D, Ojeda C (1980) Properties of the current  $i_f$  in the sino-atrial node of the rabbit compared with those of the current  $i_K$ , in Purkinje fibres. *J Physiol* 308:353-367. doi:10.1113/jphysiol.1980.sp013475
25. Brown H, Kimura J, Noble S (1982) The Relative Contributions of Various Time-Dependent Membrane Currents to Pacemaker Activity in the Sino Atrial Node. In: Bouman LN, Jongsma HJ (eds) *Cardiac Rate and*

- Rhythm: Physiological, Morphological and Developmental Aspects. Springer Netherlands, Dordrecht, pp 53-68. doi:10.1007/978-94-009-7535-4\_5
26. Brown HF, Kimura J, Noble D, Noble SJ, Taupignon A (1984) The ionic currents underlying pacemaker activity in rabbit sino-atrial node: experimental results and computer simulations. *Proc R Soc Lond B Biol Sci* 222 (1228):329-347. doi:10.1098/rspb.1984.0067
  27. Zaza A, Micheletti M, Brioschi A, Rocchetti M (1997) Ionic currents during sustained pacemaker activity in rabbit sino-atrial myocytes. *J Physiol* 505 ( Pt 3):677-688. doi:10.1111/j.1469-7793.1997.677ba.x
  28. Reuter H (1967) The dependence of slow inward current in Purkinje fibres on the extracellular calcium-concentration. *J Physiol* 192 (2):479-492. doi:10.1113/jphysiol.1967.sp008310
  29. Dolphin AC (2006) A short history of voltage-gated calcium channels. *Br J Pharmacol* 147 Suppl 1:S56-62. doi:10.1038/sj.bjp.0706442
  30. Benitah J-P, Alvarez JL, Gómez AM (2010) L-type Ca<sup>2+</sup> current in ventricular cardiomyocytes. *Journal of Molecular and Cellular Cardiology* 48 (1):26-36. doi:https://doi.org/10.1016/j.yjmcc.2009.07.026
  31. Mangoni ME, Trouboulis A, Leoni A-L, Couette B, Marger L, Le Quang K, Kupfer E, Cohen-Solal A, Vilar J, Shin H-S (2006) Bradycardia and slowing of the atrioventricular conduction in mice lacking Ca<sub>v</sub>3.1/α1G T-type calcium channels. *98 (11):1422-1430*
  32. Mangoni ME, Nargeot J (2008) Genesis and Regulation of the Heart Automaticity. *88 (3):919-982*. doi:10.1152/physrev.00018.2007
  33. Tanabe T, Beam KG, Powell JA, Numa SJN (1988) Restoration of excitation—contraction coupling and slow calcium current in dysgenic muscle by dihydropyridine receptor complementary DNA. *336 (6195):134-139*
  34. McRory JE, Hamid J, Doering CJ, Garcia E, Parker R, Hamming K, Chen L, Hildebrand M, Beedle AM, Feldcamp L (2004) The CACNA1F gene encodes an L-type calcium channel with unique biophysical properties and tissue distribution. *24 (7):1707-1718*
  35. Lipscombe D, Helton TD, Xu W (2004) L-type calcium channels: the low down. *J Neurophysiol* 92 (5):2633-2641. doi:10.1152/jn.00486.2004
  36. Bodi I, Mikala G, Koch SE, Akhter SA, Schwartz AJ (2005) The L-type calcium channel in the heart: the beat goes on. *115 (12):3306-3317*
  37. Seisenberger C, Specht V, Welling A, Platzer J, Pfeifer A, Kühbandner S, Striessnig J, Klugbauer N, Feil R, Hofmann F (2000) Functional embryonic cardiomyocytes after disruption of the L-type α1C (Ca<sub>v</sub>1.2) calcium channel gene in the mouse. *275 (50):39193-39199*
  38. Fabiato A, Fabiato F (1975) Contractions induced by a calcium-triggered release of calcium from the sarcoplasmic reticulum of single skinned cardiac cells. *249 (3):469-495*
  39. Gomez AM, Valdivia HH, Cheng H, Lederer MR, Santana LF, Cannell MB, McCune SA, Altschuld RA, Lederer WJ (1997) Defective excitation-contraction coupling in experimental cardiac hypertrophy and heart failure. *Science* 276 (5313):800-806. doi:10.1126/science.276.5313.800
  40. Benitah JP, Gomez AM, Fauconnier J, Kerfant BG, Perrier E, Vassort G, Richard S (2002) Voltage-gated Ca<sup>2+</sup> currents in the human pathophysiologic heart: a review. *Basic Res Cardiol* 97 Suppl 1:11-18. doi:10.1007/s003950200023
  41. Benitah JP, Kerfant BG, Vassort G, Richard S, Gomez AM (2002) Altered communication between L-type calcium channels and ryanodine receptors in heart failure. *Front Biosci* 7:e263-275. doi:10.2741/benitah
  42. Koschak A, Reimer D, Huber I, Grabner M, Glossmann H, Engel J, Striessnig J (2001) α1D (Cav1.3) subunits can form L-type Ca<sup>2+</sup> channels activating at negative voltages. *276 (25):22100-22106*
  43. Mesirca P, Torrente AG, Mangoni ME (2015) Functional role of voltage gated Ca<sup>2+</sup> channels in heart automaticity. *Front Physiol* 6:19. doi:10.3389/fphys.2015.00019
  44. Mangoni ME, Couette B, Bourinet E, Platzer J, Reimer D, Striessnig J, Nargeot J (2003) Functional role of L-type Cav1.3 Ca<sup>2+</sup> channels in cardiac pacemaker activity. *Proc Natl Acad Sci U S A* 100 (9):5543-5548. doi:10.1073/pnas.0935295100
  45. Torrente AG, Mesirca P, Neco P, Rizzetto R, Dubel S, Barrere C, Sinegger-Brauns M, Striessnig J, Richard S, Nargeot J, Gomez AM, Mangoni ME (2016) L-type Cav1.3 channels regulate ryanodine receptor-dependent Ca<sup>2+</sup> release during sino-atrial node pacemaker activity. *Cardiovascular Research* 109 (3):451-461. doi:10.1093/cvr/cvw006
  46. Hagiwara S, Ozawa S, Sand O (1975) Voltage clamp analysis of two inward current mechanisms in the egg cell membrane of a starfish. *J Gen Physiol* 65 (5):617-644. doi:10.1085/jgp.65.5.617

47. Carbone E, Lux HD (1984) A low voltage-activated, fully inactivating Ca channel in vertebrate sensory neurones. *Nature* 310 (5977):501-502. doi:10.1038/310501a0
48. Nowycky MC, Fox AP, Tsien RW (1985) Three types of neuronal calcium channel with different calcium agonist sensitivity. *Nature* 316 (6027):440-443. doi:10.1038/316440a0
49. Marionneau C, Couette B, Liu J, Li H, Mangoni ME, Nargeot J, Lei M, Escande D, Demolombe S (2005) Specific pattern of ionic channel gene expression associated with pacemaker activity in the mouse heart. *J Physiol* 562 (Pt 1):223-234. doi:10.1113/jphysiol.2004.074047
50. Catterall WA, Striessnig J, Snutch TP, Perez-Reyes E, International Union of P (2003) International Union of Pharmacology. XL. Compendium of voltage-gated ion channels: calcium channels. *Pharmacol Rev* 55 (4):579-581. doi:10.1124/pr.55.4.8
51. Mangoni ME, Traboulsie A, Leoni AL, Couette B, Marger L, Le Quang K, Kupfer E, Cohen-Solal A, Vilar J, Shin HS, Escande D, Charpentier F, Nargeot J, Lory P (2006) Bradycardia and slowing of the atrioventricular conduction in mice lacking CaV3.1/alpha1G T-type calcium channels. *Circ Res* 98 (11):1422-1430. doi:10.1161/01.RES.0000225862.14314.49
52. Leuranguer V, Monteil A, Bourinet E, Dayanithi G, Nargeot J (2000) T-type calcium currents in rat cardiomyocytes during postnatal development: contribution to hormone secretion. *Am J Physiol Heart Circ Physiol* 279 (5):H2540-2548. doi:10.1152/ajpheart.2000.279.5.H2540
53. Huser J, Blatter LA, Lipsius SL (2000) Intracellular Ca<sup>2+</sup> release contributes to automaticity in cat atrial pacemaker cells. *J Physiol* 524 Pt 2:415-422. doi:10.1111/j.1469-7793.2000.00415.x
54. Lipsius SL, Huser J, Blatter LA (2001) Intracellular Ca<sup>2+</sup> release sparks atrial pacemaker activity. *News Physiol Sci* 16:101-106. doi:10.1152/physiologyonline.2001.16.3.101
55. Mangoni ME, Nargeot J (2008) Genesis and regulation of the heart automaticity. *Physiol Rev* 88 (3):919-982. doi:10.1152/physrev.00018.2007
56. Lei M, Jones SA, Liu J, Lancaster MK, Fung SS, Dobrzynski H, Camelliti P, Maier SK, Noble D, Boyett MR (2004) Requirement of neuronal- and cardiac-type sodium channels for murine sinoatrial node pacemaking. *J Physiol* 559 (Pt 3):835-848. doi:10.1113/jphysiol.2004.068643
57. Tellez JO, Dobrzynski H, Greener ID, Graham GM, Laing E, Honjo H, Hubbard SJ, Boyett MR, Billeter R (2006) Differential expression of ion channel transcripts in atrial muscle and sinoatrial node in rabbit. *Circ Res* 99 (12):1384-1393. doi:10.1161/01.RES.0000251717.98379.69
58. Maier SK, Westenbroek RE, Yamanushi TT, Dobrzynski H, Boyett MR, Catterall WA, Scheuer T (2003) An unexpected requirement for brain-type sodium channels for control of heart rate in the mouse sinoatrial node. *Proc Natl Acad Sci U S A* 100 (6):3507-3512. doi:10.1073/pnas.2627986100
59. Lei M, Goddard C, Liu J, Leoni AL, Royer A, Fung SS, Xiao G, Ma A, Zhang H, Charpentier F, Vandenberg JL, Colledge WH, Grace AA, Huang CL (2005) Sinus node dysfunction following targeted disruption of the murine cardiac sodium channel gene *Scn5a*. *J Physiol* 567 (Pt 2):387-400. doi:10.1113/jphysiol.2005.083188
60. Baruscotti M, DiFrancesco D, Robinson RB (1996) A TTX-sensitive inward sodium current contributes to spontaneous activity in newborn rabbit sino-atrial node cells. *J Physiol* 492 ( Pt 1):21-30. doi:10.1113/jphysiol.1996.sp021285
61. Baruscotti M, Westenbroek R, Catterall WA, DiFrancesco D, Robinson RB (1997) The newborn rabbit sino-atrial node expresses a neuronal type I-like Na<sup>+</sup> channel. *J Physiol* 498 ( Pt 3):641-648. doi:10.1113/jphysiol.1997.sp021889
62. Baruscotti M, DiFrancesco D, Robinson RB (2000) Na<sup>(+)</sup> current contribution to the diastolic depolarization in newborn rabbit SA node cells. *Am J Physiol Heart Circ Physiol* 279 (5):H2303-2309. doi:10.1152/ajpheart.2000.279.5.H2303
63. Maltsev VA, Yaniv Y, Maltsev AV, Stern MD, Lakatta EG (2014) Modern Perspectives on Numerical Modeling of Cardiac Pacemaker Cell. *Journal of Pharmacological Sciences* 125 (1):6-38. doi:https://doi.org/10.1254/jphs.13R04CR
64. Ibarra J, Morley GE, Delmar M (1991) Dynamics of the inward rectifier K<sup>+</sup> current during the action potential of guinea pig ventricular myocytes. *Biophys J* 60 (6):1534-1539. doi:10.1016/S0006-3495(91)82187-7
65. Satoh H (2003) Sino-atrial nodal cells of mammalian hearts: ionic currents and gene expression of pacemaker ionic channels. *J Smooth Muscle Res* 39 (5):175-193. doi:10.1540/jsmr.39.175
66. Shinagawa Y, Satoh H, Noma A (2000) The sustained inward current and inward rectifier K<sup>+</sup> current in pacemaker cells dissociated from rat sinoatrial node. *J Physiol* 523 Pt 3:593-605. doi:10.1111/j.1469-7793.2000.t01-2-00593.x

67. Cho HS, Takano M, Noma A (2003) The electrophysiological properties of spontaneously beating pacemaker cells isolated from mouse sinoatrial node. *J Physiol* 550 (Pt 1):169-180. doi:10.1113/jphysiol.2003.040501
68. DiFrancesco D, Ducouret P, Robinson RB (1989) Muscarinic modulation of cardiac rate at low acetylcholine concentrations. *Science* 243 (4891):669-671. doi:10.1126/science.2916119
69. Giles W, Noble SJ (1976) Changes in membrane currents in bullfrog atrium produced by acetylcholine. *J Physiol* 261 (1):103-123. doi:10.1113/jphysiol.1976.sp011550
70. Noma A, Trautwein W (1978) Relaxation of the ACh-induced potassium current in the rabbit sinoatrial node cell. *Pflugers Arch* 377 (3):193-200. doi:10.1007/BF00584272
71. Mesirca P, Bidaud I, Briec F, Evain S, Torrente AG, Le Quang K, Leoni A-L, Baudot M, Marger L, Chung You Chong A, Nargeot J, Striessnig J, Wickman K, Charpentier F, Mangoni ME (2016) G protein-gated  $KACH$  channels as therapeutic targets for treatment of sick sinus syndrome and heart block. 201517181. doi:10.1073/pnas.1517181113 %J Proceedings of the National Academy of Sciences
72. Reuveny E, Slesinger PA, Inglese J, Morales JM, Iniguez-Lluhi JA, Lefkowitz RJ, Bourne HR, Jan YN, Jan LY (1994) Activation of the cloned muscarinic potassium channel by G protein beta gamma subunits. *Nature* 370 (6485):143-146. doi:10.1038/370143a0
73. Mesirca P, Marger L, Toyoda F, Rizzetto R, Audoubert M, Dubel S, Torrente AG, DiFrancesco ML, Muller JC, Leoni AL, Couette B, Nargeot J, Clapham DE, Wickman K, Mangoni ME (2013) The G-protein-gated  $K^+$  channel,  $IKACH$ , is required for regulation of pacemaker activity and recovery of resting heart rate after sympathetic stimulation. *J Gen Physiol* 142 (2):113-126. doi:10.1085/jgp.201310996
74. Vergara C, Latorre R, Marrion NV, Adelman JP (1998) Calcium-activated potassium channels. *Curr Opin Neurobiol* 8 (3):321-329. doi:10.1016/s0959-4388(98)80056-1
75. Weisbrod D, Khun SH, Bueno H, Peretz A, Attali B (2016) Mechanisms underlying the cardiac pacemaker: the role of SK4 calcium-activated potassium channels. *Acta Pharmacol Sin* 37 (1):82-97. doi:10.1038/aps.2015.135
76. Knaus HG, Schwarzer C, Koch RO, Eberhart A, Kaczorowski GJ, Glossmann H, Wunder F, Pongs O, Garcia ML, Sperk G (1996) Distribution of high-conductance  $Ca^{2+}$ -activated  $K^+$  channels in rat brain: targeting to axons and nerve terminals. *J Neurosci* 16 (3):955-963
77. Nelson MT, Cheng H, Rubart M, Santana LF, Bonev AD, Knot HJ, Lederer WJ (1995) Relaxation of arterial smooth muscle by calcium sparks. *Science* 270 (5236):633-637. doi:10.1126/science.270.5236.633
78. Imlach WL, Finch SC, Miller JH, Meredith AL, Dalziel JE (2010) A role for BK channels in heart rate regulation in rodents. *PLoS One* 5 (1):e8698. doi:10.1371/journal.pone.0008698
79. Lai MH, Wu Y, Gao Z, Anderson ME, Dalziel JE, Meredith AL (2014) BK channels regulate sinoatrial node firing rate and cardiac pacing in vivo. *Am J Physiol Heart Circ Physiol* 307 (9):H1327-1338. doi:10.1152/ajpheart.00354.2014
80. Klumpp L, Sezgin EC, Skardelly M, Eckert F, Huber SM (2018)  $KCa_{3.1}$  Channels and Glioblastoma: In Vitro Studies. *Curr Neuropharmacol* 16 (5):627-635. doi:10.2174/1570159X15666170808115821
81. Thompson-Vest N, Shimizu Y, Hunne B, Furness JB (2006) The distribution of intermediate-conductance, calcium-activated, potassium ( $IK$ ) channels in epithelial cells. *J Anat* 208 (2):219-229. doi:10.1111/j.1469-7580.2006.00515.x
82. Attali B, Weisbrod D, Bueno H, Behar J, Haron-Khun S, Yadin D, Peretz A, Arad M, Yaniv Y (2017)  $SK4$   $Ca^{2+}$ -Activated  $K^+$  Channels Regulate Sinoatrial Node Firing Rate and Cardiac Pacing In Vivo. *Biophysical Journal* 112:35a. doi:10.1016/j.bpj.2016.11.225
83. Xu Y, Tuteja D, Zhang Z, Xu D, Zhang Y, Rodriguez J, Nie L, Tuxson HR, Young JN, Glatter KA, Vazquez AE, Yamoah EN, Chiamvimonvat N (2003) Molecular identification and functional roles of a  $Ca^{2+}$ -activated  $K^+$  channel in human and mouse hearts. *J Biol Chem* 278 (49):49085-49094. doi:10.1074/jbc.M307508200
84. Tuteja D, Xu D, Timofeyev V, Lu L, Sharma D, Zhang Z, Xu Y, Nie L, Vazquez AE, Young JN, Glatter KA, Chiamvimonvat N (2005) Differential expression of small-conductance  $Ca^{2+}$ -activated  $K^+$  channels SK1, SK2, and SK3 in mouse atrial and ventricular myocytes. *Am J Physiol Heart Circ Physiol* 289 (6):H2714-2723. doi:10.1152/ajpheart.00534.2005
85. Li N, Timofeyev V, Tuteja D, Xu D, Lu L, Zhang Q, Zhang Z, Singapuri A, Albert TR, Rajagopal AV, Bond CT, Periasamy M, Adelman J, Chiamvimonvat N (2009) Ablation of a  $Ca^{2+}$ -activated  $K^+$  channel ( $SK2$  channel) results in action potential prolongation in atrial myocytes and atrial fibrillation. *J Physiol* 587 (Pt 5):1087-1100. doi:10.1113/jphysiol.2008.167718

86. Qi XY, Diness JG, Brundel BJ, Zhou XB, Naud P, Wu CT, Huang H, Harada M, Aflaki M, Dobrev D, Grunnet M, Nattel S (2014) Role of small-conductance calcium-activated potassium channels in atrial electrophysiology and fibrillation in the dog. *Circulation* 129 (4):430-440. doi:10.1161/CIRCULATIONAHA.113.003019
87. Liu DW, Antzelevitch C (1995) Characteristics of the delayed rectifier current (IKr and IKs) in canine ventricular epicardial, midmyocardial, and endocardial myocytes. A weaker IKs contributes to the longer action potential of the M cell. *Circ Res* 76 (3):351-365. doi:10.1161/01.res.76.3.351
88. Ito H, Ono K (1995) A rapidly activating delayed rectifier K<sup>+</sup> channel in rabbit sinoatrial node cells. *Am J Physiol* 269 (2 Pt 2):H443-452. doi:10.1152/ajpheart.1995.269.2.H443
89. Lei M, Brown HF (1996) Two components of the delayed rectifier potassium current, IK, in rabbit sino-atrial node cells. *Exp Physiol* 81 (5):725-741. doi:10.1113/expphysiol.1996.sp003972
90. Ono K, Shibata S, Iijima T (2000) Properties of the delayed rectifier potassium current in porcine sino-atrial node cells. *J Physiol* 524 Pt 1:51-62
91. Ono K, Ito H (1995) Role of rapidly activating delayed rectifier K<sup>+</sup> current in sinoatrial node pacemaker activity. *Am J Physiol* 269 (2 Pt 2):H453-462. doi:10.1152/ajpheart.1995.269.2.H453
92. Matsuura H, Ehara T, Ding WG, Omatsu-Kanbe M, Isono T (2002) Rapidly and slowly activating components of delayed rectifier K(+) current in guinea-pig sino-atrial node pacemaker cells. *J Physiol* 540 (Pt 3):815-830. doi:10.1113/jphysiol.2001.016741
93. Verheijck EE, Wilders R, Bouman LN (2002) Atrio-sinus interaction demonstrated by blockade of the rapid delayed rectifier current. *Circulation* 105 (7):880-885. doi:10.1161/hc0702.104128
94. Honjo H, Lei M, Boyett MR, Kodama I (1999) Heterogeneity of 4-aminopyridine-sensitive current in rabbit sinoatrial node cells. *J Physiol* 524 (Pt 2):H1295-H1304. doi:10.1152/ajpheart.1999.276.4.H1295
95. Han X, Light PE, Giles WR, French RJ (1996) Identification and properties of an ATP-sensitive K<sup>+</sup> current in rabbit sino-atrial node pacemaker cells. *J Physiol* 490 ( Pt 2):337-350. doi:10.1113/jphysiol.1996.sp021148
96. Venkatachalam K, Montell C (2007) TRP channels. *Annu Rev Biochem* 76:387-417. doi:10.1146/annurev.biochem.75.103004.142819
97. Löf C, Viitanen T, Sukumaran P, Törnquist K (2011) TRPC2: Of Mice But Not Men. In: Islam MS (ed) *Transient Receptor Potential Channels*. Springer Netherlands, Dordrecht, pp 125-134. doi:10.1007/978-94-007-0265-3\_6
98. Nilius B, Owsianik G, Voets T, Peters JA (2007) Transient receptor potential cation channels in disease. *Physiol Rev* 87 (1):165-217. doi:10.1152/physrev.00021.2006
99. Abramowitz J, Birnbaumer L (2009) Physiology and pathophysiology of canonical transient receptor potential channels. *FASEB J* 23 (2):297-328. doi:10.1096/fj.08-119495
100. Ju YK, Chu Y, Chaulet H, Lai D, Gervasio OL, Graham RM, Cannell MB, Allen DG (2007) Store-operated Ca<sup>2+</sup> influx and expression of TRPC genes in mouse sinoatrial node. *Circ Res* 100 (11):1605-1614. doi:10.1161/CIRCRESAHA.107.152181
101. Ju YK, Allen DG (2007) Store-operated Ca<sup>2+</sup> entry and TRPC expression; possible roles in cardiac pacemaker tissue. *Heart Lung Circ* 16 (5):349-355. doi:10.1016/j.hlc.2007.07.004
102. Frischauf I, Schindl R, Derler I, Bergsmann J, Fahrner M, Romanin C (2008) The STIM/Orai coupling machinery. *Channels (Austin)* 2 (4):261-268. doi:10.4161/chan.2.4.6705
103. Yuan JP, Zeng W, Huang GN, Worley PF, Muallem S (2007) STIM1 heteromultimerizes TRPC channels to determine their function as store-operated channels. *Nat Cell Biol* 9 (6):636-645. doi:10.1038/ncb1590
104. Liao Y, Plummer NW, George MD, Abramowitz J, Zhu MX, Birnbaumer L (2009) A role for Orai in TRPC-mediated Ca<sup>2+</sup> entry suggests that a TRPC:Orai complex may mediate store and receptor operated Ca<sup>2+</sup> entry. *Proc Natl Acad Sci U S A* 106 (9):3202-3206. doi:10.1073/pnas.0813346106
105. Pani B, Ong HL, Liu X, Rauser K, Ambudkar IS, Singh BB (2008) Lipid rafts determine clustering of STIM1 in endoplasmic reticulum-plasma membrane junctions and regulation of store-operated Ca<sup>2+</sup> entry (SOCE). *J Biol Chem* 283 (25):17333-17340. doi:10.1074/jbc.M800107200
106. Bush EW, Hood DB, Papst PJ, Chapo JA, Minobe W, Bristow MR, Olson EN, McKinsey TA (2006) Canonical transient receptor potential channels promote cardiomyocyte hypertrophy through activation of calcineurin signaling. *J Biol Chem* 281 (44):33487-33496. doi:10.1074/jbc.M605536200
107. Kuwahara K, Wang Y, McAnally J, Richardson JA, Bassel-Duby R, Hill JA, Olson EN (2006) TRPC6 fulfills a calcineurin signaling circuit during pathologic cardiac remodeling. *J Clin Invest* 116 (12):3114-3126. doi:10.1172/JCI27702
108. Salido GM, Sage SO, Rosado JA (2009) TRPC channels and store-operated Ca(2+) entry. *Biochim Biophys Acta* 1793 (2):223-230. doi:10.1016/j.bbamcr.2008.11.001

109. Demion M, Bois P, Launay P, Guinamard R (2007) TRPM4, a Ca<sup>2+</sup>-activated nonselective cation channel in mouse sino-atrial node cells. *Cardiovasc Res* 73 (3):531-538. doi:10.1016/j.cardiores.2006.11.023
110. Hof T, Simard C, Rouet R, Salle L, Guinamard R (2013) Implication of the TRPM4 nonselective cation channel in mammalian sinus rhythm. *Heart Rhythm* 10 (11):1683-1689. doi:10.1016/j.hrthm.2013.08.014
111. Little SC, Mohler PJ (2013) TRPM4 modulates sinus node diastolic depolarization. *Heart Rhythm* 10 (11):1690-1691. doi:10.1016/j.hrthm.2013.08.026
112. Sah R, Mesirca P, Van den Boogert M, Rosen J, Mably J, Mangoni ME, Clapham DE (2013) Ion channel-kinase TRPM7 is required for maintaining cardiac automaticity. *Proc Natl Acad Sci U S A* 110 (32):E3037-3046. doi:10.1073/pnas.1311865110
113. Mitsuiye T, Shinagawa Y, Noma A (2000) Sustained inward current during pacemaker depolarization in mammalian sinoatrial node cells. *Circ Res* 87 (2):88-91. doi:10.1161/01.res.87.2.88
114. Sakai R, Hagiwara N, Matsuda N, Kassanuki H, Hosoda S (1996) Sodium--potassium pump current in rabbit sino-atrial node cells. *J Physiol* 490 ( Pt 1):51-62. doi:10.1113/jphysiol.1996.sp021126
115. DiFrancesco D, Noble D (2012) The funny current has a major pacemaking role in the sinus node. *Heart Rhythm* 9 (2):299-301. doi:10.1016/j.hrthm.2011.09.021
116. Chen PS, Joung B, Shinohara T, Das M, Chen Z, Lin SF (2010) The initiation of the heart beat. *Circ J* 74 (2):221-225. doi:10.1253/circj.cj-09-0712
117. Rubenstein DS, Lipsius SL (1989) Mechanisms of automaticity in subsidiary pacemakers from cat right atrium. *Circ Res* 64 (4):648-657. doi:10.1161/01.res.64.4.648
118. Rigg L, Terrar DA (1996) Possible role of calcium release from the sarcoplasmic reticulum in pacemaking in guinea-pig sino-atrial node. *Exp Physiol* 81 (5):877-880. doi:10.1113/expphysiol.1996.sp003983
119. Lyashkov AE, Juhaszova M, Dobrzynski H, Vinogradova TM, Maltsev VA, Juhasz O, Spurgeon HA, Sollott SJ, Lakatta EG (2007) Calcium cycling protein density and functional importance to automaticity of isolated sinoatrial nodal cells are independent of cell size. *Circ Res* 100 (12):1723-1731. doi:10.1161/CIRCRESAHA.107.153676
120. Bround MJ, Asghari P, Wambolt RB, Bohunek L, Smits C, Philit M, Kieffer TJ, Lakatta EG, Boheler KR, Moore ED, Allard MF, Johnson JD (2012) Cardiac ryanodine receptors control heart rate and rhythmicity in adult mice. *Cardiovasc Res* 96 (3):372-380. doi:10.1093/cvr/cvs260
121. Vinogradova TM, Bogdanov KY, Lakatta EG (2002) beta-Adrenergic stimulation modulates ryanodine receptor Ca<sup>2+</sup> release during diastolic depolarization to accelerate pacemaker activity in rabbit sinoatrial nodal cells. *Circ Res* 90 (1):73-79. doi:10.1161/hh0102.102271
122. Vinogradova TM, Bogdanov KY, Lakatta EG (2002) Novel perspectives on the beating rate of the heart. *Circ Res* 91 (4):e3. doi:10.1161/01.res.0000031164.28289.55
123. Vinogradova TM, Zhou YY, Maltsev V, Lyashkov A, Stern M, Lakatta EG (2004) Rhythmic ryanodine receptor Ca<sup>2+</sup> releases during diastolic depolarization of sinoatrial pacemaker cells do not require membrane depolarization. *Circ Res* 94 (6):802-809. doi:10.1161/01.RES.0000122045.55331.0F
124. Vinogradova TM, Brochet DX, Sirenko S, Li Y, Spurgeon H, Lakatta EG (2010) Sarcoplasmic reticulum Ca<sup>2+</sup> pumping kinetics regulates timing of local Ca<sup>2+</sup> releases and spontaneous beating rate of rabbit sinoatrial node pacemaker cells. *Circ Res* 107 (6):767-775. doi:10.1161/CIRCRESAHA.110.220517
125. Vinogradova TM, Lakatta EG (2009) Regulation of basal and reserve cardiac pacemaker function by interactions of cAMP-mediated PKA-dependent Ca<sup>2+</sup> cycling with surface membrane channels. *J Mol Cell Cardiol* 47 (4):456-474. doi:10.1016/j.yjmcc.2009.06.014
126. Maltsev VA, Vinogradova TM, Bogdanov KY, Lakatta EG, Stern MD (2004) Diastolic calcium release controls the beating rate of rabbit sinoatrial node cells: numerical modeling of the coupling process. *Biophys J* 86 (4):2596-2605. doi:10.1016/S0006-3495(04)74314-3
127. Bassani JW, Bassani RA, Bers DM (1995) Calibration of indo-1 and resting intracellular [Ca]<sub>i</sub> in intact rabbit cardiac myocytes. *Biophys J* 68 (4):1453-1460. doi:10.1016/S0006-3495(95)80318-8
128. Maltsev VA, Yaniv Y, Maltsev AV, Stern MD, Lakatta EG (2014) Modern perspectives on numerical modeling of cardiac pacemaker cell. *J Pharmacol Sci* 125 (1):6-38. doi:10.1254/jphs.13r04cr
129. Bers DM (2002) Cardiac excitation-contraction coupling. *Nature* 415 (6868):198-205. doi:10.1038/415198a
130. Maltsev AV, Yaniv Y, Stern MD, Lakatta EG, Maltsev VA (2013) RyR-NCX-SERCA local cross-talk ensures pacemaker cell function at rest and during the fight-or-flight reflex. *Circ Res* 113 (10):e94-e100. doi:10.1161/CIRCRESAHA.113.302465

131. Ju YK, Allen DG (1998) Intracellular calcium and Na<sup>+</sup>-Ca<sup>2+</sup> exchange current in isolated toad pacemaker cells. *J Physiol* 508 ( Pt 1):153-166. doi:10.1111/j.1469-7793.1998.153br.x
132. Bogdanov KY, Vinogradova TM, Lakatta EG (2001) Sinoatrial nodal cell ryanodine receptor and Na<sup>(+)</sup>-Ca<sup>(2+)</sup> exchanger: molecular partners in pacemaker regulation. *Circ Res* 88 (12):1254-1258. doi:10.1161/hh1201.092095
133. Quednau BD, Nicoll DA, Philipson KD (1997) Tissue specificity and alternative splicing of the Na<sup>+</sup>/Ca<sup>2+</sup> exchanger isoforms NCX1, NCX2, and NCX3 in rat. *Am J Physiol* 272 (4 Pt 1):C1250-1261. doi:10.1152/ajpcell.1997.272.4.C1250
134. Levitsky DO (2007) Three types of muscles express three sodium-calcium exchanger isoforms. *Ann N Y Acad Sci* 1099:221-225. doi:10.1196/annals.1387.063
135. Lee SL, Yu AS, Lytton J (1994) Tissue-specific expression of Na<sup>(+)</sup>-Ca<sup>2+</sup> exchanger isoforms. *J Biol Chem* 269 (21):14849-14852
136. Koushik SV, Wang J, Rogers R, Moskophidis D, Lambert NA, Creazzo TL, Conway SJ (2001) Targeted inactivation of the sodium-calcium exchanger (Ncx1) results in the lack of a heartbeat and abnormal myofibrillar organization. *FASEB J* 15 (7):1209-1211. doi:10.1096/fj.00-0696fje
137. Gao Z, Rasmussen TP, Li Y, Kutschke W, Koval OM, Wu Y, Wu Y, Hall DD, Joiner ML, Wu XQ, Swaminathan PD, Purohit A, Zimmerman K, Weiss RM, Philipson KD, Song LS, Hund TJ, Anderson ME (2013) Genetic inhibition of Na<sup>+</sup>-Ca<sup>2+</sup> exchanger current disables fight or flight sinoatrial node activity without affecting resting heart rate. *Circ Res* 112 (2):309-317. doi:10.1161/CIRCRESAHA.111.300193
138. Herrmann S, Lipp P, Wiesen K, Stieber J, Nguyen H, Kaiser E, Ludwig A (2013) The cardiac sodium-calcium exchanger NCX1 is a key player in the initiation and maintenance of a stable heart rhythm. *Cardiovasc Res* 99 (4):780-788. doi:10.1093/cvr/cvt154
139. Yaniv Y, Lakatta EG, Maltsev VA (2015) From two competing oscillators to one coupled-clock pacemaker cell system. *Front Physiol* 6:28. doi:10.3389/fphys.2015.00028
140. Kort AA, Lakatta EG, Marban E, Stern MD, Wier WG (1985) Fluctuations in intracellular calcium concentration and their effect on tonic tension in canine cardiac Purkinje fibres. *J Physiol* 367:291-308. doi:10.1113/jphysiol.1985.sp015825
141. Kort AA, Lakatta EG (1984) Calcium-dependent mechanical oscillations occur spontaneously in unstimulated mammalian cardiac tissues. *54* (4):396-404. doi:doi:10.1161/01.RES.54.4.396
142. Maltsev VA, Lakatta EG (2012) The funny current in the context of the coupled-clock pacemaker cell system. *Heart Rhythm* 9 (2):302-307. doi:10.1016/j.hrthm.2011.09.022
143. Mattick P, Parrington J, Odia E, Simpson A, Collins T, Terrar D (2007) Ca<sup>2+</sup>-stimulated adenylyl cyclase isoform AC1 is preferentially expressed in guinea-pig sino-atrial node cells and modulates the I(f) pacemaker current. *J Physiol* 582 (Pt 3):1195-1203. doi:10.1113/jphysiol.2007.133439
144. Younes A, Lyashkov AE, Graham D, Sheydina A, Volkova MV, Mitsak M, Vinogradova TM, Lukyanenko YO, Li Y, Ruknudin AM, Boheler KR, van Eyk J, Lakatta EG (2008) Ca<sup>(2+)</sup> -stimulated basal adenylyl cyclase activity localization in membrane lipid microdomains of cardiac sinoatrial nodal pacemaker cells. *J Biol Chem* 283 (21):14461-14468. doi:10.1074/jbc.M707540200
145. Yaniv Y, Spurgeon HA, Ziman BD, Lakatta EG (2013) Ca<sup>(2+)</sup>/calmodulin-dependent protein kinase II (CaMKII) activity and sinoatrial nodal pacemaker cell energetics. *PLoS One* 8 (2):e57079. doi:10.1371/journal.pone.0057079
146. Lakatta EG, DiFrancesco D (2009) What keeps us ticking: a funny current, a calcium clock, or both? *J Mol Cell Cardiol* 47 (2):157-170. doi:10.1016/j.yjmcc.2009.03.022
147. Monfredi O, Maltseva LA, Spurgeon HA, Boyett MR, Lakatta EG, Maltsev VA (2013) Beat-to-Beat Variation in Periodicity of Local Calcium Releases Contributes to Intrinsic Variations of Spontaneous Cycle Length in Isolated Single Sinoatrial Node Cells. *PLoS One* 8 (6):e67247. doi:10.1371/journal.pone.0067247
148. Stern MD, Maltseva LA, Juhaszova M, Sollott SJ, Lakatta EG, Maltsev VA (2014) Hierarchical clustering of ryanodine receptors enables emergence of a calcium clock in sinoatrial node cells. *J Gen Physiol* 143 (5):577-604. doi:10.1085/jgp.201311123
149. Yaniv Y, Lyashkov AE, Sirenko S, Okamoto Y, Guiriba TR, Ziman BD, Morrell CH, Lakatta EG (2014) Stochasticity intrinsic to coupled-clock mechanisms underlies beat-to-beat variability of spontaneous action potential firing in sinoatrial node pacemaker cells. *J Mol Cell Cardiol* 77:1-10. doi:10.1016/j.yjmcc.2014.09.008

150. Rysevaite K, Saburkina I, Pauziene N, Noujaim SF, Jalife J, Pauza DH (2011) Morphologic pattern of the intrinsic ganglionated nerve plexus in mouse heart. *Heart Rhythm* 8 (3):448-454. doi:10.1016/j.hrthm.2010.11.019
151. Weihe E, Schutz B, Hartschuh W, Anlauf M, Schafer MK, Eiden LE (2005) Coexpression of cholinergic and noradrenergic phenotypes in human and nonhuman autonomic nervous system. *J Comp Neurol* 492 (3):370-379. doi:10.1002/cne.20745
152. Duraes Campos I, Pinto V, Sousa N, Pereira VH (2018) A brain within the heart: A review on the intracardiac nervous system. *J Mol Cell Cardiol* 119:1-9. doi:10.1016/j.yjmcc.2018.04.005
153. Armour JA, Murphy DA, Yuan BX, Macdonald S, Hopkins DA (1997) Gross and microscopic anatomy of the human intrinsic cardiac nervous system. *Anat Rec* 247 (2):289-298. doi:10.1002/(SICI)1097-0185(199702)247:2<289::AID-AR15>3.0.CO;2-L
154. Wake E, Brack K (2016) Characterization of the intrinsic cardiac nervous system. *Auton Neurosci* 199:3-16. doi:10.1016/j.autneu.2016.08.006
155. Shen MJ, Zipes DP (2014) Role of the autonomic nervous system in modulating cardiac arrhythmias. *Circ Res* 114 (6):1004-1021. doi:10.1161/CIRCRESAHA.113.302549
156. Armour JA (2008) Potential clinical relevance of the 'little brain' on the mammalian heart. *Exp Physiol* 93 (2):165-176. doi:10.1113/expphysiol.2007.041178
157. Nakamura K, Ajjola OA, Aliotta E, Armour JA, Ardell JL, Shivkumar K (2016) Pathological effects of chronic myocardial infarction on peripheral neurons mediating cardiac neurotransmission. *Auton Neurosci* 197:34-40. doi:10.1016/j.autneu.2016.05.001
158. Gordan R, Gwathmey JK, Xie LH (2015) Autonomic and endocrine control of cardiovascular function. *World J Cardiol* 7 (4):204-214. doi:10.4330/wjc.v7.i4.204
159. Oldham WM, Hamm HE (2008) Heterotrimeric G protein activation by G-protein-coupled receptors. *Nature Reviews Molecular Cell Biology* 9 (1):60-71. doi:10.1038/nrm2299
160. Rosenbaum DM, Rasmussen SG, Kobilka BK (2009) The structure and function of G-protein-coupled receptors. *Nature* 459 (7245):356-363. doi:10.1038/nature08144
161. Zhang P, Kofron CM, Mende U (2015) Heterotrimeric G protein-mediated signaling and its non-canonical regulation in the heart. *Life Sci* 129:35-41. doi:10.1016/j.lfs.2015.02.029
162. MacDonald EA, Rose RA, Quinn TA (2020) Neurohumoral Control of Sinoatrial Node Activity and Heart Rate: Insight From Experimental Models and Findings From Humans. 11 (170). doi:10.3389/fphys.2020.00170
163. Madamanchi A (2007) Beta-adrenergic receptor signaling in cardiac function and heart failure. *McGill J Med* 10 (2):99-104
164. Tobise K, Ishikawa Y, Holmer SR, Im MJ, Newell JB, Yoshie H, Fujita M, Susannie EE, Homcy CJ (1994) Changes in type VI adenylyl cyclase isoform expression correlate with a decreased capacity for cAMP generation in the aging ventricle. *Circ Res* 74 (4):596-603. doi:10.1161/01.res.74.4.596
165. Baldwin TA, Dessauer CW (2018) Function of Adenylyl Cyclase in Heart: the AKAP Connection. *J Cardiovasc Dev Dis* 5 (1). doi:10.3390/jcdd5010002
166. Hanoune J, Defer N (2001) Regulation and role of adenylyl cyclase isoforms. *Annu Rev Pharmacol Toxicol* 41:145-174. doi:10.1146/annurev.pharmtox.41.1.145
167. Behar J, Ganesan A, Zhang J, Yaniv Y (2016) The Autonomic Nervous System Regulates the Heart Rate through cAMP-PKA Dependent and Independent Coupled-Clock Pacemaker Cell Mechanisms. *Front Physiol* 7:419. doi:10.3389/fphys.2016.00419
168. Harzheim D, Pfeiffer KH, Fabritz L, Kremmer E, Buch T, Waisman A, Kirchhof P, Kaupp UB, Seifert R (2008) Cardiac pacemaker function of HCN4 channels in mice is confined to embryonic development and requires cyclic AMP. *EMBO J* 27 (4):692-703. doi:10.1038/emboj.2008.3
169. Bobin P, Varin A, Lefebvre F, Fischmeister R, Vandecasteele G, Leroy J (2016) Calmodulin kinase II inhibition limits the pro-arrhythmic Ca<sup>2+</sup> waves induced by cAMP-phosphodiesterase inhibitors. *Cardiovascular Research* 110 (1):151-161. doi:10.1093/cvr/cvw027
170. Wolfgang WJ, Roberts IJ, Quan F, O'Kane C, Forte M (1996) Activation of protein kinase A-independent pathways by Gs alpha in *Drosophila*. *Proc Natl Acad Sci U S A* 93 (25):14542-14547. doi:10.1073/pnas.93.25.14542
171. Liao Z, Lockhead D, Larson ED, Proenza C (2010) Phosphorylation and modulation of hyperpolarization-activated HCN4 channels by protein kinase A in the mouse sinoatrial node. *J Gen Physiol* 136 (3):247-258. doi:10.1085/jgp.201010488

172. De Jongh KS, Murphy BJ, Colvin AA, Hell JW, Takahashi M, Catterall WA (1996) Specific phosphorylation of a site in the full-length form of the alpha 1 subunit of the cardiac L-type calcium channel by adenosine 3',5'-cyclic monophosphate-dependent protein kinase. *Biochemistry* 35 (32):10392-10402. doi:10.1021/bi953023c
173. Yatani A, Imoto Y, Codina J, Hamilton SL, Brown AM, Birnbaumer L (1988) The stimulatory G protein of adenylyl cyclase, Gs, also stimulates dihydropyridine-sensitive Ca<sup>2+</sup> channels. Evidence for direct regulation independent of phosphorylation by cAMP-dependent protein kinase or stimulation by a dihydropyridine agonist. *J Biol Chem* 263 (20):9887-9895
174. Hagiwara N, Irisawa H, Kameyama M (1988) Contribution of two types of calcium currents to the pacemaker potentials of rabbit sino-atrial node cells. *J Physiol* 395:233-253. doi:10.1113/jphysiol.1988.sp016916
175. Glaves JP, Trieber CA, Ceholski DK, Stokes DL, Young HS (2011) Phosphorylation and mutation of phospholamban alter physical interactions with the sarcoplasmic reticulum calcium pump. *J Mol Biol* 405 (3):707-723. doi:10.1016/j.jmb.2010.11.014
176. Marx SO, Reiken S, Hisamatsu Y, Jayaraman T, Burkhoff D, Rosemblyt N, Marks AR (2000) PKA phosphorylation dissociates FKBP12.6 from the calcium release channel (ryanodine receptor): defective regulation in failing hearts. *Cell* 101 (4):365-376. doi:10.1016/s0092-8674(00)80847-8
177. El-Armouche A, Eschenhagen T (2009) Beta-adrenergic stimulation and myocardial function in the failing heart. *Heart Fail Rev* 14 (4):225-241. doi:10.1007/s10741-008-9132-8
178. Rockman HA, Koch WJ, Lefkowitz RJ (2002) Seven-transmembrane-spanning receptors and heart function. *Nature* 415 (6868):206-212. doi:10.1038/415206a
179. Wu Y, Gao Z, Chen B, Koval OM, Singh MV, Guan X, Hund TJ, Kutschke W, Sarma S, Grumbach IM, Wehrens XH, Mohler PJ, Song LS, Anderson ME (2009) Calmodulin kinase II is required for fight or flight sinoatrial node physiology. *Proc Natl Acad Sci U S A* 106 (14):5972-5977. doi:10.1073/pnas.0806422106
180. Rigg L, Heath BM, Cui Y, Terrar DA (2000) Localisation and functional significance of ryanodine receptors during beta-adrenoceptor stimulation in the guinea-pig sino-atrial node. *Cardiovasc Res* 48 (2):254-264. doi:10.1016/s0008-6363(00)00153-x
181. Vinogradova TM, Lyashkov AE, Zhu W, Ruknudin AM, Sirenko S, Yang D, Deo S, Barlow M, Johnson S, Caffrey JL, Zhou YY, Xiao RP, Cheng H, Stern MD, Maltsev VA, Lakatta EG (2006) High basal protein kinase A-dependent phosphorylation drives rhythmic internal Ca<sup>2+</sup> store oscillations and spontaneous beating of cardiac pacemaker cells. *Circ Res* 98 (4):505-514. doi:10.1161/01.RES.0000204575.94040.d1
182. Bers DM, Morotti S (2014) Ca<sup>2+</sup> current facilitation is CaMKII-dependent and has arrhythmogenic consequences. *Front Pharmacol* 5:144. doi:10.3389/fphar.2014.00144
183. Ai X, Curran JW, Shannon TR, Bers DM, Pogwizd SM (2005) Ca<sup>2+</sup>/Calmodulin-Dependent Protein Kinase Modulates Cardiac Ryanodine Receptor Phosphorylation and Sarcoplasmic Reticulum Ca<sup>2+</sup> Leak in Heart Failure. *Circ Res* 97 (12):1314-1322. doi:10.1161/01.RES.0000194329.41863.89
184. Vinogradova TM, Zhou YY, Bogdanov KY, Yang D, Kuschel M, Cheng H, Xiao RP (2000) Sinoatrial node pacemaker activity requires Ca<sup>2+</sup>/calmodulin-dependent protein kinase II activation. *Circ Res* 87 (9):760-767. doi:10.1161/01.res.87.9.760
185. Wu Y, Anderson ME (2014) CaMKII in sinoatrial node physiology and dysfunction. *Front Pharmacol* 5:48. doi:10.3389/fphar.2014.00048
186. Li Y, Sirenko S, Riordon DR, Yang D, Spurgeon H, Lakatta EG, Vinogradova TM (2016) CaMKII-dependent phosphorylation regulates basal cardiac pacemaker function via modulation of local Ca<sup>2+</sup> releases. *Am J Physiol Heart Circ Physiol* 311 (3):H532-544. doi:10.1152/ajpheart.00765.2015
187. Lei M, Brown HF, Terrar DA (2000) Modulation of delayed rectifier potassium current, iK, by isoprenaline in rabbit isolated pacemaker cells. *Exp Physiol* 85 (1):27-35
188. Shimoni Y (1999) Hormonal control of cardiac ion channels and transporters. *Prog Biophys Mol Biol* 72 (1):67-108. doi:10.1016/s0079-6107(99)00005-x
189. Abrams P, Andersson KE, Buccafusco JJ, Chapple C, de Groat WC, Fryer AD, Kay G, Laties A, Nathanson NM, Pasricha PJ, Wein AJ (2006) Muscarinic receptors: their distribution and function in body systems, and the implications for treating overactive bladder. *Br J Pharmacol* 148 (5):565-578. doi:10.1038/sj.bjp.0706780
190. Harvey RD (2012) Muscarinic receptor agonists and antagonists: effects on cardiovascular function. *Handb Exp Pharmacol* (208):299-316. doi:10.1007/978-3-642-23274-9\_13
191. Accili EA, Redaelli G, DiFrancesco D (1998) Two distinct pathways of muscarinic current responses in rabbit sino-atrial node myocytes. *Pflugers Arch* 437 (1):164-167. doi:10.1007/s004240050763

192. Corey S, Krapivinsky G, Krapivinsky L, Clapham DE (1998) Number and stoichiometry of subunits in the native atrial G-protein-gated K<sup>+</sup> channel, IKACH. *J Biol Chem* 273 (9):5271-5278. doi:10.1074/jbc.273.9.5271
193. Renaudon B, Bois P, Bescond J, Lenfant J (1997) Acetylcholine modulates I(f) and IK(ACh) via different pathways in rabbit sino-atrial node cells. *J Mol Cell Cardiol* 29 (3):969-975. doi:10.1006/jmcc.1996.0340
194. Wickman K, Nemecek J, Gendler SJ, Clapham DE (1998) Abnormal heart rate regulation in GIRK4 knockout mice. *Neuron* 20 (1):103-114. doi:10.1016/s0896-6273(00)80438-9
195. van Borren MM, Verkerk AO, Wilders R, Hajji N, Zegers JG, Bourrier J, Tan HL, Verheijck EE, Peters SL, Alewijnse AE, Ravensloot JH (2010) Effects of muscarinic receptor stimulation on Ca<sup>2+</sup> transient, cAMP production and pacemaker frequency of rabbit sinoatrial node cells. *Basic Res Cardiol* 105 (1):73-87. doi:10.1007/s00395-009-0048-9
196. Lyashkov AE, Vinogradova TM, Zahanich I, Li Y, Younes A, Nuss HB, Spurgeon HA, Maltsev VA, Lakatta EG (2009) Cholinergic receptor signaling modulates spontaneous firing of sinoatrial nodal cells via integrated effects on PKA-dependent Ca(2+) cycling and I(KACH). *Am J Physiol Heart Circ Physiol* 297 (3):H949-959. doi:10.1152/ajpheart.01340.2008
197. Yaniv Y, Sirenko S, Ziman BD, Spurgeon HA, Maltsev VA, Lakatta EG (2013) New evidence for coupled clock regulation of the normal automaticity of sinoatrial nodal pacemaker cells: bradycardic effects of ivabradine are linked to suppression of intracellular Ca(2+)(+) cycling. *J Mol Cell Cardiol* 62:80-89. doi:10.1016/j.yjmcc.2013.04.026
198. Behar J, Ganesan A, Zhang J, Yaniv Y (2016) The Autonomic Nervous System Regulates the Heart Rate through cAMP-PKA Dependent and Independent Coupled-Clock Pacemaker Cell Mechanisms. *Frontiers in physiology* 7:419-419. doi:10.3389/fphys.2016.00419
199. Han X, Shimoni Y, Giles WR (1994) An obligatory role for nitric oxide in autonomic control of mammalian heart rate. *J Physiol* 476 (2):309-314. doi:10.1113/jphysiol.1994.sp020132
200. Han X, Shimoni Y, Giles WR (1995) A cellular mechanism for nitric oxide-mediated cholinergic control of mammalian heart rate. *J Gen Physiol* 106 (1):45-65. doi:10.1085/jgp.106.1.45
201. Opthof T, Coronel R (2000) The normal range and determinants of the intrinsic heart rate in man. *Cardiovascular Research* 45 (1):175-176. doi:10.1016/S0008-6363(99)00321-1
202. D'Souza A, Sharma S, Boyett MR (2015) CrossTalk opposing view: bradycardia in the trained athlete is attributable to a downregulation of a pacemaker channel in the sinus node. *J Physiol* 593 (8):1749-1751. doi:10.1113/jphysiol.2014.284356
203. Fukuda K, Kanazawa H, Aizawa Y, Ardell JL, Shivkumar K (2015) Cardiac innervation and sudden cardiac death. *Circ Res* 116 (12):2005-2019. doi:10.1161/CIRCRESAHA.116.304679
204. Schwerdtfeger AR, Schwarz G, Pfuertscheller K, Thayer JF, Jarczok MN, Pfuertscheller G (2020) Heart rate variability (HRV): From brain death to resonance breathing at 6 breaths per minute. *Clin Neurophysiol* 131 (3):676-693. doi:10.1016/j.clinph.2019.11.013
205. Hon EH, Lee ST (1963) Electronic Evaluation of the Fetal Heart Rate. VIII. Patterns Preceding Fetal Death, Further Observations. *Am J Obstet Gynecol* 87:814-826
206. Thome J, Densmore M, Frewen PA, McKinnon MC, Théberge J, Nicholson AA, Koenig J, Thayer JF, Lanius RA (2017) Desynchronization of autonomic response and central autonomic network connectivity in posttraumatic stress disorder. *Psychiatry* 38 (1):27-40. doi:10.1002/hbm.23340
207. Appelhans BM, Luecken LJJRogp (2006) Heart rate variability as an index of regulated emotional responding. *Psychophysiology* 10 (3):229-240
208. Thayer JF, Lane RDJN, Reviews B (2009) Claude Bernard and the heart-brain connection: Further elaboration of a model of neurovisceral integration. *Psychophysiology* 33 (2):81-88
209. Benarroch EE The central autonomic network: functional organization, dysfunction, and perspective. In: *Mayo Clinic Proceedings*, 1993. vol 10. Elsevier, pp 988-1001
210. Friedman BH, Thayer JFJopr (1998) Autonomic balance revisited: panic anxiety and heart rate variability. *Psychophysiology* 44 (1):133-151
211. Shaffer F, McCraty R, Zerr CLJFip (2014) A healthy heart is not a metronome: an integrative review of the heart's anatomy and heart rate variability. *Psychophysiology* 51:1040
212. Shaffer F, Ginsberg JP (2017) An Overview of Heart Rate Variability Metrics and Norms. *Psychophysiology* 5 (258). doi:10.3389/fpubh.2017.00258

213. Schwerdtfeger AR, Schwarz G, Pfurtscheller K, Thayer JF, Jarczok MN, Pfurtscheller G (2020) Heart rate variability (HRV): From brain death to resonance breathing at 6 breaths per minute. *Clinical Neurophysiology* 131 (3):676-693. doi:<https://doi.org/10.1016/j.clinph.2019.11.013>
214. Feng J, Wang A, Gao C, Zhang J, Chen Z, Hou L, Luo C, Jiang Y, Pan JJAjoc (2015) Altered heart rate variability depend on the characteristics of coronary lesions in stable angina pectoris. 15 (6):496
215. Malliani A, Lombardi F, Pagani M, Cerutti S (1994) Power spectral analysis of cardiovascular variability in patients at risk for sudden cardiac death. 5 (3):274-286
216. Saul JP, Albrecht P, Berger RD, Cohen RJ (1988) Analysis of long term heart rate variability: methods, 1/f scaling and implications. *Comput Cardiol* 14:419-422
217. Politano L, Palladino A, Nigro G, Scutifero M, Cozza V (2008) Usefulness of heart rate variability as a predictor of sudden cardiac death in muscular dystrophies. *Acta Myol* 27:114-122
218. Sayers BM (1973) Analysis of heart rate variability. *Ergonomics* 16 (1):17-32. doi:10.1080/00140137308924479
219. Malliani A, Pagani M, Lombardi F, Cerutti S (1991) Cardiovascular neural regulation explored in the frequency domain. *Circulation* 84 (2):482-492. doi:10.1161/01.cir.84.2.482
220. Stein PK, Bosner MS, Kleiger RE, Conger BM (1994) Heart rate variability: a measure of cardiac autonomic tone. *Am Heart J* 127 (5):1376-1381. doi:10.1016/0002-8703(94)90059-0
221. Stein PK, Kleiger RE (1999) Insights from the study of heart rate variability. *Annu Rev Med* 50:249-261. doi:10.1146/annurev.med.50.1.249
222. Behar JA, Rosenberg AA, Weiser-Bitoun I, Shemla O, Alexandrovich A, Konyukhov E, Yaniv Y (2018) PhysioZoo: A Novel Open Access Platform for Heart Rate Variability Analysis of Mammalian Electrocardiographic Data. 9 (1390). doi:10.3389/fphys.2018.01390
223. Malpas SC (2010) Sympathetic nervous system overactivity and its role in the development of cardiovascular disease. *Physiol Rev* 90 (2):513-557. doi:10.1152/physrev.00007.2009
224. Singh N, Moneghetti KJ, Christle JW, Hadley D, Plews D, Froelicher V (2018) Heart Rate Variability: An Old Metric with New Meaning in the Era of using mHealth Technologies for Health and Exercise Training Guidance. Part One: Physiology and Methods. *Arrhythm Electrophysiol Rev* 7 (3):193-198. doi:10.15420/aer.2018.27.2
225. Huikuri HV, Stein PK (2012) Clinical application of heart rate variability after acute myocardial infarction. *Front Physiol* 3:41. doi:10.3389/fphys.2012.00041
226. Sessa F, Anna V, Messina G, Cibelli G, Monda V, Marsala G, Ruberto M, Biondi A, Cascio O, Bertozzi G, Pisanelli D, Maglietta F, Messina A, Mollica MP, Salerno M (2018) Heart rate variability as predictive factor for sudden cardiac death. *Aging (Albany NY)* 10 (2):166-177. doi:10.18632/aging.101386
227. Disease GBD, Injury I, Prevalence C (2016) Global, regional, and national incidence, prevalence, and years lived with disability for 310 diseases and injuries, 1990-2015: a systematic analysis for the Global Burden of Disease Study 2015. *Lancet* 388 (10053):1545-1602. doi:10.1016/S0140-6736(16)31678-6
228. Metra M, Teerlink JR (2017) Heart failure. *Lancet* 390 (10106):1981-1995. doi:10.1016/S0140-6736(17)31071-1
229. McMurray JJ, Pfeffer MA (2005) Heart failure. *Lancet* 365 (9474):1877-1889. doi:10.1016/S0140-6736(05)66621-4
230. Dickstein K, Cohen-Solal A, Filippatos G, McMurray JJ, Ponikowski P, Poole-Wilson PA, Stromberg A, van Veldhuisen DJ, Atar D, Hoes AW, Keren A, Mebazaa A, Nieminen M, Priori SG, Swedberg K, Guidelines ESCCfP (2008) ESC Guidelines for the diagnosis and treatment of acute and chronic heart failure 2008: the Task Force for the Diagnosis and Treatment of Acute and Chronic Heart Failure 2008 of the European Society of Cardiology. Developed in collaboration with the Heart Failure Association of the ESC (HFA) and endorsed by the European Society of Intensive Care Medicine (ESICM). *Eur Heart J* 29 (19):2388-2442. doi:10.1093/eurheartj/ehn309
231. Ziaeian B, Fonarow GC (2016) Epidemiology and aetiology of heart failure. *Nat Rev Cardiol* 13 (6):368-378. doi:10.1038/nrcardio.2016.25
232. Cherney BLMaK (2019) Congestive Heart Failure (CHF).
233. Inamdar AA, Inamdar AC (2016) Heart Failure: Diagnosis, Management and Utilization. *J Clin Med* 5 (7). doi:10.3390/jcm5070062
234. Ahmed A (2003) American College of Cardiology/American Heart Association Chronic Heart Failure Evaluation and Management guidelines: relevance to the geriatric practice. *J Am Geriatr Soc* 51 (1):123-126. doi:10.1034/j.1601-5215.2002.51020.x

235. Yancy CW, Jessup M, Bozkurt B, Butler J, Casey DE, Colvin MM, Drazner MH, Filippatos GS, Fonarow GC, Givertz MM, Hollenberg SM, Lindenfeld J, Masoudi FA, McBride PE, Peterson PN, Stevenson LW, Westlake C (2017) 2017 ACC/AHA/HFSA Focused Update of the 2013 ACCF/AHA Guideline for the Management of Heart Failure. A Report of the American College of Cardiology/American Heart Association Task Force on Clinical Practice Guidelines and the Heart Failure Society of America 70 (6):776-803. doi:10.1016/j.jacc.2017.04.025 %J Journal of the American College of Cardiology
236. Jessup M, Brozena S (2003) Heart failure. *N Engl J Med* 348 (20):2007-2018. doi:10.1056/NEJMra021498
237. Bristow MR, Gilbert EM, Abraham WT, Adams KF, Fowler MB, Hershberger RE, Kubo SH, Narahara KA, Ingersoll H, Krueger S, Young S, Shusterman N (1996) Carvedilol produces dose-related improvements in left ventricular function and survival in subjects with chronic heart failure. MOCHA Investigators. *Circulation* 94 (11):2807-2816. doi:10.1161/01.cir.94.11.2807
238. Greenberg B, Quinones MA, Koilpillai C, Limacher M, Shindler D, Benedict C, Shelton B (1995) Effects of long-term enalapril therapy on cardiac structure and function in patients with left ventricular dysfunction. Results of the SOLVD echocardiography substudy. *Circulation* 91 (10):2573-2581. doi:10.1161/01.cir.91.10.2573
239. Hall SA, Cigarroa CG, Marcoux L, Risser RC, Grayburn PA, Eichhorn EJ (1995) Time course of improvement in left ventricular function, mass and geometry in patients with congestive heart failure treated with beta-adrenergic blockade. *J Am Coll Cardiol* 25 (5):1154-1161. doi:10.1016/0735-1097(94)00543-y
240. Saxon LA, De Marco T, Schafer J, Chatterjee K, Kumar UN, Foster E, Investigators VCHF (2002) Effects of long-term biventricular stimulation for resynchronization on echocardiographic measures of remodeling. *Circulation* 105 (11):1304-1310. doi:10.1161/hc1102.105730
241. Cazeau S, Leclercq C, Lavergne T, Walker S, Varma C, Linde C, Garrigue S, Kappenberger L, Haywood GA, Santini M, Bailleul C, Daubert JC, Multisite Stimulation in Cardiomyopathies Study I (2001) Effects of multisite biventricular pacing in patients with heart failure and intraventricular conduction delay. *N Engl J Med* 344 (12):873-880. doi:10.1056/NEJM200103223441202
242. Auricchio A, Stellbrink C, Block M, Sack S, Vogt J, Bakker P, Klein H, Kramer A, Ding J, Salo R, Tockman B, Pochet T, Spinelli J (1999) Effect of pacing chamber and atrioventricular delay on acute systolic function of paced patients with congestive heart failure. The Pacing Therapies for Congestive Heart Failure Study Group. The Guidant Congestive Heart Failure Research Group. *Circulation* 99 (23):2993-3001. doi:10.1161/01.cir.99.23.2993
243. Abraham WT, Fisher WG, Smith AL, Delurgio DB, Leon AR, Loh E, Kocovic DZ, Packer M, Clavell AL, Hayes DL, Ellestad M, Trupp RJ, Underwood J, Pickering F, Truex C, McAtee P, Messenger J, Evaluation MSGMIRC (2002) Cardiac resynchronization in chronic heart failure. *N Engl J Med* 346 (24):1845-1853. doi:10.1056/NEJMoa013168
244. Jessup M (2001) Mechanical cardiac-support devices--dreams and devilish details. *N Engl J Med* 345 (20):1490-1493. doi:10.1056/NEJMed010109
245. Senni M, Redfield MM (2001) Heart failure with preserved systolic function. A different natural history? *J Am Coll Cardiol* 38 (5):1277-1282. doi:10.1016/s0735-1097(01)01567-4
246. Lyon RC, Zanella F, Omens JH, Sheikh FJCr (2015) Mechanotransduction in cardiac hypertrophy and failure. *116* (8):1462-1476
247. Francis GS, McDonald KM, Cohn JNJC (1993) Neurohumoral activation in preclinical heart failure. Remodeling and the potential for intervention. *87* (5 Suppl):IV90-96
248. Mailliet M, Van Berlo JH, Molkentin JDJNrMcb (2013) Molecular basis of physiological heart growth: fundamental concepts and new players. *14* (1):38-48
249. Shimizu I, Minamino T (2016) Physiological and pathological cardiac hypertrophy. *Journal of Molecular and Cellular Cardiology* 97:245-262. doi:https://doi.org/10.1016/j.jmcc.2016.06.001
250. Weeks KL, McMullen JRJP (2011) The athlete's heart vs. the failing heart: can signaling explain the two distinct outcomes?
251. Belke DD, Betuing S, Tuttle MJ, Graveleau C, Young ME, Pham M, Zhang D, Cooksey RC, McClain DA, Litwin SEJTJoci (2002) Insulin signaling coordinately regulates cardiac size, metabolism, and contractile protein isoform expression. *109* (5):629-639
252. Kim J, Wende AR, Sena S, Theobald HA, Soto J, Sloan C, Wayment BE, Litwin SE, Holzenberger M, LeRoith DJMe (2008) Insulin-like growth factor I receptor signaling is required for exercise-induced cardiac hypertrophy. *22* (11):2531-2543

253. McMullen JR, Shioi T, Huang W-Y, Zhang L, Tarnavski O, Bisping E, Schinke M, Kong S, Sherwood MC, Brown JJ*JoBC* (2004) The insulin-like growth factor 1 receptor induces physiological heart growth via the phosphoinositide 3-kinase (p110 $\alpha$ ) pathway. 279 (6):4782-4793
254. Stubbe P, Gatz J, Heidemann P, vz Mühlen A, Hesch RJH, Research M (1978) Thyroxine-binding globulin, triiodothyronine, thyroxine and thyrotropin in newborn infants and children. 10 (01):58-61
255. Kinugawa K, Jeong MY, Bristow MR, Long CS*JME* (2005) Thyroid hormone induces cardiac myocyte hypertrophy in a thyroid hormone receptor  $\alpha$ 1-specific manner that requires TAK1 and p38 mitogen-activated protein kinase. 19 (6):1618-1628
256. Hill JA, Olson EN*JNEJoM* (2008) Cardiac plasticity. 358 (13):1370-1380
257. Shimizu I, Minamino T, Toko H, Okada S, Ikeda H, Yasuda N, Tateno K, Moriya J, Yokoyama M, Nojima AJ*TJoci* (2010) Excessive cardiac insulin signaling exacerbates systolic dysfunction induced by pressure overload in rodents. 120 (5):1506-1514
258. Sano M, Minamino T, Toko H, Miyauchi H, Orimo M, Qin Y, Akazawa H, Tateno K, Kayama Y, Harada MJN (2007) p53-induced inhibition of Hif-1 causes cardiac dysfunction during pressure overload. 446 (7134):444-448
259. Grossman W, Jones D, McLaurin LP (1975) Wall stress and patterns of hypertrophy in the human left ventricle. *J Clin Invest* 56 (1):56-64. doi:10.1172/JCI108079
260. Grossman W, Jones D, McLaurin LJ*TJoci* (1975) Wall stress and patterns of hypertrophy in the human left ventricle. 56 (1):56-64
261. Sandler H, Dodge HT*JCr* (1963) Left ventricular tension and stress in man. 13 (2):91-104
262. Tham YK, Bernardo BC, Ooi JYY, Weeks KL, McMullen JR (2015) Pathophysiology of cardiac hypertrophy and heart failure: signaling pathways and novel therapeutic targets. *Archives of Toxicology* 89 (9):1401-1438. doi:10.1007/s00204-015-1477-x
263. Katz AM, Konstam MA*JHFP, Molecular Biology,, Clinical Management*. 2nd ed. Baltimore MLW, Wilkins (2008) Definition, historical aspects.
264. Cho GW, Altamirano F, Hill JA (2016) Chronic heart failure: Ca(2+), catabolism, and catastrophic cell death. *Biochim Biophys Acta* 1862 (4):763-777. doi:10.1016/j.bbadis.2016.01.011
265. Ferrantini C, Crocini C, Coppini R, Vanzi F, Tesi C, Cerbai E, Poggese C, Pavone FS, Sacconi L (2013) The transverse-axial tubular system of cardiomyocytes. *Cell Mol Life Sci* 70 (24):4695-4710. doi:10.1007/s00018-013-1410-5
266. Bers DM (2014) Cardiac sarcoplasmic reticulum calcium leak: basis and roles in cardiac dysfunction. *Annu Rev Physiol* 76:107-127. doi:10.1146/annurev-physiol-020911-153308
267. Lou Q, Janardhan A, Efimov IR (2012) Remodeling of calcium handling in human heart failure. *Adv Exp Med Biol* 740:1145-1174. doi:10.1007/978-94-007-2888-2\_52
268. Stammers AN, Susser SE, Hamm NC, Hlynsky MW, Kimber DE, Kehler DS, Duhamel TA (2015) The regulation of sarco(endo)plasmic reticulum calcium-ATPases (SERCA). *Canadian Journal of Physiology and Pharmacology* 93 (10):843-854. doi:10.1139/cjpp-2014-0463
269. Chen Y, Escoubet B, Prunier F, Amour J, Simonides WS, Vivien B, Lenoir C, Heimbürger M, Choqueux C, Gellen B, Riou B, Michel J-B, Franz WM, Mercadier J-J (2004) Constitutive Cardiac Overexpression of Sarcoplasmic/Endoplasmic Reticulum Ca<sup>2+</sup>-ATPase Delays Myocardial Failure After Myocardial Infarction in Rats at a Cost of Increased Acute Arrhythmias. 109 (15):1898-1903. doi:doi:10.1161/01.CIR.0000124230.60028.42
270. Mercadier JJ, Lompre AM, Duc P, Boheler KR, Fraysse JB, Wisnewsky C, Allen PD, Komajda M, Schwartz K (1990) Altered sarcoplasmic reticulum Ca<sup>2+</sup>-ATPase gene expression in the human ventricle during end-stage heart failure. *J Clin Invest* 85 (1):305-309. doi:10.1172/JCI114429
271. Guo A, Zhang C, Wei S, Chen B, Song LS (2013) Emerging mechanisms of T-tubule remodelling in heart failure. *Cardiovasc Res* 98 (2):204-215. doi:10.1093/cvr/cvt020
272. Meissner G (2010) Regulation of Ryanodine Receptor Ion Channels Through Posttranslational Modifications. *Curr Top Membr* 66:91-113. doi:10.1016/S1063-5823(10)66005-X
273. Anderson ME, Brown JH, Bers DM (2011) CaMKII in myocardial hypertrophy and heart failure. *J Mol Cell Cardiol* 51 (4):468-473. doi:10.1016/j.yjmcc.2011.01.012
274. Santulli G, Xie W, Reiken SR, Marks AR (2015) Mitochondrial calcium overload is a key determinant in heart failure. *Proc Natl Acad Sci U S A* 112 (36):11389-11394. doi:10.1073/pnas.1513047112

275. Kranias EG, Hajjar RJ (2012) Modulation of cardiac contractility by the phospholamban/SERCA2a regulatome. *Circ Res* 110 (12):1646-1660. doi:10.1161/CIRCRESAHA.111.259754
276. Bhupathy P, Babu GJ, Periasamy M (2007) Sarcolipin and phospholamban as regulators of cardiac sarcoplasmic reticulum Ca<sup>2+</sup> ATPase. *J Mol Cell Cardiol* 42 (5):903-911. doi:10.1016/j.yjmcc.2007.03.738
277. Haghighi K, Bidwell P, Kranias EG (2014) Phospholamban interactome in cardiac contractility and survival: A new vision of an old friend. *J Mol Cell Cardiol* 77:160-167. doi:10.1016/j.yjmcc.2014.10.005
278. Shareef MA, Anwer LA, Poizat C (2014) Cardiac SERCA2A/B: therapeutic targets for heart failure. *Eur J Pharmacol* 724:1-8. doi:10.1016/j.ejphar.2013.12.018
279. Li L, Louch WE, Niederer SA, Aronsen JM, Christensen G, Sejersted OM, Smith NP (2012) Sodium accumulation in SERCA knockout-induced heart failure. *Biophys J* 102 (9):2039-2048. doi:10.1016/j.bpj.2012.03.045
280. Kawase Y, Ly HQ, Prunier F, Lebeche D, Shi Y, Jin H, Hadri L, Yoneyama R, Hoshino K, Takewa Y, Sakata S, Peluso R, Zsebo K, Gwathmey JK, Tardif JC, Tanguay JF, Hajjar RJ (2008) Reversal of cardiac dysfunction after long-term expression of SERCA2a by gene transfer in a pre-clinical model of heart failure. *J Am Coll Cardiol* 51 (11):1112-1119. doi:10.1016/j.jacc.2007.12.014
281. Studer R, Reinecke H, Bilger J, Eschenhagen T, Bohm M, Hasenfuss G, Just H, Holtz J, Drexler H (1994) Gene expression of the cardiac Na<sup>(+)</sup>-Ca<sup>2+</sup> exchanger in end-stage human heart failure. *Circ Res* 75 (3):443-453. doi:10.1161/01.res.75.3.443
282. Braunwald E (2015) The war against heart failure: the Lancet lecture. *Lancet* 385 (9970):812-824. doi:10.1016/S0140-6736(14)61889-4
283. Shattock MJ, Ottolia M, Bers DM, Blaustein MP, Boguslavskyi A, Bossuyt J, Bridge JH, Chen-Izu Y, Clancy CE, Edwards A, Goldhaber J, Kaplan J, Lingrel JB, Pavlovic D, Philipson K, Sipido KR, Xie ZJ (2015) Na<sup>+</sup>/Ca<sup>2+</sup> exchange and Na<sup>+</sup>/K<sup>+</sup>-ATPase in the heart. *J Physiol* 593 (6):1361-1382. doi:10.1113/jphysiol.2014.282319
284. Eder P, Molkentin JD (2011) TRPC channels as effectors of cardiac hypertrophy. *Circ Res* 108 (2):265-272. doi:10.1161/CIRCRESAHA.110.225888
285. Eltit JM, Ding X, Pessah IN, Allen PD, Lopez JR (2013) Nonspecific sarcolemmal cation channels are critical for the pathogenesis of malignant hyperthermia. *FASEB J* 27 (3):991-1000. doi:10.1096/fj.12-218354
286. Wu X, Eder P, Chang B, Molkentin JD (2010) TRPC channels are necessary mediators of pathologic cardiac hypertrophy. *Proc Natl Acad Sci U S A* 107 (15):7000-7005. doi:10.1073/pnas.1001825107
287. Makarewich CA, Zhang H, Davis J, Correll RN, Trapanese DM, Hoffman NE, Troupes CD, Berretta RM, Kubo H, Madesh M, Chen X, Gao E, Molkentin JD, Houser SR (2014) Transient receptor potential channels contribute to pathological structural and functional remodeling after myocardial infarction. *Circ Res* 115 (6):567-580. doi:10.1161/CIRCRESAHA.115.303831
288. Shan D, Marchase RB, Chatham JC (2008) Overexpression of TRPC3 increases apoptosis but not necrosis in response to ischemia-reperfusion in adult mouse cardiomyocytes. *Am J Physiol Cell Physiol* 294 (3):C833-841. doi:10.1152/ajpcell.00313.2007
289. Wei S, Guo A, Chen B, Kutschke W, Xie YP, Zimmerman K, Weiss RM, Anderson ME, Cheng H, Song LS (2010) T-tubule remodeling during transition from hypertrophy to heart failure. *Circ Res* 107 (4):520-531. doi:10.1161/CIRCRESAHA.109.212324
290. Song LS, Sobie EA, McCulle S, Lederer WJ, Balke CW, Cheng H (2006) Orphaned ryanodine receptors in the failing heart. *Proc Natl Acad Sci U S A* 103 (11):4305-4310. doi:10.1073/pnas.0509324103
291. Nikolaev VO, Moshkov A, Lyon AR, Miragoli M, Novak P, Paur H, Lohse MJ, Korchev YE, Harding SE, Gorelik J (2010) Beta2-adrenergic receptor redistribution in heart failure changes cAMP compartmentation. *Science* 327 (5973):1653-1657. doi:10.1126/science.1185988
292. Ibarra C, Vicencio JM, Varas-Godoy M, Jaimovich E, Rothermel BA, Uhlen P, Hill JA, Lavandero S (2014) An integrated mechanism of cardiomyocyte nuclear Ca<sup>(2+)</sup> signaling. *J Mol Cell Cardiol* 75:40-48. doi:10.1016/j.yjmcc.2014.06.015
293. Lai NC, Tang T, Gao MH, Saito M, Miyanohara A, Hammond HK (2012) Improved function of the failing rat heart by regulated expression of insulin-like growth factor I via intramuscular gene transfer. *Hum Gene Ther* 23 (3):255-261. doi:10.1089/hum.2011.094
294. Zhang Y, Yuan M, Bradley KM, Dong F, Anversa P, Ren J (2012) Insulin-like growth factor 1 alleviates high-fat diet-induced myocardial contractile dysfunction: role of insulin signaling and mitochondrial function. *Hypertension* 59 (3):680-693. doi:10.1161/HYPERTENSIONAHA.111.181867

295. Peana D, Domeier TL (2017) Cardiomyocyte Ca(2+) homeostasis as a therapeutic target in heart failure with reduced and preserved ejection fraction. *Curr Opin Pharmacol* 33:17-26. doi:10.1016/j.coph.2017.03.005
296. Opthof T, Coronel R, Rademaker HM, Vermeulen JT, Wilms-Schopman FJ, Janse MJ (2000) Changes in sinus node function in a rabbit model of heart failure with ventricular arrhythmias and sudden death. *Am J Physiol* 278(25):2975-2980
297. Witte K, Hu K, Swiatek J, Müssig C, Ertl G, Lemmer BJ (2000) Experimental heart failure in rats: effects on cardiovascular circadian rhythms and on myocardial  $\beta$ -adrenergic signaling. *Am J Physiol* 278(2):350-358
298. Verkerk AO, Wilders R, Coronel R, Ravesloot JH, Verheijck EE (2003) Ionic remodeling of sinoatrial node cells by heart failure. *Circulation* 108(6):760-766
299. Du Y, Huang X, Wang T, Han K, Zhang J, Xi Y, Wu G, Ma A (2007) Downregulation of neuronal sodium channel subunits Nav1.1 and Nav1.6 in the sinoatrial node from volume-overloaded heart failure rat. *Am J Physiol* 293(3):451-459
300. Sanders P, Kistler PM, Morton JB, Spence SJ, Kalman JM (2004) Remodeling of sinus node function in patients with congestive heart failure: reduction in sinus node reserve. *Circulation* 110(8):897-903. doi:10.1161/01.CIR.0000139336.69955.AB
301. Verkerk AO, van Borren MM, van Ginneken AC, Wilders R (2015) Ca(2+) cycling properties are conserved despite bradycardic effects of heart failure in sinoatrial node cells. *Front Physiol* 6:18. doi:10.3389/fphys.2015.00018
302. Chan CS, Chen YC, Chang SL, Lin YK, Kao YH, Chen SA, Chen YJ (2018) Heart Failure Differentially Modulates the Effects of Ivabradine on the Electrical Activity of the Sinoatrial Node and Pulmonary Veins. *J Card Fail* 24(11):763-772. doi:10.1016/j.cardfail.2018.09.016
303. Yanni J, Tellez JO, Maczewski M, Mackiewicz U, Beresewicz A, Billeter R, Dobrzynski H, Boyett MR (2011) Changes in ion channel gene expression underlying heart failure-induced sinoatrial node dysfunction. *Circ Heart Fail* 4(4):496-508. doi:10.1161/CIRCHEARTFAILURE.110.957647
304. Melenovsky V, Hwang SJ, Redfield MM, Zakeri R, Lin G, Borlaug BA (2015) Left atrial remodeling and function in advanced heart failure with preserved or reduced ejection fraction. *Circ Heart Fail* 8(2):295-303. doi:10.1161/CIRCHEARTFAILURE.114.001667
305. Sridhar A, Nishijima Y, Terentyev D, Khan M, Terentyeva R, Hamlin RL, Nakayama T, Gyorke S, Cardounel AJ, Carnes CA (2009) Chronic heart failure and the substrate for atrial fibrillation. *Cardiovasc Res* 84(2):227-236. doi:10.1093/cvr/cvp216
306. Lange G, Lu HH, Chang A, Brooks CM (1966) Effect of stretch on the isolated cat sinoatrial node. *Am J Physiol* 211(5):1192-1196. doi:10.1152/ajplegacy.1966.211.5.1192
307. Brooks CM, Lu HH, Lange G, Mangi R, Shaw RB, Geoly K (1966) Effects of localized stretch of the sinoatrial node region of the dog heart. *Am J Physiol* 211(5):1197-1202. doi:10.1152/ajplegacy.1966.211.5.1197
308. Chan CS, Lin YK, Chen YC, Lu YY, Chen SA, Chen YJ (2019) Heart Failure Differentially Modulates Natural (Sinoatrial Node) and Ectopic (Pulmonary Veins) Pacemakers: Mechanism and Therapeutic Implication for Atrial Fibrillation. *Int J Mol Sci* 20(13). doi:10.3390/ijms20133224
309. Verkerk AO, Wilders R, Coronel R, Ravesloot JH, Verheijck EE (2003) Ionic remodeling of sinoatrial node cells by heart failure. *Circulation* 108(6):760-766. doi:10.1161/01.CIR.0000083719.51661.B9
310. Zicha S, Fernandez-Velasco M, Lonardo G, L'Heureux N, Nattel S (2005) Sinus node dysfunction and hyperpolarization-activated (HCN) channel subunit remodeling in a canine heart failure model. *Cardiovasc Res* 66(3):472-481. doi:10.1016/j.cardiores.2005.02.011
311. Du Y, Huang X, Wang T, Han K, Zhang J, Xi Y, Wu G, Ma A (2007) Downregulation of neuronal sodium channel subunits Nav1.1 and Nav1.6 in the sinoatrial node from volume-overloaded heart failure rat. *Pflugers Arch* 454(3):451-459. doi:10.1007/s00424-007-0216-4
312. Chang SL, Chuang HL, Chen YC, Kao YH, Lin YK, Yeh YH, Chen SA, Chen YJ (2017) Heart failure modulates electropharmacological characteristics of sinoatrial nodes. *Exp Ther Med* 13(2):771-779. doi:10.3892/etm.2016.4015
313. Kannel WB, Kannel C, Paffenbarger RS, Jr., Cupples LA (1987) Heart rate and cardiovascular mortality: the Framingham Study. *Am Heart J* 113(6):1489-1494. doi:10.1016/0002-8703(87)90666-1
314. Cook S, Togni M, Schaub MC, Wenaweser P, Hess OM (2006) High heart rate: a cardiovascular risk factor? *Eur Heart J* 27(20):2387-2393. doi:10.1093/eurheartj/ehl259
315. Palatini P, Julius S (1997) Association of tachycardia with morbidity and mortality: pathophysiological considerations. *J Hum Hypertens* 11 Suppl 1:S19-27

316. Reil JC, Bohm M (2007) The role of heart rate in the development of cardiovascular disease. *Clin Res Cardiol* 96 (9):585-592. doi:10.1007/s00392-007-0537-5
317. Kaye DM, Lefkovits J, Jennings GL, Bergin P, Broughton A, Esler MD (1995) Adverse consequences of high sympathetic nervous activity in the failing human heart. *J Am Coll Cardiol* 26 (5):1257-1263. doi:10.1016/0735-1097(95)00332-0
318. Custodis F, Reil JC, Laufs U, Bohm M (2013) Heart rate: a global target for cardiovascular disease and therapy along the cardiovascular disease continuum. *J Cardiol* 62 (3):183-187. doi:10.1016/j.jcc.2013.02.018
319. Laskey WK, Alomari I, Cox M, Schulte PJ, Zhao X, Hernandez AF, Heidenreich PA, Eapen ZJ, Yancy C, Bhatt DL, Fonarow GC, Program AHAGWTG-HF (2015) Heart rate at hospital discharge in patients with heart failure is associated with mortality and rehospitalization. *J Am Heart Assoc* 4 (4). doi:10.1161/JAHA.114.001626
320. McAlister FA, Wiebe N, Ezekowitz JA, Leung AA, Armstrong PW (2009) Meta-analysis: beta-blocker dose, heart rate reduction, and death in patients with heart failure. *Ann Intern Med* 150 (11):784-794. doi:10.7326/0003-4819-150-11-200906020-00006
321. Badu-Boateng C, Jennings R, Hammersley D (2018) The therapeutic role of ivabradine in heart failure. *Ther Adv Chronic Dis* 9 (11):199-207. doi:10.1177/2040622318784556
322. Du XJ, Feng X, Gao XM, Tan TP, Kiriazis H, Dart AM (2004) I(f) channel inhibitor ivabradine lowers heart rate in mice with enhanced sympathoadrenergic activities. *Br J Pharmacol* 142 (1):107-112. doi:10.1038/sj.bjp.0705696
323. Tardif JC, Ford I, Tendera M, Bourassa MG, Fox K, Investigators I (2005) Efficacy of ivabradine, a new selective I(f) inhibitor, compared with atenolol in patients with chronic stable angina. *Eur Heart J* 26 (23):2529-2536. doi:10.1093/eurheartj/ehi586
324. Vilaine JP (2006) The discovery of the selective I(f) current inhibitor ivabradine. A new therapeutic approach to ischemic heart disease. *Pharmacol Res* 53 (5):424-434. doi:10.1016/j.phrs.2006.03.016
325. DiFrancesco D (2006) Funny channels in the control of cardiac rhythm and mode of action of selective blockers. *Pharmacol Res* 53 (5):399-406. doi:10.1016/j.phrs.2006.03.006
326. Bucchi A, Baruscotti M, DiFrancesco D (2002) Current-dependent block of rabbit sino-atrial node I(f) channels by ivabradine. *J Gen Physiol* 120 (1):1-13. doi:10.1085/jgp.20028593
327. Stillitano F, Lonardo G, Zicha S, Varro A, Cerbai E, Mugelli A, Nattel S (2008) Molecular basis of funny current (I<sub>f</sub>) in normal and failing human heart. *J Mol Cell Cardiol* 45 (2):289-299. doi:10.1016/j.yjmcc.2008.04.013
328. Kuwabara Y, Kuwahara K, Takano M, Kinoshita H, Arai Y, Yasuno S, Nakagawa Y, Igata S, Usami S, Minami T, Yamada Y, Nakao K, Yamada C, Shibata J, Nishikimi T, Ueshima K, Nakao K (2013) Increased expression of HCN channels in the ventricular myocardium contributes to enhanced arrhythmicity in mouse failing hearts. *J Am Heart Assoc* 2 (3):e000150. doi:10.1161/JAHA.113.000150
329. Plotnikov AN, Bucchi A, Shlapakova I, Danilo P, Jr., Brink PR, Robinson RB, Cohen IS, Rosen MR (2008) HCN212-channel biological pacemakers manifesting ventricular tachyarrhythmias are responsive to treatment with I(f) blockade. *Heart Rhythm* 5 (2):282-288. doi:10.1016/j.hrthm.2007.09.028
330. Musialek P (2013) If current inhibition and mortality reduction in heart failure: more than just a 'pure' effect of lowering heart rate. *Kardiol Pol* 71 (7):764-767. doi:10.5603/KP.2013.0168
331. Cerbai E, Sartiani L, DePaoli P, Pino R, Maccherini M, Bizzarri F, DiCiolla F, Davoli G, Sani G, Mugelli A (2001) The properties of the pacemaker current I(F)in human ventricular myocytes are modulated by cardiac disease. *J Mol Cell Cardiol* 33 (3):441-448. doi:10.1006/jmcc.2000.1316
332. Mert KU, Mert GO, Morrad B, Tahmazov S, Mutlu F, Cavusoglu Y (2017) Effects of ivabradine and beta-blocker therapy on dobutamine-induced ventricular arrhythmias. *Kardiol Pol* 75 (8):786-793. doi:10.5603/KP.a2017.0094
333. Musialek P (2017) Drug action(s), drug marketing, and clinical medicine. Suppression of ventricular arrhythmogenicity with If blockade in human heart failure: emerging clinical evidence for ivabradine treatment benefit beyond heart rate control. *Kardiol Pol* 75 (12):1368-1371. doi:10.5603/KP.2017.0238
334. Dias P, Terracciano CM (2013) Hyperpolarization-activated cyclic nucleotide-gated channels and ventricular arrhythmias in heart failure: a novel target for therapy? *J Am Heart Assoc* 2 (3):e000287. doi:10.1161/JAHA.113.000287
335. Shinohara T, Park HW, Han S, Shen MJ, Maruyama M, Kim D, Chen PS, Lin SF (2010) Ca<sup>2+</sup> clock malfunction in a canine model of pacing-induced heart failure. *Am J Physiol Heart Circ Physiol* 299 (6):H1805-1811. doi:10.1152/ajpheart.00723.2010

336. Swaminathan PD, Purohit A, Soni S, Voigt N, Singh MV, Glukhov AV, Gao Z, He BJ, Luczak ED, Joiner ML, Kutschke W, Yang J, Donahue JK, Weiss RM, Grumbach IM, Ogawa M, Chen PS, Efimov I, Dobrev D, Mohler PJ, Hund TJ, Anderson ME (2011) Oxidized CaMKII causes cardiac sinus node dysfunction in mice. *J Clin Invest* 121 (8):3277-3288. doi:10.1172/JCI57833
337. Swaminathan PD, Purohit A, Hund TJ, Anderson ME (2012) Calmodulin-dependent protein kinase II: linking heart failure and arrhythmias. *Circ Res* 110 (12):1661-1677. doi:10.1161/CIRCRESAHA.111.243956
338. Yano M, Kobayashi S, Kohno M, Doi M, Tokuhisa T, Okuda S, Suetsugu M, Hisaoka T, Obayashi M, Ohkusa T, Kohno M, Matsuzaki M (2003) FKBP12.6-mediated stabilization of calcium-release channel (ryanodine receptor) as a novel therapeutic strategy against heart failure. *Circulation* 107 (3):477-484. doi:10.1161/01.cir.0000044917.74408.be
339. Toischer K, Lehnart SE, Tenderich G, Milting H, Korfer R, Schmitto JD, Schondube FA, Kaneko N, Loughrey CM, Smith GL, Hasenfuss G, Seidler T (2010) K201 improves aspects of the contractile performance of human failing myocardium via reduction in Ca<sup>2+</sup> leak from the sarcoplasmic reticulum. *Basic Res Cardiol* 105 (2):279-287. doi:10.1007/s00395-009-0057-8
340. Hunt DJ, Jones PP, Wang R, Chen W, Bolstad J, Chen K, Shimoni Y, Chen SR (2007) K201 (JTV519) suppresses spontaneous Ca<sup>2+</sup> release and [3H]ryanodine binding to RyR2 irrespective of FKBP12.6 association. *Biochem J* 404 (3):431-438. doi:10.1042/BJ20070135
341. Gomes A, Falcão-Pires I, Pires A, Brás-Silva C, Leite Moreira A (2012) Rodent models of heart failure: An updated review. *Heart failure reviews* 18. doi:10.1007/s10741-012-9305-3
342. Camacho P, Fan H, Liu Z, He JQ (2016) Small mammalian animal models of heart disease. *Am J Cardiovasc Dis* 6 (3):70-80
343. Rockman HA, Ross RS, Harris AN, Knowlton KU, Steinhilber ME, Field LJ, Ross J, Chien KRJPotNAoS (1991) Segregation of atrial-specific and inducible expression of an atrial natriuretic factor transgene in an in vivo murine model of cardiac hypertrophy. *88* (18):8277-8281
344. Luo T, Chen B, Wang X (2015) 4-PBA prevents pressure overload-induced myocardial hypertrophy and interstitial fibrosis by attenuating endoplasmic reticulum stress. *Chem Biol Interact* 242:99-106. doi:10.1016/j.cbi.2015.09.025
345. Heineke J, Molkentin JDJNrMcb (2006) Regulation of cardiac hypertrophy by intracellular signalling pathways. *7* (8):589-600
346. deAlmeida AC, van Oort RJ, Wehrens XHJJ (2010) Transverse aortic constriction in mice. (38):e1729
347. Barrick CJ, Rojas M, Schoonhoven R, Smyth SS, Threadgill DWJAJoP-H, Physiology C (2007) Cardiac response to pressure overload in 129S1/SvImJ and C57BL/6J mice: temporal- and background-dependent development of concentric left ventricular hypertrophy. *292* (5):H2119-H2130
348. Mohammed SF, Storlie JR, Oehler EA, Bowen LA, Korinek J, Lam CS, Simari RD, Burnett Jr JC, Redfield MMJCP (2012) Variable phenotype in murine transverse aortic constriction. *21* (3):188-198
349. Balakumar P, Singh AP, Singh MJJop, methods t (2007) Rodent models of heart failure. *56* (1):1-10
350. Hampton C, Rosa R, Campbell B, Kennan R, Gichuru L, Ping X, Shen X, Small K, Madwed J, Lynch JJ (2017) Early echocardiographic predictors of outcomes in the mouse transverse aortic constriction heart failure model. *Journal of Pharmacological and Toxicological Methods* 84:93-101. doi:https://doi.org/10.1016/j.vascn.2016.12.001
351. Van den Bosch B, Lindsey P, Van den Burg C, Van der Vlies S, Lips D, Van der Vusse G, Ayoubi T, Doevendans P, Smeets HJG (2006) Early and transient gene expression changes in pressure overload-induced cardiac hypertrophy in mice. *88* (4):480-488
352. Izumiya Y, Shiojima I, Sato K, Sawyer DB, Colucci WS, Walsh KJH (2006) Vascular endothelial growth factor blockade promotes the transition from compensatory cardiac hypertrophy to failure in response to pressure overload. *47* (5):887-893
353. Bryan PM, Xu X, Dickey DM, Chen Y, Potter LRJAJoP-RP (2007) Renal hyporesponsiveness to atrial natriuretic peptide in congestive heart failure results from reduced atrial natriuretic peptide receptor concentrations. *292* (5):F1636-F1644
354. Ling H, Zhang T, Pereira L, Means CK, Cheng H, Gu Y, Dalton ND, Peterson KL, Chen J, Bers DJTJoci (2009) Requirement for Ca<sup>2+</sup>/calmodulin-dependent kinase II in the transition from pressure overload-induced cardiac hypertrophy to heart failure in mice. *119* (5):1230-1240
355. Hunter JJ, Chien KRJNEJoM (1999) Signaling pathways for cardiac hypertrophy and failure. *341* (17):1276-1283

356. Haq S, Choukroun G, Lim H, Tymitz KM, del Monte F, Gwathmey J, Grazette L, Michael A, Hajjar R, Force TJC (2001) Differential activation of signal transduction pathways in human hearts with hypertrophy versus advanced heart failure. *Circulation* 103 (5):670-677
357. McMullen JR, Sherwood MC, Tarnavski O, Zhang L, Dorfman AL, Shioi T, Izumo SJC (2004) Inhibition of mTOR signaling with rapamycin regresses established cardiac hypertrophy induced by pressure overload. *Circulation* 109 (24):3050-3055
358. Moens A, Takimoto E, Tocchetti C, Chakir K, Bedja D, Cormaci GJC (2008) Ketner EA, Majmudar M, Gabrielson K, Halushka MK et al. Reversal of Cardiac Hypertrophy and Fibrosis From Pressure Overload by Tetrahydrobiopterin: Efficacy of Recoupling Nitric Oxide Synthase as a Therapeutic Strategy. *Circulation* 117:2626-2626
359. Mohammed SF, Storlie JR, Oehler EA, Bowen LA, Korinek J, Lam CS, Simari RD, Burnett JC, Jr., Redfield MM (2012) Variable phenotype in murine transverse aortic constriction. *Cardiovasc Pathol* 21 (3):188-198. doi:10.1016/j.carpath.2011.05.002
360. Vinet L, Rouet-Benzineb P, Marniquet X, Pellegrin N, Mangin L, Louedec L, Samuel JL, Mercadier JJ (2008) Chronic doxycycline exposure accelerates left ventricular hypertrophy and progression to heart failure in mice after thoracic aorta constriction. *Am J Physiol Heart Circ Physiol* 295 (1):H352-360. doi:10.1152/ajpheart.01101.2007
361. Au - McCauley MD, Au - Wehrens XHT (2010) Ambulatory ECG Recording in Mice. *JoVE* (39):e1739. doi:doi:10.3791/1739
362. Behar JA, Rosenberg AA, Weiser-Bitoun I, Shemla O, Alexandrovich A, Konyukhov E, Yaniv Y (2018) PhysioZoo: A Novel Open Access Platform for Heart Rate Variability Analysis of Mammalian Electrocardiographic Data. *Front Physiol* 9:1390. doi:10.3389/fphys.2018.01390
363. Janse MJ (2004) Electrophysiological changes in heart failure and their relationship to arrhythmogenesis. *Cardiovasc Res* 61 (2):208-217. doi:10.1016/j.cardiores.2003.11.018
364. Opthof T, Coronel R, Rademaker HME, Vermeulen JT, Wilms-Schopman FJG, Janse MJ (2000) Changes in Sinus Node Function in a Rabbit Model of Heart Failure With Ventricular Arrhythmias and Sudden Death. *Circulation* 101 (25):2975-2980. doi:doi:10.1161/01.CIR.101.25.2975
365. Pereira L, Matthes J, Schuster I, Valdivia HH, Herzig S, Richard S, Gomez AM (2006) Mechanisms of [Ca<sup>2+</sup>]<sub>i</sub> transient decrease in cardiomyopathy of db/db type 2 diabetic mice. *Diabetes* 55 (3):608-615. doi:10.2337/diabetes.55.03.06.db05-1284

**Titre :** Changements dans le cycle du calcium et ses mécanismes dans le nœud sino-auriculaire sous-jacent à l'insuffisance cardiaque induite par le TAC chez la souris

**Mots clés :** Insuffisance cardiaque ; nœud sino-auriculaire ; récepteurs de la ryanodine ;  $Ca^{2+}$

**Résumé :** L'insuffisance cardiaque (IC) est le résultat final de plusieurs maladies chroniques qui affectent la fonction cardiaque et se manifeste par l'incapacité du cœur à maintenir le flux sanguin pour répondre aux besoins de l'organisme, d'abord à l'effort, puis au repos. L'IC est généralement accompagnée d'anomalies du rythme, y compris un dysfonctionnement du nœud sinusal (SAN).

Le SAN, stimulateur cardiaque principal, fixe le rythme cardiaque de par son activité de génération automatique des potentiels d'action (PA). Le déclenchement du PA du SAN dépend de la dépolarisation diastolique, qui amène le potentiel membranaire au seuil du PA. Cette dépolarisation est provoquée par l'ouverture de canaux ioniques situés au niveau de la membrane plasmique (horloge membranaire), et au niveau du réticulum sarcoplasmique (RS) (horloge calcique), travaillant ensemble dans ce qu'il a été appelé horloge couplée. Bien que certaines études aient signalé une altération de l'horloge membranaire dans l'IC, les mécanismes de l'horloge calcique n'ont été que peu étudiés.

Ainsi, dans cette thèse, nous avons analysé l'horloge calcique dans un modèle expérimental d'IC par constriction aortique transverse (TAC) chez la souris. Les animaux témoins ont été soumis à une chirurgie factice. L'IC a été déterminée par une fraction d'éjection réduite par échocardiographie en mode M. L'IC congestive a été déterminée par une augmentation du rapport poids de poumons/longueur du tibia. Les électrocardiogrammes enregistrés par télémétrie n'ont pas montré de modification du rythme cardiaque (HR) de base. Cependant, la variabilité du HR était plus faible chez les souris IC, ainsi que le HR intrinsèque, sous blocage du système nerveux autonome (SNA) par injection intrapéritonéale d'atropine et de propranolol (2 mg / kg chacun). Ces résultats montrent un dysfonctionnement intrinsèque du SAN chez les souris IC.

Afin d'analyser le mécanisme sous-jacent, le SAN a été disséqué, chargé avec un indicateur fluorescent de  $Ca^{2+}$ , le fluo-4 AM et observé par microscopie confocale. La fréquence des transitoires  $[Ca^{2+}]_i$  était plus lente dans l'IC et leur décroissance significativement plus longue, suggérant une altération de la fonction de la  $Ca^{2+}$ -ATPase du RS (SERCA) et/ou de l'échangeur  $Na^+/Ca^{2+}$  (NCX). De fait, dans le groupe IC l'expression protéique de NCX était déprimée, avec une expression accrue de phospholamban (PLB, un inhibiteur naturel de SERCA lorsqu'il n'est pas phosphorylé) ainsi qu'une moindre phosphorylation au site T17, site phosphorylation par la  $Ca^{2+}$ /Camoduline kinase II (CaMKII). Ainsi, le temps de décroissance plus long des transitoires  $[Ca^{2+}]_i$  pourrait être le résultat d'une moindre d'expression de NCX et/ou d'une plus grande inhibition de SERCA. La diminution de la fonction de la SERCA pourrait diminuer la charge calcique du SR, comme cela a été constaté par une perfusion rapide de caféine dans les cellules isolées du SAN du groupe IC.

Afin d'évaluer l'activité des récepteurs de la ryanodine (RyR2), nous avons analysé les étincelles calciques ( $Ca^{2+}$  sparks), événements élémentaires produits par l'activation d'un cluster de RyR2s. La fréquence des  $Ca^{2+}$  sparks était significativement plus petit dans le groupe IC, avec une amplitude et une durée réduites. Ainsi, la quantité de  $Ca^{2+}$  libéré pendant la diastole par les  $Ca^{2+}$  sparks était plus petit dans le groupe IC, indiquant une altération de l'horloge  $Ca^{2+}$ .

Nous avons ensuite étudié plus avant les altérations des RyR2s au niveau moléculaire, par immunoblot. Avec l'IC, le niveau d'expression des RyR2s était significativement diminué, ainsi que la phosphorylation relative au site S2814. Combiné avec la réduction de phosphorylation relative du phospholambane (PLB) au site T17, ces résultats suggéraient une moindre activation de la CaMKII dans IC SAN. De fait, si l'expression de CaMKII était similaire dans les deux groupes, son niveau de phosphorylation était significativement diminué, indiquant moins d'activation. Pour tester la signification fonctionnelle, nous avons perfusé un inhibiteur de CaMKII, le KN93 sur le tissu SAN et analysé les mouvements de  $Ca^{2+}$ . Si le KN93 réduisait significativement la fréquence spontanée des transitoires  $[Ca^{2+}]_i$  dans les deux groupes, indiquant une certaine activation basale, son effet était proportionnellement moindre dans le groupes IC, conduisant à une fréquence encore plus rapide.

Pour conclure, nous avons mis en évidence que la CaMKII est moins activé dans le SAN des souris IC. Par conséquent, PLB et RyR2 sont moins phosphorylés, ce qui ralentit l'horloge  $Ca^{2+}$ . De plus, le niveau d'expression de RyR2 et NCX, deux facteurs principaux de l'horloge  $Ca^{2+}$ , est diminué, ce qui altère davantage la fonction du nœud sinusal avec l'IC.

**Title:** Changes in calcium cycling and its mechanisms in sinoatrial-node underlying the TAC-induced heart failure in mouse

**Keywords:** Heart failure sinoatrial node; Ryanodine receptors;  $Ca^{2+}$

**Abstract:** Heart failure (HF) is the final outcome of several chronic diseases that affect the heart function, and manifests as the inability of the heart to maintain blood flow to meet the body's needs first at effort and then at rest. HF is usually accompanied by rhythm abnormalities including sinus node dysfunction.

Heart rhythm is controlled by the automatic activity of the primary pacemaker, the sinoatrial node (SAN), which controls the heart rhythm by automatically generating action potentials (AP). The firing of the AP depends on the diastolic depolarization, which brings the membrane potential to the AP threshold. This depolarization is caused by the opening of ion channels located at the sarcolemmal membrane (voltage clock), and at the sarcoplasmic reticulum (SR) (calcium clock), working together in what it has been named coupled clock. Although some studies have pointed to alteration of the voltage clock in HF, the calcium clock mechanisms are understudied. Thus, in this thesis we aim to analyse the calcium clock in an experimental model of HF by transverse aortic constriction (TAC) in the mouse. Control animals were subjected to sham surgery. HF was determined by reduced ejection fraction by M-mode echocardiography. Congestive HF was determined by enhanced lung weight/tibia length. Electrocardiograms recorded by telemetry showed similar basal HR in both sham and HF mice. However, the HR variability was lower in HF mice, as well as the intrinsic HR under autonomous nervous system (ANS) blockade by intraperitoneal injection of atropine and propranolol (2mg/kg each). These results show pacemaker dysfunction in HF mice.

In order to analyze the underlying mechanism, we dissected the SAN and loaded it with a fluorescent  $Ca^{2+}$  indicator, fluo-4 and viewed it by confocal microscopy. The  $[Ca^{2+}]_i$  transient rate was slower in HF and its decay significantly longer suggesting alteration in SERCA and/or NCX function.

Indeed, Western Blot assays showed depressed expression of NCX and increased expression of Phospholamban (PLB, a natural SERCA inhibitor when not phosphorylated) in HF group. Moreover, PLB was relatively less phosphorylated at the site phosphorylated by CaMKII (T17). Taken together, the longer decay time could be the result of less NCX expression and more SERCA inhibition. The decreasing of the SERCA function could decrease the SR  $Ca^{2+}$  load, as was found by rapid caffeine perfusion in HF SAN cells.

In order to assess the RyR2 activity, we analyzed  $Ca^{2+}$  sparks, elementary events produced by activation of a RyR2s cluster.  $Ca^{2+}$  sparks frequency was significantly smaller in HF group, along with reduced peak amplitude and duration. Thus, the calcium released during diastole through  $Ca^{2+}$  sparks were smaller in HF group, indicating impairment of the  $Ca^{2+}$  clock.

In order to further investigate the change in RyR2 at the molecular level, we performed Western Blot. The expression level of RyR2 in HF SAN was significantly decreased, and the relative phosphorylation at S2814 site (CaMKII site) was significantly decreased. Together with the reduced PLB phosphorylation at T17 suggested that the activation level of CaMKII in HF SAN might be altered. However, the CaMKII expression was similar in the two groups, although its phosphorylation level was significantly decreased, indicating less activation. To test functional significance, we perfused a CaMKII inhibitor, KN93 on the SAN tissue and analysed  $Ca^{2+}$  movements. KN93 significantly decreased transient rate in both groups, indicating some basal activation, but the effect was proportionally less in HF SAN, making the rate even faster in HF SAN.

To conclude, we have found that CaMKII is less activated in SAN from HF mice. Therefore, PLB and RyR2 are less phosphorylated, slowing the  $Ca^{2+}$  clock. Moreover, the expression level of RyR2 and NCX, two main factors of the  $Ca^{2+}$  clock are decreased, further impairing the sinus node function in HF.